FAKULTNÍ NEMOCNICE OSTRAVA

SBORNÍK VYBRANÝCH IMPAKTOVANÝCH PRACÍ ZA ROK 2014

Sborník vybraných impaktovaných prací za rok 2014
Vydavatel: Fakultní nemocnice Ostrava
Periodicita: roční
Počet výtisků: 100 ks

ISBN 978-80-905684-9-5 (print)
ISBN 978-80-906002-0-1 (on-line)

ISSN 2336-4041 (Print)
ISSN 2336-405X (On-line)

Obsah / Content

Úvodní slovo

Vážení kolegové,

druhé číslo sborníku nejlepších vědeckých prací publikovaných v impaktovaných časopisech v roce 2014 je opět zajímavým ohlédnutím za uplynulým rokem. Sborník je souhrnem 18 prací, které v roce 2014 získaly nejvyšší impakt faktor a představují přehled vynikajících autorských prací odborníků ve Fakultní nemocnici Ostrava.

Špičkový autorský text je odrazem kvalitní vědecké práce, která je nedílnou součástí poskytované zdravotní péče. Stoupající počet výzkumných projektů a počtů impaktovaných publikací je důkazem vynikající odborné úrovně napříč lékařskými obory ve Fakultní nemocnici Ostrava.

Fakultní nemocnice, jako výzkumná organizace, vykazuje již několik let tuto stoupající úroveň a řadí se tak mezi kvalitní vědecké instituce, které jsou registrovány a hodnoceny v rámci RIV. Naším dlouhodobým cílem je zvyšovat úroveň vědecké práce a tuto prezentovat na významných domácích i zahraničních konferencích.

Sborník nejlepších impaktovaných prací tak přináší zajímavý náhled na hloubku a rozsah vědecké práce v naší nemocnici.

Přeji Vám hodně úspěchů ve Vaší vědecké a publikační činnosti, kterou Fakultní nemocnice Ostrava bude vždy podporovat.

MUDr. Václav Procházka, Ph.D., MSc
Náměstek ředitele FNO pro vědu a výzkum

Foreword

Dear Colleagues

The second volume of the Collection of the best scientific works published in journals with an impact factor in 2014 is again a very interesting retrospect of the past year. The Collection presents a summary of eighteen works, which obtained the highest impact factor in 2014, and which present an overview of excellent author works of specialists from the University Hospital Ostrava.

A top-class author text is a reflection of a high--quality scientific work, which is an integral part of the provided medical care. The increasing number of research projects, together with the number of publications in journals with high impact factor is a proof of the excellent expert level across all medical specialties at the University Hospital Ostrava.

University Hospital Ostrava, as a research organization, has been demonstrating this increasing level for several years, and truly belongs among high-quality scientific institutions, which are registered and evaluated within the RIV register. Our long-term aim is to increase the level of the scientific work and present it at significant domestic and international conferences.

The Collection of the best scientific articles with an impact factor also brings an interesting perspective at the depth and extent of the scientific work performed at our hospital.

I wish you much success in your scientific and publication activities, which will be always supported by the University Hospital Ostrava.

Václav Procházka, MD, Ph.D., MSc
Deputy director for Science and Research

1.

Acute kidney injury due to rhabdomyolysis and renal replacement therapy: a critical review

Petejová Naděžda and Martínek Arnošt

Originally published in Critical Care, 2014, vol. 18, no. 3, p. 224

Consent to the publication of June 2015

Petejova and Martinek *Critical Care* 2014, 18:224
http://ccforum.com/content/18/3/224

CRITICAL CARE

REVIEW

Acute kidney injury due to rhabdomyolysis and renal replacement therapy: a critical review

Nadezda Petejova* and Arnost Martinek

Abstract

Rhabdomyolysis, a clinical syndrome caused by damage to skeletal muscle and release of its breakdown products into the circulation, can be followed by acute kidney injury (AKI) as a severe complication. The belief that the AKI is triggered by myoglobin as the toxin responsible appears to be oversimplified. Better knowledge of the pathophysiology of rhabdomyolysis and following AKI could widen treatment options, leading to preservation of the kidney: the decision to initiate renal replacement therapy in clinical practice should not be made on the basis of the myoglobin or creatine phosphokinase serum concentrations.

Introduction

Rhabdomyolysis (RM) is a clinical syndrome characterized by injury to skeletal muscle fibers with disruption and release of their contents into the circulation. Myoglobin, creatine phosphokinase (CK) and lactate dehydrogenase are the most important substances for indicating muscle damage [1].

Brief history

The history of RM goes back to the Second World War in 1941 when the condition was described for the first time. The London Blitz was the sustained strategic bombing of many cities in the United Kingdom and the ensuing crush injuries led to typical symptoms of RM [2]. Today, we know the causes of RM are legion and include trauma, drugs such as statins, infections, toxins, extreme physical exertion, temperature extremes, hereditary and acquired metabolic myopathies [3].

* Correspondence: petejova@seznam.cz
Department of Internal Medicine, University Hospital Ostrava, 17 listopadu 1790, 708 52 Ostrava, Czech Republic

Clinical symptoms

The clinical symptoms of RM are well known: myalgia, weakness and swelling involving injured muscles, usually associated with myoglobinuria. The clinical symptoms might include nonspecific symptoms such as fever, nausea, dyspepsia and/or vomiting. Mild and subclinical cases of RM, called in clinical practice myopathies, are typically characterized by elevated serum CK and myalgias [4].

The severity of RM escalates from myoglobinuria, which can result in acute kidney injury (AKI), to other severe systemic complications such as disseminated intravascular coagulopathy and acute compartment syndrome from swelling muscle, and reduced macrocirculation and microcirculation of injured limbs. Extracted fluid from the circulation into the swollen muscle groups leads to hypotension and shock. Typical metabolic alterations accompanying RM are hyperkalemia, metabolic acidosis, hypocalcemia or hypercalcemia, hyperuricemia, hyponatremia and hyperphosphatemia with possible cardiac dysrhythmias [5,6]. AKI due to rhabdomyolysis occurs in 13 to 50% of all cases [7].

Etiology

As already mentioned, the development of RM is associated with a large number of conditions and pathological disorders. Medical research, reviews, studies and case reports describe different possible causes of RM (Table 1) [3,8,9].

Pathophysiology of rhabdomyolysis and following acute kidney injury

Under physiological conditions, skeletal muscle cell contraction requires a nervous impulse originating in a voluntary process. The nervous impulse is then transferred to a thin muscle cell membrane called the sarcolemma. The sarcolemma is a physical barrier and mediator between cell and external signals. In healthy myocytes, the sarcolemma contains different pumps for regulating the

Table 1 Etiology of rhabdomyolysis and myopathies

Acquired	Hereditary
Extreme physical activity	Metabolic myopathies caused by disorders of:
Influence of extreme temperatures	Fatty acid oxidation
Metabolic disorders of water and salts	Mitochondrial metabolism
Trauma and crush syndrome	Glycolysis/glycogenolysis
Vascular ischemia	Purine nucleotide cycle
Influence of drugs	Pentose phosphate pathway
Infections, sepsis	
Toxins	
Malignant hyperthermia	
Endocrine disorders	
Electrical current	

process of cellular electrochemical gradients [10]. The most important is Na-K-ATP-ase for sodium and potassium exchange. Under normal conditions, sodium ions are actively excluded from the muscle cell and potassium ions are allowed passage. This process is energy dependent and builds on calcium removal in Na/Ca by changing the intracellular electrical gradient during active removal of sodium. Both processes depend on ATP as a source of energy [11,12].

The sarcoplasm is the specialized cytoplasm of the muscle cell that contains the usual subcellular elements along with Golgi apparatus, myofibrils, a modified endoplasmic reticulum known as the sarcoplasmic reticulum, myoglobin and mitochondria. The primary function of the sarcoplasmic reticulum is to store calcium, which is released by muscular contraction. The most serious consequence of RM is ATP depletion, resulting in membrane cell pump dysfunction. The extrusion of sodium is impaired and the efflux of calcium from the cell is impaired [13]. If a high concentration of calcium persists in the sarcoplasm this activates cytolytic enzymes such as hydroxylases, proteases, nucleases and many others. The following impairment of cell organelles, especially of mitochondria, leads to progressive decrease in ATP, the production of free oxygen radicals and cell damage [12]. The result of cell impairment is release of potassium, phosphates, myoglobin, CK, lactate dehydrogenase and aldolase into the blood circulation with typical clinical presentation of RM.

Acute kidney injury is one of the most severe complications of rhabdomyolysis

The pathophysiology of RM-induced AKI is believed to be triggered by myoglobin as the toxin causing renal dysfunction [14]. This claim is given substance from studies in animal models of glycerol-induced AKI. Intramuscular injection of glycerol in the rabbit induces a model of AKI at a dose of 10 mg/kg that resembles the AKI caused by massive release of myoglobin in crush syndrome in humans [15]. Glycerol-induced AKI is characterized by myoglobinuria, tubular necrosis and renal vasoconstriction [16]. The most important role in glycerol-induced nephrotoxicity has been attributed to reactive oxygen metabolites (reactive oxygen species), in particular the hydroxyl radical ($OH^{\cdot}$), the same cause as for myoglobin-induced AKI [17].

Myoglobin is an oxygen and iron binding protein with a molecular weight of 17,500 Da. Myoglobin is found in the muscle tissue of vertebrates, has a higher affinity for oxygen than hemoglobin and assists myocytes to acquire energy. Myoglobin can be detected in urine in small concentrations <5 μg/l, but meets the diagnostic criteria for myoglobinuria at concentrations >20 μg/l [9].

Myoglobin – which may undergo reabsorption from the glomerular filtrate, is catabolized within proximal tubule cells and is easily filtered through the glomerular basement membrane – has been recognized as playing a part in the development of AKI in the setting of myoglobinuria. The clinical study by Gburek and colleagues demonstrated that renal uptake of myoglobin is mediated by the endocytic receptors, megalin and cubilin [18]. The same membrane cell receptors play an important role in nephrotoxicity; for example, those of antibiotics.

The three different mechanisms of renal toxicity by myoglobin are usually reported as renal vasoconstriction, formation of intratubular casts and the direct toxicity of myoglobin to kidney tubular cells [19-27] (Figure 1).

Renal vasoconstriction is caused by reduced renal blood flow due to excessive leakage of extracellular fluid into the damaged muscle cells and by secondary activation of the renin–angiotensin–aldosterone system. However, a second theory favors the effect of the nitric oxide scavenging characteristics of myoglobin and release of cytokines [25,26]. The formation of intratubular casts explains the urine concentration and the following reaction of myoglobin with Tamm–Horsfall tubular protein. Further, renal vasoconstriction, the decrease in renal blood flow due to volume depletion and the low pH of urine promote this pathological process by formation of stronger and more rapid bonds between Tamm–Horsfall protein and myoglobin [12,20].

Heme released from myoglobin is, under normal conditions, degraded by the enzyme heme oxygenase-1 with marked vasodilatating effect. Heme oxygenase-1 is upregulated in proximal tubular cells in response to oxidant stress and exerts cytoprotective and anti-inflammatory effects [14,21,22]. Zager and colleagues [19] studied intrarenal heme oxygenase-1 induction in

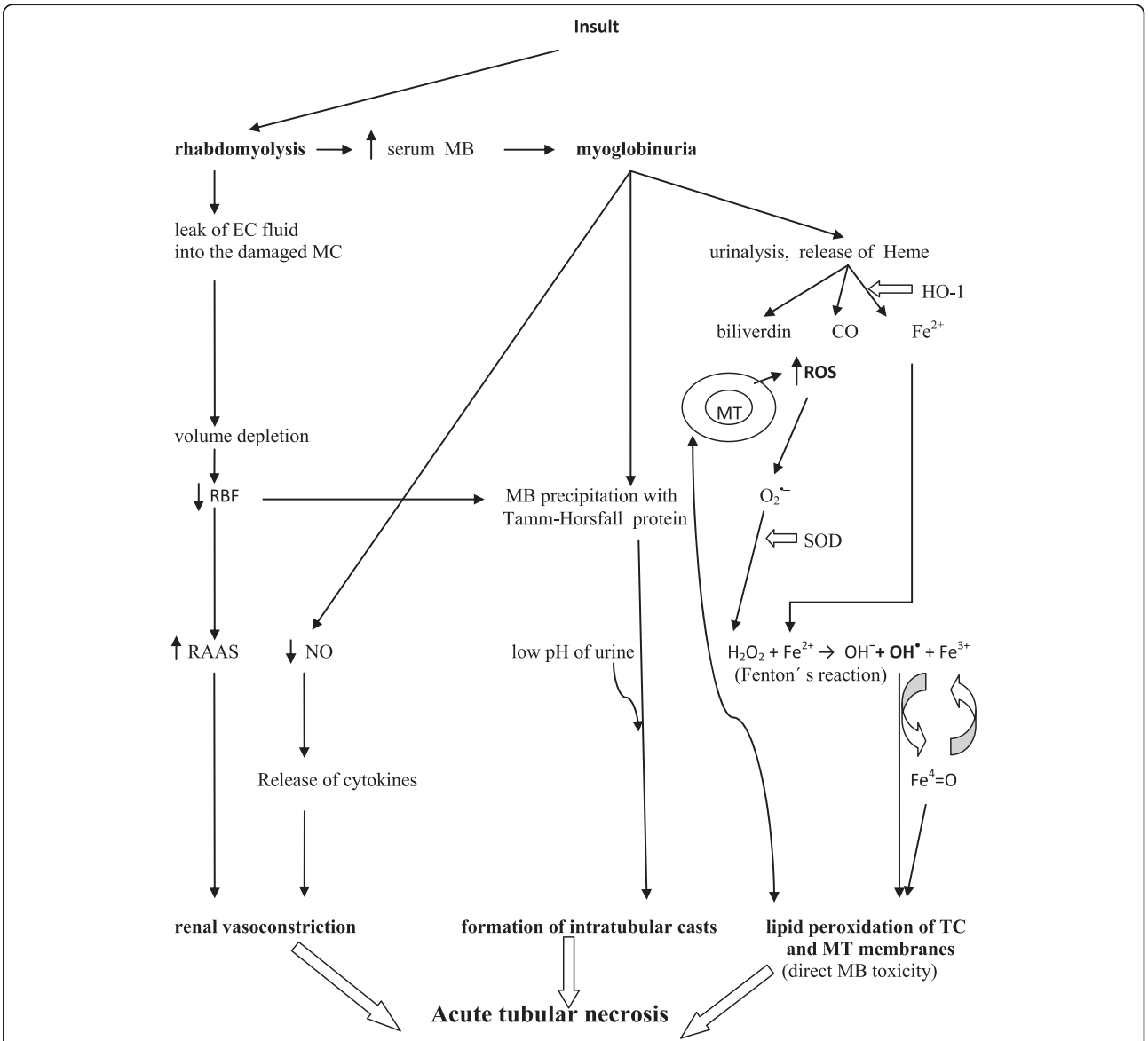

Figure 1 Pathophysiology of rhabdomyolysis-induced acute kidney injury. CO, carbon monoxide; EC, extracellular; Fe^{2+}, ferrous iron; Fe^{3+}, ferric iron; $Fe^{4}=O$, ferryl iron; HO-1, heme oxygenase-1; H_2O_2, hydrogen peroxide; MB, myoglobin; MC, muscle cell; MT, mitochondria; NO, nitric oxide; OH^-, hydroxyl anion; $O_2^{\bullet-}$, superoxide radical; $OH^{\bullet}$, hydroxyl radical, RAAS, renin–angiotensin–aldosterone system; RBF, renal blood flow; ROS, reactive oxygen species; SOD, superoxide dismutase; TC, tubular cell.

response to four different experimental AKI models: glycerol, cisplatin, ischemic–reperfusion and a bilateral ureteral obstruction model. In the glycerol AKI model that best reflects kidney damage during myoglobinuric AKI, heme oxygenase-1 was detectable in plasma and the renal cortex, and these changes were associated with an approximately 10-fold increase in renal heme oxygenase-1 mRNA. With the urinary heme oxygenase-1 concentration increase in the glycerol AKI model, further increases were observed 4 and 24 hours after glycerol injection. Finally, the authors tested whether the above findings might have clinical relevance in 20 critically ill patients: one-half of the patients had AKI and one-half had no AKI. Only the AKI group had significantly elevated plasma and urinary heme oxygenase-1 concentrations, and these investigations led to the conclusion that AKI can evoke heme oxygenase-1 elevation in plasma and urine [19]. However, the whole molecular pathophysiology of myoglobin-induced AKI is based on the deleterious effects of reactive oxygen species directly on the tubular cells and their organelles.

Reactive oxygen species also play an important and protective role in the living organism against pathogens and cancer during phagocytosis and other, especially

metabolic, reactions. But overproduction of reactive oxygen species may lead to damage to living cells via lipid peroxidation of fatty acids and to the production of malondialdehyde, which can cause the polymerization of protein and DNA [23]. The hydroxyl radical is the most reactive of the reactive oxygen species group and is produced by the reaction between superoxide and hydrogen peroxide catalyzed by iron in Fenton's reaction (Figure 1).

In previous years, iron-mediated hydroxyl radical production with resultant oxidant stress was hypothesized to be the dominant pathway for heme protein nephrotoxicity [17]. However, it was later shown that Fe-mediated proximal tubular system lipid peroxidation was more hydrogen peroxide dependent than hydroxyl anion (OH^-) dependent and that blockage of myoglobin cytotoxicity via only decreasing hydroxyl anion generation may be inadequate [24]. For myoglobin to catalyze lipid peroxidation, ferrous (Fe^{2+}) myoglobin must be oxidized to the ferric (Fe^{3+}) form, which leads to induced lipid peroxidation by redox cycling with ferryl ($Fe^4 = O$) myoglobin. This is a highly reactive form of myoglobin, which can potently induce lipid peroxidation [27]. Redox cycling between ferric and ferryl myoglobin yields radical species that cause severe oxidative damage to the kidney [28].

This process has been shown to be pH dependent and alkaline conditions prevent myoglobin-induced lipid peroxidation by stabilizing the reactive ferryl–myoglobin complex [29,30]. Alkaline conditions stabilize the ferryl species, making myoglobin considerably less reactive towards lipids and lipid hydroperoxides [31]. The fact that RM can be considered an oxidative stress-mediated pathology also with mitochondria as the primary target, and possibly the source of reactive oxygen and nitrogen species, has been reported in a study by Plotnikov and colleagues [32]. However, the authors speculate that RM-induced kidney damage involves direct interaction of myoglobin with mitochondria possibly resulting in iron ion release from myoglobin's heme, and this promotes the peroxidation of mitochondrial membranes [32]. This problem, however, appears to be more complicated.

In summary, better knowledge of the pathophysiology can optimize prevention and treatment measures in cases of RM kidney injury.

Diagnosis

In typical clinical conditions, patients with RM experience muscular weakness, myalgia, swelling, tenderness or stiffness and dark brown urine [1]. Correct diagnosis is the most important step to initiating proper treatment. The clinical and laboratory diagnostics summarized in Table 2 are the basic approach in differential diagnosis.

Table 2 Diagnosis of rhabdomyolysis and following acute kidney injury

Clinical presentation
Muscular weakness, myalgia, swelling, tenderness, stiffness
Fever, feelings of nausea, vomiting, tachycardia
Oligoanuria or anuria in connection with renal damage or in the presence of volume depletion
Signs of the underlying disease
Laboratory findings
Serum: creatinine, urea nitrogen, creatine phosphokinase, myoglobin, ions (potassium, phosphorus, calcium), lactate dehydrogenase, transaminases, acid–base balance
Urine: myoglobin or positive dipstick test without any erythrocytes

Serum myoglobin is normally bound to plasma globulins such as haptoglobin and α_2-globulin and has a rapid renal clearance to maintain a low plasma concentration of 3 μg/l [33]. Radioimmunoassays or imunolatex, imunoturbidimetric methods can detect myoglobin in plasma or urine. Normal serum levels are 30 to 80 μg/l and normal urine levels are 3 to 20 μg/l [3]. After the development of RM, free serum myoglobin increases due to exceeding the binding capacity of plasma globulins and then kidney filtrate appears in the urine which contributes to the brownish (tea) urine color. Furthermore, urine myoglobin concentrations are normally measured to assess RM; surprisingly, one *in vitro* study observed that low pH is not by itself a cause of urine myoglobin instability. The extent of instability depended not only on urine pH and temperature but also on unidentified urinary factors and initial urinary myoglobin concentrations [34]. Another way to diagnose myoglobinuria is a positive test for the presence of blood in urine without finding erythrocytes.

Serum levels of CK correlate with the severity of RM but less so with myoglobinuric AKI. Normal serum levels are 0.15 to 3.24 μkat/l or 9 to 194 U/l in men and 0.15 to 2.85 μkat/l or 9 to 171 U/l in women. To predict AKI following RM, the clinician needs a better marker than serum CK, which is routinely used as a marker in the assessment of these disorders. Very important findings about the use of myoglobin as a marker and predictor in AKI were described by Premru and colleagues [35]. The authors investigated and restrospectively analyzed the incidence of myoglobin-induced AKI (serum creatinine >200 μmol/l) and the need for hemodialysis in 484 patients with suspected RM. The median peak myoglobin was 7,163 μg/l. The incidence of myoglobin-induced AKI was significantly higher (64.9%) in patients with a peak serum myoglobin >15,000 μg/l (P <0.01). Most of these patients needed treatment with hemodialysis (28%). Myoglobin levels >15,000 μg/l were most significantly related to the development of AKI and the need for hemodialysis. Based on these results, serum myoglobin

was recommended as a valuable early predictor and marker of RM and myoglobinuric AKI [35].

In another retrospective observational cohort study, El-Abdellati and colleagues studied CK, serum myoglobin and urinary myoglobin as markers of RM and AKI in 1,769 adult patients. The results for the best cutoff values for prediction of AKI were CK >773 U/l, serum myoglobin >368 μg/l and urine myoglobin >38 μg/l, respectively [36].

Conservative measures in rhabdomyolysis to prevent acute kidney injury

The first step in medical intervention is usually treatment of underlying disease. In the case of preserved diuresis in the setting of RM, we must initiate conservative measures, which usually include massive hydration, use of mannitol, urine alkalization and forced diuresis [25,37-39] (Figure 2).

Early and aggressive fluid resuscitation to restore renal perfusion and increase the urine flow rate is agreed on as the main intervention for preventing and treating AKI [6]. Fluid resuscitation with crystalloid solutions is the ubiquitous intervention in critical care medicine [40]. One caveat, however, is that these therapeutic measures are not useful in the context of severe oliguria or anuria and may lead to interstitial and pulmonary edema. Clinicians have to be careful about oliguria which is a normal response to hypovolemia and should not be used solely as a trigger or end point for fluid resuscitation, particularly in the post-resuscitation period [41]. Further, while aggressive volume resuscitation may preserve cardiac output and renal perfusion pressure, in

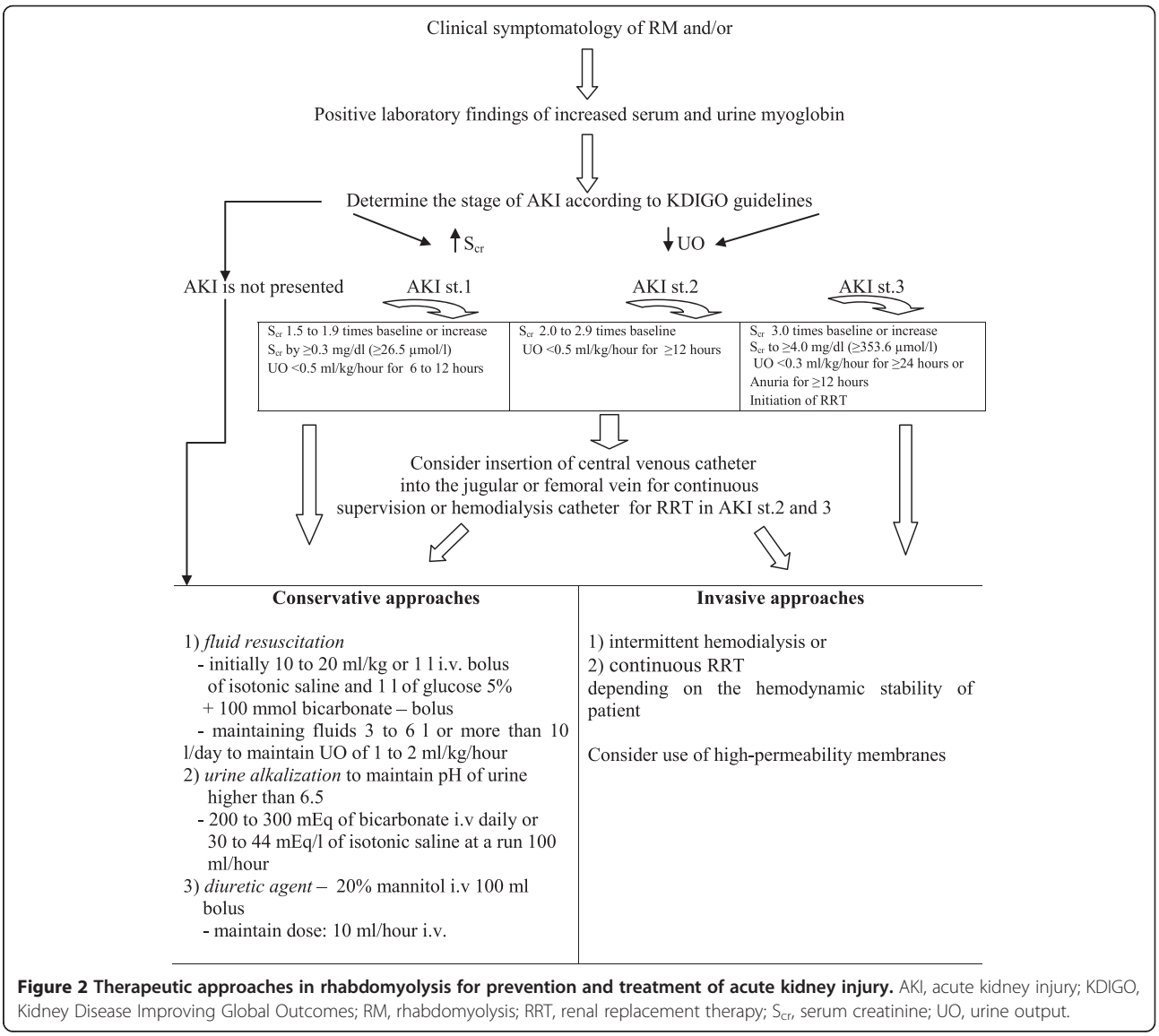

Figure 2 Therapeutic approaches in rhabdomyolysis for prevention and treatment of acute kidney injury. AKI, acute kidney injury; KDIGO, Kidney Disease Improving Global Outcomes; RM, rhabdomyolysis; RRT, renal replacement therapy; S_{cr}, serum creatinine; UO, urine output.

the presence of oliguria it is an independent predictor for developing secondary abdominal compartment syndrome with decreased renal perfusion pressure or can lead to acute respiratory distress syndrome [42].

Diuretic agent – mannitol

Mannitol is an osmotic agent that attracts the fluid of the interstitial space and so may reduce muscular swelling. As a diuretic agent, mannitol prevents intrarenal heme pigment trapping, decreasing cast formation. Mannitol can increase renal blood flow and glomerular filtration. Several studies have highlighted its hydroxyl anion-scavenging effect, although in an experimental study Zager and colleagues concluded that its protective influence is probably more due to a diuretic than to antioxidant effect [43]. Bragadottir and colleagues [44] studied the effects of mannitol on renal blood flow, the glomerular filtration rate, renal oxygen consumption and extraction in 11 postoperative cardiac patients with AKI. In all patients, a bolus dose of mannitol 225 mg/kg was given, followed by an infusion at a rate of 75 mg/kg/hour for two 30-minute periods. The authors reported that mannitol treatment in these cases increased urine flow by 61% (P <0.001), induced renal vasodilation and redistributed systemic blood flow to the kidney. In addition, mannitol does not affect the filtration fraction or renal oxygenation [44].

There are some controversial views on post-traumatic RM, where the recommendation is to re-evaluate the standards of therapy with bicarbonate and mannitol because this combination does not prevent renal failure, dialysis or mortality in patients with CK levels >5,000 U/l [45]. Knowledge of the timing of adequate hydration in severe post-traumatic patients would be valuable.

Antioxidant therapy

Based on the pathophysiology of myoglobinuric AKI, we can predict protective effects of antioxidative therapy by inhibition of lipid peroxidation of the proximal tubular cells and redox cycling between ferric and ferryl myoglobin [28]. Acetaminophen, which inhibits hemoprotein-catalyzed lipid peroxidation, is one of several investigated drugs that attenuate RM-induced AKI. Acetaminophen inhibits prostaglandin hydrogen synthase by reducing the protoporphyrin radical cation and blocking formation of the catalytic tyrosyl radical [46,47]. However, one experimental *in vitro* study showed that its administration is necessary after RM to achieve the desired outcome in blocking lipid peroxidation [28].

Renal replacement therapy

The first factor we need to recognize is that the greatest filter for removing myoglobin is the kidney, and in critical care nephrology there is no preventive kidney replacement therapy. However, the kidneys need a perfusion pressure and fluid volume to help them eliminate the toxin. The initiation of renal replacement therapy in clinical practice should not be managed by the myoglobin or CK serum concentration but by the status of renal impairment, with complications such as life-threatening hyperkalemia, hypercalcemia, hyperazotemia, anuria or hyperhydration without response to diuretic therapy. For better orientation to the requirements of renal replacement therapy initialization in AKI on critical care, we can use the Kidney Disease Improving Global Outcomes guidelines. These guidelines include a comprehensive therapeutic approach for management of AKI (Figure 2) [39,48]. Renal replacement therapies are mostly efficient in cases of RM-induced AKI, but they are extracorporeal circuits with many potential complications. However, in clinical practice it is very important to take into account all coincident factors in the patient's illness and to individualize treatment if necessary.

The possibility of using a method of renal replacement therapy, either intermittent hemodialysis or continuous kidney replacement methods in the case of RM, has been investigated in several studies [49-51]. Plasmapheresis has also been used with described success. When we proceed to treat patients with these procedures, we must take into account that myoglobin has a molecular mass of 17 kDa and is poorly removed from circulation using conventional extracorporeal techniques. Intermittent hemodialysis is mostly mandated by renal or metabolic indications and preventive extracorporeal elimination is not recommended. Sorrentino and colleagues [52] reported the effective removal of myoglobin by extended dialysis performed using a single-pass batch dialysis system and a polysulphone high-flux dialyzer (surface area 1.8 m^2), allowing elimination of substances with a molecular weight of up to 30 kDa. In six patients with myoglobinuric AKI, a median myoglobin clearance of 90.5 ml/minute (range 52.4 to 126.3 ml/minute) was achieved, resulting in a median myoglobin removal per treatment hour of 0.54 g (range 0.15 to 2.21 g) [52].

Myoglobin clearance by super high-flux hemofiltration in a 53-year-old female suffering from RM and AKI was investigated by Naka and colleagues [53]. Continuous venovenous hemofiltration was performed with a high-permeability membrane (cutoff point 100 kDa) at 2 to 4 l/hour ultrafiltration in an attempt to clear myoglobin. The sieving coefficient was 68 to 72%, myoglobin clearance was up to 56.4 l/day and the amount of myoglobin removed was 4.4 to 5.1 g/day [53]. The effect of high cutoff membrane hemodiafiltration on myoglobin removal was investigated in six patients with myoglobinuric AKI using a 45 kDa cutoff hemofilter with a surface area 2.1 m^2. Postdilutional fluid substitution was 2 to 3 l/hour, resulting in a mean myoglobin clearance of

81 ml/minute (range 42 to 131 ml/minute). The reduction ratio ranged from 62 to 89% [54].

The use of plasmapheresis to remove serum myoglobin sounds controversial but successful therapy of RM induced by statins was reported by Swaroop and colleagues [55]. The plasmapheresis was performed in addition to hemodialysis daily for 5 days. The effect of hemodialysis alone is questionable, and the authors did not describe the type of hemodialysis or membrane used [55]. The undeniable fact is the obligation to treat underlying disease that led to RM. If we do not eliminate the cause of the RM – especially in trauma, infectious disorders and septic disorders – the removal of myoglobin is only a supportive measure for increasing its clearance in the case of AKI. However, inefficient removal of myoglobin also results in a persistent high circulating level of the molecule with kidney damage and delay in renal function recovery [56]. From all these data, the effect of high-permeability membranes on eliminating circulating myoglobin has been demonstrated but care must be taken to prevent unwanted albumin loss. It is questionable whether a percentage of myoglobin clearance is not hepatic because of a decrease in serum myoglobin in patients with oligoanuric AKI. The recommended most useful mode of renal replacement therapy used to be hemofiltration, but in recent years we use high-permeability membranes in daily clinical practice for continuous venovenous hemodialysis without undesirable decrease in albumin levels. The molecular weight of albumin is 67 kDa and high-permeability membranes with a cutoff value <67 kDa in a predominantly diffusion type of elimination can be a prospective measure for the supplementary treatment of RM if necessary.

Conclusions

This review provides a comprehensive view on AKI induced by RM. Thorough knowledge of the pathophysiology will lead to new approaches for diagnosis and treatment, leading to the preservation of the kidney. Renal replacement methods have a supportive role but they are not the first line of treatment for AKI-induced RM, especially in cases of preserved diuresis. The kidney is a miraculous organ but it can be overwhelmed if the threshold is exceeded. We should try to preserve kidney function where possible by looking at the whole picture.

Abbreviations

AKI: Acute kidney injury; CK: Creatine phosphokinase; RM: Rhabdomyolysis.

Competing interests

The authors declare that they have no competing interests.

Published: 28 May 2014

References

1. Bagley WH, Yang H, Shah KH: **Rhabdomyolysis.** *Intern Emerg Med* 2007, **2:**210–218.
2. Beall D, Bywaters EG, Belsey RH, Miles JA: **Crush injury with renal failure.** *Br Med J* 1941, **1:**432–434.
3. Vanholder R, Sever MS, Erek E, Lameire N: **Rhabdomyolysis.** *J Am Soc Nephrol* 2000, **11:**1553–1561.
4. Owczarek J, Jasińska M, Orszulak-Michalak D: **Drug-induced myopathies. An overview of the possible mechanisms.** *Pharmacol Res* 2005, **57:**23–34.
5. Cervellin G, Comelli I, Lippi G: **Rhabdomyolysis: historical background, clinical, diagnostic and therapeutic features.** *Clin Chem Lab Med* 2010, **48:**749–756.
6. Zimmerman JL, Shen MC: **Rhabdomyolysis.** *Chest* 2013, **144:**1058–1065.
7. Zager RA: **Studies of mechanisms and protective maneuvers in myoglobinuric acute renal injury.** *Lab Invest* 1989, **60:**619–629.
8. Lima RS, da Silva Junior GB, Liborio AB, Daher Ede F: **Acute kidney injury due to rhabdomyolysis.** *Saudi J Kidney Dis Transpl* 2008, **19:**721–729.
9. David WS: **Myoglobinuria.** *Neurol Clin* 2000, **18:**215–243.
10. Hirsch NP: **Neuromuscular junction in health and disease.** *Br J Anaesth* 2007, **99:**132–138.
11. Knochel JP: **Mechanisms of rhabdomyolysis.** *Curr Opin Rheumatol* 1993, **5:**725–731.
12. Zager RA: **Rhabdomyolysis and myohemoglobinuric acute renal failure.** *Kidney Int* 1996, **49:**314–326.
13. Better OS, Abassi Z, Rubinstein I, Marom S, Winaver Y, Silberman M: **The mechanism of muscle injury in the crush syndrome: ischemic versus pressure-stretch myopathy.** *Miner Electrolyte Metab* 1990, **16:**181–184.
14. Nath KA, Balla G, Vercellotti GM, Balla J, Jacob HS, Levitt MD, Rosenberg ME: **Induction of heme oxygenase is a rapid, protective response in rhabdomyolysis in the rat.** *J Clin Invest* 1992, **90:**267–270.
15. Trillaud H, Degrèze P, Combe C, Deminière C, Palussière J, Benderbous S, Grenier N: **USPIO-enhanced MR imaging of glycerol-induced acute renal failure in the rabbit.** *Magn Reson Imaging* 1995, **13:**233–240.
16. Singh AP, Junemann A, Muthuraman A, Jaggi AS, Singh N, Grover K, Dhawan R: **Animal models of acute renal failure.** *Pharmacol Rep* 2012, **64:**31–44.
17. Shah SV, Walker PD: **Evidence suggesting a role for hydroxyl radical in glycerol-induced acute renal failure.** *Am J Physiol* 1988, **255:**F438–F443.
18. Gburek J, Birn H, Verroust PJ, Goj B, Jacobsen C, Moestrup SK, Willnow TE, Christensen EI: **Renal uptake of myoglobin is mediated by the endocytic receptors megalin and cubilin.** *Am J Physiol Renal Physiol* 2003, **285:**451–458.
19. Zager RA, Johnson AC, Becker K: **Plasma and urinary heme oxygenase-1 in AKI.** *J Am Soc Nephrol* 2012, **23:**1048–1057.
20. Krouzecky A, Matejovic M, Rokyta R, Novak I: **Rhabdomyolysis – mechanisms of origin, causes, consequences and therapy.** *Vnitr Lek* 2003, **49:**668–672.
21. Agarwal A, Balla J, Alam J, Croatt AJ, Nath KA: **Induction of heme oxygenase in toxic renal injury: a protective role in cisplatin nephrotoxicity in the rat.** *Kidney Int* 1995, **48:**1298–1307.
22. Nath KA: **Heme oxygenase-1: a provenanc pathways in the kidney and other tissues.** *Kidney Int* 2006, **70:**432–443.
23. Závada J: *Multiple Organ Dysfunction Syndrome.* Praha: Grada Publishing s.r.o; 2001.
24. Zager RA, Foerder CA: **Effects of inorganic iron and myoglobin on in vitro proximal tubular lipid peroxidation and cytotoxicity.** *J Clin Invest* 1992, **89:**989–995.
25. Ronco C, Bellomo R, Kellum JA: **Critical care nephrology**. In *Myoglobin as a Toxin.* 2nd edition. Philadelphia, PA: Saunders, Elsevier; 2009:1103–1109.
26. Blomberg LM, Blomberg MR, Siegbahn PE: **A theoretical study of myoglobin working as a nitric oxide scavenger.** *J Biol Inorg Chem* 2004, **9:**923–935.
27. Moore KP, Holt SG, Patel RP, Svistunenko DA, Zackert W, Goodier D, Reeder BJ, Clozel M, Anand R, Cooper CE, Morrow JD, Wilson MT, Darley-Usmar V, Roberts LJ 2nd: **A causative role for redox cycling of myoglobin and its inhibition by alkalinization in the pathogenesis and treatment of rhabdomyolysis-induced renal failure.** *J Biol Chem* 1998, **273:**31731–31737.
28. Boutaud O, Moore KP, Reeder BJ, Harry D, Howie AJ, Wang S, Carney CK, Masterson TS, Amin T, Wright DW, Wilson MT, Oates JA, Roberts LJ 2nd: **Acetaminophen inhibits hemoprotein-catalyzed lipid peroxidation and attenuates rhabdomyolysis-induced renal failure.** *Proc Natl Acad Sci U S A* 2010, **107:**2699–2704.

29. Holt S, Moore K: **Pathogenesis of renal failure in rhabdomyolysis: the role of myoglobin.** *Exp Nephrol* 2000, **8:**72–76.
30. Holt S, Reeder B, Wilson M, Harvey S, Morrow JD, Roberts LJ 2nd, Moore K: **Increased lipid peroxidation in patients with rhabdomyolysis.** *Lancet* 1999, **353:**1241.
31. Reeder BJ, Wilson MT: **The effects of pH on the mechanism of hydrogen peroxide and lipid hydroperoxide consumption by myoglobin: a role for the protonated ferryl species.** *Free Radic Biol Med* 2001, **30:**1311–1318.
32. Plotnikov EY, Chupyrkina AA, Pevzner IB, Isaev NK, Zorov DB: **Myoglobin causes oxidative stress, increase of NO production and dysfunction of kidney's mitochondria.** *Biochim Biophys Acta* 2009, **1792:**796–803.
33. Khan FY: **Rhabdomyolysis: a review of the literature.** *Neth J Med* 2009, **67:**272–283.
34. Chen-Levy Z, Wener MH, Toivola B, Daum P, Reyes M, Fine JS: **Factors affecting urinary myoglobin stability in vitro.** *Am J Clin Pathol* 2005, **123:**432–438.
35. Premru V, Kovač J, Ponikvar R: **Use of myoglobin as a marker and predictor in myoglobinuric acute kidney injury.** *Ther Apher Dial* 2013, **17:**391–395.
36. El-Abdellati E, Eyselbergs M, Sirimsi H, Hoof VV, Wouters K, Verbrugghe W, Jorens PG: **An observational study on rhabdomyolysis in the intensive care unit, Exploring its risk factors and main complication: acute kidney injury.** *Ann Intensive Care* 2013, **3:**8.
37. Huerta-Alardín AL, Varon J, Marik PE: **Bench-to-bedside review: Rhabdomyolysis – an overview for clinicians.** *Crit Care* 2005, **9:**158–169.
38. Malik GH: **Rhabdomyolysis and myoglobin-induced acute renal failure.** *Saudi J Kidney Dis Transpl* 1998, **9:**273–284.
39. *KDIGO Clinical Practice Guideline for Acute Kidney Injury.* [http://www.kidney-international.org]
40. Finfer S, Liu B, Taylor C, Bellomo R, Billot L, Cook D, Du B, McArthur C, Myburgh J, SAFE TRIPS Investigators: **Resuscitation fluid use in critically ill adults: an international cross-sectional study in 391 intensive care units.** *Crit Care* 2010, **14:**R185.
41. Myburgh JA, Mythen MG: **Resuscitation fluids.** *N Engl J Med* 2013, **369:**1243–1251.
42. Petejova N, Martinek A: **Acute kidney injury following acute pancreatitis: a review.** *Biomed Pap Med* 2013, **157:**105–113.
43. Zager RA, Foerder C, Bredl C: **The influence of mannitol on myoglobinuric acute renal failure: functional, biochemical, and morphological assessments.** *J Am Soc Nephrol* 1991, **2:**848–855.
44. Bragadottir G, Redfors B, Ricksten SE: **Mannitol increases renal blood flow and maintains filtration fraction and oxygenation in postoperative acute kidney injury: a prospective interventional study.** *Crit Care* 2012, **16:**R159.
45. Brown CV, Rhee P, Chan L, Evans K, Demetriades D, Velmahos GC: **Preventing renal failure in patients with rhabdomyolysis: do bicarbonate and mannitol make a difference?** *J Trauma* 2004, **56:**1191–1196.
46. Ouellet M, Percival MD: **Mechanism of acetaminophen inhibition of cyclooxygenase isoforms.** *Arch Biochem Biophys* 2001, **387:**273–280.
47. Boutaud O, Aronoff DM, Richardson JH, Marnett LJ, Oates JA: **Determinants of the cellular specificity of acetaminophen as an inhibitor of prostaglandin H(2) synthases.** *Proc Natl Acad Sci U S A* 2002, **99:**7130–7135.
48. Bellomo R, Kellum JA, Ronco C: **Acute kidney injury.** *Lancet* 2012, **380:**756–766.
49. Heyne N, Guthoff M, Krieger J, Haap M, Häring HU: **High cut-off renal replacement therapy for removal of myoglobin in severe rhabdomyolysis and acute kidney injury: a case series.** *Nephron Clin Pract* 2012, **121:**159–164.
50. Tang W, Chen Z, Wu W, Qiu H, Bo H, Zhang L, Fu P: **Renal protective effects of early continuous venovenous hemofiltration in rhabdomyolysis: improved renal mitochondrial dysfunction and inhibited apoptosis.** *Artif Organs* 2013, **37:**390–400.
51. Amyot SL, Leblanc M, Thibeault Y, Geadah D, Cardinal J: **Myoglobin clearance and removal during continuous venovenous hemofiltration.** *Intensive Care Med* 1999, **25:**1169–1172.
52. Sorrentino SA, Kielstein JT, Lukasz A, Sorrentino JN, Gohrbandt B, Haller H, Schmidt BM: **High permeability dialysis membrane allows effective removal of myoglobin in acute kidney injury resulting from rhabdomyolysis.** *Crit Care Med* 2011, **39:**184–186.
53. Naka T, Jones D, Baldwin I, Fealy N, Bates S, Goehl H, Morgera S, Neumayer HH, Bellomo R: **Myoglobin clearance by super high-flux hemofiltration in a case of severe rhabdomyolysis: a case report.** *Crit Care* 2005, **9:**R90–R95.
54. Premru V, Kovač J, Buturović-Ponikvar J, Ponikvar R: **High cut-off membrane hemodiafiltration in myoglobinuric acute renal failure: a case series.** *Ther Apher Dial* 2011, **15:**287–291.
55. Swaroop R, Zabaneh R, Parimoo N: **Plasmapheresis in a patient with rhabdomyolysis: a case report.** *Cases J* 2009, **2:**8138.
56. Ronco C: **Extracorporeal therapies in acute rhabdomyolysis and myoglobin clearance.** *Crit Care* 2005, **9:**141–142.

10.1186/cc13897
Cite this article as: Petejova and Martinek: Acute kidney injury due to rhabdomyolysis and renal replacement therapy: a critical review. *Critical Care* 2014, 18:224

2. Incidence of the urological tumours in patients suffering from multiple sclerosis

Krhut J, Hradílek P, Němec D, Tvrdík J, Zapletalová O, Zvara P

Originally published in Acta Neurologica Scandinavica, 2014, vol. 130, no. 3, p. 193-196

Consent to the publication of 24th March 2015

Acta Neurologica Scandinavica

Acta Neurol Scand 2014: 130: 193–196 DOI: 10.1111/ane.12264

ACTA NEUROLOGICA
SCANDINAVICA

Incidence of the urological tumours in patients suffering from multiple sclerosis

Krhut J, Hradilek P, Nemec D, Tvrdik J, Zapletalova O, Zvara P. Incidence of the urological tumours in patients suffering from multiple sclerosis.
Acta Neurol Scand 2014: 130: 193–196.

Objectives – The goal of this study was to evaluate the incidence of urological malignancies in MS patients using active screening. *Material and Methods* – A total of 495 MS patients (141 men, 354 women, age of 42 ± 13.4) were included in the study. The duration of disease was 12.3 ± 11 years, and the EDSS score was 4.3 (±2.5). Patients, regardless of specific urological symptoms, were referred for urological evaluation. The outcomes of these evaluations were compared with data from the 2009 National Oncology Register of the Czech Republic. *Results* – The standardized incidence ratio (SIR) for the whole MS study population was 38.8 (95% CI 12.6–90.6). This incidence of urological malignancies in the MS study population was higher (statistically significant) than that of the general population. The SIR for females was 66.0 (95% CI 18.0–169.1) in the MS study population, representing a statistically significant increase over that of the general female population. The increase in incidence of urological malignancies in men with MS did not reach statistical significance over that of the general male population (SIR 14.7, 95% CI 0.4–81.7). *Conclusions* – The incidence of urological cancer in MS patients as determined by active screening is significantly higher than that found in general population.

J. Krhut[1,2], P. Hradilek[3], D. Nemec[2], J. Tvrdik[4], O. Zapletalova[3], P. Zvara[1,5]

[1]Department of Urology, Ostrava University, Ostrava, Czech Republic, VT, USA; [2]Department of Urology, University Hospital, Ostrava, Czech Republic, VT, USA; [3]Department of Neurology, University Hospital, Ostrava, Czech Republic, VT, USA; [4]Department of Computer Science, Ostrava University, Ostrava, Czech Republic, VT, USA; [5]Division of Urology, Department of Surgery, University of Vermont, Burlington, VT, USA

Key words: multiple sclerosis; urological cancer; incidence; active screening

J. Krhut, Department of Urology, Ostrava University, 17 listopadu 1790, 708 52 Ostrava, Czech Republic
Tel.: +420 597375301
Fax: +420 596918347
e-mail: jan.krhut@fno.cz

Accepted for publication April 16, 2014

Introduction

Multiple sclerosis (MS) is an immune-mediated disease of the central nervous system with a variable course and rate of progression. MS is the most common immune-mediated disease in Europe, with a prevalence of 30–150/100,000 people (1). The currently employed immunosuppressive (IS) and immunomodulative (IM) therapies have proven effective in lowering the risk for disease exacerbation and disability, thereby improving quality of life for those affected (2). It is theoretically possible that alteration of the immune system (by the therapeutic medications or the disease itself) could lead to an increased incidence of malignancy in patients with MS, but the literature on the subject is inconclusive. Increased cancer risk has been documented in patients suffering from various autoimmune diseases, as well as those using systemic IS and IM therapies following allotransplantation, but the specific risk of malignancy as it pertains to MS has not been conclusively addressed (3). The most prevailing opinion is that MS does not lead to an overall increase in the cancer risk. A population-based study by Nielsen et al. (4) documented a 16% overall reduction in cancer risk in men with MS, specifically citing malignancies of the digestive, respiratory and genital organs. The goal of this study was to evaluate the incidence of urogenital malignancies in patients with MS using active screening.

Materials and methods

We have conducted an active screening study of patients with MS who presented to a single, tertiary referral centre for diagnosis and treatment of the disease. The study was approved by an Institutional Review Board of the University

Hospital, Ostrava and was performed according to the Declaration of Helsinki, World Health Organization. Each subject gave informed consent before enrolment in the study. A total of 141 men and 354 women, with an average age of 42 ± 13.4 were included in the study. The average duration of the disease, as determined by first occurrence of first symptoms, was 12.3 ± 11 years. The average time since diagnosis was 11.2 ± 9 years. Three hundred twenty-three patients (62.3%) suffered from relapsing-remitting MS, 47 (9.5%) were affected by primary progressive disease and 125 (25.2%) were affected by secondary progressive disease. The average Expanded Disability Status Scale (EDSS) score of the study population was 4.3 (±2.5). Three hundred and thirty (66.7%) of patients were treated with corticosteroids, 52 (23.4%) were treated with glatiramer acetate and 45 (9%) of patients received immunoglobulin therapy. Azathioprine was used in 274 (55.3%) patients, with an average exposure time of 53.5 ± 42.4 months and a cumulative dose of 101.0 ± 73.1 g/patient. Between January 1 and December 31, 2012, all patients with MS regardless of specific urological symptoms were referred for urological evaluation. A detailed urological history was taken, followed by a full physical evaluation (including digital rectal evaluation, urinalysis, urine culture and kidney ultrasound). Prostatic specific antigen was evaluated in all men 50 years and older. Patients with abnormal findings on initial screening went on to have cystoscopy, followed by evaluation using the appropriate imaging methods or prostate biopsy. The outcomes of these evaluations were compared with the data of the 2009 National Oncology Register of the Czech Republic (www.uzis.cz). The focus was on the following diagnoses (ICD-10): C 61 – malignant neoplasm of prostate, C 62 – malignant neoplasm of testis, C 63 – malignant neoplasm of other or unspecified male genital organs, C 64 – malignant neoplasm of kidney, C 65 – malignant neoplasm of renal pelvis, C 66 – malignant neoplasm of ureter, C 67 – malignant neoplasm of bladder, C 68 – malignant neoplasm of other or unspecified urinary organs.

Unless stated otherwise, all values are expressed as mean ± standard deviation in the descriptive part of the statistics. Standardized incidence ratio (SIR) was calculated as a ratio of frequency of tumours in the MS population and expected frequency of tumours categorized with respect to age and sex derived from the incidence of tumours in the general population. The calculations were based on Poisson probability distribution of the cancer (5). 95% confidence interval (95% CI) was calculated. If 95% CI includes one, the difference in frequency of tumours in the MS and general population is not statistically significant. If 95% CI does not include one, the difference in frequency of tumours in the MS and general population is considered to be statistically significant at the level of 0.05.

Results

The active screening technique identified a total of five patients with MS with urological cancer. The characteristics of each of these five patients are summarized in Table 1. According to data from the National Oncology Registry of the Czech Republic, the overall incidence of malignant neoplasm of the kidney (C64) in 2009 was 35.4/100,000 in males and 19.4/100,000 in females. In our study population of MS patients, the incidence calculated based on the size of the study population and the number of identified kidney cancers was 709.2/100,000 in males and 282.5/100,000 in females. The incidence of malignant neoplasm of the bladder in the general population (C 67) was 36.1/100,000 in males and 13.6/100,000 in females. In the studied cohort of MS patients, the estimated incidence of bladder cancer was 0/100,000 in males and 847.5 in females. SIR for both cancers (C64 + C67) was 38.8 (95% CI 12.6–90.6). This represents a statistically significant increase in urological cancer in the MS group as compared to the general population. SIR in females for both diagnoses (C64 + C67) was 66.0 (95% CI 18.0–169.1), representing a statistically significant increase in urological cancer in female patients with MS as compared to that of the general female population. The difference in incidence for both diagnoses (C64 + C67) in men with MS as compared to the general male population (SIR 14.7, 95% CI 0.4–81.7) did not reach statistical significance. Age-specific incidence of the urological cancer (C64 + C67) in patients with MS and in the general population is summarized in Table 2.

Discussion

MS is one of the most common neurological diseases, and because the resulting demyelination affects innervation of the lower urinary tract in 35–97% of cases, a urologist is frequently involved in the interdisciplinary care of these patients (6). It is therefore surprising that only limited attention has been given to investigating the possibility of increased urological malignancy

Table 1 Characteristics of patients with MS with urogenital cancer

Patient	Female 58 years old	Female 46 years old	Female 65 years old	Female 46 years old	Male 35 years old
Tumour type	C 67	C 67	C 67	C 64	C 64
Tumour histology	Moderately differentiated urothelial carcinoma	Moderately differentiated urothelial carcinoma	Muscle- invasive poorly differentiated urothelial carcinoma	Moderately differentiated renal cell carcinoma	Well-differentiated renal cell carcinoma
MS characteristics					
MS course	Secondary progressive	Secondary progressive	Secondary progressive	Primary progressive	Relapsing-remitting
Time since first symptoms (years)	20	6	32	12	12
Time since MS diagnosis (years)	10	6	32	12	12
EDSS	7	7	6.5	7	3
MS treatment					
Corticosteroids	Yes	Yes	Yes	Yes	Yes
Azatioprine	Yes	No	Yes	Yes	No
Mitoxantron	Yes	Yes	No	No	No
Interferon	No	No	No	No	Yes
Glatiramer acetate	No	No	No	No	Yes
Immunoglobulins	No	No	No	No	No

Table 2 Age-specific incidence of the urogenital tumours (C64 + C67) in the patients with MS and general population

	Study population				General population	
Age	Number of MS patients (*n*)	Distribution of MS patients (age groups) (%)	Number of tumours/ age group (*n*)	Tumour incidence/100,000	Tumour incidence/100,000	Expected frequency of tumours
0–4	0	0	0	0	1.57	0
5–9	0	0	0	0	0.41	0
10–14	0	0	0	0	0.12	0
15–19	16	3.23	0	0	0.18	0.000029
20–24	34	6.87	0	0	0.38	0.000129
25–29	55	11.11	0	0	0.77	0.000424
30–34	48	9.7	1	2083.3	1.76	0.000845
35–39	71	14.34	0	0	4.47	0.003174
40–44	58	11.72	0	0	10.3	0.005974
45–49	63	12.73	2	3174.6	22.1	0.013923
50–54	60	12.12	0	0	40.56	0.024336
55–59	44	8.89	1	2272.7	63.78	0.028063
60–64	25	5.05	1	4000	94.33	0.023583
65–69	11	2.22	0	0	124.21	0.013663
70–74	3	0.61	0	0	150.81	0.004524
75–79	4	0.81	0	0	161.75	0.00647
80–84	1	0.2	0	0	160.09	0.001601
85+	2	0.4	0	0	143.38	0.002868
Total	495	100	5			0.129605

in these immune-compromised patients. A study performed by Lebrun et al. in 2011 did not identify an increased risk of malignancy in patients with MS, but the authors did conclude that patients receiving IS therapy had a 300% increase in cancer risk compared to those receiving alternative treatments. This same study reported that in patients with MS receiving IS therapy, urogenital malignancies are the fourth most common cancer (7). These findings are further supported by Achiron et al., who concluded that MS patients who did not receive IS or IM therapy had a lower risk of developing cancer than that of the general healthy population. These authors point to the possibility that IS or IM therapy could eliminate the immunoprotective effect of MS (8). Both of the aforementioned studies presented data that was extracted from oncologic registers, meaning that only the patients who were symptomatic were included in their analyses. Our study focused on the incidence of urological malignancies in all patients with MS. We performed active screening using the algorithm outlined by the European Association of Urology Guidelines (9, 10). All patients with MS, including those who did not present with symptoms of lower urinary tract

disease, were included in our study group. Even using this relatively small sample size, we were able to identify cases of urological cancer before they presented with symptoms. All five cancers that we identified were diagnosed in asymptomatic patients, whose malignancies would not otherwise have been discovered at this stage. We therefore believe that our data provide a much more accurate picture of the true incidence of urological cancer among patients with MS. Due to the low number of identified cancers, we were unable to come to a conclusion regarding the effect of IS and/or IM therapies, as well as the correlation between disease stage and incidence of urological malignancy. It is still unclear whether the use of azathioprine increases the risk of cancer development.

Confavreux et al. (11) suggested that there is a dose–response relationship between cancer risk and long-term treatment with azathioprine. This study did not observe an increased risk of cancer during the first years of treatment. However, they did observe an increased risk after approximately 10 years of continuous treatment (or a cumulative dose above 600 g). In our study, three of five patients with detected cancer were treated with azathioprine in the MS group. Their cumulative dose was 18, 78 and 122 g, with a total exposure time of 12, 81 and 52 months respectively. According to the results from this study, which document the incidence of urological cancer in a group of patients with MS to be 38 times higher than that of the general population, further research, including larger studies to address this correlation, is warranted.

Conclusion

The incidence of urological cancer in patients suffering from MS as determined by active screening is significantly higher than that found in the healthy population. This study points out the need for further investigation as to the cause and warrants that increased attention be given to possible early signs of these diseases, such as microscopic haematuria.

Acknowledgments

The authors have no acknowledgments to declare.

Conflict of interest

The authors declare no conflict of interests.

Funding

None.

References

1. Ford HL, Gerry E, Johnson M et al. A prospective study of the incidence, prevalence and mortality of multiple sclerosis in Leeds. J Neurol 2002;**249**:260–5.
2. Derwenskus J. Current disease-modifying treatment of multiple sclerosis. Mt Sinai J Med 2011;**78**:161–75.
3. Végso G, Tóth M, Hídvégi M et al. Malignancies after renal transplantation during 33 years at a single center. Pathol Oncol Res 2007;**13**:63–9.
4. Nielsen NM, Rostgaard K, Rasmussen S et al. Cancer risk among patients with multiple sclerosis: a population-based register study. Int J Cancer 2006;**118**:979–84.
5. Sahai H, Khurshid A. Confidence intervals for the mean of a Poisson distribution: a review. Biom J 1993;**35**:857–67.
6. Tubaro A, Puccini F, de Nunzio C et al. The treatment of lower urinary tract symptoms in patients with multiple sclerosis: a systematic review. Curr Urol Rep 2012;**13**:335–42.
7. Lebrun C, Vermersch P, Brassat D et al. Cancer and multiple sclerosis in the era of disease-modifying treatments. J Neurol 2011;**258**:1304–11.
8. Achiron A, Barak Y, Gail M et al. Cancer incidence in multiple sclerosis and effects of immunomodulatory treatments. Breast Cancer Res Treat 2005;**89**:265–70.
9. Babjuk M, Oosterlinck W, Sylvester R et al. European Association of Urology (EAU). EAU guidelines on non-muscle-invasive urothelial carcinoma of the bladder, the 2011 update. Eur Urol 2011;**59**:997–1008.
10. Ljungberg B, Cowan NC, Hanbury DC et al. European Association of Urology Guideline Group. EAU guidelines on renal cell carcinoma: the 2010 update. Eur Urol 2010;**58**:398–406.
11. Confavreux C, Saddier P, Grimaud J et al. Risc of cancer from azathioprine therapy in multiple sclerosis: a case control study. Neurology 1996;**46**:1607–12.

3

The analysis of respiration-induced pancreatic tumor motion based on reference measurement

Knybel L, Cvek J, Otáhal B, Jonszta T, Molenda L, Czerný D, Skácelíková E, Rybář M, Dvořák P, Feltl D
Originally published in Radiation Oncology, 2014, vol. 9, no. Article ID 192, p. 1-8.
Consent to the publication of 13th March 2015

Knybel et al. Radiation Oncology 2014, 9:192
http://www.ro-journal.com/content/9/1/192

RADIATION ONCOLOGY

RESEARCH Open Access

The analysis of respiration-induced pancreatic tumor motion based on reference measurement

Lukas Knybel[1*], Jakub Cvek[1], Bretislav Otahal[1], Tomas Jonszta[2], Lukas Molenda[1], Daniel Czerny[2], Eva Skacelikova[1], Marian Rybar[1], Pavel Dvorak[3] and David Feltl[1]

Abstract

Background: To evaluate pancreatic tumor motion and its dynamics during respiration.

Methods and materials: This retrospective study includes 20 patients with unresectable pancreatic cancer who were treated with stereotactic ablative radiotherapy. An online respiratory tumor tracking system was used. Periodical maximum and minimum tumor positions with respiration in superior-inferior (SI), latero-lateral (LL), and anterior-posterior (AP) directions were collected for tumor motion evaluation. The predictability of tumor motion in each axis, based on reference measurement, was analyzed.

Results: The use of a 20-mm and 5-mm constant margins for SI and LL/AP directions, avoids target underdosage, without the need for reference measurement. Pearson's correlation coefficient indicated only a modest correlation between reference and subsequent measurements in the SI direction ($r = 0.50$) and no correlation in LL ($r = 0.17$) and AP ($r = 0.35$) directions. When margins based on the reference measurement of respiratory tumor motion are used, then 30% of patients have a risk zone of underdosage >3 mm (in average). ITV (internal target volume) optimization based on the reference measurement is possible, but allows only modest margin reduction (approximately from 20 mm to 16-17 mm) in SI direction and no reduction in AP and LL directions.

Conclusion: Our results support the use of 20-mm margin in the SI direction and 5-mm margins in the LL and AP directions to account for respiratory motion without reference measurement. Single measurement of tumor motion allows only modest margin reduction. Further margin reduction is only possible when there is on-line tumor motion control according to internal markers.

Keywords: Pancreatic cancer, Tumor motion, Internal target volume

Background

Pancreatic carcinoma is a leading cause of cancer-related mortality. Although surgery is the standard treatment of pancreatic cancer, only 20% of patients are diagnosed with resectable disease [1]. The outcomes after chemoradiation for unresectable pancreatic cancer are poor, mainly because commonly used doses are not lethal for adenocarcinoma. The irradiated volume is correlated with significant gastrointestinal toxicity [2]. Moreover, dose escalation is not possible without exceeding normal tissue dose constraints while including regional lymph nodes [3]. The reduction of the conformal fields to include only the gross tumor volume (GTV) plus margins to account for microscopic disease (clinical target volume, CTV), tumor motion (internal target volume, ITV) and treatment setup, (planning target volume, PTV) results in better tolerance [4-6]. The recently published American-French Consensus proposes that PTV includes the GTV, with a shaped aperture margin of 15 to 20 mm in LL and AP directions and a margin of 20 to 30 mm in the SI direction, to take into account microscopic spreading, respiratory movements and set-up margin [7].

Performance of four-dimensional computed tomography (4D-CT) simulation with the creation of an ITV might reduce the margins used to account for respiration [8]. Controversy exists regarding whether one measurement of tumor motion can predict future movement [9,10]. Excessive volume reduction can lead to excursions

* Correspondence: lukas.knybel@fno.cz
[1]Department of Oncology, University Hospital Ostrava, 17. listopadu 1790, 708 52 Ostrava, Czech Republic
Full list of author information is available at the end of the article

outside the designated PTV margin, resulting in underdosage of the target. On the other hand, larger margins will lead to unnecessary irradiation of organs at risk (OARs).

In this study we analyzed pancreatic tumor motion in detail during a period of >3 h for each case and evaluated the application of several compensatory mechanisms to avoid systemic errors.

Materials and methods

This retrospective study includes 20 patients with unresectable pancreatic cancer (11 women, 9 men) who were treated between December 2011 and August 2012. We used the CyberKnife® Robotic Radiosurgery System and Synchrony respiratory tracking system (Accuray Inc., Sunnyvale, CA). Plans were designed to cover 95% of PTV (CTV based on CT/MRI registration during relaxed exhale + 3-mm safety margin) with the prescribed dose. A total of 20 tumors were treated with three fractions of 10 Gy every other day. In total, 60 fractions were analyzed. Four gold markers (fiducials) were implanted percutaneously under the CT control (each fiducial within 30 mm from tumor center and fiducial constellation centroid within 10 mm of the tumor center). It is assumed that motion of the fiducial's center of mass (COM) closely approximates to the motion of the tumor's COM. Constrains for OARs were set: 10 ml < 21Gy, 5 ml < 15Gy, 700 ml < 17Gy and 0,25 ml < 18Gy for stomach, duodenum, liver and spinal cord respectively. Patients were asked to breathe normally during the irradiation.

Tumor motion detection

The Synchrony® Respiratory Tracking System [11] records the breathing light signal from external markers on the chest and relates this signal to the X-ray coordinates of internal markers. The system calculates modelling error and an adaptive algorithm is used for online estimation of internal/external marker correlation error during the entire session (image frequency > 1 per minute). The geometrical coordinates representing position of the fiducials in SI, LL and AP directions in time are extracted from the treatment X-ray images to "log" files. This method has been proven to have high accuracy regarding the evaluation of tumor motion [12].

Reference measurement was calculated prior to treatment (in the day of planning CT) from the correlation model, based on the average value of tumor motion amplitudes within 2-5 minutes (at least 8 X-ray images to make correlation model, 5 X-ray images for confirmation of correlation model stability) or using constant upper/lower margins from American – French consensus. All CyberKnife treatments involve an initial intrafraction alignment step (checking the position of both spine structures and fiducial markers), followed by continuous intrafraction respiratory motion monitoring and determination [11]. According to the patient's precise setup (spine alignment with error less than 1 mm), no other data corrections were needed. Before each fraction, the correlation model must have been created. The analyzed data covered 95% of the total treatment time. Over 5000 positions of COM were recorded during the respiration cycles; approximately 800 of these, representing the maximum or minimum amplitude of tumor motion (periodical expiration or inspiration peak), were used for analysis.

Tumor motion analysis

To evaluate possible margins, under/overestimation of the tumor motion based on the reference measurement, we have derived the following formulas:

$$TAU = \frac{\sum_{j=1}^{u} \left(x_j - x_{margin}\right) \cdot t_j}{t_1 + t_2 + \ldots t_n}$$

$$TAO = \frac{\sum_{j=1}^{o} \left(x_{margin} - x_j\right) \cdot t_j}{t_1 + t_2 + \ldots t_n}$$

Where:

TAU - the time averaged margin underestimation,

TAO - the time averaged margin overestimation,

x_{margin} - the margin used for ITV determination (value from reference measurement or predefined value from American- French consensus),

x_j - the periodical tumor motion amplitude during the j-th portion of treatment,

t_j - the duration of the j-th portion of treatment (period with stable correlation model),

$t_1 + t_2 + \ldots t_n$ – the duration of the whole treatment (n is number of correlation models),

u - the number of portions of the treatment with underestimated margins,

o - the number of portions of the treatment with overestimated margins.

We used regression analysis to evaluate whether one or more measurements of tumor motion can adequately represent the motion of pancreatic tumors and to describe intra- and interfractional variation of tumor motion. We used linear regression function for modeling of influence of the reference and subsequent measurements in the SI direction. The linear function has the form $y = b_0 + b_1 * x$, where b_0 equals a constant of the function (intercept on the vertical axis), b_1 equals the slope of the linear function, x represents the first reference measurement and y represents subsequent measurements (Figure 1A). Our margin optimization uses the shift of the linear regression line. This approach was selected in order to lower the TAO when TAU is predefined (the same as in the American-French approach). Our

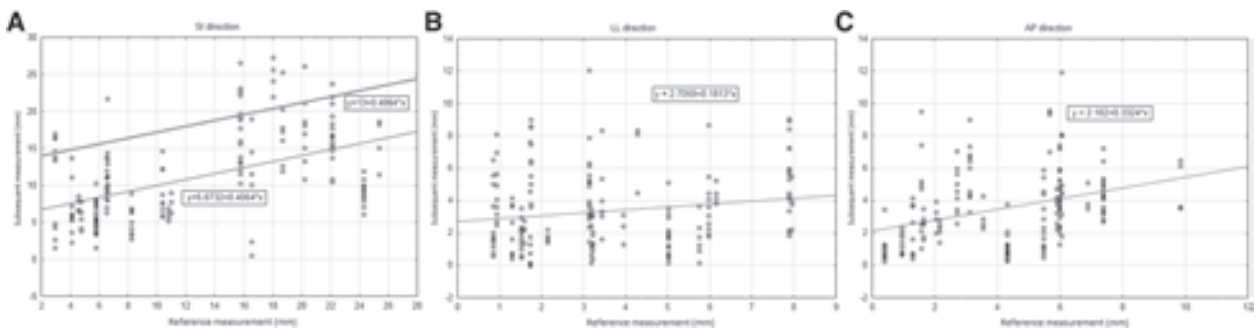

Figure 1 Regression analysis with equations for SI (A), LL (B), and AP (C) directions. Pearson's correlation coefficient was 0.501 (p = 0.000), 0.1719 (p = 0.0225), and 0.3461 (p = 0.000) for SI, LL, and AP, respectively. Same and similar values are overlapping. 1A: The lowest line (y = 5,8732 + 0,4064*x) is the result of regression analysis. The upper line (y = 13 + 0,4064*x) is the result of TAU and TAO optimization.

new approach respects individual patient amplitudes of tumor movements caused by respiration, and enables the setting of margins of radiation to individual patients based on their reference measurement. The shift of the linear regression line along the vertical axis is made experimentally in order to find TAU nearest to the predefined value. The constant part of equation (b_0) is changed by the shift, while the slope (which is defined by the function) remains constant. TAO is calculated from the formula afterwards.

Statistical analysis

Statistical analysis was performed using STATISTICA 10 software (Statsoft, Tulsa, OK). We used the Test for Difference Between Two Correlation or Regression Coefficients to distinguish between males and females, and the Test for Difference Between Two Regression Coefficients to distinguish between the slope of influence of respiration amplitudes on the reference measurement.

Results

The amplitude of COM motion during respiration varied widely among patients (range 7.3-27.3 mm in SI direction) and could vary intra-fractionally with a variation coefficient greater than 25%, for 25% of patients; moreover, the change of the tumor movement could be seen unexpectedly.

Margins to account respiration without a reference measurement

Using a margin from the upper limit (20 mm) for the SI direction (considered in the American-French consensus) resulted in low average TAU, and only one tumor has been presented with TAU >3 mm. Unfortunately, the use of this margin caused TAO greater than 8 mm, on average (Table 1). When a margin from the lower limit (10 mm) for the SI direction was used, the risk zone of TAU was >3 mm; moreover, 8 out of 20 tumors (40%) can be missed by >3 mm (range 3.5-13 mm).

Results were different for the LL and AP directions; the use of a margin close to the lower range of recommendation (5 mm) generated low TAU and TAO. When

Table 1 Pancreas movement in SI direction during three fractions, TAO and TAU for lower and upper limit for SI direction considered in the American-French consensus

Superior- Inferior							
	Motion (mm)			Margin 10mm		Margin 20mm	
Patient	Max	Mean	Std	TAU	TAO	TAU	TAO
1	19.1	10.7	7.0	4.3	2.5	0.0	8.2
2	11.0	8.5	2.0	0.3	0.8	0.0	10.9
3	10.8	7.0	2.2	0.2	2.4	0.0	13.0
4	7.3	4.8	1.6	0.0	4.6	0.0	14.6
5	25.3	17.8	5.1	8.8	0.0	0.7	2.0
6	13.7	6.5	3.5	1.6	1.3	0.0	9.6
7	13.8	9.3	2.6	0.6	0.6	0.0	9.9
8	26.6	16.9	4.6	9.9	0.0	1.8	1.9
9	24.3	9.8	3.8	1.1	1.0	0.3	10.2
10	17.0	9.8	6.4	2.0	4.0	0.0	12.0
11	14.6	9.2	3.0	0.8	1.6	0.0	10.7
12	21.7	11.7	3.9	3.5	0.2	0.3	6.9
13	27.3	23.4	2.2	13.0	0.0	3.6	0.7
14	23.7	17.1	3.6	7.6	0.0	0.5	2.8
15	10.3	7.1	1.8	0.1	2.6	0.0	12.6
16	8.9	5.3	2.1	0.0	4.1	0.0	14.1
17	26.1	17.6	4.4	10.2	0.0	1.9	1.7
18	8.5	6.8	1.5	0.0	2.8	0.0	12.8
19	25.2	17.5	4.3	7.3	0.0	0.2	2.5
20	7.9	5.2	1.5	0.0	3.8	0.0	13.8
Mean (range)	17.2 (7.3-27.3)	11.1 (4.8-23.4)		3.6	1.6	0.5	8.5

a higher limit (10 mm) was used, only a very small improvement of TAU was calculated, and TAO increased unnecessarily (Tables 2 and 3).

Margins to account respiration with a reference measurement

Pearson's correlation coefficient indicated a modest correlation in the SI direction (Figure 1A) and very poor correlations in the LL and AP directions (Figure 1B, C). Given these results, we could not hypothesize any way to predict margins that would account for motions in the LL and AP directions based on reference measurements.

Using margins in the SI direction based on the reference measurement of respiratory tumor motion allowed us to avoid overdosage, with the average geometrical miss better than 3 mm (Table 4). However, 30% of patients had a risk zone of underdosage that measured >3 mm (range 3.6 – 7.4 mm)

Closer evaluation of the results clearly revealed the segregation of our patients into two groups, one with movement more than 15 mm, and the second with movement less than 15 mm in the SI direction (Figure 1A). To keep TAO and TAU as low as possible for patients with both types of breathing patterns, ITV margins had to be adjusted accordingly: 15 mm for shallow breathing and 20 mm for deep breathing (Table 4). Similar segregation was not observed for LL or AP directions (Figure 1B, C).

For the SI direction, we derived a "regression model" that added an extra margin to those acquired from the reference measurement (Figure 1A). As the results were far from optimal (only 2-3 mm margin reduction compared to a constant margin without reference measurement), we evaluated patient's variability more closely. Women and men are known to favor different types of breathing (chest vs. abdominal). Our results did not indicate any significant difference regarding tumor motion amplitudes (Figure 2A-C) for all three directions, while the tumor motion prediction was higher for men, especially in the SI direction (Test for Difference Between Two Correlation Coefficients, p = 0.0000; Test for Difference Between Two Regression Coefficients, p = 0.0001)

Table 2 Pancreas movement in LL direction during three fractions, TAO and TAU for lower and upper limit for LL direction considered in the American-French consensus

Latero-Lateral							
	Motion (mm)			Margin 5mm		Margin 10mm	
Patient	Max	Mean	Std	TAU	TAO	TAU	TAO
1	3.5	2.0	1.4	0.0	2.9	0.0	7.9
2	3.9	2.7	1.1	0.0	2.3	0.0	7.3
3	6.1	4.8	0.9	0.3	0.5	0.0	5.4
4	6.5	2.6	1.9	0.2	2.3	0.0	7.1
5	7.9	4.7	2.2	0.6	1.1	0.0	5.5
6	7.7	1.9	2.4	0.9	0.9	0.0	5.5
7	4.2	2.1	1.5	0.0	3.2	0.0	8.3
8	9.1	5.5	2.3	1.9	0.4	0.0	3.5
9	5.0	1.9	1.5	0.0	2.7	0.0	7.7
10	8.7	4.0	2.1	0.2	2.2	0.0	7.0
11	3.2	1.8	0.9	0.0	2.9	0.0	7.9
12	8.6	6.0	2.0	2.2	0.1	0.0	2.9
13	8.3	6.7	1.8	1.8	0.3	0.0	3.5
14	12.1	4.8	2.4	0.9	1.1	0.0	5.1
15	2.2	1.8	0.3	0.0	3.2	0.0	8.2
16	2.9	1.8	0.9	0.0	3.0	0.0	8.0
17	8.1	4.3	2.2	0.8	0.9	0.0	5.1
18	2.8	2.0	0.6	0.0	2.9	0.0	7.9
19	5.7	2.0	1.9	0.2	2.2	0.0	7.0
20	8.3	4.2	2.2	1.1	1.0	0.0	4.8
Mean (range)	6.2 (6.5-8.3)	3.4 (2.6-6.7)		0.5	1.8	0.0	6.3

Table 3 Pancreas movement in AP direction during three fractions, TAO and TAU for lower and upper limit for AP direction considered in the American-French consensus

Anterior-Posterior							
	Motion (mm)			Margin 5mm		Margin 10mm	
Patient	Max	Mean	Std	TAU	TAO	TAU	TAO
1	6.0	3.0	1.6	0.2	1.7	0.0	6.4
2	6.9	4.8	1.6	0.7	0.5	0.0	4.8
3	4.3	3.1	0.8	0.0	2.1	0.0	7.1
4	5.9	2.9	1.9	0.3	2.1	0.0	6.9
5	9.8	5.9	2.6	1.5	0.1	0.0	3.7
6	9.5	4.7	2.9	0.4	0.1	0.0	3.2
7	4.9	3.3	1.2	0.0	2.1	0.0	7.1
8	7.4	4.9	1.5	0.9	0.3	0.0	4.5
9	4.3	1.3	1.1	0.0	3.4	0.0	8.4
10	6.0	4.3	1.5	0.4	1.3	0.0	5.9
11	2.4	1.4	0.6	0.0	3.6	0.0	8.6
12	9.0	5.6	1.8	1.3	0.3	0.0	4.0
13	9.5	8.2	1.2	2.8	0.0	0.0	2.2
14	7.4	4.6	1.4	0.4	0.9	0.0	5.5
15	2.8	2.2	0.4	0.0	2.7	0.0	7.7
16	3.4	0.9	0.8	0.0	4.1	0.0	9.1
17	11.9	5.6	3.0	2.7	0.4	0.5	3.2
18	3.9	2.8	0.8	0.0	2.2	0.0	7.2
19	5.9	3.8	1.2	0.3	1.0	0.0	5.7
20	3.5	2.4	0.7	0.0	2.8	0.0	7.8
Mean (range)	6.2 (5.9-9.5)	3.8 (2.9-8.2)		0.6	1.6	0.0	5.9

Table 4 Summary table of the different concepts to determine ITV in SI direction

Margin strategy	Constant 10mm	Constant 20mm	Reference measurement	Constant 15 or 20 mm	Constant 15 or 20 mm- man	Constant 15 or 20 mm- woman	Regression analysis all, $y = 13 + 0.4064 \cdot x$	Regression analysis- man $y = 8.5 + 0.7015 \cdot x$	Regression anylysis- woman $y = 17 + 0.1804 \cdot x$
TAU (mm)	3.6	0.5	2.3	0.5	0.3	0.7	0.5	0.3	0.7
TAU > 3mm (%)	40%	5%	30%	5%	0%	9%	5%	0%	9%
TAU > 1mm (%)	55%	15%	50%	20%	11%	27%	15%	11%	18%
TAO (mm)	1.6	8.5	2.7	5.6	6.2	5.1	6.7	5.6	7.4
TAO > 3mm (%)	20%	70%	25%	65%	78%	55%	85%	67%	73%
TAO > 1mm (%)	55%	95%	50%	95%	100%	91%	95%	100%	91%
Margin- average (mm)	10	20	12.1	17	16.7	17.3	17.9	15.8	19.4

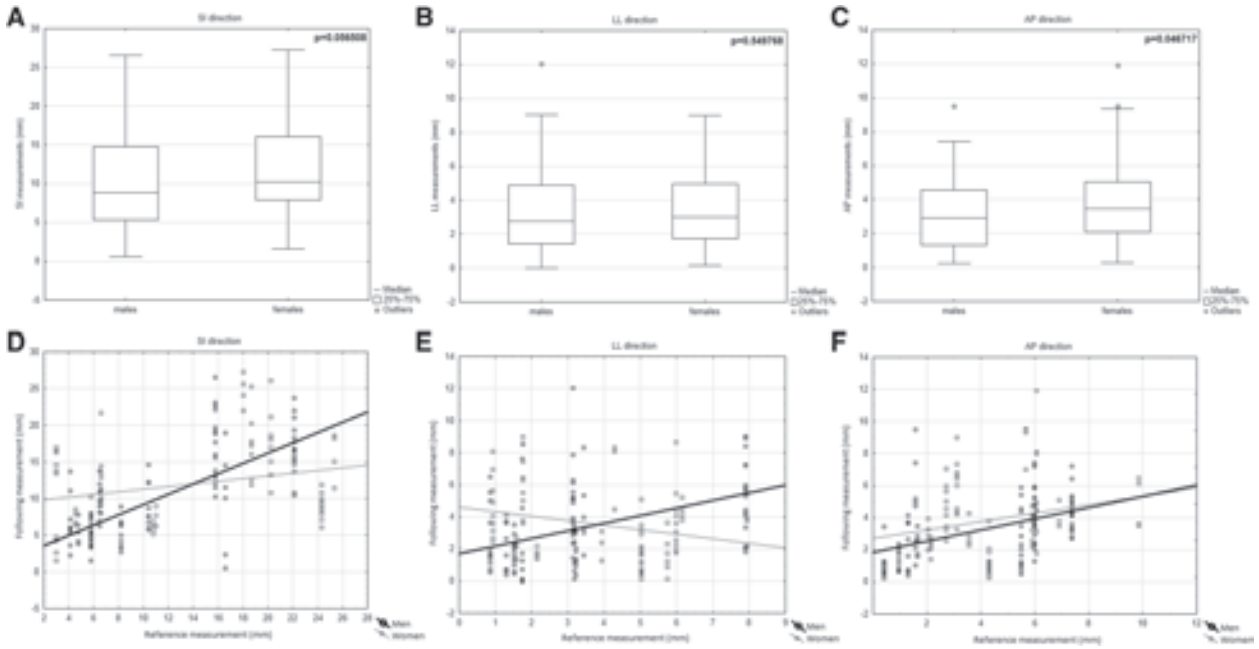

Figure 2 Tumor motion amplitudes and variability of prediction for men and women. We observed no significant difference between men and women regarding tumor motion amplitudes in all three directions: SI p = 0.056 **(A)**; LL p = 0.549 **(B)**; and AP p = 0.052 **(C)**. Variability of prediction for the SI direction **(D)**, men: y = 2.2008 + 0.7015*x; r = 0.7285; p = 0.0000; and women: y = 9.4583 + 0.1804*x; r = 0.2695; p = 0.0163. Test for difference between two correlation coefficients, p = 0.0000. Test for difference between two regression coefficients, p = 0.0001. LL direction **(E)**, men: y = 1.7543 + 0.4717*x; r = 0.4572; p = 0.000; and women: y = 4.6229-0.2843*x; r = -0.2505; p = 0.026. Test for difference between two correlation coefficients, p = 0.0000. Test for difference between two regression coefficients, p = 0.0001. AP direction **(F)**, men: y = 1.8117 + 0.346*x; r = 0.4538; p = 0.0000; and women: y = 2.7144 + 0.261*x; r = 0.1993; p = 0.0802. Test for difference between two correlation coefficients, p = 0.07. Test for difference between two regression coefficients, p = 0.57.

(Figure 2D; Table 4). Unfortunately, only modest margin reduction (1 mm) was seen.

Correlation between internal and external markers during respiration

To get correlation error less than 3 mm (median 1.53 mm, range 0.01-3.09 mm), we had to establish more than 3 correlation models per treatment (median 9.5 times, range 4-18) whenever we observed a correlation error between internal and external markers greater than 3 mm. The median duration of one model was 19 min (range 1-87 min). 10 out of 20 patients (50%) were presented with low stability between internal and external markers and more than 9 models had to been done per treatment (3 fractions).

Discussion

The treatment response of pancreatic tumors to radiotherapy treatment remains poor. Given the strong radioresistance of adenocarcinomas, dose escalation is needed but it is not possible without margin reduction [3-6].

In the present study, tumor motion was greatest in the SI direction, in agreement with data from other institutions [2,9,10,13,14]. According to our measurements (20 patients, monitoring time 4676 min), the mean respiration amplitude between inhalation and exhalation was 11 mm (range 5-23 mm), which appears to be comparable to previously published results from larger studies. Bussels et al. obtained their data by using dynamic MRI to quantify pancreatic motion in 12 patients; instead of placing fiducials, they acquired one image every second for 1 min. They observed a larger degree of movement in the SI direction: 24 mm ±16 mm [15,16] compared to our result (1 minute of monitoring seems to be short and MRI tumor detection could be less precise). Although smaller tumor motion amplitudes have also been presented, those studies are based on a much smaller number of measurements [10,13,14]. Murphy et al. reported the results of only one patient imaged fluoroscopically for 1 min; the patient had three gold fiducials sutured into the tumor, and the maximal SI movement was 6 mm with breathing (13). Gierga et al. published a study of six patients who also underwent invasive marker placement and were observed fluoroscopically for 30 sec. The range of average SI motions was 4.4–12 mm (14). Hallman et al. concluded that the mean COM motion for pancreatic tumors was 5 mm (standard deviation 1 mm), with a range of 3 to 7 mm (10). We observed mean tumor motion of approximately

3 mm (range 3-7 mm) and 4 mm (range 3-8 mm) in the LL and AP directions respectively, which supports the recommendation for asymmetrical margins as published by Goldstein et al. [9].

To the best of our knowledge, this is the first study to quantify under- or overestimation of tumor motion during a longer time period. With the use of TAO and TAU, we were able to derive margins for the optimization of underdosage and overdosage. Our analysis clearly shows the feasibility of the concept of larger margin (20 mm) considered by the American-French consensus [7] for the SI direction, and lower (5 mm) for the LL and AP directions to account respiration. The use of smaller margins in the SI direction would cause an average underdosage zone of approximately 3 mm; moreover, 40% of patients would have an average geometrical miss of >3 mm. Abdominal compression might be useful [17] to minimize tumor motion, especially for the 50% of patients that presented with an average tumor motion of >15 mm. Limitations of our study could be using the tumor tracking system to simulate reference measurement instead of 4DCT and short time of monitoring (3 fractions in 1 week compared to 5 weeks of fractionated radiotherapy).

Planning 4D-CT is commonly used to customize the internal margin in patients with abdominal tumors [8]. Our results show that the motion of pancreatic tumors is modestly predictable with respiration in the SI direction (correlation coefficient $r = 0.50$) and unpredictable in the LL ($r = 0.17$) and AP ($r = 0.35$) directions when derived from the reference measurement. Margins based on the reference measurement of tumor motion avoid overdosage with an average geometrical miss of <3 mm in our group. However, 30% of patients have a risk zone of underdosage >3 mm caused by inter-/intrafractional changes of breathing pattern, that seems unacceptable. When Minn et al. [18] compared the planning of 4D-CT motion with intrafractional motion measured in a single-fraction respiratory tracking radiotherapy; they found that the geometrical miss could exceed 10% for 16 out of 20 patients. Compared with our results, they found an additional modest correlation for the AP direction. However, only the average value from all consequential measurement points was used, compared to our approach assessing the correlation between reference and subsequent measurements [18]. In a study of four pancreatic tumors monitored during 38 fractions, Ge et al. concluded that the motion measured with 4D-CT did not adequately represent actual motion during radiation therapy. The 4D-CT disagreed with 95% of the fractions, 55% of which were underestimated and 40% of which were overestimated [19]. Cai et al. found that gated internal volume based on 4D-CT could underestimate tumor motion in respiratory-gated therapy, mainly because of breathing variability [20]. James et al. found that the instability of internal target volume varied from 46% to 127% [21].

Our results are not in compliance with recommendations for the use of 4D-CT [9,10]. Goldstein et al. observed that the volumes and excursions were relatively unchanged during the treatment course, obviating the need for re-planning during treatment [9]. However, the monitoring time was short, only two measurements were taken for 50% of patients, and inter-/intrafractional variability may have remained hidden; the duration of few breaths could not represent the entire treatment time. Hallman et al. recommend using respiratory gating towards the end of exhalation, which might substantially reduce the range of motion. They found an average shift of 5 mm (range 3-7 mm) for SI direction [10]. Abdominal motion was determined by one respiratory cycle, which could be a limitation of this study.

We have derived two methods of ITV optimization based on the reference measurement. Our algorithms allow us to reduce the margin (approximately from 20 mm to 17 mm for women and from 20 mm to 16 mm for men) in the SI direction, compared with the use of constant margins without reference measurement. No additional risk of underdosage was found. Our preliminary results showed much better prediction capability for men than for women, resulting in a smaller ITV and lower risk of overdosage for men. The amplitude analysis has not shown any significant difference between men and women (Figure 2A-C). Even after detailed analysis, the predictability of movement in both the LL and AP directions remains poor. Moreover, we have detected occasional unpredictable COM shifts caused by intestinal and duodenal peristalsis; therefore, another extra margin might be added.

Finally, we had to create approximately 200 correlation models with median duration of 19 min (range 1-87 min) to obtain good correlation between tumor motion and skin markers (error smaller than 3 mm). This finding is in agreement with the results of Feng et al., who demonstrated poor correlation between the tumor position and the abdominal wall and diaphragm. Poor reproducibility in breathing pattern has also been shown [16]. These additional uncertainties should be accounted for when image guidance with external markers (without fiducials) is used.

Conclusion

Our results support the use of a 20-mm margin in the SI direction and a 5-mm margin in the LL and AP directions to account respiratory motion without a reference measurement. ITV optimization, based on the reference measurement, allows a small margin reduction in the SI direction (approximately from 20 mm to 16-17 mm) and no margin reduction in the LL/AP directions, with no

additional risk of underdosage when compared with the use of constant margins. Further margin reduction is only possible when there is on-line tumor motion control according to internal markers.

Competing interests
The authors declare that they have no competing of interests.

Authors' contributions
LK collected data, analysed data and wrote article. JC design the study and wrote article. LM, BO analysed data. ES, TJ, DC performed contouring and analysis of relationship between fiducials and contours. MR performed the statistical analysis. PD carried out a critical review of the manuscript. DF participated in study design and coordination. All authors read and approved the final manuscript.

Acknowledgements
We would like to thank M.S. Petr Jordan Ph.D., Imaging Research Manager (Accuray Inc.) for his valuable and constructive suggestions.
This work was supported by MH CZ - DRO – FNOs/2013.

Author details
[1]Department of Oncology, University Hospital Ostrava, 17. listopadu 1790, 708 52 Ostrava, Czech Republic. [2]Department of Radiology, University Hospital Ostrava, Ostrava, Czech Republic. [3]Medical Physics, The London Clinic, London, UK.

Received: 23 January 2014 Accepted: 23 August 2014
Published: 30 August 2014

References

1. Geer RJ, Brennan MF: **Prognostic indicators for survival after resection of pancreatic adenocarcinoma.** *Am J Surg* 1993, **165:**68–73.
2. Murphy JD, Adusumilli S, Griffith KA, Ray ME, Zalupski MM, Lawrence TS, Ben-Josef E: **Full-dose gemcitabine and concurrent radiotherapy for unresectable pancreatic cancer.** *Int J Radiat Oncol Biol Phys* 2007, **68:**801–808.
3. Brown MW, Ning H, Arora B, Albert PS, Poggi M, Camphausen K, Citrin D: **A dosimetric analysis of dose escalation using two intensity-modulated radiation therapy techniques in locally advanced pancreatic carcinoma.** *Int J Radiat Oncol Biol Phys* 2006, **65:**274–283.
4. Gurka MK, Collins SP, Slack R, Tse G, Charabaty A, Ley L, Berzcel L, Lei S, Suy S, Haddad N, Jha R, Johnson CD, Jackson P, Marshall JL, Pishvaian MJ: **Stereotactic body radiation therapy with concurrent full-dose gemcitabine for locally advanced pancreatic cancer: a pilot trial demonstanting safety.** *Radiation Oncol* 2013, **8:**44.
5. Kim Y, Lee WJ, Woo SM, Kim TH, Han S, Kim BH, Moon SH, Kim SS, Koh YH, Park S, Kim J, Kim DY, Park J: **Comparison of capecitabine and 5-fluorouracil in chemoradiotherapy for locally advanced pancreatic cancer.** *Radiation Oncol* 2013, **8:**160.
6. Van der Geld YG, Van Triest B, Verbakel WF, Van Sörnsen de Koste JR, Senan S, Slotman BJ, Lagerwaard FJ: **Evaluation of four-dimensional computed tomography-based intensity-modulated and respiratory-gated radiotherapy techniques for pancreatic carcinoma.** *Int J Radiat Oncol Biol Phys* 2008, **72**(4):1215–1220.
7. Huguet F, Goodman KA, Azria D, Racadot S, Abrams RA: **Radiotherapy technical considerations in the management of locally advanced pancreatic cancer: American-French concensus recommendations.** *Int J Radiat Oncol Biol Phys* 2012, **83:**1355–1364.
8. Aruga T, Itami J, Aruga M, Nakajima K, Shibata K, Nojo T, Yasuda S, Uno T, Hara R, Isobe K, Machida N, Ito H: **Target volume definition for upper abdominal irradiation using CT scans obtained during inhale and exhale phases.** *Int J Radiat Oncol Biol Phys* 2000, **48:**465–469.
9. Goldstein SD, Ford EC, Duhon M, McNutt T, Wong J, Herman JM: **Use of respiratory-correlated four-dimensional computed tomography to determine acceptable treatment margins for locally advanced pancreatic adenocarcinoma.** *Int J Radiat Oncol Biol Phys* 2010, **76:**597–602.
10. Hallman JL, Mori S, Sharp GC, Lu HM, Hong TS, Chen GT: **A four-dimensional computed tomography analysis of multiorgan abdominal motion.** *Int J Radiat Oncol Biol Phys* 2012, **83:**435–441.
11. Kilby W, Dooley JR, Kuduvalli G, Sayeh S, Maurer CR Jr: **The CyberKnife robotic radiosurgery system in 2010.** *Technol Cancer Res Treat* 2010, **9:**433–452.
12. Hoogeman M, Prevost JB, Nuyttens J, Pöll J, Levendag P, Heijmen B: **Clinical accuracy of the respiratory tumor tracking system of the cyberknife: assessment by analysis of log files.** *Int J Radiat Oncol Biol Phys* 2009, **74:**297–303.
13. Murphy MJ, Martin D, Whyte R, Hai J, Ozhasoglu C, Le QT: **The effectiveness of breath-holding to stabilize lung and pancreas tumors during radiosurgery.** *Int J Radiat Oncol Biol Phys* 2002, **53:**475–482.
14. Gierga DP, Chen GT, Kung JH, Betke M, Lombardi J, Willett CG: **Quantification of respiration-induced abdominal tumor motion and its impact on IMRT dose distributions.** *Int J Radiat Oncol Biol Phys* 2004, **58:**1584–1595.
15. Bussels B, Goethals L, Feron M, Bielen D, Dymarkowski S, Suetens P, Haustermans K: **Respiration-induced movement of the upper abdominal organs: a pitfall for the three-dimensional conformal radiation treatment of pancreatic cancer.** *Radiother Oncol* 2003, **68:**69–74.
16. Feng M, Balter JM, Normolle D, Adusumilli S, Cao Y, Chenevert TL, Ben-Josef E: **Characterization of pancreatic tumor motion using cine MRI: surrogates for tumor position should be used with caution.** *Int J Radiat Oncol Biol Phys* 2009, **74:**884–891.
17. Wunderink W, Romero AM, Osorio EMV, De Boer HC, Brandwijk RP, Levendag PC, Heijmen BJ: **Target coverage in image-guided stereotactic body radiotherapy of liver tumors.** *Int J Radiat Oncol Biol Phys* 2007, **68:**282–290.
18. Minn AY, Schellenberg D, Maxim P, Suh Y, McKenna S, Cox B, Dieterich S, Xing L, Graves E, Goodman KA, Chang D, Koong AC: **Pancreatic tumor motion on a single planning 4D-CT does not correlate with intrafraction tumor motion during treatment.** *Am J Clin Oncol* 2009, **32:**364–368.
19. Ge J, Santanam L, Noel C, Parikh PJ: **Planning 4-dimensional computed tomography (4DCT) cannot adequately represent daily intrafractional motion of abdominal tumors.** *Int J Radiat Oncol Biol Phys* 2013, **85:**999–1005.
20. Cai J, McLawhorn R, Read PW, Larner JM, Yin FF, Benedict SH, Sheng K, Berbeco RI, Lewis JH: **Effects of breathing variation on gating window internal target volume in respiratory gated radiation therapy.** *Med Phys* 2010, **37:**3927–3934.
21. James SS, Mishra P, Hacker F, Berbeco RI, Lewis JH: **Quantifying ITV instabilities arising from 4DCT: a simulation study using patient data.** *Phys Med Biol* 2012, **57:**L1–L7.

doi:10.1186/1748-717X-9-192
Cite this article as: Knybel *et al.*: The analysis of respiration-induced pancreatic tumor motion based on reference measurement. *Radiation Oncology* 2014 **9**:192.

4 Lacrimal sac dacryoliths (86 samples): chemical and mineralogic analyses

Komínek P, Doškářová Š, Švagera Z, Lach K, Červenka S, Zeleník K, Matoušek P

Originally published in Graefes Archive for Clinical and Experimental Ophthalmology, 2014, vol. 252, no. 3, p. 523-529

Consent to the publication of 19th March 2015

(licence no. 3592390559772)

Graefes Arch Clin Exp Ophthalmol (2014) 252:523–529
DOI 10.1007/s00417-013-2501-6

OCULOPLASTICS AND ORBIT

Lacrimal sac dacryoliths (86 samples): chemical and mineralogic analyses

Pavel Komínek · Šárka Doškářová · Zdeněk Švagera · Karel Lach · Stanislav Červenka · Karol Zeleník · Petr Matoušek

Received: 11 April 2013 / Revised: 2 October 2013 / Accepted: 8 October 2013 / Published online: 30 October 2013

Abstract
Background Because dacryoliths occur at low frequency, few studies have focused on their composition. We aimed to present findings from morphological, chemical, and mineralogic analysis of 86 dacryoliths.
Methods We studied 86 dacryoliths obtained during 832 dacryocystorhinostomies (DCR) performed for postsaccal obstruction. We examined the samples with atomic infrared spectrometry (80 samples), amino acid analysis (17 samples), scanning electron microscopy, and an electron microprobe with an energy dispersive detector (seven samples).
Results Dacryoliths were found in 86/832 DCRs (10.3 %), mostly in patients with primary acquired nasolacrimal duct obstruction. All the dacryoliths were soft, composed of organic material, including proteins and mucoproteins, with approximately 20 % amino acid content. There were no "hard" dacryoliths composed of calcium phosphate. The stones were composed of lobes and lobules built on an amorphous core material with small cavities, probably as a result of various chemical processes that produced a gaseous product. The most frequent elements found in inorganic inclusions were silicon, magnesium, sulfur, potassium, calcium, sodium, and chlorine. Also, some particles had high contents of bismuth, titanium, iron, and organic fibers. The fibers found in the core of dacryoliths suggested a potential origin from cotton swabs used in cosmetics.
Conclusion Dacryoliths are composed almost exclusively of organic material, including proteins and mucoproteins, with approximately 20 % amino acid content.

Keywords Dacryolith · Dacryocystorhinostomy · Composition · Chemical analysis · Infrared spectrometry · Scanning electron microscopy · Elemental analysis

P. Komínek (✉) · S. Červenka · K. Zeleník · P. Matoušek
Department of Otolaryngology, University Hospital Ostrava, 17. listopadu Street 1790, 708 52 Ostrava Poruba, Czech Republic
e-mail: pavel.kominek@fno.cz

Š. Doškářová · K. Lach
Public Health Institute of Ostrava, Centre of Hygiene Laboratories, Ostrava, Czech Republic

Z. Švagera
Institut of Laboratory Diagnostics, University Hospital Ostrava, Ostrava, Czech Republic

Z. Švagera · K. Zeleník · P. Matoušek
Faculty of Medicine, University of Ostrava, Ostrava, Czech Republic

S. Červenka
Department of Ophthalmology, Otrokovice, Czech Republic

Introduction

It is not unusual to find a stone in the lacrimal sac during dacryocystorhinostomy (DCR). Although patients with dacryolithiasis often have a history of long-term intermittent epiphora, lacrimal sac distention, and/or partial obstruction of the nasolacrimal duct (NLD), dacryoliths are often only detected during DCR. The incidence of dacryoliths has not been evaluated in the general population; the incidence of dacryoliths in the lacrimal sac of patients that undergo DCR ranges from 6.0–18.0 % [1–3]. Most published studies on dacryoliths have included quite a small number of samples [4–6].

Canalicular concretions have long been associated with canaliculitis caused by actinomycotic infection. Despite recent, significant progress, we lack understanding of the pathophysiology of lacrimal sac dacryoliths [1–3]. Several predisposing factors have been suggested to contribute to the mechanism that gives rise to dacryolith formation. These factors include age (under 50 years old), sex (increased frequency in females), cigarette smoking, and previous occurrence of chronic dacryocystitis and primary acquired

nasolacrimal duct obstruction (PANDO) [1–3, 5, 7]. Recent analyses have shown that dacryolith development may be related to lacrimal sac epithelial and NLD production of a broad spectrum of mucins and expression of two peptide members of the trefoil factor family (TFF), TFF1 and TFF3 [1, 8, 9]. Because dacryoliths occur at low frequency, few studies have focused on their composition.

In this study, we aimed to present findings from morphological, chemical, and mineralogic analysis of 86 dacryoliths.

Materials and methods

A total of 967 primary EDCRs were performed at the Department of Otorhinolaryngology of the University Hospital of Ostrava and at the Department of Otorhinolaryngology of the Frydek–Mistek City Hospital between 1994 and April 2012. Only endonasal dacryocystorhinostomies (EDCRs) performed for postsaccal stenosis/obstruction (832 procedures) were included in the study. Exclusion criteria were presaccal obstruction treatment, revision EDCRs, and incomplete follow-ups. The indication for EDCRs were made preoperatively according to the history, clinical examination with syringing of the lacrimal system, and diagnostic probing and dacryocystography in some cases.

The study was performed in accordance with the Declaration of Helsinki, Good Clinical Practice, and applicable regulatory requirements. Written consent was obtained from all patients before the initiation of surgery and dacryolith analysis.

Among the group of 832 EDCRs, 86 stones of the lacrimal sac (dacryoliths) were found, including 61/86 (70.9 %) in women and 25/86 (29.1 %) in men. Clinical information was obtained from patient medical records, including the involved side, the etiology of the nasolacrimal duct (NLD) obstruction, the outcome of EDCR at 1 year after surgery, the size of the dacryolith, and data from dacryolith analysis. The association with cigarette smoking was not studied due to lack of relevant information. For the chemical and morphologic analysis, the infrared spectrometry, chemical amino acid analysis, and scanning electron microscopy were used. The culture examination as well as histology were not performed.

Infrared spectroscopy

We examined the dacryoliths with Fourier transform infrared spectrometry (FTIR; IMPACT 410, fy Nicolet) using KBr pellets. Evaluations were performed with OMNIC software, and the obtained spectra were compared with a library of spectra from kidney stones.

Amino acids analysis

Proteins in the samples (≤ 20 mg) were hydrolyzed with hydrochloric acid [1, 2]. Then, 1 ml of distilled water was added, the solution was filtered, then evaporated at 90 °C under nitrogen, and the residue was dissolved in 2 ml of 1 % aqueous NaOH. An aliquot (~0.5 mg of the initial sample) was transferred to another tube, the volume adjusted to ± 100 μl with 1 % NaOH, and a derivatization was performed with ethyl chloroformate (4). Next, we performed gas chromatography in tandem with mass spectrometry with a 7890A and MSD5975C (Agilent), equipped with a 30-m, VF-17 ms capillary column (0.25 mm×0.15 μm; CP8981 from HPST, Praque). Samples were run at temperatures ramped from 60 to 300 °C at a rate of 6 °C /min; split injection (10:1) was employed. We performed electron impact (EI) mass spectrometry detection at 70 eV at temperatures of 230 °C for the ion source, 250 °C for the transfer line, and 150 °C for the quad. We performed full-scan analyses with a helium-carrier gas flow of 1.2 ml/min.

Imaging and morphological analysis

Morphological analyses were performed with a scanning electron microscope (QUANTA FEG 450, FEI Company, Redmond, WA, USA). An electron microprobe with an energy dispersive detector (EDS) was used for the elemental analysis of the organic matrix of the stone and for the analysis of fine inorganic particulates in the stone.

Statistical analysis

For statistical analysis, we calculated binomial confidence intervals (CI) for the success rates at the 95 % CI. The two-sample t-test and χ^2 test were used to evaluate differences in age, sex, and surgical success between groups I and II; $p < 0.05$ was considered statistically significant.

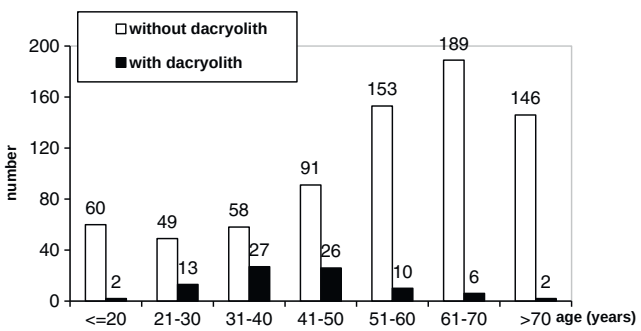

Fig. 1 Distribution of EDCRs (n = 832) with dacryoliths (86 procedures) and without dacryoliths (746 procedures) in different age groups

Fig. 2 Dacryoliths take on the shape of the internal lumen of the main lacrimal sac cavity and the upper nasolacrimal duct

Results

We evaluated a total of 832 EDCRs, performed for the treatment of postsaccal obstructions in 1994–2012.

Dacryoliths were found in 86/832 procedures (10.3 %); 76 patients had unilateral and five patients had bilateral procedures. The most common initial cause of the obstruction was PANDO for patients with or without dacryolithiasis.

The group with dacryoliths (group I) had an average age of 41.2 years (range 16–74 years, median=41, SD=12.6); the group without dacryoliths (group II) had an average age of 53.7 years (range 3 months–90 years; median=41, SD=20.1; $p<0.001$). EDCRs were performed significantly more frequently in individuals aged 31–50 years old in group I, and in patients aged 51–70 years old in group II (Fig. 1). There was no significant difference in the female-to-male ratio in the two groups (2.3:1 group I; 2.4:1 group II; $p=0.834$). EDCR achieved complete improvement and resolution of symptoms

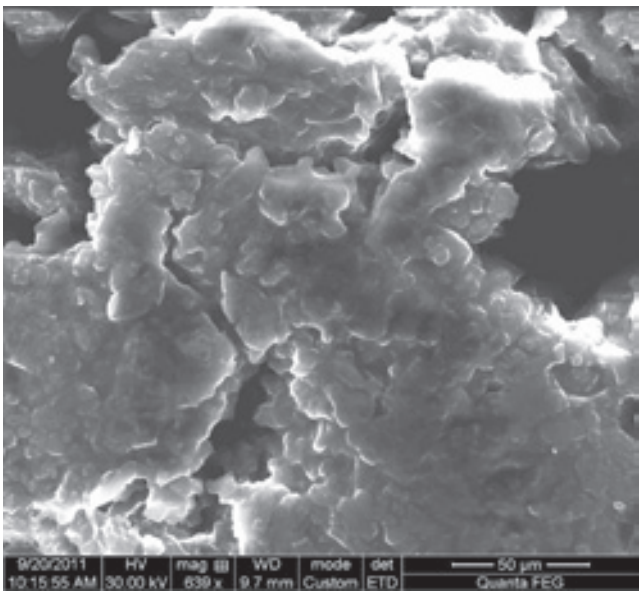

Fig. 3 Scanning electron micrograph of the dacryolith surface shows a lobular structure

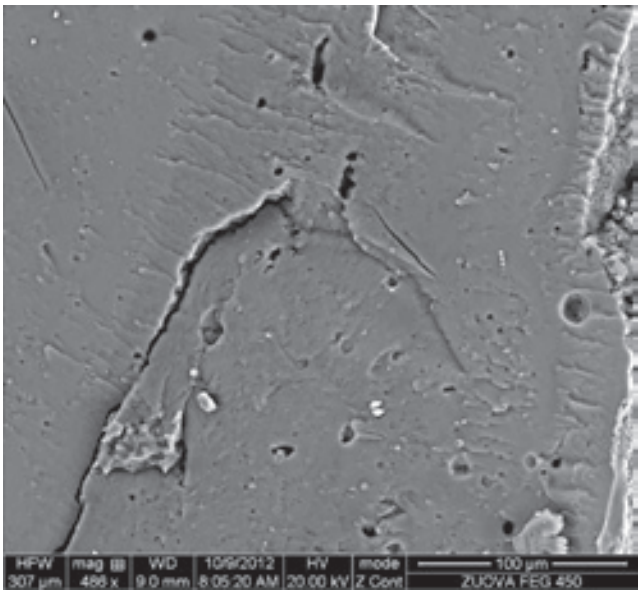

Fig. 4 Scanning electron micrograph of a dacryolith shows an amorphous matrix with small cavities

significantly more frequently in group I (86/86; 100.0 %) than in group II (678/746; 90.9 %; 95 % CI: 88.6 % – 92.9 %).

In all cases, the dacryoliths were yellowish or light brownish in color. Macroscopically, the dacryoliths took on the shape of the internal lumen of the main lacrimal sac cavity or the upper nasolacrimal duct (Fig. 2). The stone surfaces were typically roughened and mostly ridged, with notches caused by the lacrimal sac mucosa. The dacryolith sizes ranged from 3 to 14 mm (mean 7.0 mm) in length, and 3 to 9 mm (mean 5.0 mm) wide. All stones were composed of soft, spongy, semi-solid tissue, with no hard substance. In one case,

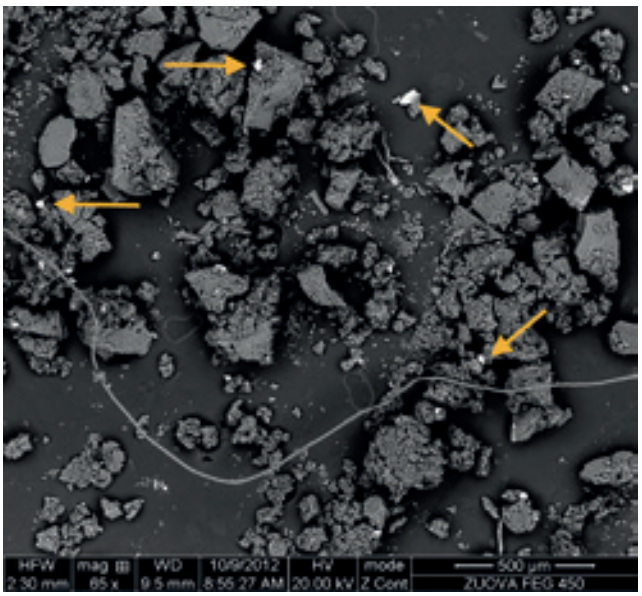

Fig. 5 Scanning electron micrograph of a dacryolith with an organic microfiber at the center of the matrix. *White particles* represent inorganic particles (some are marked with an *arrow*)

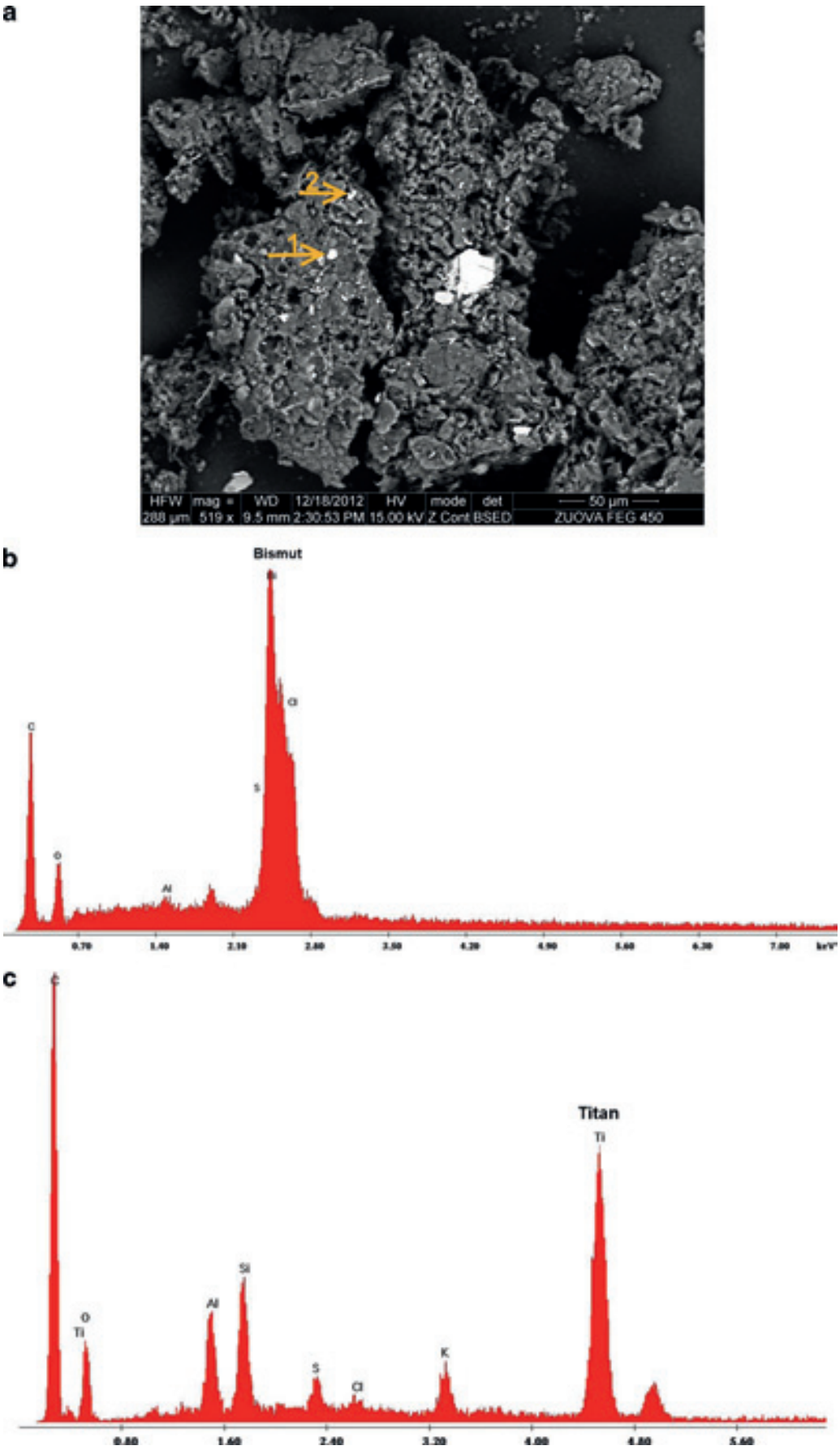

Fig. 6 Elemental analyses of the organic matrix of a dacryolith with a scanning electron microscope and electron microprobe with an energy dispersive detector. **a** Inorganic particles in the matrix appear as *white dots* (iron = *arrow 1*, bismuth = *arrow* 2). **b** A dacryolith with a high proportion of bismuth. **c** A dacryolith with a high proportion of iron

the dacryolith had a hard core covered with soft spongy material; the nidus (core) was composed of grass seed (confirmed histologically), but the matrix around the nidus had the same composition as the other stones and contained no fungal hyphae. Overall, 80 dacryoliths were examined with FTIR. The spectra of all samples demonstrated that the stones consisted of protein. No stones showed bands consistent with phosphate, oxalate, or cholesterol. A chemical analysis of 17 samples revealed that the stones had, on average, 19.8 % amino acid content. The most common amino acids found were leucine (2.8 %), glutamic acid (2.5 %), aspartic acid (1.6 %), and alanine (1.6 %). Other amino acids were present at less than 1 %.

Scanning electron microscopy of seven dacryoliths (four from females, three from males) showed very similar surface structures. Dacryoliths were composed of lobes and lobules built on an amorphous core material; in the solid, amorphous, organic matrix, inorganic particles of different composition were unevenly, sparsely dispersed. The matrix of the samples contained many small cavities (Figs. 3 and 4). Three samples (three females) exhibited organic fibers, visible in the center of the dacryoliths (Fig. 5).

The most frequent inorganic particles (>90 % of all investigated) were silicates of magnesium. Minor amounts of potassium, sodium, sulfur, and chlorine were observed. Inorganic particles were also found with higher levels of calcium and phosphorus; these corresponded to the presence of fine phosphate particles. Inorganic inclusions were predominantly in the size range of <1 to 10 μm. In one case (a female with organic fibers in dacryolith) the inorganic particles were found to have high contents of bismuth, titanium, and iron (Fig. 6 a,b,c).

A quantitative, elemental analysis of the organic amorphous matrix showed that the predominant elements were, as expected, carbon and oxygen (hydrogen content was not evaluable with EDS). In addition, minor elements were detected, including sulfur, phosphorus, chlorine, and sodium (Table 1). Sulfur was mostly present only in the organic matrix, and calcium was mostly bound to the phosphorus (calcium phosphate).

Discussion

The incidence of dacryoliths has not been established in the general population. Most published studies on dacryoliths included quite small numbers [4–6]. Among patients undergoing EDCR, dacryoliths are observed in approximately in 6.0–18 % of cases [1, 2]. In the present study, probably the largest in current literature, dacryolithiasis was observed in 10.3 % of patients (predominantly women) that underwent EDCR.

Dacryoliths develop most frequently in PANDO [1–3, 10]. Though the pathophysiology of the stones was unclear, there seemed to be a relationship between stones and chronic dacryocystitis with stagnation secondary to nasolacrimal stenosis, and it is difficult to determine clearly whether dacryocystitis or dacryolithiasis was the primary driver in the development process [3, 10]. Some studies have described morphological characteristics consistent with fungus or hyphae-like structures [5, 11]. Although it seems that fungi may accentuate the process of the dacryolith formation, unfortunately there is lack of relevant information on the culture of lacrimal sac stones in literature, further research is needed. We did not examine culture to detect fungi, and did not perform a microscopic analysis to investigate presence of fungi in the dacryoliths.

Few studies have analyzed the composition of lacrimal system stones [12]. At first glance, it might be expected that lacrimal sac dacryoliths would have compositions similar to that of stones that form in other parts of the human body (rhinoliths, sialoliths, etc.), which consist mainly of inorganic calcium compounds [13]. However, in reality, they are quite different. Veirs described two types of dacryoliths; those with and those without amino acid content. Hard stones, composed mostly of calcium, have only been mentioned in some papers [3, 7, 10]. Cassotis studied a lacrimal stone in a horse; that calculus primarily comprised carbonate hydroxylapatite with a minor constituent of NaCl halite [14]. In the present study, we did not observe any “hard“ stones that comprised mainly calcium phosphate composites. All the stones in this study comprised predominantly proteins (mucoproteins), as shown by FTIR. This was consistent with several previous studies [4, 5, 12, 15]. In a study by Iliadelis et al., dacryoliths were mainly composed of organic material (99.53 to 99.85 %) [4].

Some dacryoliths include various cells and cellular debris, like epithelial cells, neutrophils, T and B lymphocytes, macrophages, and cellular debris [3, 4, 6]. Those cells or debris may have formed the basis of the dacryolith, such as the eyelash observed by Barath et al. or the grass seed observed in the present study [1, 16]. Lew et al. suggested that lacrimal fluid from patients with dacryoliths contained less lysozyme and calcium than normal lacrimal fluid [17].

Table 1 Elemental analysis of dacryolith organic matrices, performed with a scanning electron microscope and an energy dispersive detector

Element (proportion by weight : %)	Carbon	Oxygen	Sodium	Magnesium	Aluminum	Phosphorus	Sulfur	Chlorine	Calcium
Sample 1	75.06	19.96	1.19	0.26	0.25	0.30	2.12	0.43	0.42
Sample 2	70.77	20.69	0.74	0.31	1.78	0.20	4.10	0.85	0.40

Paulsen et al. found that dacryoliths were composed mostly of proteins and mucoproteins produced by the epithelium of the lacrimal sac and the NLD [1, 8, 9]. In their studies, a broad spectrum of mucins and TFF peptides (TFF1 and TFF3) were identified. They suggested that these proteins probably played a role in dacryolithogenesis. TFF-containing dacryoliths consisted of ~40 % amino acids, and had several well-conserved features. Their reported dacryolith composition corresponded well with results from the present study; our amino acid analysis showed that amino acids accounted for 19.8 % of the dacryolith weight.

Chemically, mucins are large, extracellular glycoproteins with molecular weights ranging from 0.5 to 20 MDa. They are highly glycosylated, typically consisting of 80 % carbohydrates. Although we did not analyze mucoproteins in our study, we confirmed their dominant presence in dacryoliths with the electron microprobe EDS. This revealed that carbon (80 %) was the main constituent of dacryoliths. In contrast, inorganic material was detected to a much lesser extent.

Our imaging and morphological analysis with the scanning electron microscope were very interesting. We found that the surface of dacryoliths was composed of lobes and lobules built on an amorphous material and many small, different-sized cavities were observed in the core material of soft dacryoliths. This type of cavity is typically formed as a result of various chemical or biochemical processes that produce gas. We could not clearly determine whether the cavities were a product of processes in the lacrimal sac or whether they were artifacts that developed, either after removing the sac or in the period between the operation and the examination.

The scanning electron microscope images of the solid, amorphous organic matrix showed unevenly, sparsely dispersed inorganic particles of different compositions. The most frequent inorganic particle (>90 % of all investigated) was composed of magnesium silicate, and ranged from <1 μm to about 10 μm in diameter. Phosphorus occurred predominantly in calcium phosphate. In three samples of females, we also observed very small organic fibers in the core material in addition to particles that contained bismuth, titanium, and iron in the surrounding matrix. These findings suggested that inorganic particles from various cosmetic products may gradually move down the tear duct and, in susceptible individuals, may cause an inflammatory reaction [3]. This notion was supported by the finding in the literature that dacryolithiasis affects mostly women [3].

Conclusion

This study of 86 dacryoliths confirmed that stones formed in the lacrimal sac are soft, composed almost exclusively of organic solid amorphous organic matrix, and consist of proteins and mucoproteins. This composition of dacryoliths corresponded with an amino acid analysis, which demonstrated that amino acids accounted for 19.8 % of dacryolith weight. The presence of small organic fibers in the core of some samples and the high content of particles that contained bismuth and titanium in one sample suggested that some dacryoliths may have originated from cosmetics and beauty aids. No hard dacryoliths composed of calcium phosphate were found in the present study.

The culture of dacryoliths was not examined in the study. Nevertheless, fungi seem to play an important role in the process of dacryolith formation, and further studies dealing with culture and/or histology of the lacrimal sac dacryoliths are needed.

Acknowledgments The authors would like to thank Mrs Hana Tomášková for her assistance in statistical analytical corrections that contributed to the final version of this paper.

Financial support None.

Proprietary interest statement There are no financial interests related to the manuscript, including stock or ownership of a business entity connected to a product described in the paper, paid consulting for the company or competing companies, or patent rights to a drug or piece of equipment.

Clinical trials reference number NCT01826734

References

1. Paulsen F (2007) Pathophysiological aspects of PANDO, dacryolithiasis, dry eye, and punctum plugs. In: Weber RK, Keerl R, Schaefer SD, Della Rocca RC (eds) Atlas of lacrimal surgery. Springer, Berlin, pp 15–27
2. Repp DJ, Burkat CN, Lucarelli MJ (2009) Lacrimal excretory system concretions: canalicular and lacrimal sac. Ophthalmology 116:2230–2235
3. Hurwitz JJ (1996) Diseases of the Sac and Duct. In: Hurwitz JJ (ed) The lacrimal system, 1st edn. Lippincott Raven, Philadelphia, pp 117–138
4. Iliadelis ED, Karabatakis VE, Sofoniou MK (2006) Dacryoliths in a series of dacryocystorhinostomies: histologic and chemical analysis. Eur J Ophthalmol 16(5):657–662
5. Orhan M, Onerci M, Dayanir V, Orhan D, Irkec T, Irkec M (1996) Lacrimal sac dacryolith: a study with atomic absorption spectrophotometry and scanning electron microscopy. Eur J Ophthalmol 6(4):478–480
6. Iliadelis E, Karabatakis V, Sofoniou M (1999) Dacryoliths in chronic dacryocystitis and their composition (spectrophotometric analysis). Eur J Ophthalmol 9(4):266–268
7. Herzig S, Hurwitz JJ (1979) Lacrimal sac calculi. Can J Ophthalmol 14(1):17–20
8. Paulsen FP, Schaudig U, Fabian A, Ehrich D, Sel S (2006) TFF peptides and mucins are major components of dacryoliths. Graefes Arch Clin Exp Ophthalmol 244(9):1160–1170
9. Paulsen FP (2008) Anatomie und Physiologie der ableitenden Tränenwege. Ophthalmologe 105:339–345
10. Viers ER (1976) Lacrimal disorders. CV Mosby, St. Louis, pp 150–180
11. Berlin AJ, Rath T, Rich L (1980) Lacrimal system dacryoliths. Ophthalmic Surg 11(7):435–6
12. Halborg J, Prause JU, Toft PB, Skjødt K, Tommerup NR, Nielsen OF, Heegaard S (2009) Stones in the lacrimal gland: a rare condition. Acta Ophthalmol 87:672–675

13. Komínek P, Červenka S, Doskářová S, Heiderová D, Slabík D, Hušek P, Buryška J (2002) Cesk Slov Oftalmol 58(3):205–211
14. Cassotis NJ, Schiffman P (2006) Calcification associated with the nasolacrimal system of a horse: case report and mineralogic composition. Vet Ophthalmol 9(3):187–190
15. McCormick SA, Linberg JV (1988) Pathology of nasolacrimal duct obstruction. clinicopathologic correlates of lacrimal excretory system disease. In: Linberg JV (ed) Lacrimal surgery. Churchill Livingstone, New York, pp 169-202
16. Baratz KH, Bartley GB, Campbell RJ, Garrity JA (1991) An eyelash nidus for dacryoliths of the lacrimal excretory and secretory systems. Am J Ophthalmol 111:624–627
17. Lew H, Lee SY, Yun YS (2004) Measurement of pH, electrolytes and electrophoretic studies of tear proteins in tear of patients with dacryoliths: a novel concept for dacryoliths. Ophthalmologica 18(2):130–135

5

Transcranial sonography and ^{123}I-FP-CIT single photon emission computed tomography in movement disorders

Bártová P, Kraft O, Bernátek J, Havel M, Ressner P, Langová K, Herzig R, Školoudík D

Originally published in Ultrasound in Medicine & Biology, 2014, vol. 40, no. 10, p. 2365-2371

Consent to the publication of 20th March 2015

(licence no. 3593080052645)

Ultrasound in Med. & Biol., Vol. 40, No. 10, pp. 2365–2371, 2014

0301-5629/$ - see front matter

http://dx.doi.org/10.1016/j.ultrasmedbio.2014.05.014

● *Original Contribution*

TRANSCRANIAL SONOGRAPHY AND ^{123}I-FP-CIT SINGLE PHOTON EMISSION COMPUTED TOMOGRAPHY IN MOVEMENT DISORDERS

Petra Bártová,* Otakar Kraft,† Jaromír Bernátek,‡ Martin Havel,† Pavel Ressner,* Kateřina Langová,§ Roman Herzig,¶ and David Školoudík*‖

*Department of Neurology, Ostrava University and University Hospital, Ostrava, Czech Republic; †Department of Nuclear Medicine, University Hospital, Ostrava, Czech Republic; ‡Department of Nuclear Medicine, Bata Hospital Zlín, Zlín, Czech Republic; §Department of Biophysics, Faculty of Medicine and Dentistry, Institute of Molecular and Translational Medicine, Palacký University, Olomouc, Czech Republic; ¶Department of Neurology, Faculty of Medicine, Charles University, Hradec Králové, Czech Republic; and ‖Department of Nursing, Faculty of Health Science, Palacký University and University Hospital, Olomouc, Czech Republic

(*Received* 7 *December* 2013; *revised* 6 *May* 2014; *in final form* 15 *May* 2014)

Abstract—Diagnosis of Parkinson's disease (PD) can be difficult in the early stages of the disease. The aim of the study described here was to assess the correlation between transcranial sonography (TCS) and ^{123}I-FP-CIT ([^{123}I] ioflupane, *N*-ω-fluoropropyl-2β-carbomethoxy-3β-(4-[^{123}I]iodophenyl)nortropane) SPECT (single photon emission computed tomography) findings and the diagnosis of PD. A total of 49 patients were enrolled in the study: 29 patients with PD, 7 patients with other parkinsonian syndromes, 11 patients with essential tremor and 2 with psychogenic movement disorder. Substantia nigra echogenicity was measured using TCS. SPECT was performed using DaTSCAN ([^{123}I]ioflupane). TCS and SPECT findings were correlated in 84% of patients, with $\kappa = 0.62$ (95% confidence interval: 0.38–0.86). TCS-measured substantia nigra echogenicity and SPECT-measured striatal binding ratio were negatively correlated ($r = -0.326$, $p = 0.003$). TCS/SPECT sensitivity, specificity and positive and negative predictive values for the diagnosis of PD were 89.7%/96.6%, 60.0%/70.0%, 76.5%/82.4% and 80.0%/93.3%, respectively. Both positive TCS and SPECT findings correlated significantly with the diagnosis of PD ($\kappa = 0.52$, 95% confidence interval: 0.27–0.76, and $\kappa = 0.69$, 95% confidence interval: 0.49–0.90, respectively).
(E-mail: petrabartova@seznam.cz)

Key Words: **Parkinson's disease, Parkinsonian syndromes, Substantia nigra, Transcranial sonography, Single photon emission computed tomography, [^{123}I]ioflupane.**

INTRODUCTION

The diagnosis of Parkinson's disease (PD) and its differential diagnosis from other parkinsonian syndromes (PS), essential tremor (ET) and psychogenic movement disorders (PMD) can be difficult, especially in the early stages of the disease (Hughes et al. 1992). Well-established diagnostic criteria based on clinical experience are commonly used for diagnosis of PD, multiple system atrophy (MSA), progressive supranuclear palsy (PSP), vascular parkinsonism and ET (Bain et al. 2000; Gilman et al. 1998; Hughes et al. 1992, 2002; Litvan et al. 1996). Differential diagnosis is important not only for prognosis, but also for the medical treatment of these various diseases.

Neuroimaging methods such as transcranial sonography (TCS) and single photon emission computed tomography (SPECT) may be used to improve diagnostic accuracy (Spiegel et al. 2006; Vlaar et al. 2008b). Nevertheless, differential diagnosis remains difficult.

Transcranial sonography is a tolerable, non-invasive diagnostic method that is used to detect structural changes in the substantia nigra (SN). Recent studies have reported elevated SN echogenicity in at least 90% of PD patients, with border enlargements between 0.20 and 0.25 cm^2 depending on the specific ultrasound system used (Walter et al. 2002). This enables differentiation of patients with PD from healthy patients and patients with ET, in whom a hyper-echogenic enlarged SN is detectable in only 8%–14% (Berg et al. 1999). The sensitivity and specificity of TCS can reach >90% (Brooks 2010; Vlaar et al. 2009). TCS assessment of SN echogenicity and area, together with evaluation of other brain structures, may also be helpful in the differential

Address correspondence to: Petra Bártová, Department of Neurology, University Hospital Ostrava, 17. listopadu 1790, CZ-708 52 Ostrava, Czech Republic. E-mail: petrabartova@seznam.cz

diagnosis of PD and atypical PS, in addition to clinical examination and paraclinical, neuroimaging and genetic methods (Walter et al. 2007a). On the other hand, elevated SN echogenicity was recently reported to have a sensitivity of only 40% and a specificity of 61% for the diagnosis of PD at early stages when examining only patients with parkinsonism (Bouwmans et al. 2013). Moreover, the sonographer's experience and the quality of the bone window influence TCS usage, representing further limitations (Skoloudik et al. 2007).

Single photon emission computed tomography using ^{123}I-FP-CIT (*N*-ω-fluoropropyl-2β-carbomethoxy-3β-(4-[^{123}I]iodophenyl)nortropane) or ^{123}I-β-CIT as a tracer of striatal dopamine transporters (DATs) is able to detect a pre-synaptic lesion of the nigrostriatal system. Decreased DAT densities have been observed in the putamen and caudate nucleus in PD patients, closely paralleling losses of dopamine. ^{123}I-ß-CIT SPECT studies performed in PD patients confirmed the relative selective loss of DAT in the putamen. The pre-synaptic dopaminergic system is not affected in healthy patients and patients with ET, and ^{123}I-FP-CIT SPECT is highly sensitive in differentiation between ET and PD, even during the early stages of the disease, with sensitivity and specificity >90% (Benamer et al. 2000a; Brooks 2010; Doepp et al. 2008; Spiegel et al. 2006). However, ^{123}I-FP-CIT SPECT results can even be negative in the early stages of PD, especially in patients in whom resting tremor is dominant (Benamer et al. 2000a; Doepp et al. 2008; Schillaci et al. 2011). ^{123}I-FP-CIT SPECT has also been used in several studies to differentiate PD from other PS (Pirker et al. 2002; Vlaar et al. 2007, 2008a, 2008b). Nevertheless, the uptake of these radiotracers has been reported to be reduced in patients with PS, such as MSA and PSP, with moderate to high sensitivity (80%–100%) but low specificity (0–46%) (Marshall et al. 2009; Pirker et al. 2002; Vlaar et al. 2007). High cost, poor availability and semi-invasiveness (mainly because of the radiation load) are the main limitations of SPECT.

One may suppose that agreement between TCS and SPECT findings in patients with movement disorders may be high. Nevertheless, the results of studies that have compared TCS-measured SN area and SPECT-measured binding ratio have been conflicting (Doepp et al. 2008; Spiegel et al. 2006; Weise et al. 2009).

The aim of this study was to assess the correlation between TCS and SPECT findings in patients with movement disorders (PD, other PS, ET and PMD).

METHODS

Patients

All consecutive patients presenting with symptoms of parkinsonism or isolated tremor at their first visit to our neurology outpatient clinic over a 3-y period who met the inclusion criteria were enrolled. Inclusion criteria were: (i) a suspected clinical diagnosis of PD (based on the diagnostic criteria of the Parkinson's Disease Society Brain Bank of the United Kingdom) (Hughes et al. 1992, 2002), ET (criteria for the diagnosis of ET) (Bain et al. 2000), MSA (consensus statement on the diagnosis of MSA) (Gilman et al. 1998), PSP (clinical research criteria for the diagnosis of PSP) (Litvan et al. 1996) or PMD (classification system of Williams et al. [1995] and *Diagnostic and Statistics Manual of Mental Disorders* [American Psychiatric Association 2000]); (ii) age of 30–75 y; and (iii) signed informed consent. The study was conducted in accordance with the Helsinki Declaration of 1975 (as revised in 2004 and 2008) and was approved by the local ethics committee. Patients with a clinical history of stroke were excluded, as were patients with ischemic infarction in the basal ganglia, hydrocephalus or a tumor identified by brain magnetic resonance imaging. Patients with disorders that affected the uptake of ^{123}I-FP-CIT (those with vascular parkinsonism and other identifiable possible causes of secondary parkinsonism, including psychiatric disorders, and a history of intake of neuroleptics, tricyclic antidepressants, other serotonin re-uptake inhibitors, reserpine, clonidine, amphetamines and phenopropanolamine) or who had an insufficient temporal bone window or an allergy to iodine were excluded.

Part III of the Unified Parkinson's Rating Scale (UPDRS) was performed on all patients in the "off" state. The Hoehn–Yahr stage was determined in PD and MSA patients. Medication, especially L-DOPA and dopamine agonists, and duration of disease symptoms were recorded for all patients.

Brain CT and magnetic resonance imaging were performed on all patients within 1 mo of clinical examination. TCS and SPECT were performed on all patients within 2 mo of clinical examination. Selegiline therapy was discontinued 2 d before SPECT evaluation.

Transcranial sonography

A 2- to 4-MHz phased P4-2 array probe (HDI 5000, Philips, Bothell, WA, USA) was used for TCS examination. The examination was performed through a temporal bone window with a penetration depth of 15 cm, dynamic range of 50 dB, tissue index of 1.9 and mechanical index of 1.3. A butterfly-shaped structure of the mesencephalic brainstem and the region of the SN were imaged as clearly as possible from the transverse plane. First the right and then the left temporal bone windows were imaged, and both images were anonymized, encoded and saved in jpg format. Only the ipsilateral SN was evaluated. All examinations were performed by an experienced sonographer (D.S.) with more than 10 y of clinical experience. The sonographer was blinded to the

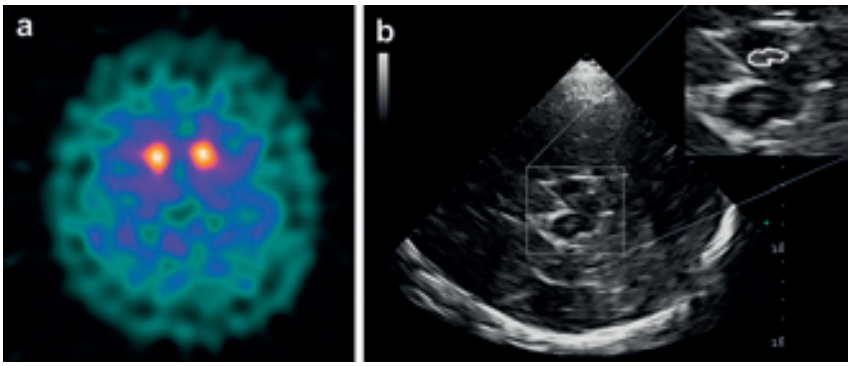

Fig. 1. Patient with Parkinson's disease. (a) Detection of pathologic visual grade 2 with striatal binding ratio 1.76 by [^{123}I] ioflupane single photon emission computed tomography. (b) Detection of pathologic finding of substantia nigra with 0.34-cm^2 echogenic area by transcranial sonography.

patient's diagnosis, but not to the movement disorder symptoms. Subsequently, SN area measurement using the VistaMatrix program (SkillCrest, Chicago, IL, USA) was evaluated in all images by a blinded rater (P.B.). This method, including intra-rater and inter-rater variability, has been described in more detail previously (Bártová et al. 2010; Skoloudik et al. 2007). On the basis of results of previous studies, an SN echogenic area >0.25 cm^2 was classified as pathologic (Figure 1) (Bártová et al. 2010; Skoloudik et al. 2007).

^{123}I-FP-CIT SPECT investigation

Single photon emission computed tomography evaluation of basal ganglia was performed using the DAT ligand [^{123}I]ioflupane (*N*-ω-fluoropropyl-2β-carbomethoxy-3β-(4-[^{123}I]iodophenyl)nortropane, DaTSCAN, Amersham Health, London, UK) within 2 mo of clinical examination. Radiotracer with an activity of 185 MBq was injected intravenously by a nuclear medicine specialist 3.5–4 h before acquisition. SPECT was performed with a dual-head variable-angle gamma camera (Symbia T2, Siemens, The Hague, The Netherlands) equipped with low-energy high-resolution collimators, with a 128 × 128 matrix and a total of 128 frames at 40 s per view. SPECT slices were created using Esoft 2000 application package software (Siemens, Erlangen, Germany), filtered backprojection (FBP) reconstruction with Chang's attenuation correction (coefficient = 11 cm^{-1}) and implementation of a Butterworth filter (cutoff 0.40, order 5). The slices were assessed visually, with normal findings defined as grade 0 and pathologic findings defined as grades 1–3 (Table 1, Figure 1).

Semiquantitative analysis was performed for the correlation with TCS findings by calculating the specific binding ratios of both the caudate nucleus and putamen. The region of interest for non-specific binding of the tracer was taken from the occipital lobe (Koch et al. 2005). The ratios were processed statistically. Reference values obtained from healthy volunteers were used for the acquisition and reconstruction parameters; the ratio was 3.64 ± 0.56 for the caudate nucleus and 3.02 ± 0.56 for the putamen. Scans were analyzed by a specialist blinded to the clinical diagnosis.

Statistics

A Shapiro–Wilk test was used to test the correspondence of the calculated parameters to a normal distribution. Data with a normal distribution are reported as means ± standard deviations. All parameters not fitting a normal distribution are presented as means, medians and interquartile ranges; the non-parametric Kruskal–Wallis test was used for comparison. Agreement, Cohen's κ and agreement coefficient 1 were determined when statistically assessing the correlation between TCS and SPECT findings. Spearman's correlation coefficient was used for correlation between TCS-measured SN echogenicity and SPECT-measured striatal binding ratio, and between the results of both methods and age and disease symptom duration. The sensitivity, specificity and positive predictive and negative predictive values for TCS and SPECT were

Table 1. Pre-synaptic radiotracer [^{123}I]ioflupane single photon emission computed tomography (^{123}I-FP-CIT SPECT) visual evaluation grading

Grade	Specification
0 = normal	Symmetric tracer uptake in the putamen and caudate nucleus bilaterally
1 = abnormal	Asymmetric unilateral reduction in visualization of the putamen in one hemisphere
2 = abnormal	Bilateral reduction in visualization of the putamen, with preserved deposition of radiotracer in the caudate nucleus bilaterally
3 = abnormal	Considerably reduced accumulation of radiotracer affecting both the putamen and caudate nucleus

evaluated. All data were analyzed using SPSS Version 15 statistical software (SPSS, Chicago, IL, USA).

RESULTS

Forty-nine (32 males and 17 females, ages 26–73 y, mean ± SD: 56.1 ± 9.1 y) of the 53 selected patients were included in the study: 29 PD patients, 7 PS patients, 11 ET patients and 2 PMD patients. Three other patients were excluded because of an insufficient temporal bone window and one patient because of an allergy to iodine. Demographic data of the study patients are summarized in Table 2. The duration of clinical symptoms was 6–48 mo (22.96 ± 13.93 mo).

Twenty-six (89.7 %) PD patients had positive TCS (SN area > 0.25 cm^2) and SPECT (visual grades 1–3) results. Ten patients (76.9 %) with ET had negative TCS and SPECT results. Complete results are summarized in Table 3.

Transcranial sonography and SPECT findings were correlated in 84% of all patients, with $\kappa = 0.62$ (95% confidence interval [CI]: 0.38–0.86) and agreement coefficient 1 (AC1) = 0.61 ($p < 0.001$). There was agreement between the clinical diagnosis and TCS findings in 90% of the patients and between the clinical diagnosis and SPECT findings in 97% of the patients.

Both positive TCS and SPECT findings significantly correlated with the diagnosis of PD, with $\kappa = 0.52$ (95% CI: 0.27–0.76) and AC1 = 0.59 ($p < 0.001$) and $\kappa = 0.69$ (95% CI: 0.49–0.90) and AC1 = 0.74 ($p < 0.001$), respectively. TCS-measured SN echogenicity and SPECT-measured striatal binding ratio were significantly negatively correlated, with a Spearman's correlation coefficient of –0.326 ($p = 0.003$) (Fig. 2). TCS and SPECT sensitivity, specificity and predictive values for PD diagnosis are listed in Table 4.

Transcranial sonography-measured SN echogenicity did not correlate with patient age ($r = 0.021$, $p = 0.85$) or disease symptom duration ($r = 0.004$, $p = 0.97$). SPECT-measured striatal binding ratio correlated significantly only with patient age ($r = –0.359$, $p = 0.001$) and not with symptom duration ($r = 0.032$, $p = 0.78$).

DISCUSSION

Results of the present study indicated high agreement between TCS and SPECT findings in patients with movement disorders. Twenty-six (89.7%) PD patients had positive findings in both TCS and SPECT examinations. On the contrary, only 1 (3.4%) patient had negative findings with both methods. Moreover, TCS-measured hyper-echogenic SN areas and SPECT-measured striatal binding ratios were significantly inversely correlated, with a correlation coefficient $r = –0.326$.

Our findings are in concordance with the results of a previous study conducted by Weise et al. (2009), who found an inverse correlation between TCS-measured SN areas and the activity of pre-synaptic striatal

Table 2. Patient demographic and clinical data

				Atypical parkinsonian syndromes	
	Parkinson's disease	Essential tremor	PMD	MSA	PSP
Number of patients	29	11	2	5	2
Age*	56.9 ± 10.3	55.5 ± 6.2	50 ± 11.3	52.6 ± 7.6	62.5 ± 3.5
Male gender*	19 (65.5%)	7 (63.6%)	0	4 (80.0%)	2 (100%)
UPDRS-III					
Mean ± SD (range)	24.87 ± 9.6 (12–47)	5.82 ± 1.25 (2–8)	13.5 ± 2.12 (12–15)	41.6 ± 7.6 (32–49)	37 ± 2.83 (35–39)
Hoehn–Yahr scale					
Median (range)	2 (1–3)		1.5 (1–2)	3 (2.5–3)	2.75 (2.5–3)
Interquartile range	1–2	NA	1.25–1.75	2.5–3	2.63–2.88
L-DOPA therapy*	19 (65.5%)	0 (0%)	1 (50.0%)	3 (60.0%)	1 (50.0%)
DA agonist therapy*	15 (51.7%)	0 (0%)	1 (50.0%)	2 (40.0%)	1 (50.0%)
Disease duration (mo)					
Mean ± SD (range)	18.67 ± 12.2 (6–48)	39.18 ± 9.64 (24–48)	10.0 ± 2.83 (8–12)	19.2 ± 6.72 (12–28)	15.0 ± 4.24 (12–18)
Tremor					
Bilateral*	19 (65.5%)	5 (45.5%)	0 (0%)	2 (40.0%)	1 (50.0%)
Unilateral*	10 (34.5%)	6 (54.5%)	2 (100%)	3 (60.0%)	0 (0%)
Tremor					
Resting*	29 (100%)	7 (63.6%)	2 (100%)	5 (100%)	1 (50.0%)
Postural tremor*	6 (20.7%)	11 (100%)	1 (50.0%)	2 (40.0%)	1 (50.0%)
Resting and postural*	6 (20.7%)	7 (63.6%)	1 (50.0%)	2 (40.0%)	1 (50.0%)
Hypokinesia*	29 (100%)	4 (36.4%)	2 (100%)	5 (100%)	2 (100%)
Rigidity*	29 (100%)	3 (27.3%)	2 (100%)	5 (100%)	2 (100%)
Postural instability*	15 (51.7%)	0 (0%)	1 (50.0%)	5 (100%)	2 (100%)

MSA = multiple system atrophy; NA = not applicable; PMD = psychogenic movement disorders; PSP = progressive supranuclear palsy; SD = standard deviation; UPDRS = Unified Parkinson's Rating Scale.

* Values are expressed as the mean ± standard deviation or n (%), unless marked otherwise.

Table 3. ^{123}I-FP-CIT SPECT and transcranial sonography evaluations in patient subgroups

	^{123}I-FP-CIT SPECT			Transcranial sonography		
Diagnosis	Striatal binding ratio	Positive	Negative	SN area	Positive	Negative
Parkinson's disease*	1.65 ± 0.80	28 (96.6%)	1 (3.4%)	0.30 ± 0.09	26 (89.6%)	3 (10.4%)
Essential tremor*	2.56 ± 0.76	1 (9.1%)	10 (90.9%)	0.18 ± 0.09	2 (18.2%)	9 (81.8%)
PMD*	1.21 ± 0.50	0 (0%)	2 (100%)	0.24 ± 0.10	0 (0%)	2 (100%)
Atypical parkinsonian syndromes						
MSA*	1.64 ± 0.15	3 (60.0 %)	2 (40%)	0.33 ± 0.07	5 (100%)	0 (0%)
PSP*	1.93 ± 0.44	2 (100%)	0 (0%)	0.22 ± 0.12?	1 (50.0%)	1 (50.0%)

^{123}I-FP-CIT SPECT = [^{123}I]ioflupane single photon emission computed tomography; MSA = multiple system atrophy; PMD = psychogenic movement disorders; PSP = progressive supranuclear palsy; SN = substantia nigra.
* Values are expressed as the mean ± standard deviation or n (%).

dopamine re-uptake transporters, assessed in the same patients by ^{123}I-FP-CIT SPECT with $r = -0.417$. These results appear to contrast with the findings presented by Spiegel et al. (2006) and Doepp et al. (2008), in which a correlation between the size of the echogenic SN area and ^{123}I-FP-CIT SPECT binding in PD patients was not found. Weise et al. (2009) hypothesized that in these studies, several patients did not actually suffer from PD, and therefore, a correlation between the echogenic SN area and dopamine re-uptake transporter activity might be more difficult to detect or absent. Nevertheless, in the present study, TCS and SPECT findings were correlated not only in PD patients, but also in patients with MSA, PSP, vascular parkinsonism, ET and PMD. This implies that more studies are needed to confirm the relationship between TCS and SPECT findings.

Results of 31 different clinical studies with a total of 1167 PD patients examined by TCS indicated increased SN echogenicity in approximately 90% of the patients, with sensitivity reaching >90 % (Brooks 2010; Vlaar et al. 2009). Also in our study, the sensitivity of TCS for diagnosis of PD was 89.7%. Nevertheless, in the recently published prospective study including 196 consecutive patients referred with unclear parkinsonism and with determination of a final diagnosis after 2 y, TCS sensitivity for the diagnosis PD was only 40% (Bouwmans et al. 2013). The lower specificity of TCS reported in our study is similar to that reported by Bouwmans et al. (2013): 60% and 61%, respectively. However, in other previously published studies, specificity ranged between 80% and 92%, for example, 82% as reported by Vlaar et al. (2008b). This may be explained by the different patient populations in the studies mentioned. For example, the specificity was higher (about 92%) in a control group consisting of healthy patients as compared with a control group consisting of patients with other movement disorders, as in our study (Doepp et al. 2008; Vlaar et al. 2008b).

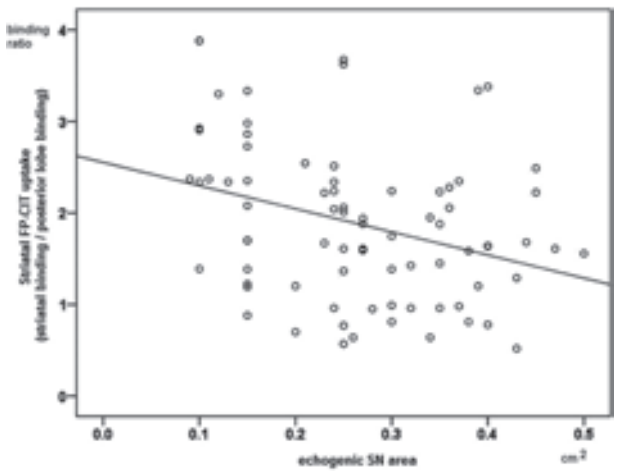

Fig. 2. Correlation between bilateral substantia nigra (SN) echogenicity measured by transcranial sonography and striatal uptake measured by [^{123}I]ioflupane single photon emission computed tomography (FP-CIT SPECT) in 49 patients.

An enlarged and hyper-echogenic SN on TCS examination was not specific for PD. The incidence of a pathologic SN on TCS in patients with atypical parkinsonian syndromes (APS) was considerably lower than that in patients with PD. Yet there was great variation between studies, and results also depended on the APS subtype (Vlaar et al. 2009). A hyper-echogenic enlarged SN was detected in 6%–43% of the patients with MSA,

Table 4. Sensitivity, specificity and predictive values of transcranial sonography and ^{123}I-FP-CIT SPECT in the diagnosis of Parkinson's disease

	Transcranial sonography		^{123}I-FP-CIT SPECT	
	Mean	95% CI	Mean	95% CI
Sensitivity	89.7%	72.7–97.8	96.6%	82.2–99.9
Specificity	60.1%	36.1–80.9	70.0%	45.7–88.1
Positive predictive value	76.5%	58.8–89.3	82.4%	65.5–93.2
Negative predictive value	80.0%	51.9–95.7	93.3%	68.1–99.8

CI = confidence interval, ^{123}I-FP-CIT SPECT = [^{123}I]ioflupane single photon emission computed tomography.

0–39% of the patients with PSP and 88% of the patients with corticobasal degeneration (Bártová et al. 2007; Vlaar et al. 2009; Walter et al. 2002, 2003). The high positivity of TCS findings in our patients with MSA (in all five patients) and PSP (in one of the two patients) may be influenced by the small numbers of patients in particular subgroups. In our previous study, a hyperechogenic enlarged SN was detected in 43% of the MSA patients (Bártová et al. 2007). In concordance with published study results, the sensitivity of TCS in the present study was lower than the sensitivity of SPECT (Doepp et al. 2008; Vlaar et al. 2007).

The dopamine transporter tracer ^{123}I-FP-CIT appears to be a very good marker of dopamine pre-synaptic activity in the brain (Kish et al. 1988; Verhoeff 2001). Its uptake in the basal ganglia is high (the ratio between specific and non-displaceable tracer uptake in striatum is about 6), allowing accurate estimates of the radioactivity concentration in the basal ganglia (Verhoeff 2001). In idiopathic PD, reduced striatal ^{123} I-FP-CIT SPECT density is caused by a reduction in the number of neurons projecting from the substantia nigra to the striatum (Kish et al. 1988; Verhoeff 2001). The number of DATs per neuron may also be lower than normal because of the attempt to increase the amount of synaptic dopamine by reducing the re-uptake (Kish et al. 1988). Many studies have reported that ^{123}I-β-CIT SPECT is helpful in PD diagnosis and has a high sensitivity (Doepp et al. 2008; Pirker et al. 2002; Vlaar et al. 2007).

In recent studies, ^{123}I-FP-CIT SPECT revealed damage to the nigrostriatal system in 70% of patients with pathologic SN hyper-echogenicity and olfactory dysfunction and in 90% of patients with pathologic SN hyper-echogenicity and mild PD (Hoehn–Yahr stage I) (Sommer et al. 2004; Spiegel et al. 2006). Normal SPECT scans in 5%–10% of clinically definitive PD patients may be explained by the disease stage of patients (Benamer et al. 2000a; Vlaar et al. 2007; Pirker et al. 2002). Previous ^{123}I-FP-CIT SPECT investigations also revealed some false-negative results, and the reported sensitivity ranged between 87% and 97% (Bouwmans et al. 2013; Doepp et al. 2008). Vlaar et al. (2008a) reported abnormal ^{123}I-FP-CIT SPECT results in 7 of 9 MSA patients, as well as in 4 of 6 PSP patients. Also, in our study, 3 of the 5 MSA patients and all PSP patients had a positive ^{123}I-FP-CIT SPECT result. The SPECT specificity obtained in our study is comparable to that reported by Bouwmans et al. (2013): 70% and 68%, respectively.

Only the SPECT-measured striatal binding ratio correlated significantly with patient age, but the agreement was only fair. This finding is in concordance with Booij et al. (2001). In our study, and also in other studies, no correlation was found between TCS-measured SN echogenicity and patient age (Berg et al. 1999; Walter et al. 2007b). Controversial results were published in studies correlating both SPECT-measured striatal binding ratios and TCS-measured SN echogenicities and disease symptom durations (Benamer et al. 2000b; Walter et al. 2007b). No such correlations were observed in the present study.

Therefore, one can hypothesize that SN hyperechogenicity can be regarded as a risk marker for PD. On the contrary, abnormal SPECT findings, as a marker of a pre-motor lesion, represent a sign of an already ongoing neurodegenerative process. Thus, it is difficult to compare TCS and SPECT findings in these subgroups of patients cross-sectionally, because PD may develop later in individuals with ET and SN hyper-echogenicity.

Some limitations of the present study should be mentioned. The main limitations of TCS examination are the insufficient bone window and the dependence on sonographer experience (Skoloudik et al. 2007; Walter et al. 2007a). The former means this method would be less useful in common clinical practice. The latter can be overcome in future studies with the use of high-end sonographic machines with fusion imaging technology and automatic detection of SN features (Verhoeff 2001; Vlaar 2007). The small numbers of patients in the subgroups, especially in the APS group, represent another limitation of the present study. It is well known that both SPECT and TCS are helpful in the differential diagnosis of PD and essential tremor, but not really useful in the differential diagnosis of PD and APS (Vlaar et al. 2007). Thus, the results of the study are dependent on the number of individuals included per subgroup.

Finally, an important fact is that TCS reveals the morphologic changes of brain structures and SPECT evaluates the functional impairment of neurotransmission. Some movement disorders differ only in structural pathology, and others differ in changes in particular neurotransmitter dysfunction. Therefore, a combination of SPECT and TCS examinations should be helpful in the diagnosis of PD and differential diagnosis of PD and APS.

CONCLUSIONS

The present study revealed a high correlation between TCS and SPECT findings in movement disorder patients, with a fair correlation between TCS-measured SN echogenic area as a marker of the morphologic changes and SPECT-measured striatal binding ratio as a marker of the functional impairment of neurotransmission in patients with parkinsonism. The sensitivity, specificity, positive predictive values and negative predictive values were similar for both methods. The combined use of TCS, as a non-invasive method, and SPECT may improve diagnosis, particularly in patients with an unclear diagnosis.

Acknowledgments—The study was supported by a grant from the Moravian-Silesian Region grant number 01947/2011/RRC.

REFERENCES

American Psychiatric Association. Diagnostic and statistical manual of mental disorders (DSM-IV-TR). 4th ed. Washington, DC: Author; 2000.

Bain P, Brin M, Deuschl G, Jankovic J, Findley L, Koller WC, Pahwa R. Criteria for the diagnosis of essential tremor. Neurology 2000;54(11, Suppl 4):S7.

Bártová P, Skoloudik D, Fadrna T, Ressner P, Kanovsky P, Herzig R. Sonographic evaluation of substantia nigra in parkinsonian syndromes. Parkinsonism Relat Disord 2007;13(Suppl 2):149.

Bártová P, Školoudík D, Ressner P, Herzig R, Kaňovský P. Correlation between substantia nigra features detected by sonography and Parkinson's disease symptoms. J Ultrasound Med 2010;29:37–42.

Benamer TS, Patterson J, Grosset DG, Booij J, de Bruin K, van Royen E, Speelman JD, Horstink MH, Sips HJ, Dierckx RA, Versijpt J, Decoo D, Van Der Linden C, Hadley DM, Doder M, Lees AJ, Costa DC, Gacinovic S, Oertel WH, Pogarell O, Hoeffken H, Joseph K, Tatsch K, Schwarz J, Ries V. Accurate differentiation of parkinsonism and essential tremor using visual assessment of [^{123}I]-FP-CIT SPECT imaging: The [^{123}I]-FP-CIT study group. Mov Disord 2000a;15:503–510.

Benamer HTS, Patterson J, Wyper DJ, Hadley DM, Macphee GJ, Grosset DG. Correlation of Parkinson's disease severity and duration with 123I-FP-CIT SPECT striatal uptake. Mov Disord 2000b; 15:692–698.

Berg D, Becker G, Zieler B, Tucha O, Hofmann E, Preier M, Benz P, Jost W, Reiners K, Lange KW. Vulnerability of the nigrostriatal system as detected by transcranial ultrasound. Neurology 1999;53: 1026–1031.

Booij J, Bermans P, Winogrodzka A, Speelman JD, Wolters EC. Imaging of dopamine transporters with [^{123}I]FP-CIT does not suggest a significant effect of age on the symptomatic threshold of disease in Parkinson's disease. Synapse 2001;39:101–108.

Bouwmans AE, Vlaar AM, Mess WH, Kessels A, Weber WE. Specificity and sensitivity of transcranial sonography of the substantia nigra in the diagnosis of Parkinson's disease: Prospective cohort study in 196 patients. BMJ Open 2013;3:4.

Brooks DJ. Imaging approaches to Parkinson disease. J Nucl Med 2010; 51:596–609.

Doepp F, Plotkin M, Siegel L, Kivi A, Gruber D, Lobsien E, Kupsch A, Schreiber SJ. Brain parenchyma sonography and 123I-FP-CIT SPECT in Parkinson's disease and essential tremor. Mov Disord 2008;23:405–410.

Gilman S, Low PA, Quinn N, Albanese A, Ben-Shlomo Y, Fowler CJ, Kaufmann H, Klockgether T, Lang AE, Lantos PL, Litvan I, Mathias CJ, Oliver E, Robertson D, Schatz I, Wenning GK. Consensus statement on the diagnosis of multiple system atrophy: American Autonomic Society and American Academy of Neurology. Clin Auton Res 1998;8:359–362.

Hughes AJ, Daniel SE, Ben-Shlomo Y, Lees AJ. The accuracy of diagnosis of parkinsonian syndromes in a specialist movement disorder service. Brain 2002;125:861–870.

Hughes AJ, Daniel SE, Kilford L, Lees AJ. Accuracy of clinical diagnosis of idiopathic Parkinson's disease: A clinico-pathologic study of 100 cases. J Neurol Neurosurg Psychiatry 1992;55:181–184.

Kish SJ, Shannak K, Hornykiewicz O. Uneven pattern of dopamine loss in the striatum of patients with idiopathic Parkinson's disease: Pathophysiologic and clinical implications. N Engl J Med 1988;318: 876–880.

Koch W, Radau PE, Hamann C, Tatsch K. Clinical testing of an optimized software solution for an automated, observer-independent evaluation of dopamine transporter SPECT studies. J Nucl Med 2005;46:1109–1118.

Litvan I, Agid Y, Calne D, Campbell G, Dubois B, Duvoisin RC, Goetz CG, Golbe LI, Grafman J, Growdon JH, Hallett M, Jankovic J, Quinn NP, Tolosa E, Zee DS. Clinical research criteria for the diagnosis of progressive supranuclear palsy (Steele– Richardson–Olszewski syndrome): Report of the NINDS-SPSP international workshop. Neurology 1996;47:1–9.

Marshall VL, Reininger CB, Marquardt M, Patterson J, Hadley DM, Oertel WH, Benamer HT, Kemp P, Burn D, Tolosa E, Kulisevsky J, Cunha L, Costa D, Booij J, Tatsch K, Chaudhuri KR, Ulm G, Pogarell O, Höffken H, Gerstner A, Grosset DG. Parkinson's disease is overdiagnosed clinically at baseline in diagnostically uncertain cases: A 3-y European multicenter study with repeat [123I]FP-CIT SPECT. Mov Disord 2009;24:500–508.

Pirker W, Djamshidian S, Asenbaum S, Gerschlager W, Tribl G, Hoffmann M, Brücke T. Progression of dopaminergic degeneration in Parkinson's disease and atypical parkinsonism: A longitudinal beta-CIT SPECT study. Mov Disord 2002;17:45–53.

Schillaci O, Chiaravalloti A, Pierantozzi M, Di Pietro B, Koch G, Bruni C, Stanzione P, Stefani A. Different patterns of nigrostriatal degeneration in tremor type versus the akinetic-rigid and mixed types of Parkinson's disease at the early stages: Molecular imaging with 123I-FP-CIT SPECT. Int J Mol Med 2011;28:881–886.

Skoloudik D, Fadrna T, Bartova P, Langova K, Ressner P, Zapletalova O, Hluštík P, Herzig R, Kaňovský P. Reproducibility of sonographic measurement of the substantia nigra. Ultrasound Med Biol 2007; 33:1347–1352.

Sommer U, Hummel T, Cormann K, Mueller A, Frasnelli J, Kropp J, Reichmann H. Detection of presymptomatic Parkinson's disease: Combining smell tests, transcranial sonography and SPECT. Mov Disord 2004;19:1196–1202.

Spiegel J, Hellwig D, Mollers MO, Behnke S, Jost W, Fassbender K, Samnick S, Dillmann U, Becker G, Kirsch CM. Transcranial sonography and [123I]FP-CIT SPECT disclose complementary aspects of Parkinson's disease. Brain 2006;129:1188–1193.

Verhoeff NPLG. Imaging presynaptic dopamine synthesis in parkinsonian syndromes. Rev Bras Psiquiatr 2001;23(Suppl I):50–52.

Vlaar AM, Bouwmans A, Mess WH, Tromp SC, Weber WE. Transcranial duplex in the differential diagnosis of parkinsonian syndromes: A systematic review. J Neurol 2009;256:530–538.

Vlaar AM, de Nijs T, Kessels AG, Vreeling FW, Winogrodzka A, Mess WH, Tromp SC, van Kroonenburgh MJ, Weber WE. Diagnostic value of 123I-ioflupane and 123I-iodobenzamide SPECT Scans in 248 patients with parkinsonian syndromes. Eur Neurol 2008a;59:258–266.

Vlaar AM, de Nijs T, van Kroomenburgh MJ, Mess WH, Winogrodzka A, Tromp SC, Weber WE. The predictive value of transcranial duplex sonography for the clinical diagnosis in undiagnosed parkinsonian syndromes: Comparison with SPECT scans. BMC Neurol 2008b;8:42.

Vlaar AM, van Kroonenburgh MJ, Kessels AG, Weber WE. Meta-analysis of the literature on diagnostic accuracy of SPECT in parkinsonian syndromes. BMC Neurol 2007;7:27.

Walter U, Behnke S, Eyding J, Niehaus L, Postert T, Seidel G, Berg D. Transcranial brain parenchyma sonography in movement disorders: State of the art. Ultrasound Med Biol 2007a;33:15–25.

Walter U, Dressler D, Wolters A, Wittstock M, Benecke R. Transcranial brain sonography findings in clinical subgroups of idiopathic Parkinson's disease. Mov Disord 2007b;22:48–54.

Walter U, Niehaus L, Probst T, Benecke R, Meyer BU, Dressle D. Brain parenchyma sonography discriminates Parkinson's disease and atypical parkinsonian syndromes. Neurology 2003;60:74–77.

Walter U, Wittstock M, Benecke R, Dressler D. Substantia nigra echogenicity is normal in non-extrapyramidal cerebral disorders but increase in Parkinson's disease. J Neural Transm 2002;109: 191–196.

Weise D, Lorenz R, Schliesser M, Schirbel A, Reiners K, Classen J. Substantia nigra echogenicity: A structural correlate of functional impairment of the dopaminergic striatal projection in Parkinson's disease. Mov Disord 2009;24:1669–1675.

Williams DT, Ford B, Fahn S. Phenomenology and psychopathology related to psychogenic movement disorders. AdvNeurol 1995;65: 231–257.

6

Changes in middle cerebral artery velocimetry of fetuses diagnosed postnatally with mild or moderate hemolytic disease

Šimetka O, Pětroš M, Lubuský M, Liska M, Doležálková E, Matura D, Wiedermannová H, Procházka M

Originally published in Acta Obstetricia et Gynecologica Scandinavica, 2014, vol. 93, no. 10, p. 1059-1064

Consent to the publication of 19th March 2015

AOGS
ACTA Obstetricia et Gynecologica Scandinavica

AOGS MAIN RESEARCH ARTICLE

Changes in middle cerebral artery velocimetry of fetuses diagnosed postnatally with mild or moderate hemolytic disease

ONDREJ SIMETKA[1,2], MICHAL PETROS[1], MAREK LUBUSKY[3], MIROSLAV LISKA[4], ERIKA DOLEZALKOVA[1], DAVID MATURA[1,2], HANA WIEDERMANNOVA[5] & MARTIN PROCHÁZKA[3]

[1]Department of Obstetrics and Gynecology, University Hospital Ostrava, Ostrava, [2]Faculty of Surgical Studies, University of Ostrava, Ostrava, [3]Department of Obstetrics and Gynecology, University Hospital Olomouc, Olomouc, [4]Department of Informatics and Computers, University of Ostrava, Ostrava, and [5]Department of Neonatology, University Hospital Ostrava, Ostrava, Czech Republic

Key words
Middle cerebral artery, peak systolic velocity, alloimmunization, Doppler ultrasound, fetal anemia

Correspondence
Marek Lubusky, Department of Obstetrics and Gynecology, University Hospital Olomouc, I.P. Pavlova 6, 77520 Olomouc, Czech Republic.
E-mail: marek@lubusky.com

Conflicts of interest
The authors have stated explicitly that there are no conflicts of interest in connection with this article.

Please cite this article as: Simetka O, Petros M, Lubusky M, Liska M, Dolezalkova E, Matura D, et al. Changes in middle cerebral artery velocimetry of fetuses diagnosed postnatally with mild or moderate hemolytic disease. Acta Obstet Gynecol Scand 2014; 93: 1059–1064.

Received: 18 February 2014
Accepted: 6 August 2014

DOI: 10.1111/aogs.12477

Abstract

Objectives. To determine the longitudinal trends of middle cerebral artery peak systolic velocity (MCA PSV) in fetuses with mild or moderate hemolytic disease according to the need for postnatal therapy. *Design.* Prospective cohort study. *Setting.* University referral center. *Sample.* Twenty-three fetuses from singleton alloimmunized pregnancies. *Methods.* Serial measurements of MCA PSV were performed. After delivery, newborns were grouped by the need for postnatal management into mild hemolytic disease, which required no or only phototherapy (n = 14, group 1), and moderate hemolytic disease, where postnatal top-up or exchange transfusions were required (n = 9, group 2). *Main outcome measures.* Serial Doppler MCA PSV data transformed to multiples of the median, analyzed with linear regression and exponential models. *Results.* We performed 83 measurements in group 1: 3-8 per fetus; mean GA at inclusion, 23 weeks and 65 measurements in group 2: 4-15 per fetus; mean GA at inclusion, 22 weeks. The estimated mean slopes of the MCA PSVs increased with the degree of postnatal therapy required (group 1: MCA PSV = 0.003 GA + 1.298; group 2: MCA PSV = 0.035 GA + 0.436). The relative average increments (RAI) were 4.7% and 7.1%, respectively. The two groups exhibited significant differences in mean slope and RAI ($p<0.05$). *Conclusions.* Fetuses that required postnatal transfusions due to hemolytic disease showed an enhanced progressive increase in MCA PSVs compared to those without transfusion requirement. This information might enable their identification during pregnancy.

Abbreviations: AAI, absolute average increment; GA, gestational age; HDN, hemolytic disease of newborns; MCA, middle cerebral artery; MoM, multiples of the median; PSV, peak systolic velocity; RAI, relative average increment.

Introduction

Middle cerebral artery (MCA) peak systolic velocity (PSV) Doppler velocimetry is a standard method for noninvasively diagnosing fetal anemia. Accelerated blood velocity in the MCA enables identification of anemic fetuses (1–3). Previous studies have demonstrated a

Key Message

Fetuses that will require postnatal transfusions due to hemolytic disease show progressive elevations in middle cerebral artery peak systolic velocity. This feature provides a tool that can be used during the pregnancy to determine whether the fetus will require transfusion therapy after delivery.

correlation between the MCA PSV and fetal hemoglobin levels (4–8). In mild fetal anemia, there is very little or no increment in blood velocity in the MCA; however, in moderate and severe fetal anemia, the MCA blood velocity increases and the detection accuracy of anemia improves. When anemia becomes very severe (hemoglobin levels of 10–30 g/L), the velocity does not increase further (7). A single MCA PSV measurement below 1.5 multiples of the median (MoM) of the Mari nomogram cannot reassure the investigator about the future well-being of fetuses at risk of hemolytic disease, as it does not describe how rapidly the anemia develops (9). Therefore, serial measurements are necessary. Nevertheless, 70% of fetuses at risk of anemia due to red blood cell alloimmunization of the mother will either have no anemia or will become only mildly anemic during the pregnancy and will therefore not require transfusion (2). To our knowledge, only one previous retrospective study analyzed longitudinal measurements (9). There it was demonstrated that by examining the slope of the values over time, instead of individual values, one could detect in advance which fetuses were at risk of developing anemia. The objective of the present study was to describe the longitudinal trends in MCA PSV Doppler measurements in fetuses diagnosed with mild or moderate hemolytic disease postnatally, and managed according to the degree of disease and to determine whether fetuses that will postnatally require top-up or exchange transfusions could be noninvasively identified during pregnancy.

Material and methods

The data were prospectively collected at the tertiary care center at the Department of Obstetrics and Gynecology, University Hospital Ostrava, Ostrava, Czech Republic. We included fetuses with red blood cell maternal alloimmunization clinically relevant antibodies in significant titer (D $\geq$ 1:32, Kell $\geq$ 1:8, other non-D antibodies $\geq$ 1:32). In one case, prenatal fetal genotyping was performed from free-fetal DNA isolated from the mother; in the remaining cases, the neonatal blood group phenotype was identified after birth. All fetuses underwent a detailed prenatal ultrasound evaluation. The expected date of delivery was established by first trimester crown–rump length. All fetuses were followed up with a minimum of three or more serial MCA PSV measurements. The first three measurements were done weekly. When the MCA PSV was <1.5 MoM and the slope of the MCA PSV did not indicate that it would cross 1.5 MoM within the next 2–3 weeks, we extended the interval to 2–3 weeks. Apart from that, the levels of antibodies were monitored every second to fourth week depending on the antibody titer. During every visit a basic ultrasound scan was performed. The decision about delivery was based on the consensus of at least two specialists in maternal fetal medicine depending on cardiotocogram, PSV and biophysical profile. Two sonographers performed the measurements on one ultrasonographic machine (Voluson E8 BT08; General Electric, GE Healthcare Technologies, Wauwatosa, WI, USA).

The MCA PSV was evaluated with the standardized technique, previously described by Mari et al. (10). In brief, a transverse section of the brain, which included the thalamus and the cavum septi pellucidi, was identified during a period of fetal rest, and the circle of Willis was imaged with color Doppler ultrasonography. The MCA proximal to the transducer was enlarged until it occupied more than 50% of the image, and could be visualized over its entire length; the sample volume (1 mm) was superimposed on the MCA, 2 mm after its origin from the internal carotid artery. The angle between the direction of blood flow and the ultrasound beam was maintained as closely as possible to 0°, and when uniform waveforms (between 15 and 30) were recorded, the highest point of the waveform (the PSV) was measured.

All newborns underwent clinical examination. Neonatal blood counts from the umbilical vein were performed immediately after delivery. Hemolytic disease of newborns (HDN) was confirmed by positive Coombs test, anemia and/or elevated bilirubin at birth or its sharp rise within 24 hours of birth. Further management and treatment indications were performed according to the American Academy of Pediatrics guidelines and the Czech Society of Neonatology guidelines (11,12). The newborns were later assigned to one of two groups: group 1 required no therapy or phototherapy only (mild HDN); group 2 required a postnatal top-up or exchange transfusion (moderate HDN).

Data analysis

Two types of the mathematical analyses were performed for both groups, based on an exponential model and a linear model. Serial Doppler measurements of MCA PSV from individual fetuses were analyzed with the exponential model ($[\text{MCA PSV}] = K.e^{RAI.GA}$), where K is a proportional parameter, RAI is the relative average increment and GA is gestational age. The data were fitted with the model to determine the rate of change. From these data, the RAI in the MCA PSV as a function of GA was calculated for the two groups. The mean RAI in the MCA PSV as function of GA was calculated for each group with the confidence interval (CI), and exponential trends were modeled.

The measurements from individual fetuses were analyzed with a simple linear regression model ($[\text{MCA PSV}] = AAI.GA + L$), where L is a proportional parameter and

Table 1. Maternal and neonatal clinical characteristics in groups with different degrees of hemolytic disease of newborn.

Parameter	Mild HDN (n = 14)	Moderate HDN (n = 9)	p-value[a]
Maternal age (years)	29 (22–41)	32 (27–38)	0.33
Parity	2 (1–7)	2 (2–5)	0.49
Gestational age at inclusion (weeks)	21.5 (18–32)	22 (18–29)	0.59
Gestational age at delivery (weeks)	38 (35–41)	36 (34–37)	0.01
Birthweight (g)	3090 (2500–3800)	2450 (1950–3420)	0.01
Number of measurements	6.5 (3–8)	7 (4–15)	0.42
Hemoglobin UV (g/L)	152 (121–179)	116 (97–173)	<0.01
Total bilirubin UV (μmol/L)	39.9 (27.2–54.9)	78.8 (58.1–107.4)	<0.01
Reticulocytes UV (%)	3.8 (1.3–7.6)	4.6 (0.2–11.3)	0.12
Neonatal intensive care unit (days)	0 (0–6)	6 (2–23)	<0.01
Phototherapy (hours)	0 (0–316)	201 (107–399)	<0.01
Neonates who received transfusions	0	9	–

Data represent the median (range).
HDN, hemolytic disease of newborn; UV, umbilical vein.
[a]Mann–Whitney *U*-test for independent samples.

AAI (absolute average increment) represents the mean rate of change in the MCA PSV (mean slope). The mean slope of the MCA PSV as a function of GA was calculated for each group,and longitudinal trends were modeled.

Differences between and within the groups were evaluated with the Mann–Whitney *U*-test for independent samples. The values of MCA PSV were expressed in units of MoM, according to Mari et al. (2). A p-value <0.05 indicated statistical significance. MedCalc software (Version 12.7.5.0; MedCalc Software, Mariakerke, Belgium) and Office Excel 2007 (Microsoft Corporation, Redmond, WA, USA) were used for calculations and trend modeling.

Results

A total of 148 measurements were performed on 23 fetuses. Group 1 (mild HDN) included 14 fetuses with 83

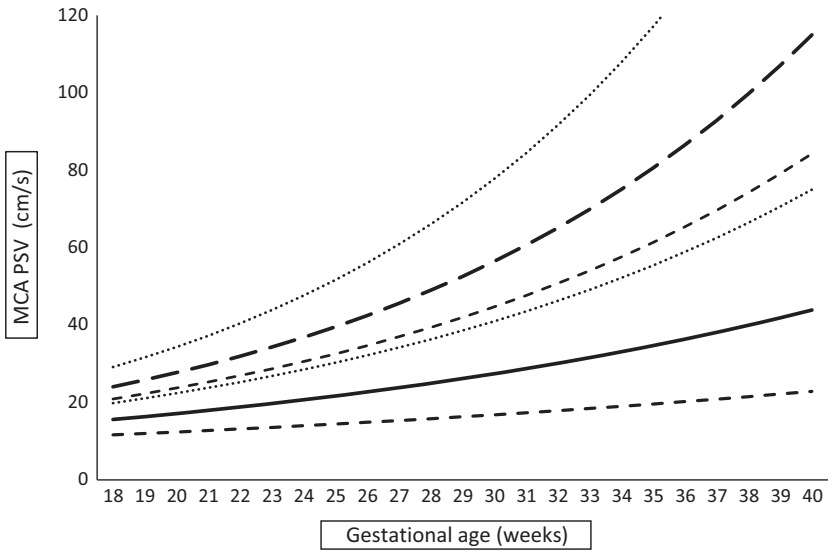

Figure 1. Serial Doppler measurements of the middle cerebral artery peak systolic velocity (MCA PSV) increased exponentially as a function of gestational age (GA). Each heavy line represents the average exponential fit to data from fetuses with either mild hemolytic disease of the newborn (continuous line, MCA PSV = $Ke^{0.047.GA}$) or moderate hemolytic disease of the newborn (heavy dashed line, MCA PSV = $Ke^{0.071.GA}$). Only the exponential lines that were fitted to at least three serial measurements were included in the average lines shown. The dotted lines represent the confidence limits.

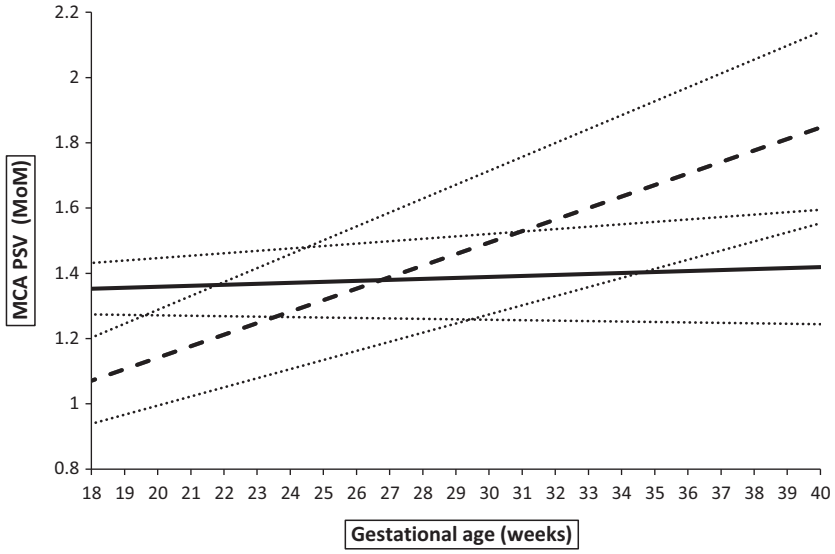

Figure 2. Serial Doppler measurements of the middle cerebral artery peak systolic velocity (MCA PSV) observed over time were transformed to multiples of median (MoM) units, according to the Mari reference curve. Lines represent the average linear regression fits for data from fetuses with either mild hemolytic disease of the newborn (continuous line, MCA PSV = 0.003.GA + 1.298) or moderate hemolytic disease of the newborn (heavy dashed line, MCA PSV = 0.035.GA + 0.436), where GA is gestational age. Only the linear regression lines that were fitted to at least three serial measurements were included in the average lines shown. The dotted lines represent the confidence limits.

measurements (range 3–8/fetus). Group 2 (moderate HDN) included nine fetuses with 65 measurements (range 4–15/fetus). The characteristics of the study population are given in Table 1. All women were Caucasian. All fetuses were delivered after 34 weeks of gestation. Red cell alloantibodies observed in the mild HDN group included D (n = 8), c (n = 1), E (n = 2), K (n = 2) and s (n = 1). Those observed in the moderate HDN group included D (n = 8) and E (n = 1). The umbilical venous blood hemoglobin levels differed significantly between the groups.

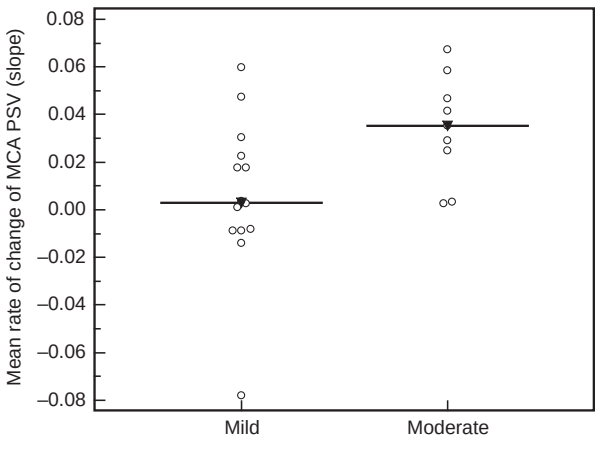

Figure 3. Mean rates of change in the middle cerebral artery peak systolic velocity in fetuses with mild or moderate hemolytic disease of newborn. Individual values and medians are shown.

In the exponential model, the estimated mean average increment for mild HDN (MCA PSV = K e $^{0.047.GA}$) was 4.7% and for moderate HDN (MCA PSV = K e $^{0.071.GAx}$) 7.1% (Figure 1). In individual cases RAI increased with the requirement for more intense postnatal therapy and was significantly different between fetuses with mild and those with moderate hemolytic disease ($p < 0.05$).

In the linear model, the estimated mean rate of change for both mild HDN (MCA PSV = 0.003.GA + 1.298) and moderate HDN (MCA PSV = 0.035.GA + 0.436) increased with the degree of required postnatal therapy. The mean slopes were 0.3 and 3.5% for fetuses with mild and moderate HDN, respectively (Figure 2) and were significantly different between the two groups ($p < 0.05$; Figure 3).

Discussion

This study demonstrated that the plot of at least three serial MCA PSV measurements over time exhibited a slope that increased with the degree of HDN. We found a significant difference in mean slope and RAI of MCA PSV between fetuses with mild and moderate HDN. This finding suggested that it may be possible to differentiate between fetuses that develop mild HDN but require little or no postnatal therapy and fetuses that develop moderate HDN, which requires a top-up or exchange transfusion

after delivery. This information might be useful in the management of at-risk pregnancies, because it can identify which fetuses will benefit from closer surveillance during pregnancy and better planning of the delivery. For example, identification of a fetus with mild HDN that will require low-intensity therapy could provide a basis for postponing the delivery, which would decrease the risk of preterm delivery. In fact, the more advanced GA in the mild HDN group (38 vs. 36 weeks; Table 1) reflects such a policy.

To our knowledge, to date, only one previous retrospective study by Detti et al. showed that, by determining the slope of the line joining at least three measurements, it was possible to identify a fetus that had developed moderate or severe anemia. They showed that the rate of increase in MCA PSV values was greater in moderate or severe anemia than when there was mild or no anemia (9). In the present study, we aimed to extend that observation. Our results showed that Doppler measurements were sufficiently sensitive to clearly distinguish between fetuses with moderate hemolytic disease and those with mild hemolytic disease. This finding represents a means to determine whether a fetus will require transfusion after delivery.

The main strengths of this study were the prospective collection of the data, the comparatively large number of measurements, that all measurements were performed with one type of ultrasound machine and only two sonographers who used one standardized protocol. The primary weakness of the study was the limited reproducibility of the results due to its monocentric character. Larger, multicenter studies are needed to confirm our findings.

We support the caution stated by Detti et al. that a single MCA PSV measurement below the cut-off point of 1.50 MoM should not reassure the investigator about the future well-being of a fetus at risk for anemia. Instead of focusing on a single value, the investigator should consider the RAI in the MCA PSV. The rate of increase informs the investigator in advance of whether the fetus is at risk for developing HDN, even when the MCA PSV values are in the healthy range. Patient counseling or planning the next visit can be based on the calculated trend in the MCA PSV, and the physician can project the approximate time that anemia is likely to develop.

We have demonstrated that fetuses that are likely to require postnatal transfusion due to hemolytic disease show a more rapid increase in MCA PSV than those who will manage without transfusions. This feature provides a tool that can be used during the pregnancy to determine whether the fetus will require transfusion therapy after delivery.

Funding

This study was supported by a grant from the Ministry of Health of the Czech Republic IGA NT-12225-4/2011.

References

1. Mari G, Adrignolo A, Abuhamad AZ, Pirhonen J, Jones DC, Ludomirsky A, et al. Diagnosis of fetal anemia with Doppler ultrasound in the pregnancy complicated by maternal blood group immunization. Ultrasound Obstet Gynecol. 1995;5:400–5.
2. Mari G, Deter RL, Carpenter RL, Rahman F, Zimmerman R, Moise KJ Jr, et al. Noninvasive diagnosis by Doppler ultrasonography of fetal anemia due to maternal red-cell alloimmunization. Collaborative Group for Doppler Assessment of the Blood Velocity in Anemic Fetuses. N Engl J Med. 2000;342:9–14.
3. Zimmerman R, Carpenter RJ Jr, Durig P, Mari G. Longitudinal measurement of peak systolic velocity in the fetal middle cerebral artery for monitoring pregnancies complicated by red cell alloimmunisation: a prospective multicentre trial with intention-to-treat. BJOG. 2002;109:746–52.
4. Teixeira JM, Duncan K, Letsky E, Fisk NM. Middle cerebral artery peak systolic velocity in the prediction of fetal anemia. Ultrasound Obstet Gynecol. 2000;15:205–8.
5. Detti L, Oz U, Guney I, Ferguson JE, Bahado-Singh RO, Mari G, et al. Doppler ultrasound velocimetry for timing the second intrauterine transfusion in fetuses with anemia from red cell alloimmunization. Am J Obstet Gynecol. 2001;185:1048–51.
6. Delle Chiaie L, Buck G, Grab D, Terinde R. Prediction of fetal anemia with Doppler measurement of the middle cerebral artery peak systolic velocity in pregnancies complicated by maternal blood group alloimmunization or parvovirus B19 infection. Ultrasound Obstet Gynecol. 2001;18:232–6.
7. Mari G, Detti L, Oz U, Zimmerman R, Duerig P, Stefos T. Accurate prediction of fetal hemoglobin by Doppler ultrasonography. Obstet Gynecol. 2002;99:589–93.
8. Stefos T, Cosmi E, Detti L, Mari G. Correction of fetal anemia on the middle cerebral artery peak systolic velocity. Obstet Gynecol. 2002;99:211–15.
9. Detti L, Mari G, Akiyama M, Cosmi E, Moise KJ Jr, Stefor T, et al. Longitudinal assessment of the middle cerebral artery peak systolic velocity in healthy fetuses and in fetuses at risk for anemia. Am J Obstet Gynecol. 2002;187:937–9.
10. Mari G, Abuhamad AZ, Cosmi E, Segata M, Altaye M, Akiyama M. Middle cerebral artery peak systolic velocity: technique and variability. J Ultrasound Med. 2005;24:425–30.

11. American Academy of Pediatrics Subcommittee on Hyperbilirubinemia. Management of hyperbilirubinemia in the newborn infant 35 or more weeks of gestation. Pediatrics. 2004;114:297–316.
12. Dort J, Tobrmanova H. Hyperbilirubinemie novorozence. Doporucený postup péce. [Hyperbilirubinemia of the newborn. Clinical Guideline] (in Czech). Available online at: http://www.neonatologie.cz/fileadmin/user_upload/Doporuceni_CNEOS/Hyperbilirubinemie.pdf (accessed 20 April, 2010).

7

Anaerobic metabolism associated with traumatic hemorrhagic shock monitored by microdialysis of muscle tissue is dependent on the levels of hemoglobin and central venous oxygen saturation: a prospective, observational study

Burša F and Pleva L

Originally published in Scandinavian Journal of Trauma Resuscitation & Emergency Medicine, 2014, vol. 22, no. Article no. 11, p. 1-9

SCANDINAVIAN JOURNAL OF
trauma, resuscitation
& emergency medicine

ORIGINAL RESEARCH Open Access

Anaerobic metabolism associated with traumatic hemorrhagic shock monitored by microdialysis of muscle tissue is dependent on the levels of hemoglobin and central venous oxygen saturation: a prospective, observational study

Filip Burša[1*] and Leopold Pleva[2]

Abstract

Background: Traumatic hemorrhagic shock resulting in tissue hypoxia is a significant cause of morbidity and mortality in polytraumatized patients. Early identification of tissue hypoxia is possible with microdialysis. The aim of this study was to determine the correlation between a marker of tissue hypoxia (L/P; lactate to pyruvate ratio) and selected parameters of systemic oxygen delivery (Hb; hemoglobin) and oxygen extraction ($ScvO_2$; central venous oxygen saturation). We also investigated the severity of tissue hypoxia over the course of care.

Methods: Adult patients with traumatic hemorrhagic shock were enrolled in this prospective, observational study. Microdialysis of the peripheral muscle tissue was performed. Demographic data and timeline of care were collected. Tissue lactate, pyruvate, glycerol, glucose levels, hemoglobin, serum lactate and oxygen saturation of the central venous blood ($ScvO_2$) levels were also measured.

Results: The L/P ratio trend may react to changes in systemic hemoglobin levels with a delay of 7 to 10 hours, particularly when systemic hemoglobin levels are increased by transfusion. Decrease in tissue L/P ratio may react to increase in $ScvO_2$ with a delay of up to 10 hours, and such a decrease may signify elimination of tissue hypoxia after transfusion. We also observed changes in the L/P trend in the 13 hours preceding a change in the hemoglobin level. Fluid administration, which is routinely used as a first-line treatment of hypovolemic shock, can cause hemodilution and decreased hemoglobin. When $ScvO_2$ decreases, increase in L/P ratio may precede the $ScvO_2$ trend by 10 or 11 hours. An increase in the L/P ratio is an early warning sign of insufficient tissue oxygenation and should lead to intensive observation of hemoglobin levels, $ScvO_2$ and other hemodynamic parameters. Patients who were treated more rapidly had lower maximal L/P values and a lower degree of tissue ischemia.

Conclusion: The L/P ratio is useful to identify tissue ischemia and can estimate the effectiveness of fluid resuscitation. An increase in the L/P ratio is an early warning sign of inadequate tissue oxygenation and should lead to more detailed hemodynamic and laboratory monitoring. This information cannot usually be obtained from global markers.

Keywords: Microdialysis, Shock, Lactate, Hemoglobin

* Correspondence: bursaf@seznam.cz
[1]Department of anesthesiology and intensive care medicine, University Hospital Ostrava, Faculty of Medicine Universitas Ostrava, 17 listopadu, 1790 Ostrava-Poruba, Czech Republic
Full list of author information is available at the end of the article

Background

Polytrauma is the most frequent cause of death in adults up to 40 years old, and the incidence of death by trauma is 60-80/100,000 traumas in developed countries. A key cause of morbidity and mortality in polytraumatized patients is hemorrhagic shock. Hemorrhage leads to decreased oxygen delivery to tissues and causes severe tissue hypoxia and oxygen debt, which is a core cause of multi-organ failure [1]. Hemoglobin is one of the determinants of oxygen delivery, and one of the first compensatory reactions to a decrease in hemoglobin is an increase in oxygen extraction and thus decreased central venous oxygen saturation ($ScvO_2$). The aim of this study was to investigate the dependence of tissue hypoxia on hemoglobin and $ScvO_2$ levels.

Adequate therapy of hemorrhagic shock is guided by the clinical status of the patient and global parameters of circulation and metabolism. Identification of both occult and inadequately resuscitated shock is a major clinical problem, and occult shock can be present with normal hemodynamics [2]. Markers for assessing the degree and duration of shock are still controversial. Clinicians can use heart rate, blood pressure, urine output, invasive hemodynamic monitoring of cardiac output including oxygen delivery and consumption, central venous oxygen saturation or metabolic markers such as lactate and base deficit to guide their therapy. Elevated blood lactate levels are associated with increased mortality and morbidity and can be elevated without clinical signs of shock [3]. Shock is a state of hypoperfusion at the cellular level that occurs when the delivery of oxygen (DO_2) to tissues falls below the tissue oxygen consumption (VO_2). Oxygen delivery is dependent on blood flow and arterial oxygen content. An imbalance between the delivery and consumption of oxygen leads to the development and accumulation of an oxygen debt. Different DO_2 distributions to various tissue beds may result in isolated organ ischemia before the occurrence of whole-body ischemia and before the detection of elevated systemic markers of ischemia. Decreased DO_2 to critical oxygen delivery levels, when increased oxygen extraction past the extraction limit is not possible, causes a proportional decrease in VO_2 and the emergence of an oxygen debt. This phenomenon leads to multi-organ dysfunction syndrome, which is a leading cause of morbidity and mortality in trauma. Resuscitation efforts should be focused on preventing further oxygen debt accumulation and repayment of the current oxygen debt. The main problem is the resolution of the emerging oxygen debt because its origin is at the cellular level [4]. Changes at the level of the macrocirculation are preceded by changes at the level of individual cells, the smallest capillaries and the extracellular fluid. Neither the effective supply of oxygen required by cells nor their ability to utilize that oxygen are known. Timely recognition of changes in metabolism at the cellular level may lead to more effective treatment of patients.

Resuscitation management in polytraumatized patients with hemorrhagic shock has been well described [5]. The major tasks are rapidly and correctly identifying severely traumatized patients and the early identification of patients with severe hemorrhagic shock. In addition to vital signs, either serum lactate levels or base deficit measurements are recommended as sensitive tests to estimate the extent of the shock. It is expected that lactate levels will track the oxygen debt, but in some clinical conditions, lactate levels may normalize without tissue oxygen debt resolution [6]. The key issue is the type and amount of fluid therapy that is needed to restore oxygen delivery and repay the oxygen debt. Low-volume resuscitation is recommended, including the use of vasopressors and fluid administration, with a hemoglobin target of 7 to 9 g/dl [5]. The administration of fluids in hemorrhagic shock can be sufficient to maintain adequate oxygen delivery to tissues but may not be high enough to dislodge clots, leading to deterioration of the coagulation pathway and increased blood loss. Eliminate of tissue hypoxia based on L/P normalization could be an exact end-point for fluid administration. Improvements in monitoring techniques could influence outcomes in these challenging patients [7].

Capillaries and the extracellular fluid envelope cells and form a network through which nutrients and oxygen are distributed and metabolic products are removed. All these molecules can be monitored by analysis of the extracellular fluid with microdialysis. Monitoring by microdialysis could help guide the therapy of critically ill patients [8].

Microdialysis consists of the continuous collection of extracellular fluid with a microdialysis probe inserted into the tissue and subsequent analysis of this dialysate using a biochemical analyzer. The microdialysis probe, due to its behavior and construction, imitates a blood capillary. The probe can be inserted into any tissue. Numerous studies have described its use in the liver, intestines, muscle and adipose tissue [9-11]. After insertion of the probe into the tissue, the probe comes into contact with the extracellular fluid. The probe is continually flushed with a solution of known composition at a set perfusion speed. This process enables an exchange of substances between the dialysis solution and the extracellular fluid. The dialysate is subsequently collected into microvials and analyzed.

The primary substances that provide information about the degree of anaerobic metabolism and energy use include lactate, pyruvate, glycerol and glucose. The serum lactate level is the result of both lactate production, which occurs during ischemia or stress, and consumption, which occurs as the lactate enters the metabolism in the form of an energetic substrate in tissues such as the liver, heart or

brain. The tissue lactate level is solely the result of lactate production. The arterial serum lactate concentration, which is routinely monitored, reflects the condition of the whole organism. However, normal serum lactate values do not provide any information about the regional state of tissues. Patients in shock exhibit a difference in the level of lactate between the tissues and the blood [12]. The most important value is the lactate/pyruvate (L/P) ratio in the extracellular fluid, which serves as a timely marker of emerging ischemia and allows for the monitoring of hemorrhagic shock [13,14]. An increase in the L/P ratio to > 25 indicates the onset of anaerobic metabolism [15]. The L/P ratio may be helpful in discriminating between different mechanisms of hyperlactatemia and to distinguish the anaerobic portion of lactate production. Hyperlactatemia and a simultaneously elevated L/P ratio in patients is associated with a higher mortality than hyperlactatemia with a normal L/P ratio. The L/P ratio is therefore a more complex and precise marker of ischemic conditions [16]. When using the L/P ratio, differences in the lactate levels between ischemic and non-ischemic tissues can be distinguished [17].

Monitoring of the tissue metabolism and microcirculation is a topic in many studies. The main development of this method has been in neurocritical care, and microdialysis has become an important component of multimodal monitoring [18]. The Brain Trauma Foundation guidelines recommend tissue metabolism monitoring. Microdialysis has been shown to be effective in septic shock [19], but septic shock exhibits a different type of microcirculatory dysfunction compared with hemorrhagic shock [20]. Blood transfusion results in a decrease in the L/P ratio in septic patients [21]. The L/P ratio may detect organ ischemia earlier than an increase in intra-abdominal pressure and much earlier than signs of organ failure due to abdominal compartment syndrome [22]. Microdialysis also allows for monitoring of the levels of pharmaceuticals in tissues, the availability of antibiotics and chemotherapeutics, and the immunological state of patients by analyzing tissue cytokines [23-27]. Microdialysis is a sufficiently sensitive method for monitoring anaerobic metabolism and it positively correlates with pro-inflammatory markers [28]. This technique can also be used during surgery or transplantation [29]. A slight modification of the method makes it suitable for monitoring the degree of blood perfusion in individual tissues through blood-flow markers, such as ethanol [30] or urea [31-33]. Microdialysis shows great theoretical potential for use in experimental and clinical medicine.

The primary goal of this study was to determine the correlation between a marker of tissue hypoxia (L/P ratio) and selected parameters of systemic oxygen delivery (Hb; hemoglobin) and oxygen extraction ($ScvO_2$; central venous oxygen saturation). The secondary goal was to investigate the severity of tissue hypoxia during the course of care (pre-hospital care, care in the emergency department and operating room care).

Methods

Polytrauma patients between 18 and 60 years of age were enrolled in this prospective, observational study. All the participants presented with signs of serious traumatic hemorrhagic shock with an estimated blood loss exceeding 1 l. Monitoring was initiated as soon as possible after admission to the emergency department and always within 6 hours. The recorded parameters included demographic data, timeline of care, hemoglobin level, $ScvO_2$ level and serum lactate level. A CMA 60 microdialysis probe (CMA Microdialysis AB, Stockholm, Sweden) was placed into the deltoid muscle. We used CMA Perfusion Fluid T1 dialysis solution (a lactate-free Ringer solution). Perfusion was accomplished with a CMA 106 pump at a constant speed of 0.3 μl/min. Subsequent analysis was performed with the CMA Iscus Flex (CMA Microdialysis AB) analyzer using a set of reagents for the analysis of lactate, pyruvate, glycerol and glucose (CMA Reagent Set A). The tissue values were analyzed in 1-hour intervals. Complete blood count and $ScvO_2$ were measured in 8-hour intervals, but at least every 2 hours following the administration of blood products, using a biochemical analyzer (Roche Cobas b221 OMNI S). The normal tissue concentrations of the examined metabolites are presented in Table 1. The ethics committee University hospital Ostrava in Czech Republic approved the study and each of the study subjects signed an informed consent form approved by the ethics committee.

We used R software version 2.15.2 for the statistical analysis. The data were divided into time intervals by linear interpolation. A total of 30 time shifts of one hour were assessed independently for hemoglobin and $ScvO_2$, resulting in 30^2 different models. For each model, we tested the dependence with a t-test adjusted by the Holm scheme for multiple comparisons. The results of the tests are depicted in the form of a heat map. On this map, every point represents an individual model for a time shift of the trends in hemoglobin and $ScvO_2$ towards the L/P ratio. The colors represent the value of statistical significance, with the deep red color representing statistical

Table 1 Cut-off values for the tissue concentrations of metabolites in muscle tissue

Glucose	5	mmol/l
Lactate	2	mmol/l
Pyruvate	120	μmol/l
Lactate/Pyruvate	>25	
Glycerol	200	μmol/l

(Valid for flow at 0.3 μl/min and a 3-cm membrane length).

significance of $p < 0.05$. We also investigated whether a correlation existed between the duration of pre-hospital care, the care provided in the emergency department, the duration of surgical procedures, and the L/P ratio (T_{ICU} = sum of prehospital care, care in the emergency department and operative time, it is time before ICU admission).

Results

A total of 36 patients were included in the statistical analysis.

The correlation between the L/P ratio and its dependence on the level of hemoglobin and $ScvO_2$ in time shifts from −15 to +15 hours is shown in Figure 1. The red areas indicate the strongest correlation ($p = 0.05$). A strong correlation was found between the trend of the L/P ratio and hemoglobin from −7 to −10 hours and in the +13 hour. In other words, the tissue L/P ratio may react to changes in systemic hemoglobin values with a 7- to 10-hour delay. However, it may also manifest up to 13 hours in advance. Similar results were obtained for the $ScvO_2$ trend, which showed a strong correlation in hour −10 and between hours +10 and +11.

Table 2 illustrates the times of care; the highest L/P ratios and the lowest hemoglobin values in the first 12 and 24 hours; the time during which the patients had L/P ratios > 25, 30 and 35; and the median and mean L/P ratios in individual patients.

Figure 2 presents the duration of tissue ischemia with L/P ratios exceeding 25 according to the length of care. In the $T_{ICU} \leq 240$ minutes treatment group, the median value of the maximal L/P ratio in the first 12 resp. 24 hours was 22.9 resp. 23.55. For the group $T_{ICU} > 240$ minutes, the corresponding values of the maximal L/P ratio was 30.3 in the first 12 hours and 29.15 in the first 24 hours. The duration of the period in which the L/P ratio was > 25 was 1 hour in the faster treatment group and 7.5 hours in the group with the longer treatment duration ($p = 0.05$). The severity of the trauma was comparable in both groups (the ISS score in the $T_{ICU} \leq 240$ minutes group was 41, and it was 45 in the $T_{ICU} > 240$ minutes group), and both groups had the same average age (41 years in the $T_{ICU} \leq 240$ minutes group and 39 years in the $T_{ICU} > 240$ minutes group).

Discussion

If we attempt to draw clinical conclusions from the monitored tissue values, it is very important to understand that the tissue values represent the state of cells in the monitored area only. The aim of this study was determine how these values correspond to the global parameters that are routinely measured in the intensive care unit, particularly

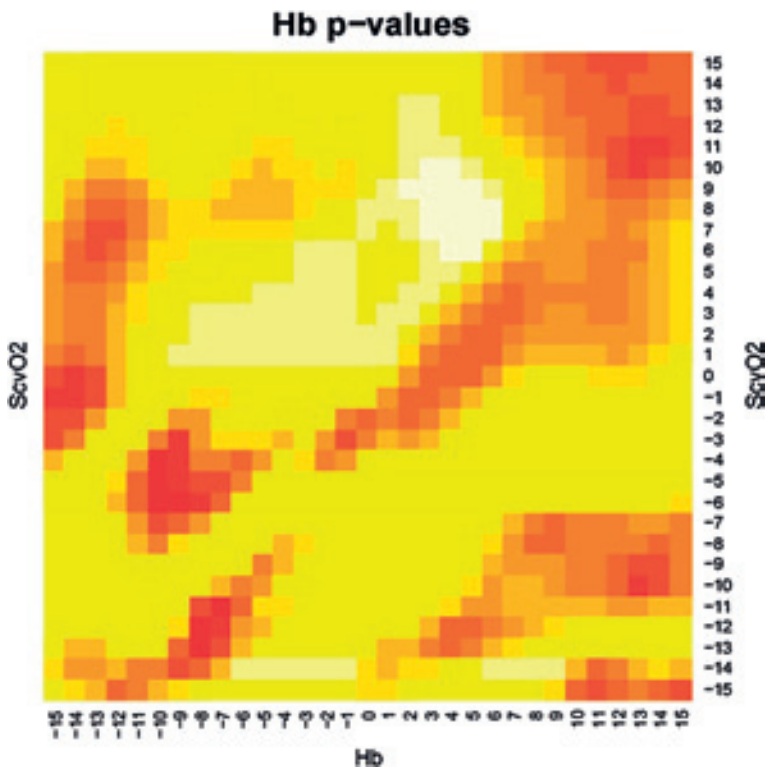

Figure 1 Correlation of the tissue lactate/pyruvate ratio with time shifts in hemoglobin levels (Hb) and central venous oxygen saturation ($ScvO_2$). Significance is indicated with colors: the areas of deep red color represent $p < 0.05$.

Table 2 Monitored values in individual patients

ID	Gender	Age	ISS	PHC	E	OT	Total	ICU	M	L/P max.12 h	Hb min.12 h	Ls 12 h	L/P max.24 h	Hb min.24 h	Ls 24 h	L/P 25	L/P 30	L/P 35	Median L/P
1MP	M	60	50	70	90	-	160	9	0	12.4	91.7	7.7	17.8	91.2	7.7	3	0	0	20.7
10LJ	M	54	25	30	100	200	330	7	0	32.9	93	4.4	32.9	93	5.2	2.5	0.5	0	16.4
11GM	M	30	41	45	90	250	385	5	0	-	70	7.9	-	70	9.6	24.5	23.8	15	34.9
12HM	M	30	41	55	160	145	360	4	0	23.7	103	3.4	23.7	103	3.4	0	0	0	13.6
13KP	M	33	41	85	115	130	330	15	0	29.8	67	3.2	29.8	67	3.2	7.5	0	0	20.5
14KM	M	51	50	70	90	160	320	28	0	50	63	5	28.5	63	6.2	54.8	18.3	10	24.4
15SM	M	21	50	45	210	100	355	24	0	17.1	72	2.3	17.4	72	2.3	12.5	2.7	1.3	18.2
16KB	M	55	25	60	60	70	190	1	1	368	9	17	368	9	17	0	0	0	368.9
17HM	M	20	29	50	90	210	350	17	0	33.9	83	4.3	33.9	75	4.3	0.8	0.3	0	17.9
18SD	M	30	59	65	80	105	250	53	0	63.7	47	13.4	63.7	47	13.4	21.3	11	3	19,1
19BZ	M	19	25	50	25	100	175	3	0	22.9	51	8.1	22.9	51	8.1	0.3	0	0	15.6
2KS	F	31	41	105	155	0	260	25	0	26	74	2.7	26	74	2,7	51.5	21.5	0.3	26.3
20BR	M	22	57	80	70	240	390	62	0	30.9	66	10.6	30.9	66	10.6	28	17.8	2.3	24.8
21NM	F	53	66	30	160	110	300	77	0	54	67	3	54	67	3.2	22.8	3.8	2.5	21
22JS	M	38	66	45	140	-	185	21	0	65	61	16	65	61	16	71	66	43.5	34.1
23SM	M	22	50	45	205	210	460	23	0	19	51	2.8	19	51	2.8	0	0	0	13.7
24PP	M	40	20	50	70	100	220	10	0	38.1	77	3.1	38.7	58	4.9	10.5	9.8	6.8	16.7
25SJ	M	42	45	60	110	-	170	7	0	19.2	126	5.2	24.2	123	5.2	0	0	0	20.5
26SF	M	62	57	55	105	480	640	7	0	12.7	71	4.6	12.7	64	6.2	5	0	0	16.8
28VJ	M	38	50	50	70	160	280	3	0	38.6	99	3.9	38.6	99	3.9	4	3	0.5	14.1
29ZM	M	23	34	40	145	-	185	29	0	-	-	-	20.3	66	6.9	16.5	9.5	5.3	16.2
3FR	M	39	41	-	-	200	200	10	0	49.9	76	2.5	52.9	76	3.9	75	64.2	53.5	38.4
30AV	M	55	59	30	130	180	340	21	1	43.8	82	9.5	43.8	82	11.8	67.8	49.2	24.8	32
32BJ	M	30	57	90	130	160	380	23	0	4	90	2.7	10	90	2.7	2	0	0	15.5
33HP	M	40	43	95	60	60	215	12	0	-	91	7.6	-	91	7.6	1	0	0	18.6
34PJ	M	50	27	40	160	370	570	22	0	28.5	69	7.3	28.5	69	7.3	6	2.3	1	19.8
35DM	M	23	48	115	65	165	345	26	0	28	79	1.4	28	79	1.4	9	0	0	16.6
36FP	M	67	50	80	155	-	235	7	1	16.7	79	6.3	16.7	79	8.8	0	0	0	13.8
38LM	F	73	50	75	60	150	285	16	0	-	87	5	24.1	87	5	2.5	0	0	21.8
39GP	F	32	41	50	40	90	180	28	0	19	70	7.4	19	70	7.4	0	0	0	12.5
40OK	M	49	41	55	80	160	295	4	0	15.9	87	4.6	15.9	87	4.6	0	0	0	10.9
41BV	M	64	57	70	80	140	290	2	1	99	48	12	99	48	12	1.8	1	1	19.1
5BB	M	34	48	40	80	170	290	6	0	-	73	5.5	19.9	73	5.5	49.5	22	4.2	29

Table 2 Monitored values in individual patients *(Continued)*

6FL	F	27	34	120	100	260	480	7	0	20.7	60	6.2	27.5	60	6.2	5	0	0	16.6
8PL	M	43	34	160	135	200	495	9	0	53.2	81	1	53.2	64	3	28.2	14.5	7.5	24.5
9KR	M	32	29	135	105	120	360	14	0	44.4	105	1.6	44.4	97	1.6	47.5	45.5	39.5	37

ISS, International Severity Score; PHC, prehospital care time; E, emergency care time; OT, operation time; Total, overall care time before ICU care; ICU, overall time (days) in ICU; M, 30-day mortality (0 = no, 1 = yes); L/P max.12 h, maximal value of L/P ratio in the first 12 hours; Hb min.12 h, minimal value of hemoglobin in the first 12 hours (g/l); Ls 12H, maximal value of serum lactate in the first 12 hours (mmol/l) (similarly for the first 24 hours); L/P 25, number of hours during which the value of the L/P was >25 (similarly, the L/P 30 and L/P 35 indicate >30 and >35, respectively).

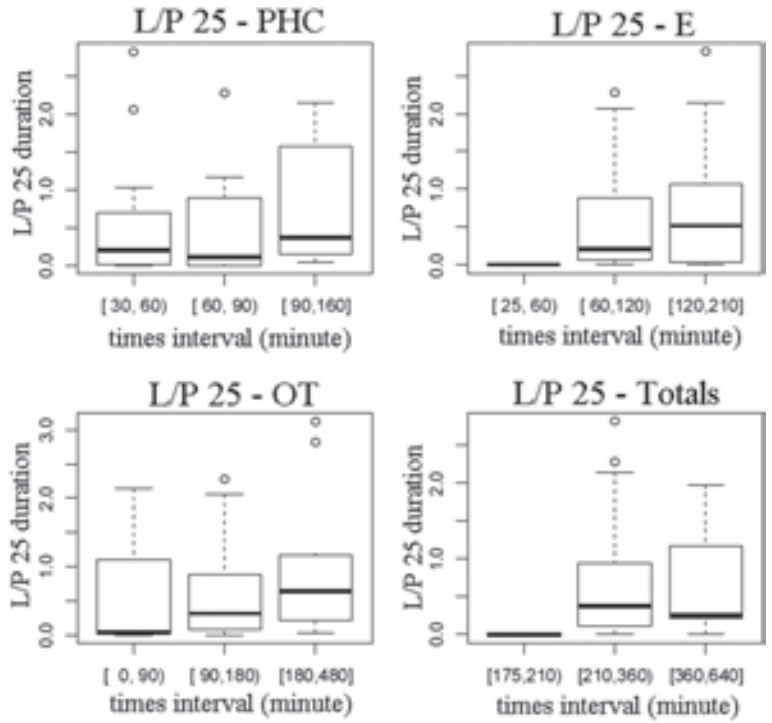

Figure 2 Duration of tissue ischemia according to the duration of the treatment period. PHC, prehospital care; E, emergency care; OT, operation time; Totals, summary of PHC + E + OT. Duration of care in intervals on the X-axis. Duration of L/P >25 on the Y-axis (relative units).

hemoglobin levels and $ScvO_2$. The microcirculation of the peripheral muscle tissue is affected very early in patients with serious forms of traumatic hemorrhagic shock [34]. The damage is very intense and requires a long period of recovery [4]. Tissue values may be influenced by the centralization of the circulation or by a stress-induced (i.e., non-ischemic) increase in lactate [35]. The interpretation of lactate values [12] and the L/P ratio [21] may also be guided by using the studies of patients with septic shock. In those studies, the highest tissue lactate values preceded the highest serum lactate values by 4 hours and the L/P ratio decreased in reaction to transfusion.

The most important parameter is the interpretation of the lactate values, particularly the L/P ratio, which is a generally accepted marker of ischemia [36]. Both lactate and pyruvate are influenced in the same way by local factors, such as the centralization of circulation that causes hypoperfusion of the peripheral tissue. The interpretation of this ratio is simpler than explaining the trend of isolated tissue lactate. The most frequently presented threshold value for the L/P ratio in ischemia is 25. Numerous papers in the literature have taken into consideration a higher trigger point of approximately 35 or 40 [37]. It seems that the best strategy for overtly ischemic conditions is to use L/P values over 30.

Figure 1 demonstrates that the L/P ratio trend may react to increase in systemic hemoglobin levels with a delay of 7 to 10 hours. Hemoglobin is one of the main determinants of oxygen delivery, and low values in conjunction with hypovolemia may cause tissue hypoxia. One of the first compensatory responses is centralization of the circulation, followed by increased cardiac output (especially via tachycardia) and increased oxygen extraction (via decreased $ScvO_2$). When the oxygen demand is higher than the oxygen extraction limit, an oxygen debt and further tissue ischemia will develop [38]. Normalization of the increased L/P ratio by transfusion occurred after a delay of the aforementioned 7 to 10 hours, which indicated restoration of aerobic metabolism in the tissues and start of redemption of the oxygen debt. Similar changes were observed in increased $ScvO_2$ levels with an L/P ratio delay of up to 10 hours. Ischemia of the peripheral muscle tissue was eliminated by a significant time interval after transfusion.

Increase in the L/P ratio may precede the $ScvO_2$ decrease by 10 or 11 hours. Exceeding the limit of oxygen extraction in tissues was reflected by the increased L/P ratio. We were able to detect this condition in advance of the $ScvO_2$, which is one of main indicators for transfusion [39].

We also observed changes in the L/P trend preceding a change in the hemoglobin level up to 13 hours in advance. Shock and centralization of the circulation could cause high and further increasing L/P ratios due to tissue ischemia. Fluid administration, which is routinely used as a

first-line treatment of hypovolemic shock, can cause hemodilution and decreased hemoglobin. The development of anemia is preceded by an increase in the L/P ratio. An increase in the L/P ratio is an early warning sign of inadequate oxygenation in tissues and should lead to early control of the hemoglobin level, $ScvO_2$ and other factors of oxygen delivery such as hemodynamic parameters.

Table 2 and Figure 2 show the dependence of the length of care on the L/P ratio within the first 12 and 24 hours. The timeline of care is divided into individual stages, i.e., pre-hospital care, care provided in the emergency department, and surgical time. Patients who are treated within a shorter time frame ($T_{ICU} \leq 240$ minutes) have lower maximal L/P ratios and generally have a shorter duration of tissue ischemia.

Conclusion

Microdialysis is a modern method that is on the border of experimental and clinical practice and the values monitored with this technique provide new insights into the condition of cells in critically ill patients. We can observe the dependence of the L/P ratio on the hemoglobin level and $ScvO_2$, which in turn inform us about anaerobic tissue metabolism and allow us to alter treatment. The L/P ratio was useful to identify tissue ischemia and could estimate the effectiveness of fluid resuscitation. Normalization of an elevated L/P ratio could help guide resuscitation efforts and could be an indicator for fluid administration. An increased L/P ratio is an early warning sign of inadequate tissue oxygenation and should lead to more detailed hemodynamic and laboratory monitoring. This information cannot usually be obtained from global markers. Microdialysis has immense potential and unlimited possibilities for monitoring the various molecules in many organs and tissues. The search for the optimal marker of adequate resuscitation continues.

Abbreviations

$ScvO_2$: Central venous oxygen saturation; L/P: Lactate/pyruvate ratio; SOFA: Sequential organ failure assessment score; ICU: Intensive care unit; DO_2: Oxygen delivery; VO_2: Oxygen consumption.

Competing interests

The authors declare that there are no other competing interests.

Authors' contribution

FB collection and analysis of data, interpretation and publication of data, co-investigator. LP principal investigator, publication of results. All authors read and approved the final manuscript.

Acknowledgments

The authors wish to thank Michal Burda from IT4Innovations Division, University of Ostrava, Institute for Research and Applications of Fuzzy Modelling, Department of Biostatistics, Czech Republic, for statistical processing. The authors would also like to express their gratitude to the staff of the intensive care unit at KARIM, University Hospital Ostrava, Czech Republic, for their help in collecting and analyzing the data and to my colleague Peter Sklienka MD to revising manuscript critically.
The manuscript was supported by a grant from the Resort Programme of Science and Development - MZ III for the period of 2010–2015, from the Internal Grant Agency of the Ministry of Health of the Czech Republic: NT11371-5/2010 "Metabolic Response of the Organism in Polytraumas"; principle investigator Leopold Pleva, MD, CSc.; co-investigators Filip Burša, MD; Tomáš Olos, MD; Jan Jahoda, MD; Roman Kula, MD, CSc.; Vaclav Prochazka, MD, PhD; and Ivo Kopáček, MD.

Source of funding

Both authors are investigators in a grant project funded by the Resort Programme of Science and Development - MZ III for the period of 2010–2015 from the Internal Grant Agency of the Ministry of Health of the Czech Republic: NT11371-5/2010 "Metabolic Response of the Organism in Polytraumas"; principle investigator Leopold Pleva, MD, CSc.; co-investigators Filip Burša, MD; Tomáš Olos, MD; Jan Jahoda, MD; Roman Kula, MD, CSc.; Vaclav Prochazka, MD, PhD; and Ivo Kopáček, MD.

Author details

[1]Department of anesthesiology and intensive care medicine, University Hospital Ostrava, Faculty of Medicine Universitas Ostrava, 17 listopadu, 1790 Ostrava-Poruba, Czech Republic. [2]Traumatology Centre, University Hospital Ostrava, Faculty of Medicine Universitas Ostrava, 17 listopadu, 1790 Ostrava-Poruba, Czech Republic.

Received: 3 June 2013 Accepted: 8 January 2014
Published: 5 February 2014

References

1. Shoemaker WC, Appel PL, Kram HB: **Tissue oxygen debt as a determinant of lethal and nonlethal postoperative organ failure.** *Crit Care Med* 1988, **16**(11):1117–1120.
2. Suistomaa M, Uusaro A, Parviainen I, *et al*: **Resolution and outcome of acute circulatory failure does not correlate with hemodynamics.** *Crit Care* 2003, **7:**R52–R58.
3. Meregalli A, Oliveira RP, Friedman G, *et al*: **Occult hypoperfusion is associated with increased mortality in hemodynamically stable, high-risk, surgical patients.** *Crit Care* 2004, **8:**R60–R65.
4. Barbee RW, Reynolds PS, Ward KR, *et al*: **Assessing shock resuscitation strategies by oxygen debt repayment.** *Shock* 2010, **33**(2):113–122.
5. Spahn DR, Bouillon B, Cerny V, *et al*: **Management of bleeding and coagulopathy following major trauma: an updated European guideline.** *Crit Care* 2013, **17**(2):R76.
6. Sakr Y, Dubois MJ, De Backer D, *et al*: **Persistent microcirculatory alterations are associated with organ failure and death in patients with septic shock.** *Crit Care Med* 2004, **32**(9):1825–1831.
7. Shere-Wolfe RF, Galvagno SM Jr, Grissom TE: **Critical care considerations in the management of the trauma patient following initial resuscitation.** *Scand J Trauma Resusc Emerg Med* 2012, **20:**68.
8. Bursa F, Olos T, Pleva L, *et al*: **Metabolism monitoring with microdialysis in the intensive care.** *Cas Lek Cesk* 2011, **150**(11):605–609.
9. Waelgaard L, Thorgersen EB, Line PD, *et al*: **Microdialysis monitoring of liver grafts by metabolic parameters, cytokine production, and complement activation.** *Transplantation* 2008, **86**(8):1096–1103.
10. Cibicek N, Zivna H, Vrublova E, *et al*: **Gastric submucosal microdialysis in the detection of rat stomach ischemia–a comparison of the 3H2O efflux technique with metabolic monitoring.** *Physiol Meas* 2010, **31**(10):1355–1368.
11. Rostami E, Bellander BM: **Monitoring of glucose in brain, adipose tissue, and peripheral blood in patients with traumatic brain injury: a microdialysis study.** *J Diabetes Sci Technol* 2011, **5**(3):596–604.
12. Kopterides P, Theodorakopoulou M, Ilias I, *et al*: **Interrelationship between blood and tissue lactate in a general intensive care unit: a subcutaneous adipose tissue microdialysis study on 162 critically ill patients.** *J Crit Care* 2012, **27**(6):742.e9–742.e18.
13. Ohashi H, Kawasaki N, Fujitani S, *et al*: **Utility of microdialysis to detect the lactate/pyruvate ratio in subcutaneous tissue for the reliable monitoring of haemorrhagic shock.** *J Smooth Muscle Res* 2009, **45**(6):269–278.
14. Larentzakis A, Toutouzas KG, Papalois A, *et al*: **Porcine model of haemorrhagic shock with microdialysis monitoring.** *J Surg Res* 2013, **179**(1):e177–e182.
15. Waelgaard L, Dahl BM, Kvarstein G, *et al*: **Tissue gas tension and tissue metabolites for detection of organ hypoperfusion and ischemia.** *Acta Anaesthesiol Scand* 2012, **56**(2):200–209.

16. Suistomaa M, Ruokonen E, Kari A, Takala J: **Time-pattern of lactate and lactate to pyruvate ratio in the first 24 hours of intensive care emergency admissions.** *Shock* 2000, **14**(1):8–12.
17. Dimopoulou, Nikitas N, Orfanos SE, *et al*: **Kinetics of adipose tissue microdialysis-derived metabolites in critically ill septic patients:associations with sepsis severity and clinical outcome.** *Shock* 2011, **35**(4):342–348.
18. Timofeev I, Czosnyka M, Carpenter KL, *et al*: **Interaction between brain chemistry and physiology after traumatic brain injury: impact of autoregulation and microdialysis catheter location.** *J Neurotrauma* 2011, **28**(6):849–860.
19. Trzeciak S, McCoy JV, Phillip DR, *et al*: **Early increases in microcirculatory perfusion during protocol-directed resuscitation are associated with reduced multi-organ failure at 24 h in patients with sepsis.** *Intensive Care Med* 2008, **34**(12):2210–2217.
20. Dubin A, Pozo MO, Ferrara G: **Systemic and microcirculatory responses to progressive haemorrhage.** *Intensive Care Med* 2009, **35**(3):556–564.
21. Kopterides P, Theodorakopoulou M, Nikitas N, *et al*: **Red blood cell transfusion affects microdialysis-assessed interstitial lactate/pyruvate ratio in critically ill patients with late sepsis.** *Intensive Care Med* 2012, **38**(11):1843–1850.
22. Benninger E, Laschke MW, Cardell M: **Early detection of subclinical organ dysfunction by microdialysis of the rectus abdominis muscle in porcine model of critical intraabdominal hypertension.** *Shock* 2012, **38**(4):420–428.
23. Liu X, Kruger PS, Roberts MS: **How to measure pharmacokinetics in critically ill patients?** *Curr Pharm Biotechnol* 2011, **12**(12):2037–2043.
24. Douglas A, Altukroni M, Udy AA, *et al*: **The pharmacokinetics of cefazolin in patients undergoing elective & semi-elective abdominal aortic aneurysm open repair surgery.** *BMC Anesthesiol* 2011, **11**:5.
25. Karlander SF, Lars E, *et al*: **Continous assessment of concentrations of cytokines in experimental injuries of the extremity.** *Int J Clin Exp Med* 2009, **2**(4):354.
26. Tyvold SS, Solligård E, Gunnes S, *et al*: **Bronchial microdialysis of cytokines in the epithelial lining fluid in experimental intestinal ischemia and reperfusion before onset of manifest lung injury.** *Shock* 2010, **34**(5):517–524.
27. Roberts JA, Roberts MS, Semark A, *et al*: **Antibiotic dosing in the 'at risk' critically ill patient: Linking pathophysiology with pharmacokinetics/ pharmacodynamics in sepsis and trauma patients.** *BMC Anesthesiol* 2011, **11**:3.
28. Jansson K, Redler B, Truedsson L, *et al*: **Postoperative on-line monitoring with intraperitoneal microdialysis is a sensitive clinical method for measuring increased anaerobic metabolism that correlates to the cytokine response.** *Scand J Gastroenterol* 2004, **39**(5):434–439.
29. Haugaa H, Almaas R, Thorgersen EB, *et al*: **Clinical experience with microdialysis catheters in pediatric liver transplants.** *Liver Transpl* 2013, **19**(3):305–314.
30. Widegren U, Hickner RC, Jorfeldt L, *et al*: **Muscle blood flow response to mental stress and adrenaline infusion in man: microdialysis ethanol technique compared to (133)Xe clearance and venous occlusion plethysmography.** *Clin Physiol Funct Imaging* 2010, **30**(2):152–161.
31. Farnebo S, Zettersten EK, Samuelsson A, *et al*: **Assessment of blood flow changes in human skin by microdialysis urea clearance.** *Microcirculation* 2011, **18**(3):198–204.
32. Samuelsson A, Farnebo S, Magnusson B, *et al*: **Implications for burn shock resuscitation of a new in vivo human vascular microdosing technique (microdialysis) for dermal administration of noradrenaline.** *Burns* 2012, **38**(7):975–983.
33. Farnebo S, Samuelsson A, Henriksson J, *et al*: **Urea clearance: a new method to register local changes in blood flow in rat skeletal muscle based on microdialysis.** *Clin Physiol Funct Imaging* 2010, **30**(1):57–63.
34. Shoemaker WC, Peitzman AB, Bellamy R, *et al*: **Resuscitation from severe hemorrhage.** *Crit Care Med* 1996, **24**(2 Suppl):S12–S23.
35. Larach DB, Kofke WA, Le Roux P: **Potential non-hypoxic/ischemic causes of increased cerebral interstitial fluid lactate/pyruvate ratio: a review of available literature.** *Neurocrit Care* 2011, **15**(3):609–622.
36. Nikitas N, Kopterides P, Ilias I, *et al*: **Elevated adipose tissue lactate to pyruvate (L/P) ratio predicts poor outcome in critically ill patients with septic shock: a microdialysis study.** *Minerva Anestesiol* 2013, **15**. Epub ahead of print.
37. Messerer M, Daniel RT, Oddo M: **Neuromonitoring after major neurosurgical procedures.** *Minerva Anestesiol* 2012, **78**(7):810–822.
38. Rixen D, Siegel JH: **Bench-to-bedside review: oxygen debt and its metabolic correlates as quantifiers of the severity of hemorrhagic and post-traumatic shock.** *Crit Care* 2005, **9**(5):441–453.
39. Vallet B, Robin E, Lebuffe G: **Venous oxygen saturation as a physiologic transfusion trigger.** *Crit Care* 2010, **14**(2):213.

doi:10.1186/1757-7241-22-11
Cite this article as: Burša and Pleva: Anaerobic metabolism associated with traumatic hemorrhagic shock monitored by microdialysis of muscle tissue is dependent on the levels of hemoglobin and central venous oxygen saturation: a prospective, observational study. *Scandinavian Journal of Trauma, Resuscitation and Emergency Medicine* 2014 **22**:11.

8

Brain activity during bladder filling and pelvic floor muscle contractions: a study using functional magnetic resonance imaging and synchronous urodynamics

Krhut J, Holý P, Tintěra J, Zachoval R, Zvara P

Originally published in International Journal of Urology, 2014, vol. 21, no. 2, p. 169-174

Consent to the publication of 19th March 2015

INTERNATIONAL JOURNAL OF UROLOGY
International Journal of Urology (2014) **21**, 169–174 doi: 10.1111/iju.12211

Original Article: Clinical Investigation

Brain activity during bladder filling and pelvic floor muscle contractions: A study using functional magnetic resonance imaging and synchronous urodynamics

Jan Krhut,[1] Petr Holy,[2] Jaroslav Tintera,[3] Roman Zachoval[2] and Peter Zvara[4]

[1]Department of Urology, University Hospital, Ostrava, Czech Republic, [2]Department of Urology, Thomayer's Hospital, Prague, Czech Republic, [3]Department of Radiodiagnostics and Interventional Radiology, Institute for Clinical and Experimental Medicine, Prague, Czech Republic; and [4]Division of Urology, University of Vermont, Burlington, Vermont, USA

Abbreviations & Acronyms
fMRI = functional magnetic resonance imaging
GLM = general linear model
ICA = independent component analysis
LUT = lower urinary tract
MPR = multiplanar reconstruction
PET = positron emission tomography
PF = pelvic floor
PMA = primary motor area
SMA = supplementary motor area

Correspondence: Jan Krhut M.D., Ph.D., Department of Urology, University Hospital, 17 Listopadu 1790, Poruba, Ostrava 708 52, Czech Republic. Email: jan.krhut@fno.cz

Received 10 November 2012; accepted 24 May 2013.
Online publication 1 July 2013

Objectives: To map the brain activity during bladder filling by functional magnetic resonance imaging using a refined scanning protocol including synchronous urodynamics and pelvic floor muscle contractions.

Methods: A total of 23 healthy female volunteers (age 20–68 years) were enrolled. Participants were asked to contract their pelvic floor muscles. This was followed by a urodynamic examination consisting of repeated filling cycles. Brain activity was measured by functional magnetic resonance imaging using a 3T magnetic resonance system. Measurements of brain activity consisted of 120 functional scans during pelvic floor contractions and 210 scans during bladder filling. Each functional magnetic resonance imaging scan covered the brain with 35 slices. Statistical analyses used the general linear model and independent component analysis. Areas of activation were visualized using group statistics.

Results: The following main clusters of activation were observed during pelvic floor muscle contractions: medial surface of the frontal lobe (primary motor area), bilaterally; supplementary motor area, bilaterally; and left gyrus precentralis. During bladder filling, activation was detected in the inferior frontal lobe bordering the frontal cingulum, left gyrus parietalis superior, left central area, right insula, brainstem and thalamus with subcortical gray matter nuclei.

Conclusions: Our work extends an existing functional magnetic resonance imaging protocol for researching the neural control of the lower urinary tract. The present results are consistent with the available literature and agree with the present hypothetical functional model of lower urinary tract neural control.

Key words: functional magnetic resonance imaging, pelvic floor, urinary bladder, urodynamics.

Introduction

In the past three decades, considerable research attention has been paid to the central neural control of various organs. However, compared with other organs and systems, relatively few studies have addressed neuroregulation of the LUT.

PET and fMRI have implicated the pons, periaqueductal grey, lobus insularis, anterior cingulate gyrus and prefrontal cortex as the structures most involved in the central control of LUT function in the human brain.[1] These findings have led to the development of a hypothetical model of the cerebral control of LUT.[2] However, our understanding of the neuroregulation of LUT and PF muscles is still incomplete, and results of existing studies are inconsistent. During the filling phase of the micturition cycle, PF muscles contribute to maintaining continence by gradually increasing their tone during bladder filling and through reflex contraction during a sudden increase in abdominal pressure.[3] In addition, it has been shown that a contraction of PF muscles inhibits detrusor contraction.[4]

We have previously mapped brain activity during micturition.[5] We observed the activation of several brain regions at the final filling phase, but we were not able to rule out the potential brain co-activations related to the PF muscles contraction. Based on these findings, we decided to carry out a study dedicated to the filling phase with respect to the potential influence of either volition or reflex PF muscles contraction.

In order to further increase precision and better correlate bladder function with central nervous system activity, we used synchronous urodynamic examination and fMRI, together with direct monitoring of the PF muscle activity.

Methods

Participants

A total of 23 right-handed healthy female volunteers aged 20–68 years were enrolled in the study. All participants were informed of the risks associated with the study, and provided written, informed consent. The study protocol was approved by the Ethics Committee of Thomayer Hospital, Prague. The study was designed in accordance with the principles of the Declaration of Helsinki, World Medical Association.

Participants with the following conditions were excluded from participation in the study: urinary infections, any LUT symptoms, significant prolapse of the pelvic organs, dementia, urolithiasis, history of previous malignant disease in the pelvic area, previous irradiation therapy of the pelvis, claustrophobia, use of medications that could influence functions of the brain or the LUT, metallic or electronic implants, or positive pregnancy test. Before enrolment, all participants were examined by a physiotherapist and trained in the use of a perineometer to ensure isolated contraction of the PF muscles.

Study design

Examinations performed on all volunteers were carried out under antibiotic prophylaxis (ofloxacin 200 mg). A Ch6 dual-channel catheter was inserted into the urinary bladder before the start of each examination for bladder filling and measurement of intravesical pressure. A catheter was also inserted into the rectal ampulla for measurement of abdominal pressure for monitoring of PF muscle activity. Both catheters were connected to urodynamic pressure transducers (MMS, Enschede, the Netherlands) located outside the examination room, and then zeroed against atmospheric pressure in the area of the symphysis, according to Good Urodynamic Practices.[6] Before the initial filling, a 10-min rest period was observed to allow catheter-induced irritation to subside.

The filling phase was evaluated by infusing the bladder with a sterile solution of 0.9% NaCl at a rate of 50 mL/min. Subjective parameters (first filling sensation, strong desire to void) were recorded by the participant using a hand-held signaling device. fMRI measurements were initiated after the bladder had been filled with 100 mL of solution. After the initial bladder filling, rapid filling and emptying of the bladder with 25 mL of the infusion solution was initiated in order to strengthen the sensory stimulus. Two trials of rapid filling and emptying were carried out according to the scheme described by Griffiths *et al*.[5] Briefly, the protocol examined the following four sequential phases: resting phase (14 s), filling phase (25 mL over 14 s), resting phase (14 s) and withdrawal phase (25 mL over 14 s). The filling cycle was continued until the participant recorded a strong desire to urinate. Then, four additional cycles of filling and emptying of the bladder were carried out simultaneously with continuous fMRI.

During another fMRI measurement, participants were asked to carry out three to four PF contractions lasting approximately 6 s, followed by a resting phase of 30 s. This procedure was repeated 10 times with 120 simultaneously carried out functional scans. This data was used in the final analysis to differentiate between brain activity that resulted from bladder sensations and activity resulting from voluntary contractions of the PF muscles.

fMRI data acquisition

All data was acquired with a 3T magnetic resonance scanner (Siemens Trio Tim 3T; Siemens, Erlangen, Germany) using a gradient-echo echo-planar imaging sequence (field of view = 192 × 192 mm; voxel size = 3 × 3 × 3 mm; repetition time/echo time = 2000/30 ms; bandwidth = 2790 Hz/pixel; parallel acquisition technique factor = 2). Measurements of brain activity during PF contractions used 120 functional scans. A total of 210 scans were used in the measurement of brain activity during bladder filling. Each fMRI dynamic covered the brain with a total of 35 slices.

Statistical processing

Statistical evaluations were carried out using SPM8 software (Wellcome Trust Center for Neuroimaging, http://www.fil.ion.ucl.ac.uk/spm). fMRI data preprocessing consisted of motion correction (realignment), slice timing and smoothing with a Gauss filter (full width at half maximum = 6 × 6 × 6 mm). Data was then normalized to standard Montreal Neurological Institute-152 space (Montreal Neurological Institute, Montreal, Canada, International Consortium for Brain Mapping, http://www.loni.ucla.edu/ICBM). Brain activity due to PF contractions was statistically evaluated using the GLM with a canonical hemodynamic response function convolved with a block scheme describing periods of contractions and rests (6 s of repeated contractions and 30 s of rest). Group level statistical maps were thresholded with an uncorrected *P*-value of 0.0001.

Both SPM8 and GLM was also used to evaluate brain activity during bladder filling using the following two protocols: (i) step function comparing empty versus full bladder (participant reporting a strong desire to void) – model A; and (ii) cyclic filling and withdrawal of 25 mL of 0.9% NaCl – model B. The procedure used for bladder filling during fMRI is shown in Figure 1. This figure also shows how the estimated brain activity was split into two models for statistical evaluation using GLM. Individual statistical maps were evaluated with a threshold of $P \leq 0.001$ (uncorrected) or $P \leq 0.05$ (adjusted for multiple observations FWE). The resulting statistical maps were included in group statistics (random effect) using a one-sample *t*-test with an uncorrected threshold of $P = 0.001$. Parallel evaluations used ICA for every measurement, with an identical number ($n = 20$) of components and the basic initial setup of the group ICA of fMRI toolbox program (version 1.3i, default values of processing parameters, infomax algorithm). This ICA analysis allowed for a comparison at the individual level of components obtained with simultaneously carried out urodynamic recording. The threshold of *Z*-score ($Z = 1.0$) was used for all components.

In addition to assigning anatomical brain regions to coordinates of activation cluster (position of maximum *t*-value within the cluster), the software package, Marina (B Walter, University of Giessen, Giessen, Germany), was used.

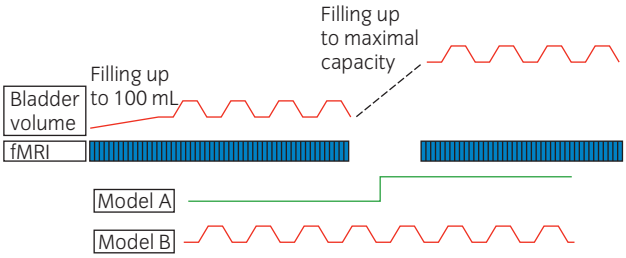

Fig. 1 Schematic summarizing the procedure used for bladder filling and the time course of fMRI. The first line represents how the volume was varied: to begin, the bladder was filled to 100 mL ("empty bladder condition") followed by a cycle of filling and withdrawing 25 mL. Scanning was stopped and the bladder was filled to maximal capacity, which was indicated by each participants ("full bladder condition"). Immediately after maximal bladder capacity was achieved, a second cycle of fMRI recording with simultaneous bladder filling and withdrawing was started. The second line shows when fMRI was carried out simultaneously. The two bottom lines indicate how both models were defined for statistical evaluation after data concatenation.

Table 1 Brain regions activated during PF contractions ($P = 0.0001$, *t*-test; uncorrected data for nine participants in group statistic using GLM)

Brain region	T	Z	x	y	z
Frontal lobe, medial surface (PMA)	10.12	4.47	±4	–27	65
Frontal lobe, medial surface (SMA)	12.47	4.88	±2	2	50
Central region, left precentral gyrus	8.22	3.62	–43	–13	63

Table 2 Brain regions activated during filling of the urinary bladder, tested using model A ($P = 0.001$, *t*-test; uncorrected)

Brain region	T	Z	x	y	z
Orbital surface of the inferior frontal lobe, olfactory cortex, bordering the frontal cingulum	5.02	3.38	–5	20	–10
Left gyrus parietalis superior	11.27	4.84	–25	–60	52
Left central area, gyrus postcentralis	6.97	3.99	–5	–35	60

Table 3 Brain regions activated during filling of the urinary bladder, tested using model B ($P = 0.001$, *t*-test; uncorrected)

Brain region	T	Z	x	y	z
Brain stem bilaterally	4,43	3,49	±14	–20	–9
Subcortical gray matter nuclei of the thalamus bilaterally	6,52	4,42	±10	–16	3
Right insula	5,38	3,95	40	14	3

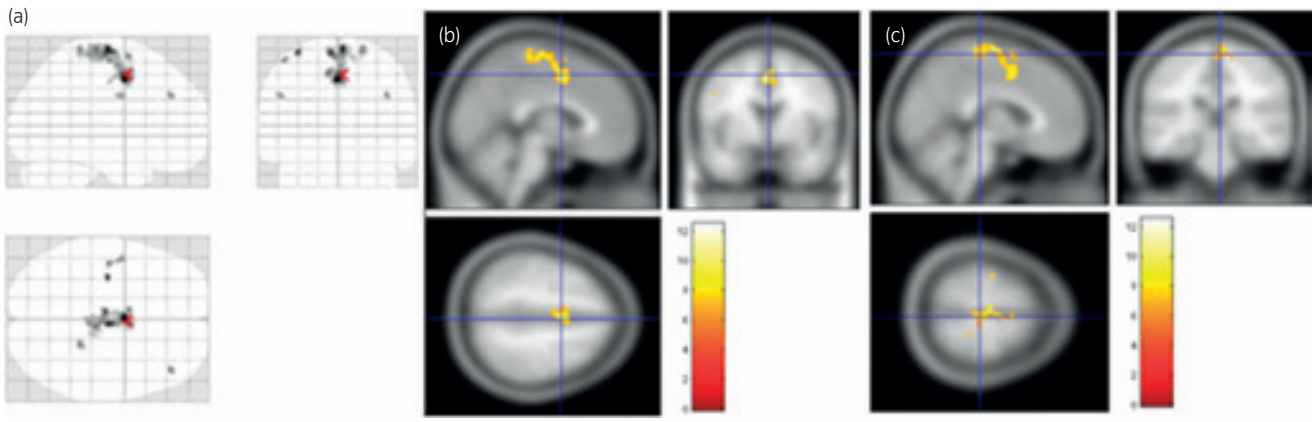

Fig. 2 Activations during PF contraction ($P = 0.0001$, *t*-test [$n = 9$]; group statistic, uncorrected). (a) 3-D projections showing all activity in sagittal, coronal and axial orientations; (b) MPR in SMA localization (±2, 2, 50); (c) MPR in localization of the primary motor cortex for the pelvic region (±4, –27, 65).

Results

Brain activation during PF contraction

The main clusters of brain activation during PF contractions were observed in the following areas: medial surface of the frontal lobe (primary motor area), bilaterally (±4, −27, 65); SMA, bilaterally (±2, 2, 50); and left gyrus precentralis (−43, −13, 63). Other, less significant, clusters of activation were observed on the left side of the medial frontal gyrus (−38, 36, 32), the right side of the medial frontal gyrus (42, 36, 32) and the right superior temporal gyrus (62, −34, 22; Table 1 and Fig. 2).

Brain activation during bladder filling

A total of 23 participants were evaluated. Meaningful data (evidence of brain activity) was obtained from 19 participants (this means data where any activation could be detected at all). The likely high level of motion could be degraded acquired data in the case of four participants without any activation. Using bladder-filling model A, we detected activations in the frontal lobe, left parietal gyrus and left central area (Table 2 and Fig. 3). Bladder-filling model B triggered activation mainly in the brainstem (7, −10, −10), the subcortical

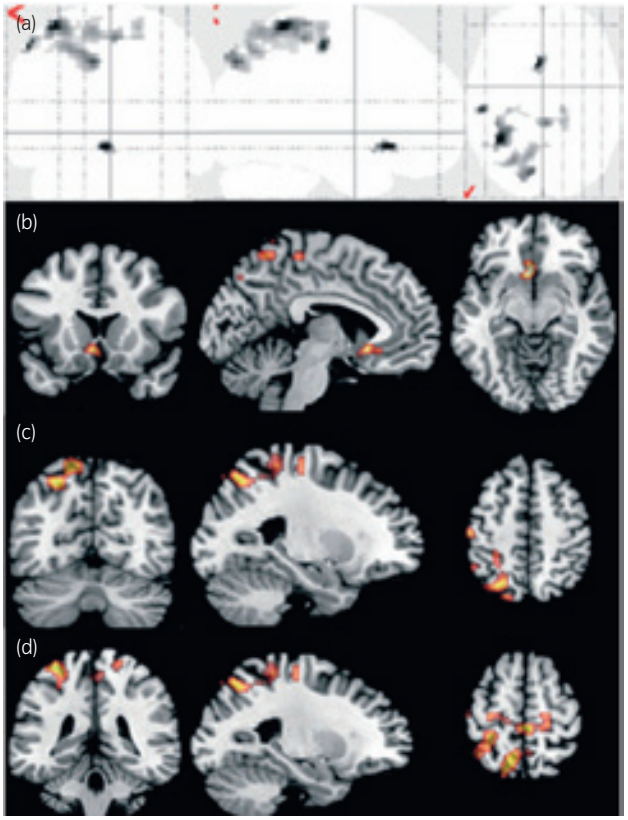

Fig. 3 Final activations stimulated by differences between empty and full bladder, calculated by GLM (model A). (a) Maximal intensity projection (frontal, sagittal, transversal) of group statistical map thresholded with $P = 0.001$ (uncorrected). (b) MPR in three orthogonal orientations centered in position (–5, 20, –10): orbital surface of the inferior frontal lobe, olfactory cortex, bordering the frontal cingulum. (c) MPR in three orthogonal orientations centered in position (–25, –60, 52): left gyrus parietalis superior. (d) MPR in three orthogonal orientations centered in position (–5, –35, 60): left central area, gyrus postcentralis.

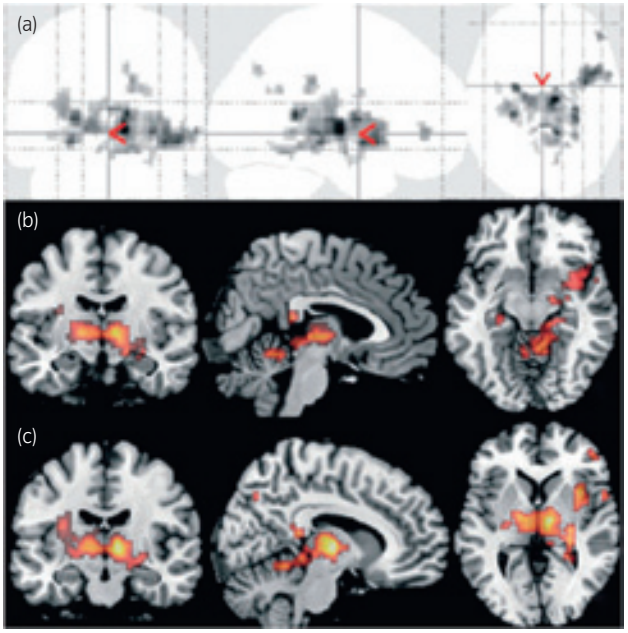

Fig. 4 Final activations stimulated by cyclic bladder filling and withdrawal (model B). (a) Maximal intensity projection (frontal, sagittal, transversal) of group statistical map thresholded with $P = 0.001$ (uncorrected). (b) MPR in three orthogonal orientations centered in position (7, –10, –10): brainstem. (c) MPR in three orthogonal orientations centered in position (10, –15, 0): thalamus with subcortical gray matter nuclei.

gray matter nuclei of the thalamus (10, −15, 0) and right insula (40, 14, 3; Table 3 and Fig. 4). Changes in brain activation during repeated filling and emptying of the bladder were also analyzed using ICA, which was carried out for each of the 23 measurements. One representative component for each of the measurements, which correlated with the simultaneously obtained urodynamic data, was identified by visual comparison (Fig. 5). Four measurements failed to identify a component associated with the change in volume of the urinary bladder. The most frequently identified areas of activation were localized to the right portion of the posterior cingulate gyrus [5, −47, 22], the left thalamus [−9, −10, 11], the middle left frontal gyrus (−36, 33, 45), and the left (−46, 20, −6) and right (47, 30, −14) orbital parts of the inferior frontal gyrus. The brain areas activated by changes in bladder volume and their relative frequencies of occurrence are presented in Table 4.

Discussion

Our understanding of the central neural mechanisms controlling the LUT is incomplete and the reproducibility of previously published data is inconsistent.[7]

The present study confirmed the reproducibility of an infusion/withdrawal protocol and provided further data in support of the feasibility of recording brain activity during bladder filling using fMRI.[8] Adding comprehensive urodynamics and direct recording of the PF muscle contractions to the fMRI scanning protocol allowed for better correlation between the detrusor, PF muscle function and brain activity. Cystometry carried out synchronously with fMRI scanning enabled a detailed visual comparison between brain activation and filling of the bladder, which allowed for selection of relevant components for ICA statistical analysis. Adding PF muscle contraction monitoring to the experimental protocol allowed for separation of brain activity caused by voluntary or reflex PF contractions at the terminal phase of the bladder filling from the activation caused by afferent signaling from mechanoreceptors in the bladder wall. PF contraction is known to cause inhibition of the micturition reflex. Patients suffering from urgency use this maneuver to suppress onset of the micturition phase. It is therefore possible that at least some components of the brain activity, recorded by fMRI during fast bladder filling, which others attributed to a strong urge to urinate, could be caused by contraction of the PF muscles. In order to precisely localize brain activity associated with PF contraction and distinguish it from activation related to bladder filling, we used a series of PF contractions at the beginning of the examination protocol. Using simultaneous urodynamics and direct PF muscle activity recording, we extended the protocol used in experiments by Kuhtz-Buschbeck *et al.*,[9,10] who evaluated the brain centers involved with control of the pelvic floor muscles. Our assessment of brain projections of PF

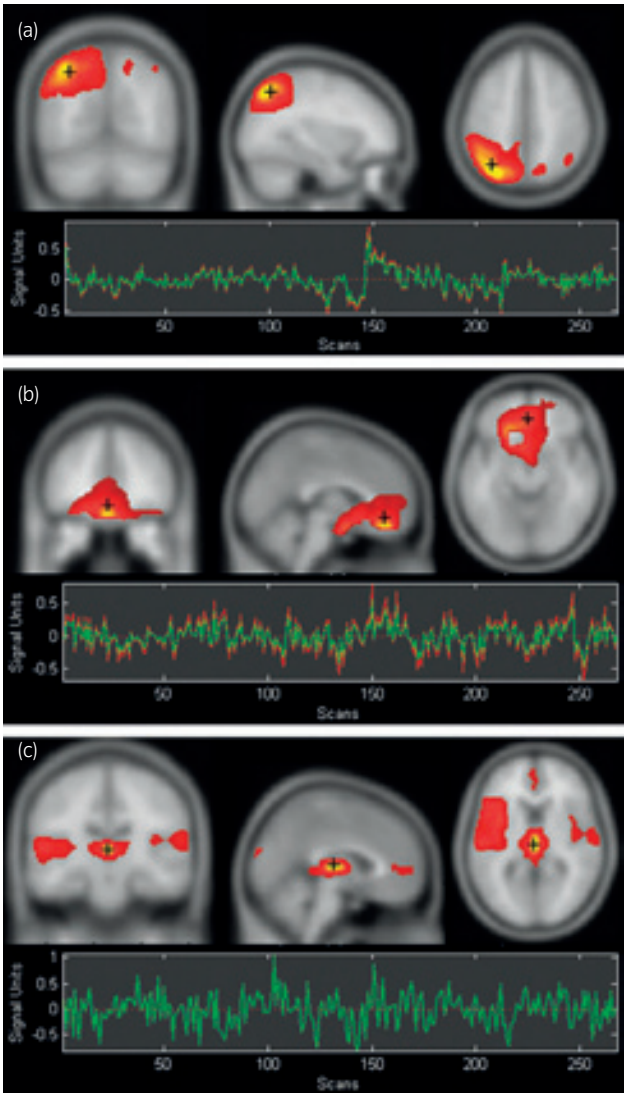

Fig. 5 Activations in the brain during changes in bladder volume recorded using group ICA: (a–c) showing three selected components with the best correlation with the time course of bladder volume changes. Each upper line shows three orthogonal sections (coronal, sagittal and axial) centered in the area marked with the black cross (a) (–34, –55, 49), (b) (–4, 42, –8) and (c) (–3, –15, 4). Corresponding time signal course in this point is shown in the lower line.

muscle activity identified bilateral activation of the SMA together with activation of the primary motor cortex for the PF muscles. This is in accord with previously published data.[10] However, contrary to the report from Di Gangi-Herms,[11] who described activation in the area of the right pre-central gyrus, we observed activation in the medial frontal gyrus. Seseke *et al*. examined activation of the cortex during the contraction of PF muscles with a full bladder. Similar to the present results, they observed activation of primary and SMA without hemispheric predominance. Furthermore, they described activation of numerous subcortical structures (hypothalamus, thalamus, periaqueductal grey) and the cerebellum.[12]

The reason for utilizing rapid filling and withdrawal during the early and final stage of bladder filling (model B) was to augment the afferent signals according to a protocol proposed by Griffith *et al*.[8] Comparison between these two models of

Table 4 Relative frequency of brain activity in nine selected brain regions during bladder volume changes (individual statistics using ICA)

Brain region	Coordinates			Relative frequency of activations in the subject population
	x	y	z	
Middle left frontal gyrus	–36	33	45	47% (9/19)
Inferior frontal gyrus, left orbital part	–46	20	–6	42% (8/19)
Inferior frontal gyrus, right orbital part	47	30	–14	42% (8/19)
Middle frontal gyrus, right orbital part	21	62	–14	26% (5/19)
Middle frontal gyrus, left orbital part	–21	45	–16	26% (5/19)
Left angular gyrus	–41	–59	57	47% (9/19)
Right posterior cingulate gyrus	5	–47	22	58% (11/19)
Anterior cingulate, left paracingulate gyri	–2	46	14	26% (5/19)
Subcortical grey nuclei, left thalamus	–9	–10	11	53% (10/19)

bladder filling allowed us to observe that the slow gradual bladder filling (model A), used in the present study, induced activation solely in the cortical regions of the brain, while the subcortical regions and insula are activated only by rapid filling and withdrawal. We speculate that rapid change in the intravesical volume and pressure triggers micturition reflex mechanisms responsible for maintaining detrusor relaxation during filling (e.g. sympathetic pelvic-to-hypogastric storage reflex or guarding somatic pelvic-to-pudendal reflex). This could possibly imitate the brain response to non-voiding detrusor contractions. In contrast, gradual filling allows time for bladder accommodation, which is predominantly under the control of the cortical centers.

The present findings are generally consistent with results of the initial works of Griffiths *et al*.[13,14] and earlier studies using PET, which describe activation in the area of the insula, cingulum, periaqueductal grey, cerebellum and occipito-parietal area with sensory stimulation during bladder filling in healthy subjects.[15,16] We did not observe any brain activation in the regions related to PF muscle contractions during the filling phase.

The present study further developed a protocol applicable for studying neural control of LUT using fMRI. The results acquired with this refined scanning protocol point to the fact that the thalamus, cingulate gyrus, and especially the lower surface of the frontal lobe play a significant role in sensation and afferent signaling from the LUT, and could therefore represent a potential target for the treatment of the cardinal LUT symptom of urgency. Future studies in this area should focus on comparing central nervous system activity of patients with various LUT dysfunctions with those of healthy controls, together with assessing the influence of pharmacotherapy.

Acknowledgments

The study was supported by a grant from the Ministry of Health, Czech Republic for Development of Research Organi-

zation 00023001 (IKEM, Prague, Czech Republic) Institutional Support and by a grant NT/14183 from Ministry of Health, Czech Republic.

Conflict of interest

None declared.

References

1 Blok BF, Sturms LM, Holstege G. Brain activation during micturition in women. *Brain* 1998; **121**: 2033–42.
2 Fowler CJ, Griffiths DJ. A decade of functional brain imaging applied to bladder control. *Neurourol. Urodyn.* 2010; **29**: 49–55.
3 de Groat WC, Fraser MO, Yoshiyama M *et al*. Neural control of the urethra. *Scand. J. Urol. Nephrol. Suppl.* 2001; **207**: 35–43.
4 Shafik A, Shafik IA. Overactive bladder inhibition in response to pelvic floor muscle exercises. *World J. Urol.* 2003; **20**: 374–7.
5 Krhut J, Tintera J, Holý P, Zachoval R, Zvara P. A preliminary report on the use of functional magnetic resonance imaging with simultaneous urodynamics to record brain activity during micturition. *J. Urol.* 2012; **188**: 474–9.
6 Schäfer W, Abrams P, Liao L *et al*. Good urodynamic practices: uroflowmetry, filling cystometry, and pressure-flow studies. *Neurourol. Urodyn.* 2002; **21**: 261–74.
7 Holstege G. Micturition and the soul. *J. Comp. Neurol.* 2005; **493**: 15–20.
8 Griffiths D, Derbyshire S, Stenger A, Resnick N. Brain control of normal and overactive bladder. *J. Urol.* 2005; **174**: 1862–7.
9 Schrum A, Wolff S, van der Horst C, Kuhtz-Buschbeck JP. Motor cortical representation of the pelvic floor muscles. *J. Urol.* 2011; **186**: 185–90.
10 Kuhtz-Buschbeck JP, van der Horst C, Wolff S *et al*. Activation of the supplementary motor area (SMA) during voluntary pelvic floor muscle contractions-an fMRI study. *Neuroimage* 2007; **35**: 449–57.
11 Di Gangi Herms AM, Veit R, Reisenauer C *et al*. Functional imaging of stress urinary incontinence. *Neuroimage* 2006; **29**: 267–75.
12 Seseke S, Baudewig J, Kallenberg K, Ringert RH, Seseke F, Dechent P. Voluntary pelvic floor muscle control – an fMRI study. *NeuroImage* 2006; **31**: 1399–407.
13 Griffiths D, Tadic SD, Schaefer W, Resnick NM. Cerebral control of the bladder in normal and urge-incontinent women. *NeuroImage* 2007; **37**: 1–7.
14 Griffiths D, Tadic SD. Bladder control, urgency, and urge incontinence: evidence from functional brain imaging. *Neurourol. Urodyn.* 2008; **27**: 466–74.
15 Athwal BS, Berkley KJ, Hussain I *et al*. Brain responses to changes in bladder volume and urge to void in healthy men. *Brain* 2001; **124**: 369–77.
16 Matsuura S, Kakizaki H, Mitsui T, Shiga T, Tamaki N, Koyanagi T. Human brain region response to distention or cold stimulation of the bladder: a positron emission tomography study. *J. Urol.* 2002; **168**: 2035–9.

Editorial Comment

Editorial Comment to Brain activity during bladder filling and pelvic floor muscle contractions: A study using functional magnetic resonance imaging and synchronous urodynamics

The frontal cortex is regarded as the higher center for micturition, because lesions in the frontal cortex; for example, the prefrontal cortex, medial superior/middle frontal gyri, anterior cingulate cortex, insula and supplemental motor area, produce marked lower urinary tract dysfunction in humans. Overactive bladder (urinary urgency and frequency) as a result of detrusor overactivity is a common bladder abnormality in the aforementioned brain areas. Functional neuroimaging in normal volunteers using single-photon emission computed tomography, positron-emission tomography, functional magnetic resonance imaging, and near infrared spectroscopy has been applied to observe brain activation in response to bladder fullness and urination; and the activated areas strikingly overlap the lesions described in clinical studies. Among the brain areas, anterior cingulate cortex and insula are thought to be "primary", and the prefrontal cortex is "secondary" (presumably modulatory) in regulating micturition. The constellation of these cortical areas seem to "switch on and off" the spino–bulbo–spinal micturition reflex involving the midbrain periaqueductal grey and the pontine micturition center.[1–3]

Krhut *et al*. studied 20 healthy female volunteers who participated in bladder push and pull, and pelvic floor contraction paradigm for urodynamics-functional magnetic resonance imaging.[4] The results were in agreement with the previously reported results. In addition, that study successfully highlighted the role of the pelvic floor, though already suggested by others,[5–7] that bilateral primary motor area (midline medial surface), bilateral supplementary motor area (similar) and left precentral gyrus are significantly activated by pelvic floor contraction. In order to manage patients' pelvic floor, for both diagnosis and treatment, the brain is worth looking at.

Ryuji Sakakibara M.D., Ph.D.
Neurology Division, Department of Internal Medicine, Sakura Medical Center, Toho University, Sakura, Japan
sakakibara@sakura.med.toho-u.ac.jp

DOI: 10.1111/iju.12222

Conflict of interest

None declared.

References

1 DasGupta R, Kavia RB, Fowler CJ. Cerebral mechanisms and voiding function. *BJU Int.* 2007; **99**: 731–4.
2 Fowler CJ, Griffiths D, de Groat WC. The neural control of micturition. *Nat. Rev. Neurosci.* 2008; **9**: 453–66.
3 Haruta H, Sakakibara R, Ogata T *et al*. Inhibitory control task is decreased in vascular incontinence patients. *Clin. Auton. Res.* 2013; **23**: 85–9.
4 Krhut J, Holy P, Tintera J, Zachoval R, Zvara P. Brain activity during bladder filling and pelvic floor muscle contractions: a study using functional magnetic resonance imaging and synchronous urodynamics. *Int. J. Urol.* 2014; **21**: 169–74.
5 Blok BFM, Sturms LM, Holstege AG. A PET study on cortical and subcortical control of pelvic floor musculature in women. *J. Comp. Neurol.* 1997; **389**: 535–44.
6 Seseke S, Baudewig J, Kallenberg K, Ringert RH, Seseke F, Dechent P. Voluntary pelvic floor muscle control – an fMRI study. *NeuroImage* 2006; **31**: 1399–407.
7 Kuhtz-Buschbeck JP, van der Horst C, Wolff BS *et al*. Activation of the supplementary motor area (SMA) during voluntary pelvic floor muscle contractions – an fMRI study. *NeuroImage* 2007; **35**: 449–57.

9

Addition of platelet concentrate to Dermo-Epidermal Skin Graft in deep burn trauma reduces scarring and need for revision surgeries

Procházka V, Klosová H, Štětinský J, Gumulec J, Vítková K, Šalounová D, Dvořáčková J, Bielniková H, Klement P, Levaková V, Ocelka T, Pavliska L, Kovanic P, Klement G L

Originally published in Biomedical Papers, 2014, vol. 158, no. 2, p. 242-258

Consent to the publication of 1st April 2015

Addition of platelet concentrate to Dermo-Epidermal Skin Graft in deep burn trauma reduces scarring and need for revision surgeries

Vaclav Prochazka[a], Hana Klosova[b], Jiri Stetinsky[b], Jaromir Gumulec[c], Katerina Vitkova[d], Dana Salounova[e], Jana Dvorackova[f], Hana Bielnikova[f], Petr Klement[g†], Veronika Levakova[h], Tomas Ocelka[i], Lubomir Pavliska[j], Pavel Kovanic[k], Giannoula Lakka Klement[l,m,n]

Backround. Deep skin burn injuries, especially those on the face, hands, feet, genitalia and perineum represent significant therapeutic challenges. Autologous dermo-epidermal skin grafts (DESG) have become standard of care for treating deep burns. Additionally, human autologous thrombin activated autologous platelet concentrate (APC) has gained acceptance in the setting of wounds. While each of these interventions has been independently shown to accelerate healing, the combination of the two has never been evaluated. We hypothesized that the addition of platelets (source of growth factors and inhibitors necessary for tissue repair) to the DESG (source of progenitor cells and of tissue proteases necessary for spatial and temporal control of growth regulators released from platelets) would create the optimal environment for the reciprocal interaction of cells within the healing tissues.
Methods. We used clinical examination (digital photography), standardised scales for evaluating pain and scarring, in combination with blood perfusion (laser Doppler imaging), as well as molecular and laboratory analyses.
Results. We show for the first time that the combination of APC and DESG leads to earlier relief of pain, and decreased use of analgesics, antipruritics and orthotic devices. Most importantly, this treatment is associated with earlier discharges from hospital and significant cost savings.
Conclusions. Our findings indicate that DESG engraftment is facilitated by the local addition of platelets and by systemic thrombocytosis. This local interaction leads to the physiological revascularization at 1-3 months. We observed significant elevation of circulating platelets in early stages of engraftment (1-7 days), which normalized over the subsequent 7 and 90 days.

Key word: deep burn trauma, dermo-epidermal skin graft, surgical debridement, necrectomy, autologous platelet concentrate (APC), human autologous thrombin (HAT), scarring, laser doppler perfusion imaging (LDPI), gnostic analysis

Received: January 31, 2013; Accepted with revision: September 13, 2013; Available online September 27, 2013
http://dx.doi.org/10.5507/bp.2013.070

[a]Institute of Radiodiagnostic and Vice-President for Science and Research, University Hospital Ostrava, Czech Republic
[b]Burn centre, University Hospital Ostrava
[c]Institute of Clinical Hematology, University Hospital Ostrava
[d]Department of Vice-President for Science and Research, University Hospital Ostrava
[e]Department of Mathematical Methods in Economy, VSB-Technical University of Ostrava
[f]Institute of Pathology, University Hospital Ostrava
[g]Vice-rector for External Affairs, VSB-Technical University of Ostrava
[h]Complex Oncologic centre, P&R Lab, Novy Jicin
[i]Institute of Public Health Ostrava, Partyzanske nam. 7, 702 00 Ostrava,
[j]E&H services, Inc., Navratilova 1421/11, Prague
[k]Retired scientist from the Czech Academy of Sciences
[l]Pediatric Hematology Oncology, Floating Hospital for Children at Tufts Medical Center, Boston, MA, USA
[m]Center of Cancer System Biology, Steward St. Elizabeth Health Center, Boston, MA, USA
[n]Tufts University School of Medicine, Boston, MA, USA
Corresponding author: Vaclav Prochazka, e-mail: angio@vol.cz

INTRODUCTION

Despite significant recent advances in wound care, therapeutic outcomes are often functionally, psychologically and cosmetically unacceptable. No solutions have been found to address the prevalence of severe scar hypertrophy, joint contractures, peripheral neuropathy, or systemic temperature dysregulation. At present, standard of care for treating deep burns consists of surgically excising necrotic tissue (necrectomy), followed by dermo-epidermal skin autografting.

The use of autologous platelet concentrates (APC) is well established[1-5], and there is ample evidence that platelets facilitate various wound healing processes such as chemotaxis[6], recruitment of progenitor cells[7], proliferation[8], angiogenesis[9], and inflammation[10]. We have previously published evidence that APC is beneficial in the treatment of chronic ischemic ulcers, and can lead to limb salvage

in the most severe cases[1]. Evidence suggests that platelets actively and selectively sequester angiogenesis regulators[11], and differentially release inhibitors and stimulators of angiogenesis[12,13]. This differential release of stimulators and inhibitors of angiogenesis from platelets is conditional on a direct platelet/stroma interaction. Similarly, the benefits of DESG are well-documented, even though no explanation is available for the excessive cicatrization that often accompanies the use of DESG. It can be thus surmised based on emerging evidence that a direct reciprocal interaction of platelets and wound matrix must occur for optimal tissue regeneration[14,15]. Moreover, we hypothesize that the combination therapy of DESG and activated platelets may be more efficacious than either individual modality. Thus, the goal of this study was to evaluate, whether the combination of DESG (a surrogate for cellular therapy) and platelet concentrate (a surrogate inflammatory modulator) leads to development of stable, non-hypertrophic scarring; thereby, preventing pain and shortening hospitalization.

Evidence suggests that platelets actively and selectively sequester angiogenesis regulators[11], and differentially release inhibitors and stimulators of angiogenesis[12,13].We explored the molecular determinants of this interaction in the present study by directly correlating physiological (laser Doppler perfusion imaging), clinical (pain scale, Vancouver scar scale and ratio of healed/total grafted area), and morphological (immunohistochemistry and epithelialization) evaluations to specific clinical endpoints such as time to wound closure, frequency of infections, inflammation and scarring.

MATERIALS AND METHODS

Selection of subjects and determination of areas to be grafted

Consecutive patients with second or third degree burns seen at the Burn Centre of University Hospital Ostrava, between January 2009 and November 2010, were approached for participation in the study. The study was registered on clinicaltrials.org under the number NCT01383187, and was approved by the Institutional Review Board (IRB-No16/b2008 on April 30th, 2008). All 18 patients who agreed to participate (9 men, 9 women) consented according to institutional guidelines, and received standard therapy, which included surgical excision of devitalised tissue, dermo-epidermal skin auto transplantation, analgesia, and wound care. The additional local application of APC to the DESG before wound application was tested for improvement over standard care.

The timing of surgery was based on real or expected clinical progression. Determination of surgical management necessity was based on daily clinical examination as well as laser Doppler perfusion imaging (LDPI) every second day for up to 7 days. Any IIb-degree burn traumas, which were not expected to heal within 21 days, and all third degree burns, were grafted with DESG.

Surgical Procedure

A radical excision of nonviable tissue was done just prior to grafting using tangential or fascial excision of necrotic tissues. DESG (split thickness skin grafts) were obtained using electric dermatome (Nouvag, Switzerland or Aesculap, Germany) from the thigh. After positioning of the DESG, it was spray-coated with APC and human autologous thrombin using a SmartJet applicator Harvest Technologies Inc, Plymouth, USA). After 20-30 seconds to allow gelling, the area was covered with Surfasoft foil (Taureon, Netherlands) and the dressing was fixed with disposable skin staplers at the margins. To prevent drying of the foil, a layer of gauze moistened with saline was applied before the final top layer of elastic roller bandage (Panep, Czech Republic).

Preparation of the APC

The APC was prepared using the Harvest SmartPRep Platelet Concentrate System [Harvest Technologies, Plymouth, MA, USA] as described previously[16].

Preparation of autologous thrombin: briefly, peripheral venous blood was obtained under aseptic conditions by venipuncture just prior to the surgery. The first 9 mL of venous blood collected into 1 mL ACD-A anticoagulant [Harvest Technologies] primed syringe and allowed to stand for 45 min at room temperature. This was centrifuged at 1000 RPM for 15 min, filtered using the set provided by Harvest technologies. During the 45 min incubation, 60 mL of venous blood was collected for preparation of APC. The 60 mL of venous blood along with the 6 mL of ACD-A (1:10 dilution) was put into the separator chamber and the gradient density centrifugation using the Harvest Technology System for 15 min at 1000 RPM was provided. After finishing the process of centrifugation we kept at disposal the 3 mL of autologous thrombin and 10 mL of aoutologous platelet rich plasma. On average, 10 mL of APC can cover ~ 4% of the total body surface area. The direct spray application of the APC and the autologous thrombin was done using the SmartJet applicator [Harvest Technologies, Plymuth, MA, USA].

Hematological, biochemical, and cytokine analyses

Hemoglobin concentration, a full white blood cell differential, platelets count, mean platelet volume, platelets distribution width and immature platelets fraction were evaluated in whole blood, platelet rich plasma and platelets-depleted plasma prior to surgery, and at 7, 14, and 90 days (Table 3). Prothrombin time, activated partial thromboplastin time, thrombin time, and fibrinogen were measured on a SYSMEX CA 7000 automated analyzer prior to surgery, and at 7, 14 and 90 days. Measured hematological values were compared to clinical ranges of normal values. Biochemical analysis such as liver function tests (ALT, AST, GGT) and inflammatory indexes (C-reactive protein), and analysis of cytokines by means of ELISA (BioVendor – Laboratorni medicina, Czech Republic) were performed according to standard procedures supplied by the manufacturer.

Histopathology analysis

Burn eschar, DESG alone, and DESG/APC specimens were fixed by immersing in 10% formalin and processed in the Clinical Pathology lab. After alcohol-xylene dehydration and automated paraffin embedding, 2-4 μm sections were cut and mounted on a glass microscope slides before staining with hematoxylin/eosin. The DESG and DESG/APC specimens were also stained by immunohistochemistry for PDGF, VEGF, bFGF, and SDF1, using monoclonal anti-PDGF, (BioGenex, San Ramnon, USA), polyclonal rabbit anti-VEGF (DakoCytomation), polyclonal mouse anti-PDGF-B (BioGenex) with secondary chromophore staining red (DakoCytomation) and brown (EXBIO). A senior clinical pathologist completed the final pathological examination in a blinded fashion.

Laser Doppler perfusion Imaging (LDPI)

A Perimed PIM3 laser Doppler perfusion imager was used to assess tissue perfusion in the burn region. The method employs color-coded mapping of skin perfusion using a laser beam to detect velocity and volume of red blood cells[17], and the evaluations were made pre-operatively, every second day for 2 weeks post operatively, and then at 1, 3, 6, 12 months.

Graft Evaluation

Viability: A visual analogue scale for graft viability was developed at our centre and consisted of the following scores: i) graft color (scale 0-3), where 0=pink, 1=pale, 2=livid (dark purplish, hyperperfused, +/- secretions), 3=necrotic; graft fixation to wound bed (scale 0-2), where 0=entire graft is fixed, 1= areas of incomplete fixation, 2=total lack of fixation; secretions (scale 0-3), where 0=no secretion through the fenestrations, 1=serous secretions, 2=seropurulent secretions, 3=purulent secretions. The evaluations were made every second day for 2 weeks post operatively, and the best total score was 0.

The Vancouver Scar Score Scale has been validated recently and uses pigmentation, vascularity, pliability and height of the scar in its scoring system[18]. The best total score is 0 (range 0-14). The scores were determined at 1, 3, 6, and 12 months.

Degree of Epithelialization Scale (0–3) was developed in our centre, and evaluations were made every second day for 2 weeks post operatively. The optimal total score is 0 (visual evidence of complete epithelialization of fenestrations) and the worst score is 3 (no evidence of epithelialization).

The scale to evaluate rate of healing was also developed at our centre, and is as follows: Percentage of burned area (affected area/total body surface) was estimated upon arrival using Dubois evaluation of total body surface of the patient. The area covered by the graft was considered 100%, and other areas, where the application of a graft was not necessary, were not included in this evaluation. Each area was assigned a value between 0 and 6 to indicate the percentage of healing, where 0=100%healed, 1>99%, 2>95%, 3>90%, 4>80%, 5>60%, and 6<60%. The evaluations were made every second day for 2 weeks post operatively.

Pain evaluation

Visual Analog Pain Scale (VAPS; best total score=0), which has been standardized for clinical application previously[19], was used for evaluation one day prior to grafting and every second day for 2 weeks post operatively.

Graft Pruritus

Visual analog pruritus scale (VAPrS) has been standardized previously[20]. Scoring ranges from between 0-10, with 0 indicating total lack of pruritus and and 10 most severe pruritus. Evaluations were made one day prior to grafting and then every second day for 2 weeks post operatively.

Data analysis

Initial statistical analysis was conducted using IBM SPSS, version 18 for Windows (ACREA CR, Inc.). All reported *P*-values are two-sided, and only *P*-values less than 0.05 were considered statistically significant. Continuous variables are reported as mean ± standard error of means (SEM), categorical variables as frequency and percentage. Standard distribution of the data could not be assumed due to small sample size, and the changes of hematological and biochemical parameters over time (prior to surgery, day 7, 14, 90 post surgery) were analyzed using non-parametric, related samples Friedman's two way analysis of variance by ranks with all pair wise multiple comparisons. Mathematical statistics was not the best tool for analysis of the data because (1) the sample size was only 18; (2) there was a high inherent inter-individual and intra-individual variability; (3) the data probability distributions were non parametric; (4) they were highly heterogeneous, and (5) the "outliers" contained very valuable information, that would have been missed if standard statistical tests were applied. We therefore used non-statistical methods based on mathematical gnostics. The method incorporates: i) robust probability distribution of different parameters at multiple time points (both static and dynamic analysis), ii) robust correlation between parameters, iii) robust multi-dimensional analysis, and iv) robust testing of hypotheses[21]. The methods were adopted from methodological sources, published applications, and the tools based on computation system of R-project™.

RESULTS

The demographics, extent and etiology of deep burn trauma of the 18 patients seen at the University Hospital Ostrava between January 2009 and December 2010 are summarized in (Table 1). The hospital stay statistics are summarized in (Table 2). Despite the length of surgery having been significantly elevated ($P<0.02$), the length of hospital stay was significantly decreased ($P<0.06$), and there was a trend to a shorter hospital stay in the DESG/APC group. Seventeen out of the 18 patients were treated by primary intent and 1 following a secondary disintegration of a partially healed wound on the face.

Table 1. Patients demographics.

Demographic	Mean +/-SEM
Age	54.94 +/-4.1
Gender	M:F 9:9
Smokers	7/18 (38.9%)
Diabetes	1/18 (5.55%)
Hyperlipidemia	2/18 (11.1%)
Cardiovascular Disease	7/18 (38.9%)
Hematological malignancy	0
Thrombocytopenia	0
Chronic renal failure	0
Systolic BP	138 ± 3.0
Diastolic BP	78.8 ± 1.4
Body temperature	36.8 ± 0.1
Height [cm]	168.4 ± 2.2
Weight [kg]	75.9 ± 3.3
BMI	26.4 ± 1.0
Average burns extent of TBSA [%]	9% (1% - 18%)
Average grafted area of TBSA [%]	3% (1% - 10%)
Liquid source of burns	8 pts
Flame source of burns	7 pts
Metallurgic slug	1 pt
Gas explosion as source of burn	1 pt
Electrical burn	1 pt

Avarage burns extent of TBSA [%] and grafted area of TBSA [%] with the etiology of deep burn trauma.

Patient evaluation

Visual Analog pain scale (VAPS) results are summarized in (Fig. 1A). Approximately 78% of patients required analgesics prior to the surgery (Fig. 1B), but by 14th post-operative day (the end of the monitoring period) only 6% of patients still required analgesics. The role of inflammation in loss of graft, edema and inflammation is shown in (Fig. 1C,D). Each individual curve represents the relationship between pain and leukocytes at a given time by means of the conditional probability function denoted Probability {x|y}. The different colors define time and condition: prior to the procedure patients had pain scores of either >2 (out of 10) (black) or < 2 (red); at 7 days patients either had no pain (magenta) or pain > 1 (blue); by the 14th day only 6% of patients had low pain (brown), with scores >1, while the rest were pain free (green).

Visual Analog Pruritus Scale (VAPrS) The use of the combination DESG/APC appeared to markedly reduce the level of pruritus (Fig. 2A), an established predictor of hypertrophic scars[20], compared to historical data (shaded area) and corresponded with greatly reduced antihistamine use (Fig. 2B). The frequency of patients using antihistamines reached a minimum (17/18 or 94%) at post-operative day 4 and remained at low levels (78% medication free) throughout the observation period (up to 12 months). The few patients remaining on anti-histamines beyond this time did not appear to benefit from the medication. Decrease in pruritus correlated to absence of scarring, and the decrease matches the fact that the majority of patients did not to need antihistamines throughout the observation period (12 months) (Fig. 2C). Most notably, the patients with pruritus had low levels of eosinophils throughout the study, suggesting that the mechanism of pruritus may not be histamine related (Fig. 2D).

Graft healing

The healing of the graft was associated with less complications from infections, decreased graft failure and better acceptance by patients than traditionally observed. The degree of wound healing was evaluated and assigned a score, as described in Materials and Methods. By the fourth day, a third of the wounds were >99% healed (Fig. 3). By the end of the study period (18 days) 94% of the wounds were 99% or greater healed.

Table 2. Cost analysis of in hospital stay.

	DESG/APC (Mean)	SEM	DESG (Mean)	SEM	T-test
Surgery time (Min)	121.5	5.45	81.25	7.63	0.002
Hospital stay (Days)	18.5	1.28	27.2	1.93	0.006
Cost (Thousands-CZK)	48.2	1.03	64.6	1.39	0.169

The highest total Vancouver Scar Scale Score was 4 (median) and occurred at 3 months post surgery. After this point, the median VSS score decreased steadily, reaching 2 (the lowest point) at 6 months and remaining at this score for 1 year. This score of 2 was due to hyperpigmentation in the 6 patients. Most importantly, all of the scars were without any marks of hypertrophy or contractures; thus, avoiding the need for secondary intervention or contraction release (Fig. 4).

While epithelialisation occurred no faster than traditionally observed, the quality of the epithelialisation, as judged by absence of inflammation and good fixation of

Table 3. Platelet Rich Plasma Analysis.

Platelet Rich Plasma	Mean	SEM
Platelet count (x10^9/L)	1011.94	69.58
Platelet volume (fL)	9.70	0.29
Platelet distribution width (%)	10.98	0.58
Immature Platelet Fraction (%)	2.75	0.66

Platelet rich plasma sample analysis of the 60 mL of peripheral blood after 15 min of gradient density centrifuge procedure with Harvest SmartPRep Platelet Concentrate System.

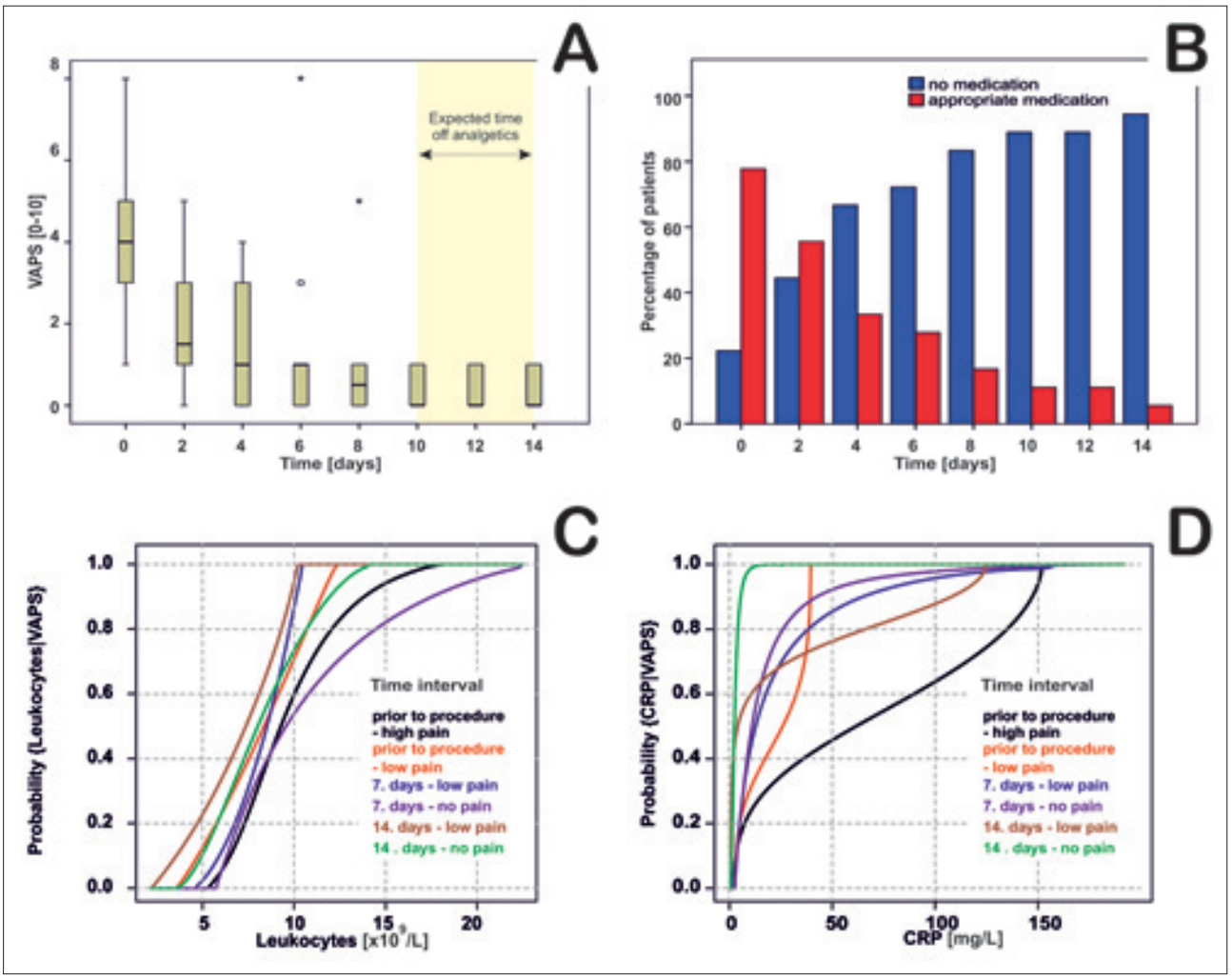

Fig. 1. Post operative pain assessment after DESG.

A) Visual Analog Pain Scale (VAPS): Patients treated with APC and DESG were evaluated using a VAPS from 0-10. As evident, most were pain free by day 6. The shaded area in A indicates historical experience with pain disappearance.

B) Percentage of Patients on analgesics. Prior to surgery, approximately 78% of patients required analgesics, by the 2nd post-operative day, the number dropped to 56%, by the 4th post operative to 33% remaining on analgesics, and by 14th post-operative day (the end of the monitoring period) only 6% of patients require analgesics.

C) Impact of Leukocytes on the Pain Evaluated in Visual Analog Pain Scale. The curves are gnostic distribution functions of leukocytes conditioned by a certain level of pain. Each individual curve represents the relationship between VAPS and leukocytes at a given time. Prior to DESG the VASPS some patients had 2/10 pain (black curve), or less than 2/10 pain(red curve), at 7 days, there are patients without pain (purple) and with pain over 1 (blue), by the 14th day only 6% of patients have pain (brown) over 1 and the rest is pain free (green).

D) Interpretation of VAPS using Distribution Functions. The curves represent the conditional probability (in this case probability of c-reactive protein influencing pain). The diversion of the probability curves indicates that 82% of the patients with high CRP also had high pain prior to procedure. At 7 days those with pain and those without pain had nearly the same concentration of CRP, and finally at 14 days those in whom inflammation persisted had high pain (brown) and those with low CRP had no pain (green).

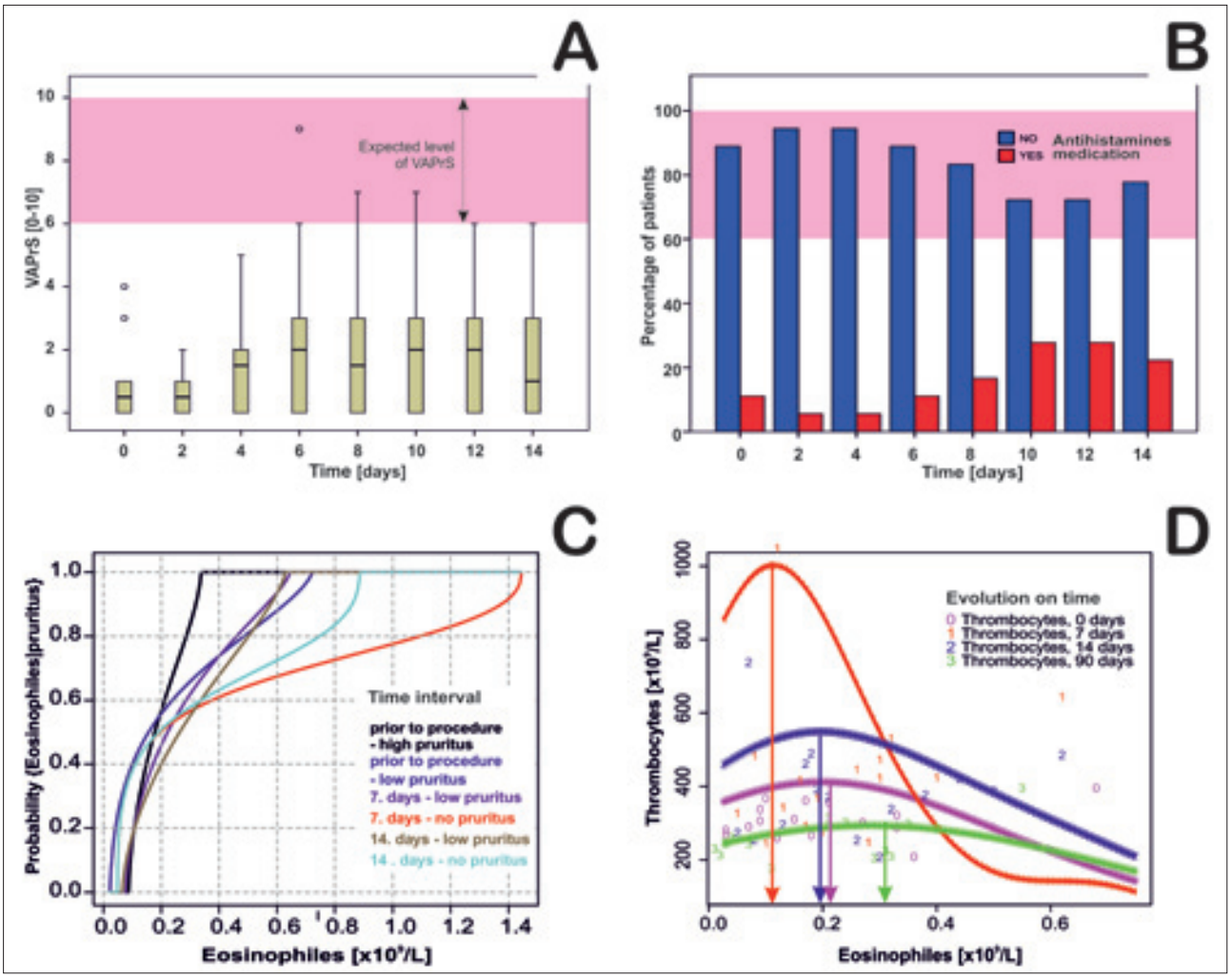

Fig. 2. Post operative pruritus assessment after DESG.

A) Visual Analog Pruritus Scale (VAPrS): The range of the scale is from 0-10. As evident, degree of pruritus was lower than in patients not treated with DESG/APC (shaded area). Pruritus drops from pre-procedural levels, reaching a nadir at 7 days, and then raising again with healing (B). B) Percentage of Patients using antihistamines. Percentage of patients on antihistamines was used as a surrogate for pruritus and scar formation. On the 2nd and 4th post-operative day 17/18 patients (94%), and on 14th postoperative 14/18 (78%) patients did not require any antihistamines. C) Interpretation of VAPrS and eosinophils using Distribution Functions. Each individual curve represents the relationship between eosinophils and pruritus at a given time. Prior to surgery there was ~55% of patients who had low levels of eosinophils and high pruritus (note the value at which blue and black curves cross) and the remainder had low eosinophils and high pruritus (blue curve). At 7 days the low pruritus line (purple) and no pruritus lines (red) intersect at about 50%. Decrease of pruritus was correlated to absence of scarring, and the decrease of pruritus is in agreement with the finding that majority of patients continued not to need antihistamines throughout the observation period (12 months). D) Relationship between platelets and eosinophiles analyzed using Distribution Functions. Their inter-relationships reveal that at 7 days there are low eosinophiles and high platelets (significant at 0·1 eosinophiles, red line). At 14 days, platelets decrease, but remain higher with a peak of $600x10^9$/L, and by 3 months both eosinophiles and platelets are in normal ranges. Most notably, the patients with pruritus had low levels of eosionophils throughout the study, suggesting that the mechanism of pruritus *may not be* histamine related. This would agree with the finding that those patients using anti-histamines to control pruritus do not get relief from the medication.

Table 4. Coagulation statistical analysis.

	Day 0 - 7	Day 0 - 14	Day 0 - 90	Day 7 - 14	Day 7 - 90	Day 14 - 90
APTT			↓*P*=0.003		↓*P*=0.026	
TT						↓*P*=0.003
Fbg		↓*P*=0.006	↓*P*=0.000	↓*P*=0.016	↓*P*=0.000	
Platelets	↑*P*=0.026				↓*P*=0.000	↓*P*=0.000
INR		↑*P*=0.032	↑*P*=0.041			

↑ Significant increase ↓ Significant decrease

Activation of the coagulation cascade. A clot is necessary for the creation of a platelet rich fibrin/collagen matrix that facilitates early phases of wound healing by providing a scaffold for the migration and homing of inflammatory and mesenchymal cells. While aPTT, TT, INR and platelets are higher than normal at 7 days suggesting a compensated disseminated intravascular coagulation in the first week post procedure, all parameters gradually improve over the 14 days and normalized by 90 days by significant decrease.

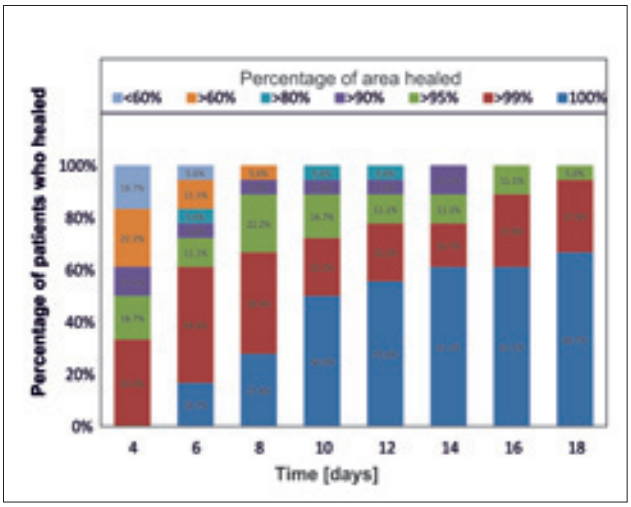

Fig. 3. Rate of Healing. The rate of wound healing was evaluated on a scale 0-100%. The majority of graft area (more than 99%) was healed in 33% of patients on the 4th post-operative day, in 61% on the 6th day, in 67 % on the 8th postoperative day, in 72% on the 10th day, 78% on the 12th day and 94% of patients on the 18th post-operative day. The healing seen with DESG and platelets occurs earlier is more robust.

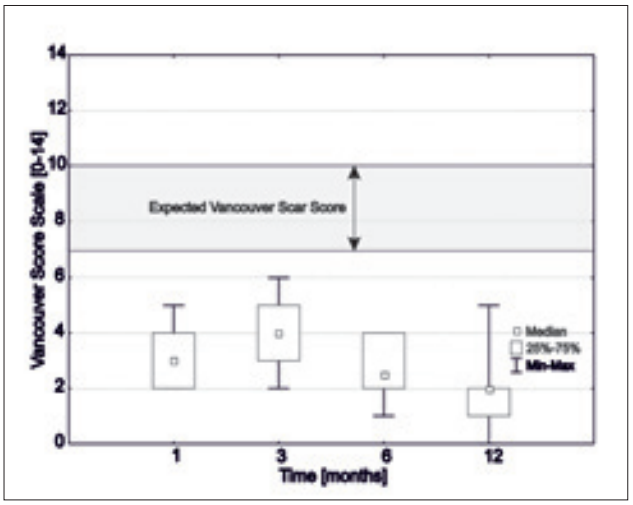

Fig. 4. Vancouver Scar Score Scale. The scale score is based on: pigmentation (0-3), vascularity (0-3), pliability (0-5), and scar height (0-3) with a maximum achievable score of 14. The Vancouver Scar Score ratings of patients not treated with DESG and platelets range between 7-10 (grey shaded area), mainly because 40-60% of these patients have scar hypertrophy (1). In our study, patients treated with the combination show a remarkable decrease of scores with maximum scores achieved at 3 month (median=4) and high quality scar (median=2) from 12 months onward.

the tissue to the wound bed, was greatly improved. Most grafts (72% of patients) were completely reepithelialised by the tenth day (Fig. 5A). Improved epithelialisation was also associated with statistically significant suppression of the inflammatory response as measured by decrease in CRP and fibrinogen levels in the plasma of those patients with faster healing wounds (Fig. 5B,5D). There was no apparent correlation with reepithelialisation rate and leukocyte counts (Fig. 5C).

Coagulation and Haematological analysis

The evolution of coagulation parameters over time following treatment with DESG/APC was evaluated (Fig. 6). The tendency for early healing (rate of graft healing <2 on day 4), or late healing (rate of graft healing <2 on day 6), was not related to platelet counts, MPV, or Immature Platelet Fraction (data not shown). The methods of analysis for Coagulation parameters (aPTT, INR, Fibrinogen, Platelets and Thrombin Time) were suggestive of compensated disseminated intravascular coagulation (Fig. 6) and are summarized in (Table 4). The levels of cellular indicators of inflammation and stress corresponded to the observed clinical decrease of inflammation (Fig. 7). The normalization of lymphocyte counts reached significance by the 7th postoperative day (*P*=0.21), and remained so throughout the early post-operative and late stages (*P*=0.27) on day 90 (Fig. 7C). A significant decrease in monocyte counts was also observed throughout the follow up period (day 0-14, *P*=0.05; day 0-90, *P*=0.03) (Fig. 7E), indicating early resolution of inflammatory response,

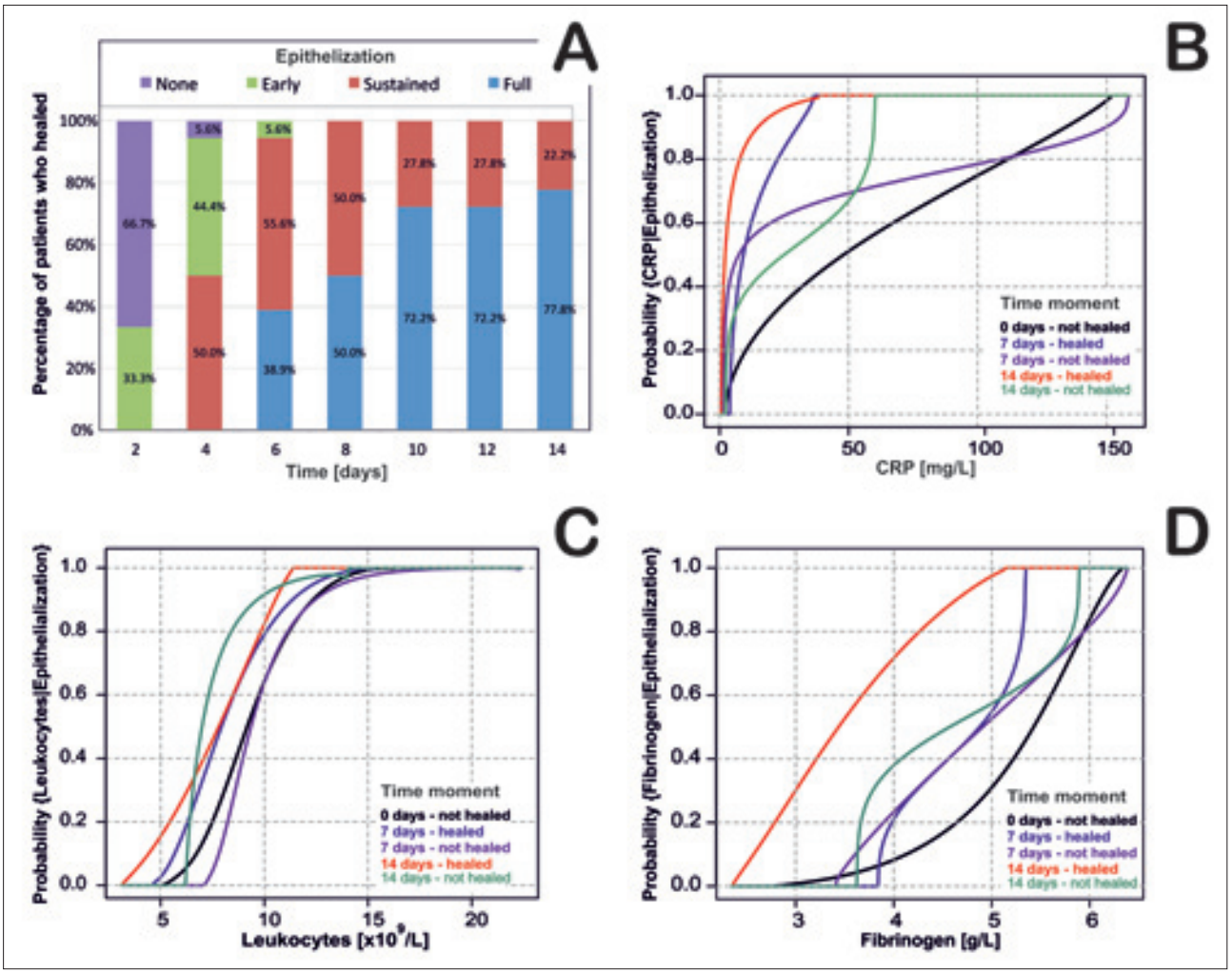

Fig. 5. Inflammation during re-epithelialization.

A) Rate of post-operative re-epithelialization. The rate of epithelization was evaluated using a scale from none=3 points, early=2, sustained=1, and full=0. We found that most grafts (72% of patients) were completely epithelialized by 10th day.

B) Conditional distribution functions correlating epithelialization and c-reactive protein (CRP) at 0, 7 and 14 days. It appears that better epithelialization on the 7th and 14th post operative day are related to a lower CRP (red and blue line).

C) Distribution functions correlating epithelization and leukocyte levels. At 7 days all patients without healing have higher leukocyte counts (purple line) than those that healed (blue line. In contrast at 14 days the patients who have not healed have lower levels of leukocytes, while higher levels of leukocytes are correlated to better healing (red line). However, because the majority of patients (78%) were healed at 14 days, leaving few patients for calculation of this curve, it is difficult to reach the later conclusion.

D) Dependence of epithelialization on the fibrinogen levels. Following healing (at 14 days) fibrinogen levels appear to have dropped (red line) to less than baseline (black line at day 0). At 7 days there appear to be only small differences between healers and non-healers.

which corresponded well with perfusion data (Fig. 10) as well as the clinical evaluation of wounds (Fig. 12). Because the initial values were obtained during acute injury, the comparison was made with the values at 3 months when all patients had healed and exhibited no evidence of inflammation (Fig. 7). A reactive increase in red blood cells hemoglobin and hematocrit was seen on days 7–90 (Fig. 7B,F), most likely reflecting no blood loss.

Cytokines analysis

The blood elements carry a cargo of growth factors, inflammatory cytokines and chemoattractants for mesenchymal cells, and we analyzed the relationships between the different cytokines in the initial platelet concentrate used for the grafting. The levels of growth factors in platelets correlated not only with platelet and neutrophil counts and mean platelets volume, but also with the rate of graft healing. A strong inverse correlation was found between the MPV levels and SDF-1 counts. Similarly strong positive correlations were observed between platelets, neutrophils and the amount of growth factors, confirming that VEGF is accumulated in platelets and neutrophils (Fig. 8).

Histolopathology

Patients with DESG containing all layers (dermal, epidermal, fibrin/collagen adventitia) (A) appeared to be healing faster and their grafts retained better integrity

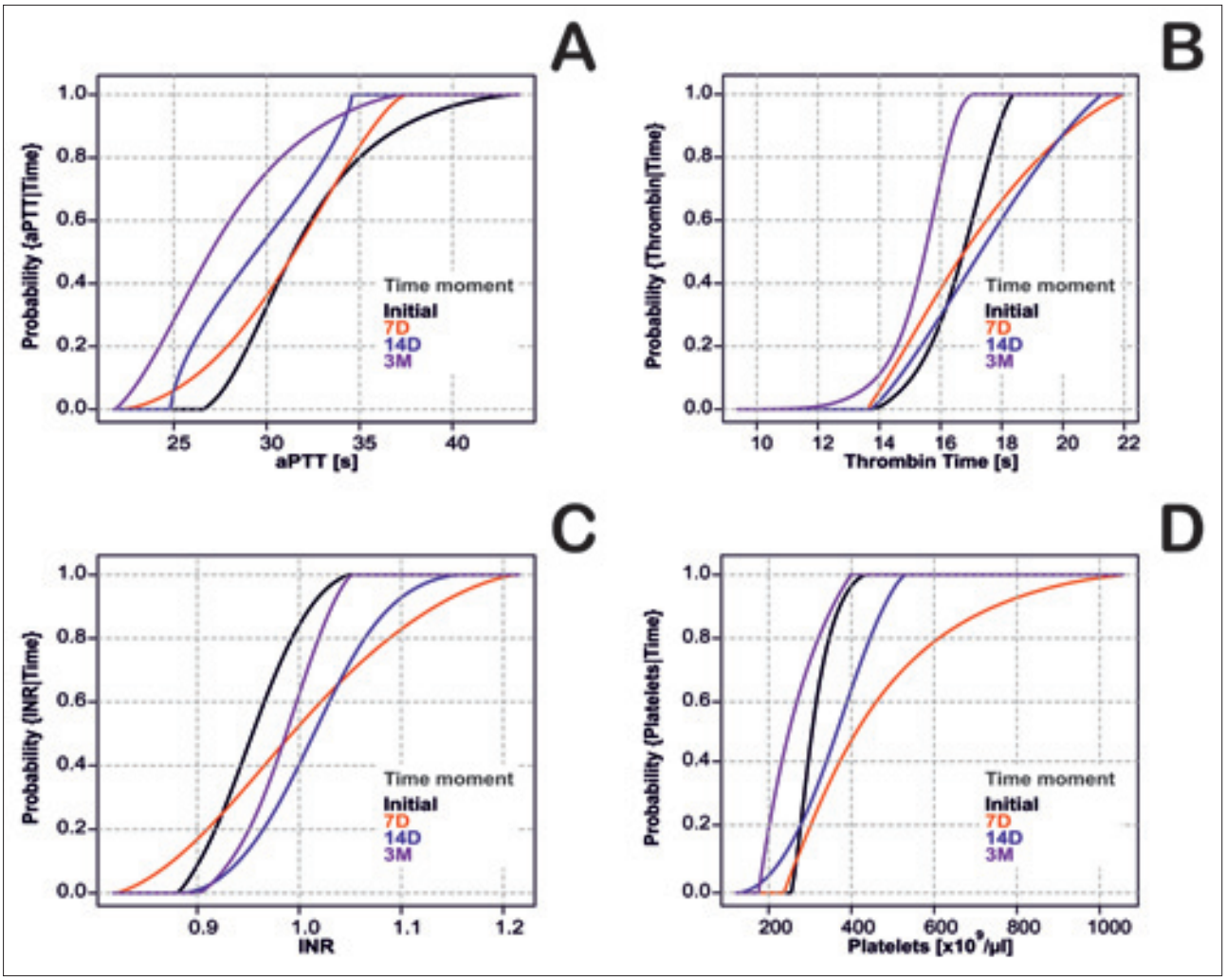

Fig. 6. Distribution of individual coagulation parameters.

A) Evolution of Distribution Functions of aPTT: While values of aPTT are higher than normal at 7 days (black curve vs red curve), they gradually normalize at 14 (blue) and 90 (purple) days.

B) Evolution of Distribution Functions of TT. The values of TT are higher than normal at 7 days in about half of cases (black vs red curve), they remain elevated at 14 days (blue), and gradually normalize by 90 days (purple). The value of TT following the surgery (cross of the black line with blue and red) remains high and very variable in over 50% patients at 7 and 14 days, but normalizes at 3 months.

C) Evolution of Distribution Functions of INR. The value of INR is elevated and very variable in nearly 80% patients at 7 days. At 14 and 90 days the values somewhat normalize, but never reach initial levels.

D) Evolution of Distribution Functions of Platelets. Platelet levels at 7 days following surgery are significantly elevated and very variable in over 90% patients (cross of the black line with red), and they gradually normalize and correct to values less than those at initial (black curve) by three months.

throughout. Thin grafts (B) usually missed sub-epidermal layers, and resulted in delayed healing, mainly due to lack of firmness and increased secretions, leading to less stable grafts at 3 months. Viable platelets and PDGF could be demonstrated in all patients who received DESG/APC. The cellularity of the germinal layer of the graft correlated with graft viability; conversely, lack of cellularity and increased number of apoptotic nuclei within the germinal layer indicated decreased rate of healing (Fig. 9). The expression of PDGF (Fig. 9E,F), and bFGF (Fig. 9C,D) was confined to the germinal layer, an area most commonly inhabited by progenitor cells. The presence of viable progenitor cells was corroborated by histochemical evidence of CD34/PDGF and CD34/ SDF-1 co-localization in the germinal layers (Fig. 9E,F,G,H).

Laser doppler perfusion, measured in perfusion units (PUs), showed a florid initial perfusion, a gradual decrease in perfusion during the first six days, followed by healing angiogenesis within a one month period (Fig. 10,11). All 18 patients had at least one pre-operative scan indicating pathologic post-traumatic inflammation with an increase in perfusion; following grafting, inflammatory reduction is reflected as a relative decrease in perfusion, before a secondary increase in perfusion after 14 days that indicates engraftment and angiogenesis. Following this

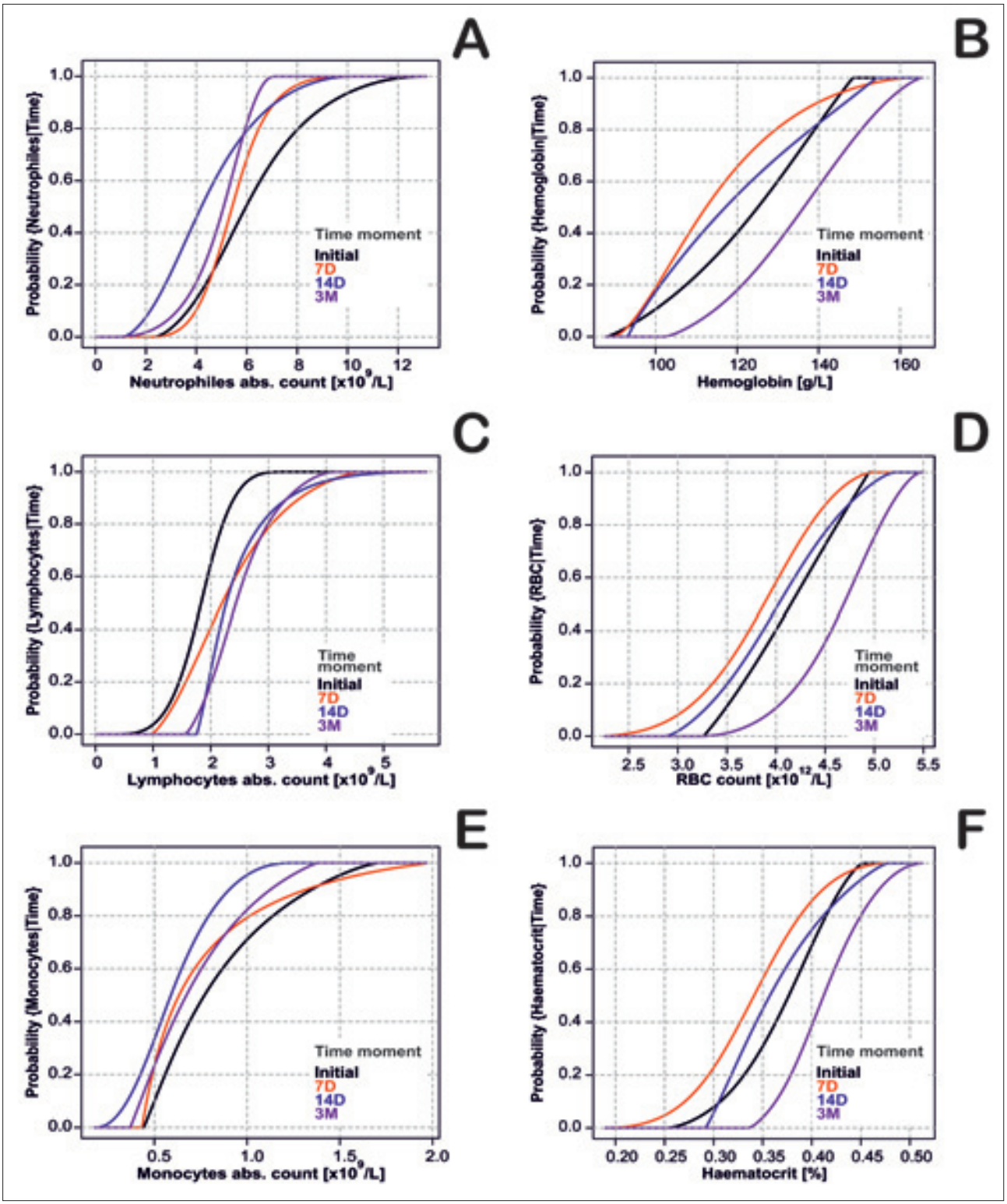

Fig. 7. Evolution of distribution functions of hematological elements. Following DESG/APC grafting. There is evidence of initial blood loss (left shift of the red curve) in hemoglobin, hematocrit and red blood cells analysis, with gradual stabililization of the curves over time on the level substantially exceeding the initial state. Dynamics of changes in neutrophile, monocyte and lymphocyte levels is less considerable but not negligible.

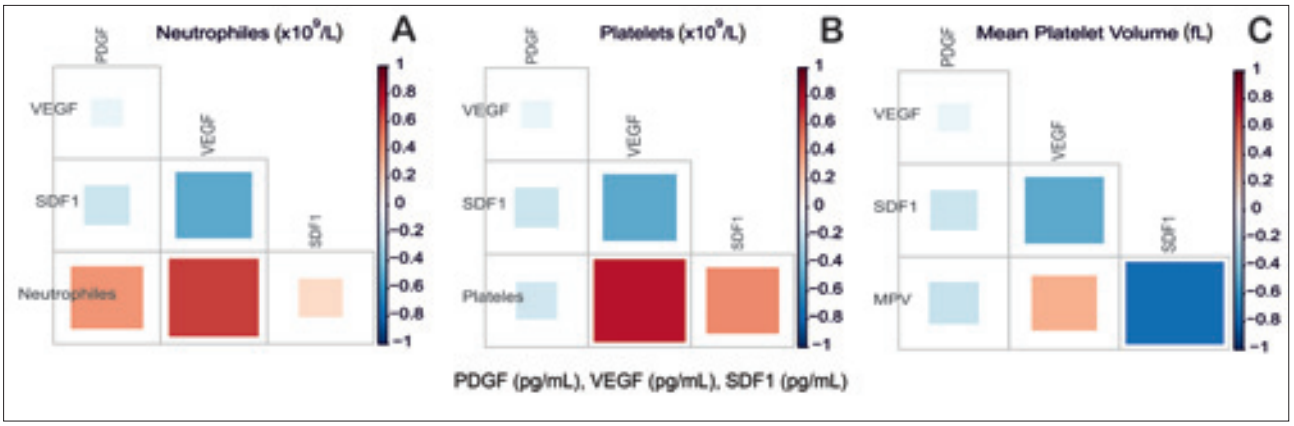

Fig. 8. Correlation diagrams for cytokines interactions. Heat map diagrams of correlation coefficients of individual selected cytokines, where blue represents a negative correlation [-1 to 1] and red represents a positive one [1 to -1]. The color and size of each individual square indicates a quantitative measure of the correlation. The diagram shows the correlations of neutrophiles, platelets or MPV (always in the left lower corner of the diagram), with 3 cytokines (VEGF, SDF1, PDGF). In the case of neutrophiles (A) and platelets (B), the strongest positive correlation is between VEGF and neutrophiles (or VEGF and platelets in B). Mean platelet volume (B) has a very strong negative correlation with SDF1. The correlation of VEGF and PDGF is very weak in all three correlations.

secondary peak and tissue regeneration, there is gradual drop in average perfusion at 360 days, indicating restoration of vascular quiescence.

Clinical evaluation by digital photography was done on day 2, 4, 6, 8, 10 and 14 after surgical procedure (see Fig. 12). Patient 1 was burned by melted metal on the job, and he was grafted on the 6th day post injury, 3rd degree burns covered 1.75% of TBSA. Complete healing was achieved by 8 days (A3), and a month later a normally pigmented, non-hypertrophic scar devoid of any contractures was noted. Patient 2 burned herself with a garden fire, and received the DESG/APC on 14th day post injury. She had 3rd degree burns of 2.5% of TBSA on the right thigh, popliteal region and calf of right leg (B1). The wound was completely healed by 8 days, and one moth post-surgery (B4) a well-healed scar devoid of contractures, ulcerations or infections is evident. Patient 3 had burned herself while cooking on the hypothenar area of the palm and dorsum of 5th and 4th finger. She had 3rd degree burns on 1% of TBSA, but involving highly sensitive area of the left hand and fingers. Complete healing was achieved on the 10th post-operative day. At one month the patient had a fully functional hand, and contraction-less scar.

DISCUSSION

The application of concentrated platelets in the setting of chronic ulcer[22,23], cardiovascular surgery[24], orthopedic surgery[25,26], sternum repair after cardiac surgery[27] and spinal injury[28] is increasing. However, in the case of burns, it has not been established whether there is any benefit of platelet therapy. The use of acellular pig dermis matrix consisting of a mesh of collagen and elastic fibres, may result in skin hypertrophy, and cultured keratinocytes lead to thin and unstable grafts[29]. Ideally, new therapies would incorporate progenitor cells capable of differentiating into various dermal cells to increase the quality of healed wounds. Additionally, application of individual agents or scaffolds do not allow for dynamic reciprocity of intercellular interactions that lead to normal tissue regeneration[30]. In this study we attempted to demonstrate benefit through the combination of Dermo-Epidermal Skin Grafts (DESG), which contain progenitor cells within the deep dermal layers, with autologous platelet concentrate (APC), which contains enhanced levels of cytokines and growth factors required to facilitate cellular cross-talk and interactions as well as to enhance recruitment of other cell types resident within bordering host tissues.

The 18 patients treated with DESG/APC were pain-free by day 6 (Fig. 1A), and since persistent pain in patients is due to delayed healing, and loss of graft, this supports an improved healing in DESG/APC treated patients. As seen in Figure 1, panel B only 6% of patients used analgesics at the end of the 14 day monitoring period. The probability of change in leukocyte counts (or CRP levels) under the condition of pain (Fig. 1C,D) indicate an initial (0-7 days) increase in inflammation, followed by a gradual drop in both CRP and leukocytes as pain disappears. This confirms the existing clinical suspicion that CRP and leukocyte counts are excellent markers/predictors of pain.

Pruritus (itching, edema and redness) could be directly correlated with healing (Fig. 2A,B,C,D). The salient finding from this measurement was that the frequency and severity of pruritus were both 2-3x less than the usually observed 6-10/10 VAPrS (shaded area in Fig. 2A). The somewhat surprising finding was a lack of correlation between eosinophils, platelets and pruritus, supporting the conclusion that pruritus is not in this case related to histamine release, and would not (and did not) respond to anti-histamine therapy. Lessening of pain and pruritus herald healing. In agreement with this are the findings in

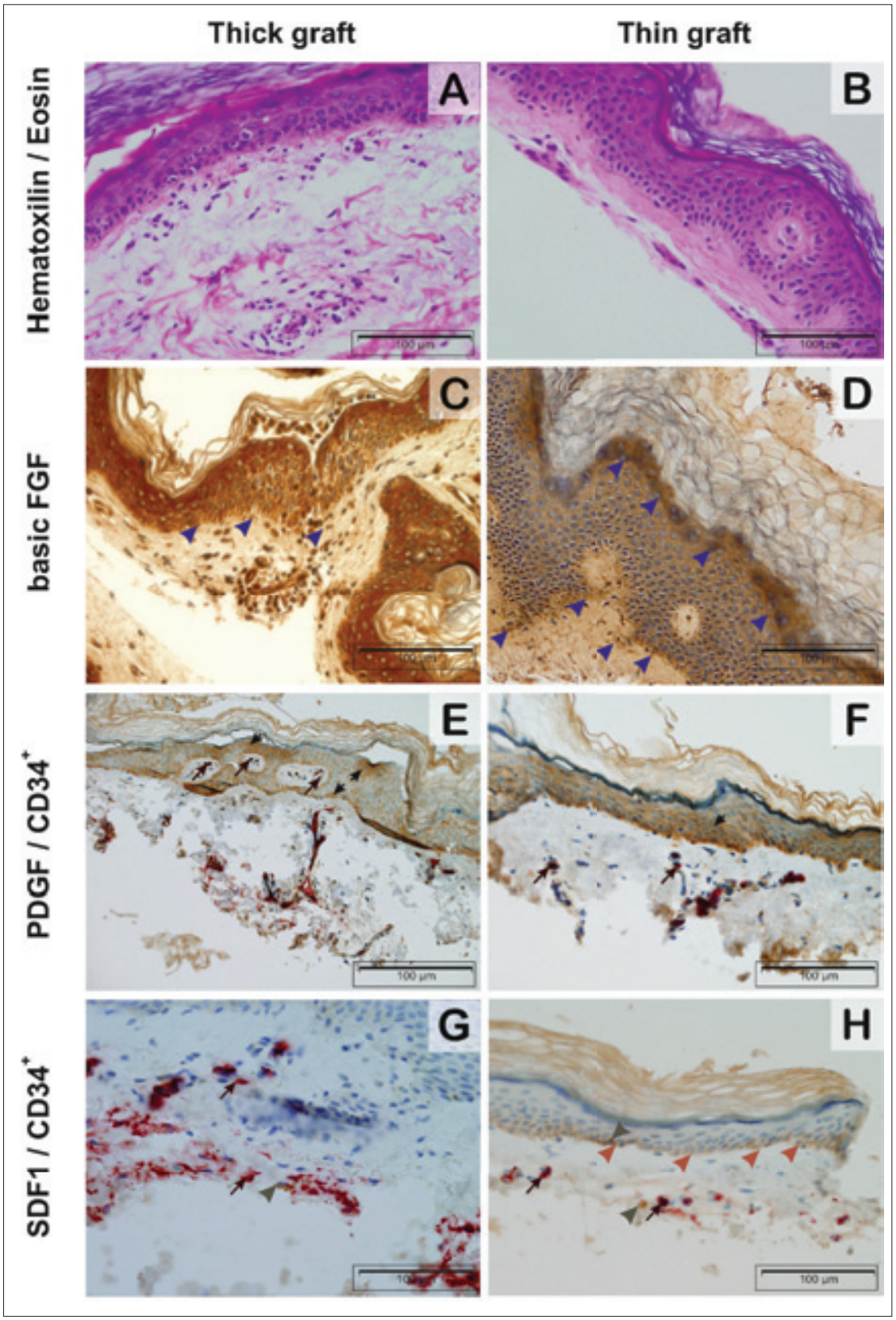

Fig. 9. Histology of DESG/APC at the time of application. Hematoxylin/Eosin: 40x; Immunohistochemistry for bFGF, Platelet Derived Growth Factor (PDGF), SDF1, CD34; was performed on the graft tissues at the time of DESG/APC application. The expression of bFGF localized to the stroma of the germinal layer (blue arrowheads in C,D), and to the junction of keratin layer and epidermis. The expression of PDGF is localized in the stroma of the germinal layer (black arrowheads in E,F), an area commonly inhabited by progenitor cells. Dark red arrows in E,F point to CD34+ cells marked by red stain. The expression of SDF1 is localized to the stroma of the germinal layer (brown arrowheads in G,H), and fibroblastic cells (dark grey arrowheads in G, H). Dark red arrows in G,H point to CD34+ cells marked by red stain.

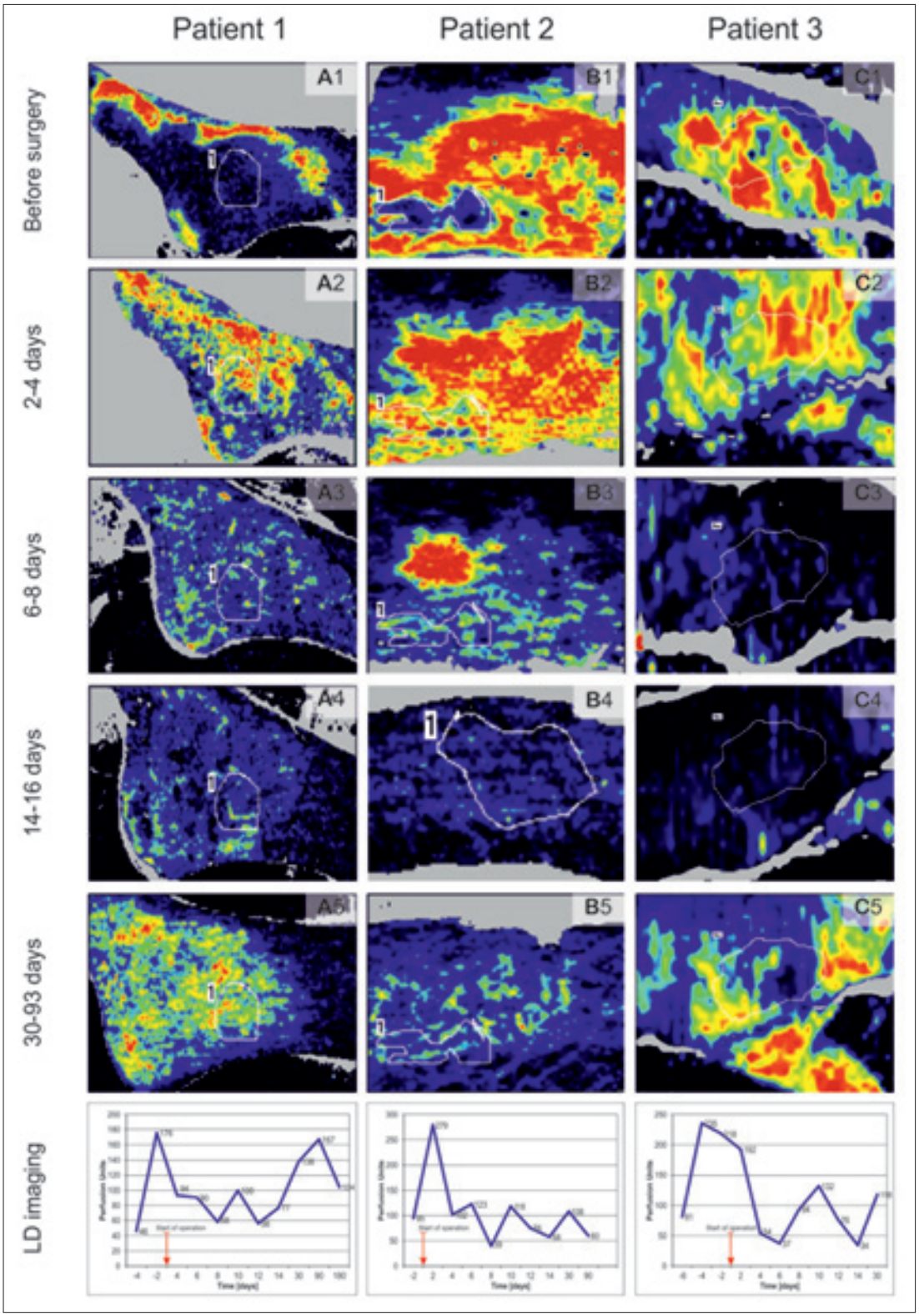

Fig. 10. Laser doppler imaging studies. Were donne on day 0, 6, 14 and 30. Day 0 is prior to any procedure. Each of the images has a defined region of interest (ROI) marked by a white border and labeled "1".

In patient 1 (A1-A5) a pre-operative scan, was done on the 4th post-traumatic day, and showed very low perfusion (46.4 perfusion units, PU), surrounded by inflammatory hallo (A1 on Fig. 10). On the 2nd post-operative day perfusion increased to 176 PU (A2). Next two scans indicate decrease in perfusion to 94 PU on day 4 and to 58 PU on day 8 before a secondary increase in perfusion that occurred with healing, and is evident by a rise to 167 at 93 days. *In patient 2 (B1-5)* the preoperative scan was acquired 12th post-traumatic day (day -2 of surgery) and showed low perfusion 94·9 PU, raising to 279·2 PU in the first 2 days post-op, before gradually decreasing to a nadir of 39·3 on the 8th post-operative day, and stabilized between 57·6-118·1 without a secondary peak. *In patient 3 (C1-C5)* was first scanned 7 days post trauma (day -1), and showed 81·5 PU, raising to 235·4 PU, dropping gradually to 37·2 on the 6th post-operative day, and stabilizing between 34·2 and 132 PU.

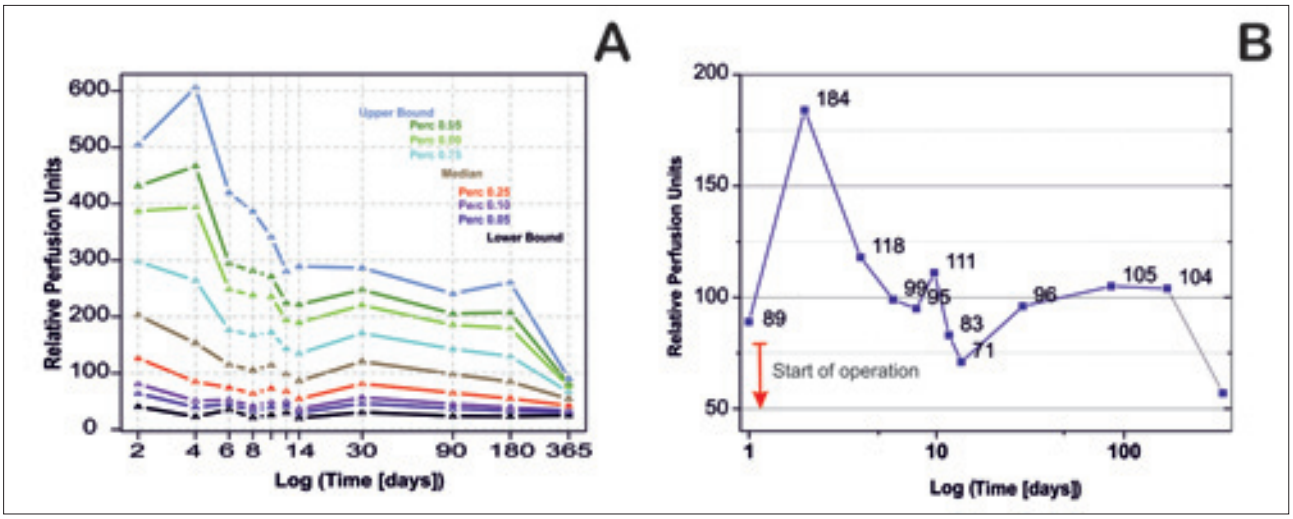

Fig. 11. Laser doppler perfusion study.

A) Dynamic summary of perfusion studies are obtained by estimating the distribution functions of the 11 data sets of RPU (Relative Perfusion Units) for each of the 11 time points. Nine values of percentiles of each of these distributions are calculated for probabilities 0, 0·05, 0·1, 0·25, 0·5, 0·75, 0·90 and 1. Percentiles are depicted in figure 11 on straight lines parallel to the Y-axis by color marks. It can be seen in Figure 11 that the large starting variability of RPU is still increasing at time 4D to fall to minimum at 365D.

B) Average perfusion units at each of the 11 time points. All 18 patients had at least one pre-operative scan indicating pathologic post-traumatic inflammation with an increase in perfusion (89); following grafting, inflammatory reduction is reflected as a relative decrease in perfusion that reaches a nadir between 6-14 days (PU 71-111 respectively), before a secondary increase in perfusion after 14 days that indicates engraftment and angiogenesis and peaks between 30-90 days (105 PU). Following this secondary peak and tissue regeneration, there is gradual drop in average perfusion to 61 PU at 360 days, indicating restoration of vascular quiescence.

(Fig. 3) showing a gradual increase in the percentage of healed area, with >94% of patients having over 99% of the burned area healed on 18th post-operative day.

One of the most attractive selling features of the combination of DESG and platelets may be the enhanced cosmesis and characteristics of the scar (Fig. 4 and Fig. 12). In patients not treated with this combination, scar hypertrophy often occurs 1-3 months post-operatively, and peaks at 3 months. The quality of scar formation and patient's ultimate functionality is best predicted by the speed and stability of epithelialization. While the rate of reepithelialization in patients treated with DESG/APC may not have been higher or faster than traditionally observed, the inflammatory markers normalized faster (Fig. 5 B,C,D), making the re-eptithelialized wound more stable. Most grafts (72% of patients) were completely reepithelialized by day 10 (Fig. 5A) creating a natural barrier to infection and preventing usual complications. Because of the minimal cicatrization in patients treated with DESG/APC, they had no need for pressure garments or other scar management.

Activation of the coagulation cascade is seen with any tissue injury (Table 4.). A clot is necessary for the creation of a platelet rich fibrin/collagen matrix that facilitates early phases of wound healing by providing a scaffold for the migration and homing of inflammatory and mesenchymal cells. While aPTT, TT, INR and platelets are higher than normal at 7 days (black and red in Fig. 7 A,B,C,D) suggesting a compensated disseminated intravascular coagulation in the first week post procedure, all parameters gradually improved over the 14 days (blue) and normalized by 90 days (magenta).

Activation of coagulation also leads to recruitment of platelets to the site. These blood elements carry a cargo of growth factors, inflammatory cytokines and chemoattractants for mesenchymal cells[9,11] and we analyzed the relationships between the different cytokines (Fig. 8) in the initial platelet concentrate used for the grafting. Both platelets and neutrophils were shown to be a great source of VEGF see (Fig. 8 A,B), and the VEGF correlated negatively with SDF1, substantiating the very distinct and temporally separated functions of these two cytokines. SDF1 is a chemoattractant for stem cells, whereas VEGF is an initiator of vascular sprouting and is needed only transiently. The histological analysis (Fig. 9) supports this interpretation of cytokine progenitor cell interaction, CD34+ progenitors are in the deep dermal crypts and in perivascular regions (Fig. 9E,F,G,H), whereas the deep epidermis stroma is rich in pro-angiogenic growth factors such as bFGF (Fig. 9 C,D) and PDGF (Fig. 9 E,F). In contrast, SDF1 co-localises with CD34+ progenitor cells (Fig. 9 G,H). The final neovascularization is the outcome of a complex network of interactions between transient expression of VEGF (vascular sprout initiation), FGF2 (vascular stalk formation), and PDGF (pericyte recruitment and vessel maturation).

From serial dynamic perfusion studies used to follow up patients grafted with DESG/APC emerged a very characteristic pattern of pathological and physiological angio-

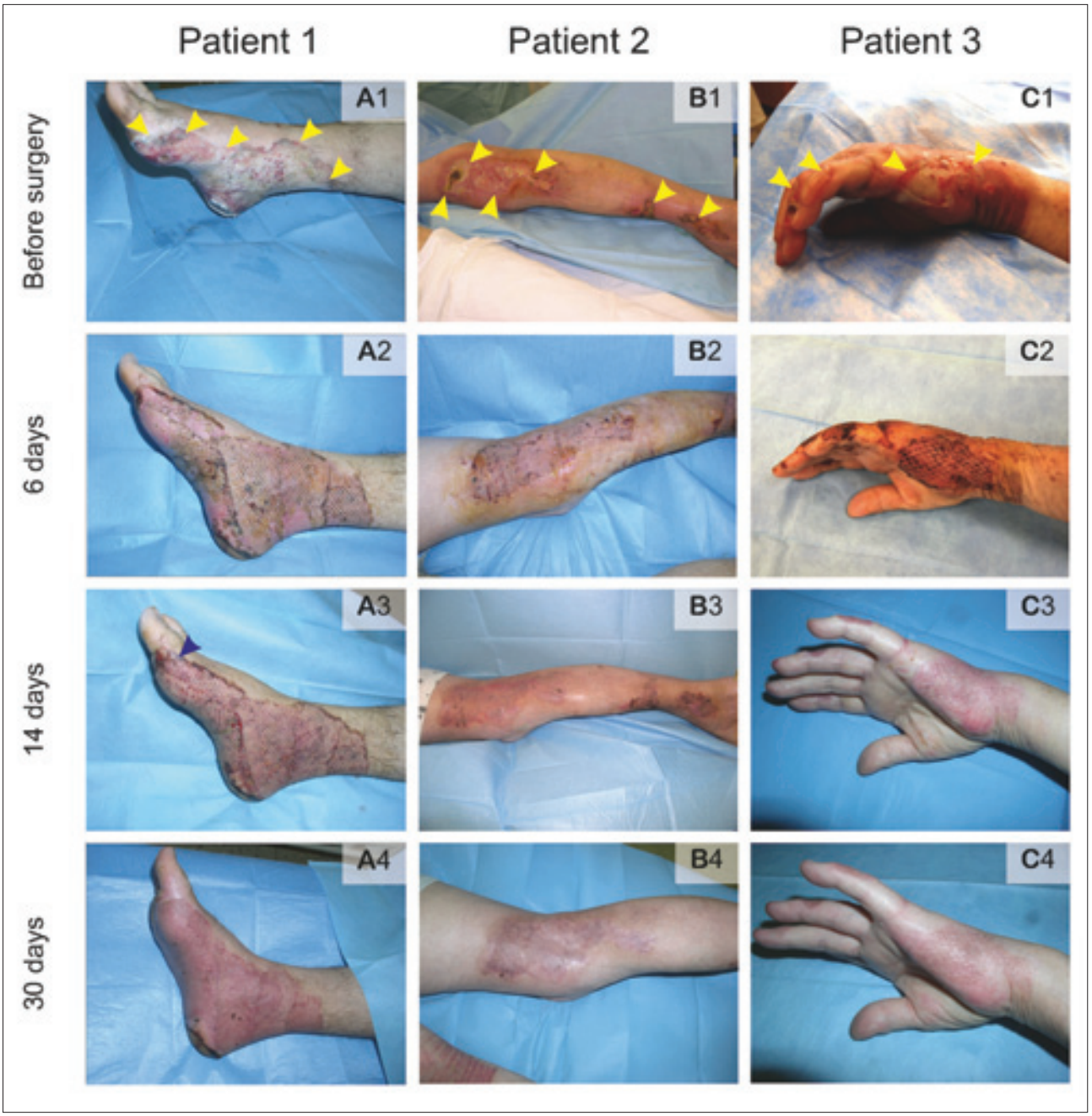

Fig. 12. Clinical evaluation photography. Serial photographs on day 6, 14 and 30 post grafting. Each vertical row represents a single patient.

Patient 1 was burned by melted metal on the job, and he was grafted on the 6th day post injury, 3rd degree burns covered 1·75% of TBSA. On the day of grafting the entire area was necrotic with full thickness damage. On the 6th day (A2) pink granulation tissue well-fixed to the wound bed, and devoid of secretion suggesting a vital skin grafts in over 99% of the surgically treated area. The blue arrowhead points to the Histoacryl® glue with which the graft is affixed to the tissue. Complete healing was achieved by 8 days (A3), and a month later a normally pigmented, non-hypertrophic scar devoid of any contractures was noted. Heal was the only hyperkeratotic area discolored by iodine. *Patient 2* burned herself with a garden fire, and received the DESG/APC on 14_{th} day post injury. She had 3rd degree burns of 2·5% of TBSA on the right thigh, popliteal region and calf of right leg (B1). On 6th day a vital skin graft was noted in over 99% of the surgically treated area. The wound was completely healed by 8 days, and one moth post-surgery (B4) a well-healed scar devoid of contractures, ulcerations or infections is evident. *Patient 3* had Patient C burned herself while cooking on the hypothenar area of the palm and dorsum of 5th and 4th finger. She had 3rd degree burns on 1% of TBSA, but involving highly sensitive area of the left hand and fingers. She underwent grafting on the 8th day. On the 6th post-surgical day, fully vital skin grafts were noted on more than 99% of the surgical area. Complete healing was achieved on the 10th post-operative day. At one month the patient had a fully functional hand, and contraction-less scar.

genesis (Fig. 11). Following the grafting, the pathologic inflammation regresses and a secondary peak occurs at the time of reperfusion, reflecting healthy regenerative angiogenesis between1-3 months.

One of the most important findings of this study was the cost effectiveness of the therapy. Despite the longer operating times, the cost of hospital stay was lower (approximately 25% less) than that of institutional controls who did not receive DESG/APC grafting.

CONCLUSIONS

Our study indicates that DESG/APC is a combination with superior outcomes to the present standard of care and should be embraced widely. Patients treated with DESG/APC had high quality of healing without evidence of scar hypertrophy or contractures. The intervention markedly benefits patients, the community, and health care in general. We showed that even though the length of time for the initial procedure may have been somewhat longer, significant cost savings in hospital stay and subsequent revisions were achieved.

ABBREVIATIONS

APC, Autologous platelet concentrate; HAT, Human autologous thrombin; LDPI, Laser doppler perfusion imaging; DESG, Dermo-epidermal skin graft; ACD-A, Acid citrate dextrose-anticoagulant; PDGF, Platelet derived growth factor; VEGF, Vascular endothelial growt factor; bFGF, Beta fibroblast growth factor; SDF1, Stromal cell derived factor 1; VAPS, Visual analog pain scale; VAPrS, Visual analog pruritus scale; TBSA, Total body surface area; MPV, Mean platele volume.

ACKNOWLEDGEMENTS

United States patent office electronically published application for this method of treatment on June 21st, 2012 with the NO: US-2012-0156184-A1. The study was supported by Moravian-Silesian governmental research grant number 02932/2009/RRC. GLK is funded by grants from the NIH NIGMS R01 GM093050-01, by the U.S. DOE DESC0002606, and the NIH NCI (1 U54 CA149233-01), and philanthropic funds from Friends for Life and Newman-Lakka Cancer Foundation. The study was approved by IRB – No·16/b2008 on April 30th, 2008 and registered on ClinTrialsGov as NCT01383187. Many thanks to Pavlina Kusinova coordinating study nurse for APC/HAT preparation in all cases and conducting the case report forms in our clinical study.

Funding was provided by the Council of the Moravian Sileasian region Czech Republic (Grant FNO-99-OVZ-09-024-Dot).

CONFLICT OF INTEREST STATEMENT

The authors state that there are no conflicts of interest regarding the publication of this article.

REFERENCES

1. Prochazka V, Gumulec J, Jaluvka F, Salounova D, Jonszta T, Czerny D, Krajca J, Urbanec R, Klement P, Martinek J, Klement GL. Cell therapy, a new standard in management of chronic critical limb ischemia and foot ulcer. Cell transplantation 2010;19(11):1413-24.
2. Akingboye AA, Giddins S, Gamston P, Tucker A, Navsaria H, Kyriakides C. Application of autologous derived-platelet rich plasma gel in the treatment of chronic wound ulcer: diabetic foot ulcer. The Journal of extra-corporeal technology 2010;42(1):20-9.
3. Kachel E, Callum J, Moussa F, Goldstein J, Fremes S. Treatment of deep sternal wound infections after coronary artery bypass grafting by means of injection of platelet gel: an evolving technology. The Journal of thoracic and cardiovascular surgery 2010;139(6):e118-20.
4. Martinez-Zapata MJ, Marti-Carvajal A, Sola I, Bolibar I, Angel Exposito J, Rodriguez L, Garcia J. Efficacy and safety of the use of autologous plasma rich in platelets for tissue regeneration: a systematic review. Transfusion 2009;49(1):44-6.
5. Morizaki Y, Zhao C, An KN, Amadio PC. The effects of platelet-rich plasma on bone marrow stromal cell transplants for tendon healing in vitro. The Journal of hand surgery 2010;35(11):1833-41.
6. Langer H, May AE, Daub K, Heinzmann U, Lang P, Schumm M, Vestweber D, Massberg S, Schonberger T, Pfisterer I, Hatzopoulos AK, Gawaz M. Adherent platelets recruit and induce differentiation of murine embryonic endothelial progenitor cells to mature endothelial cells in vitro. Circulation research 2006;98(2):e2-10.
7. Stellos K, Seizer P, Bigalke B, Daub K, Geisler T, Gawaz M. Platelet aggregates-induced human CD34+ progenitor cell proliferation and differentiation to macrophages and foam cells is mediated by stromal cell derived factor 1 in vitro. Seminars in thrombosis and hemostasis 2010;36(2):139-45.
8. Pintucci G, Froum S, Pinnell J, Mignatti P, Rafii S, Green D. Trophic effects of platelets on cultured endothelial cells are mediated by platelet-associated fibroblast growth factor-2 (FGF-2) and vascular endothelial growth factor (VEGF). Thrombosis and haemostasis 2002;88(5):834-42.
9. Pietramaggiori G, Scherer SS, Cervi D, Klement G, Orgill DP. Tumors stimulate platelet delivery of angiogenic factors in vivo: an unexpected benefit. The American journal of pathology 2008;173(6):1609-16.
10. Lindemann S, Kramer B, Seizer P, Gawaz M. Platelets, inflammation and atherosclerosis. Journal of thrombosis and haemostasis: JTH 2007;5 Suppl 1:203-11.
11. Klement GL, Yip TT, Cassiola F, Kikuchi L, Cervi D, Podust V, Italiano JE, Wheatley E, Abou-Slaybi A, Bender E, Almog N, Kieran MW, Folkman J. Platelets actively sequester angiogenesis regulators. Blood 2009;113(12):2835-42.
12. Italiano JE, Jr., Richardson JL, Patel-Hett S, Battinelli E, Zaslavsky A, Short S, Ryeom S, Folkman J, Klement GL. Angiogenesis is regulated by a novel mechanism: pro- and antiangiogenic proteins are organized into separate platelet alpha granules and differentially released. Blood 2008;111(3):1227-33.
13. Ma L, Perini R, McKnight W, Dicay M, Klein A, Hollenberg MD, Wallace JL. Proteinase-activated receptors 1 and 4 counter-regulate endostatin and VEGF release from human platelets. Proceedings of the National Academy of Sciences of the United States of America 2005;102(1):216-20.
14. Bottcher-Haberzeth S, Biedermann T, Reichmann E. Tissue engineering of skin. Burns : journal of the International Society for Burn Injuries 2010;36(4):450-60.
15. Crkvenjas Z, Tymonova J, Adamkova M, Kadlcik M, Klosova H, Zamecnikova I. Surgical treatment of electrical burns by local flap plastic surgery. Acta chirurgiae plasticae 2005;47(1):10-12.
16. Hermann PC, Huber SL, Herrler T, von Hesler C, Andrassy J, Kevy SV, Jacobson MS, Heeschen C. Concentration of bone marrow total nucleated cells by a point-of-care device provides a high

yield and preserves their functional activity. Cell transplantation 2008;16(10):1059-69.
17. Kloppenberg FW, Beerthuizen GI, ten Duis HJ. Perfusion of burn wounds assessed by laser doppler imaging is related to burn depth and healing time. Burns : journal of the International Society for Burn Injuries 2001;27(4):359-63.
18. Draaijers LJ, Tempelman FR, Botman YA, Kreis RW, Middelkoop E, van Zuijlen PP. Colour evaluation in scars: tristimulus colorimeter, narrow-band simple reflectance meter or subjective evaluation? Burns : journal of the International Society for Burn Injuries 2004;30(2):103-7.
19. Kabes AM, Graves JK, Norris J. Further validation of the nonverbal pain scale in intensive care patients. Critical care nurse 2009;29(1):59-66.
20. Elman S, Hynan LS, Gabriel V, Mayo MJ. The 5-D itch scale: a new measure of pruritus. The British journal of dermatology 2010;162(3):587-93.
21. Kovanic PH, Huber MB. The Economics of Information-Mathematical Gnostics for Data Analysis: http://www.math-gnostics.com 2003.
22. Mazzucco L, Balbo V, Cattana E, Borzini P. Platelet-rich plasma and platelet gel preparation using Plateltex. Vox sanguinis 2008;94(3):202-8.
23. Mazzucco L, Medici D, Serra M, Panizza R, Rivara G, Orecchia S, Libener R, Cattana E, Levis A, Betta PG, Borzini P. The use of autologous platelet gel to treat difficult-to-heal wounds: a pilot study. Transfusion 2004;44(7):1013-8.
24. Gunaydin S, McCusker K, Sari T, Onur M, Gurpinar A, Sevim H, Atasoy P, Yorgancioglu C, Zorlutuna Y. Clinical impact and biomaterial evaluation of autologous platelet gel in cardiac surgery. Perfusion 2008;23(3):179-86.
25. Coetzee JC, Pomeroy GC, Watts JD, Barrow C. The use of autologous concentrated growth factors to promote syndesmosis fusion in the Agility total ankle replacement. A preliminary study. Foot & ankle international / American Orthopaedic Foot and Ankle Society [and] Swiss Foot and Ankle Society 2005;26(10):840-6.
26. Gardner MJ, Demetrakopoulos D, Klepchick PR, Mooar PA. The efficacy of autologous platelet gel in pain control and blood loss in total knee arthroplasty. An analysis of the haemoglobin, narcotic requirement and range of motion. International orthopaedics 2007;31(3):309-13.
27. Khalafi RS, Bradford DW, Wilson MG. Topical application of autologous blood products during surgical closure following a coronary artery bypass graft. European journal of cardio-thoracic surgery : official journal of the European Association for Cardio-thoracic Surgery 2008;34(2):360-4.
28. Akeda K, An HS, Pichika R, Attawia M, Thonar EJ, Lenz ME, Uchida A, Masuda K. Platelet-rich plasma (PRP) stimulates the extracellular matrix metabolism of porcine nucleus pulposus and anulus fibrosus cells cultured in alginate beads. Spine 2006; 31(9):959-66.
29. Xu W, Jong Hong S, Jia S, Zhao Y, Galiano RD, Mustoe TA. Application of a partial-thickness human ex vivo skin culture model in cutaneous wound healing study. Laboratory investigation; a journal of technical methods and pathology 2012;92(4): 584-99.
30. Xu R, Boudreau A, Bissell MJ. Tissue architecture and function: dynamic reciprocity via extra- and intra-cellular matrices. Cancer metastasis reviews 2009;28(1-2):167-76.

10 Autoimmune pankreatitis

Dítě P, Nechutová H, Uvírová M, Dvořáčková J, Kianička B, Martínek A

Originally published in Biomedical Papers, 2014, vol. 158, no. 1, p. 17-22

Consent to the publication of 1st April 2015

Autoimmune pancreatitis

Petr Dite[a], Hana Nechutova[b,c], Magdalena Uvirova[d], Jana Dvorackova[a,e], Bohuslav Kianicka[b], Arnost Martinek[a]

Introduction. Autoimmune pancreatitis (AIP) is the specific type of chronic pancreatitis due to autoimmune background and mechanism.
Characteristics. The main clinical symptoms of AIP are obstructive jaundice and abdominal discomfort. The typical histological findings are lymphocytes and IgG4 plasma cells infiltration, fibrosis and venulitis within pancreatic gland. Plasma level of IgG4 is usually extremely high.
Objectives. Diagnosis: High level IgG4 positive plasma cells in serum, lymphoplasmatic infiltration found on histological staining of pancreatic tissue, "sausage-like" pancreas in ultrasound and CT scans, and response to steroid therapy are crucial for making of diagnosis.
Classification of AIP: AIP can be classified into two subtypes. Type 1 was recognized as the pancreatic manifestation of multiorgan disorder, called IgG4 related disease. Type 2 is a pancreas-specific disorder not associated with IgG4, with similar histological signs as type 1, but also with the positivity of GEL (granulocythic epithelial lesion).
Results. Therapy: Due to its high effectivity in AIP treatment, steroid therapy is the first-line option. The alternative therapy is using immunosuppressants (azathioprine). Recently, there are also first experience in biological therapy already published.
Conslusion. Before the start of AIP therapy - the differential diagnosis between pancreatic cancer and AIP is essential.

Key words: chronic pancreatitis, autoimmune pancreatitis, immunoglobulines, IgG4, steroids, extrapancreatic lesions, pancreatic biopsy

Received: June 29, 2013; Accepted with revision: December 13, 2013; Available online: February 24, 2014
http://dx.doi.org/10.5507/bp.2013.094

[a]Academic Center of Gastroenterology, Department of Internal Medicine, University Hospital Ostrava and Faculty of Medicine, University of Ostrava, Czech Republic
[b]2nd Department of Internal Medicine, St. Anne's University Hospital Brno and Medical Faculty, Masaryk University, Brno
[c]International Clinical Research Center, St. Anne's University Hospital Brno
[d]Agel Research and Training Institute, CGB Laboratory, Ostrava-Vitkovice Branch
[e]Department of Pathology, Faculty of Medicine, University of Ostrava and University Hospital Ostrava
Corresponding author: Petr Dite, e-mail: pdite.epc@gmail.com

INTRODUCTION

Chronic pancreatitis is an inflammatory process, during which the pancreatic parenchyma is replaced with fibrotic tissue. This morphological change leads to irreversible destruction of both the exocrine and the endocrine glandular pancreatic parenchyma. The terminal point of these changes is exocrine and endocrine pancreatic insufficiency. The literature on the incidence and prevalence of chronic pancreatitis in not voluminous and time trends in incidence rates are lacking. The study in Copenhagen area in the 1970's reported an e incidence of 6.9 - 10.0 new cases per 100 000 inhabitants per year[1] In the Cantabria region of Spain between 1981 and 1991 the incidence was found to be 14 per 100000 per year, of which 80% were alcohol induced[2]. In 2002, Lankisch and co-workers published their results of chronic pancreatitis incidence in the region of Northern Germany. The incidence in the period 1988 to 1995 was 6.4 per 100000 per year[3,4]. In 2001, Dite and co-workers reported an incidence of 7.9/100000/year in the Czech Republic and the incidence was similar to thatof other European countries /France, Denmark Germany, Hungary/. The highest incidence of chronic pancreatitis, 23/100000/year, was found in Finland[5]. Some studies have found a serious increase in the number of patients admitted to hospital with chronic pancreatitis, e.g. in the UK an increase of 100% from 1989/90 to 1999/2000 was documented[6] (Table 1). Japan also registered an increase in prevalence from 28.5 to 32.9/100000 and from 5.4 to 5.7/100000/year during the period 1994 to 1999 (ref.[6]).

In 2001, the TIGAR-O classification system of etiological factors for chronic pancreatitis was published[7]. This system is based on the mechanism of injury of pancreatic tissue, and it addresses the risk, etiology, and complexity of the disease. Chronic pancreatitis is a complex disorder that may involve the interaction of two or more environmental or genetic factors. The TIGAR-O model addresses this potential synergistic role of multiple risk factors in a single individual with chronic pancreatitis and allows assessment of the contributory level of each of the interacting risk factors. Although the critical information about different forms of chronic pancreatitis is not fully available, the TIGAR-O system lays the foundation for further advancement in the field. The major categories include toxic-metabolic (T), idiopathic (I), genetic (G),

autoimmune (A), recurrent severe acute pancreatitis (R), and obstructive (O) mechanisms.

In 1961, Sarles and co-workers described the idiopathic form of pancreatitis with minimal subjective symptoms, obstructive jaundice and hypergammaglobulinemia and they were the first to suspect an autoimmune process as an etiological factor[8]. In 1995, Yoshida and co-workers described a patient with obstructive jaundice, with diffusely enlarged pancreas, irregular pancreatic duct and hypergammaglobulinemia. The pancreatic biopsy revealed pancreatic fibrosis. The symptoms resolved after steroid therapy. The term "AUTOIMMUNE PANCREATITIS" was used for the first time[9]. Recent knowledge supports the concept of autoimmune pancreatitis (AIP) as a unique clinical entity within putative IgG4 systemic diseases. The pathogenetic mechanisms remain unclear[10] , but autoimmune etiology is presumed.

EPIDEMIOLOGY

Epidemiological data on AIP is still very poor. A nationwide study in Japan estimated the prevalence of AIP to be 0.82 per 100 000 habitants[11], when diagnostic criteria for AIP proposed by the Japanese Pancreas Society in 2002 were used[12]. AIP is at least twice as common in men as in women. The onset of the disease is typical in patients over 55 years of age[11,13,14]. The incidence of AIP appears to have risen in last few years - from 2.0 to 4.0 in our series.

Clinical feature

- mild abdominal symptoms
- occasional presence of obstructive jaundice
- high level of serum gammaglobulin IgG and IgG4
- presence of non-specific antibodies
- diffuse enlargement of the pancreas ("sausage-like"), in CT scan with capsule-like low density rim
- diffuse irregular of pancreatic duct on ERCP
- histomorphologically lymphocyte and IgG4-positive plasmacyte infiltration and fibrosis, obliterative phlebitis
- association with extrapancreatic lesions
- responsibility to steroid therapy

HISTOLOGY

Histopathological features support the hypothesis of two histological and clinical subtypes of AIP (ref.[14,15]).

The histological pattern in type 1 is identical to the classic description of the disease and is associated with the histological pattern known as lymphoplasmatic sclerosing pancreatitis - LPSP. Typical histological signs are dense periductal lymphoplasmacytic infiltrates, swirling fibrosis, obliterative venulitis and IgG4 tissue positivity. The main serological marker is elevation of serum immunoglobulin IgG4. Type-1 AIP is considered to be a part of IgG4-associated systemic disease for which extrapancreatic involvement is typical. The bile ducts, kidneys, salivary glands, retroperitoneum and mediastinum are among the most commonly affected extrapancreatic organs[16-20] (Table 2).

Table 1. Incidence of Chronic Pancreatitis.

Country	Incidence
Switzerland	1.2/100 000/year
Poland	4.0/100 000/year
Germany	7.4/100 000/year
Czech Rep.	7.9/100 000/year
Hungary	8.0/100 000/year
Denmark	10.0/100 000/year
Sweden	10.0/100 000/year
Finland	23.0/100 000/year
United States	5.7-7.6/100 000/year

Table 2. Autoimmune pancreatitis – subtypes.

Type 1 Lymphoplasmatic sclerosing pancreatitis (LPSP)	– periductal lymphoplasmatic infiltrates – high amount IgG4 – positive plasma cells – swirling fibrosis – obliterative venulitis
Type 2 Idiopathic duct-centric pancreatitis (IDCP) „non-alcoholic duct destructive pancreatitis"	– ductal epithelial granulocytic infiltration – ductal damage – obliteration

The most frequent clinical symptom in type 1 AIP is obstructive jaundice. In patients with AIP type 2 features typical for acute or chronic pancreatitis can be occasionally seen. IgG4 elevation is very rare in type 2 AIP, but very frequent (about 80%) in patients with type 1 AIP. Association between inflammatory bowel disease, primary biliary cirrhosis and AIP is connected with type 2 AIP. In contrast, type 1 AIP is combined with extrapancreatic manifestations, as are IgG4 sclerosing cholangitis, sialoadenitis, retroperitoneal fibrosis, etc.[21] (Table 3). According to the TIGAR-O classification system[7] AIP can be subdivided into isolated and syndromic subgroups with syndromic AIP being associated with inflammatory bowel disease and primary biliary cirrhosis[21]. In our sample of patients with AIP, we also identified IgG4 mastitis and Mikulicz syndrome (Table 4).

DIAGNOSIS

Asian consensus criteria (Table 5) and/or HISORt criteria of AIP (table 6) are generally accepted[22-24]. The problem with the Japanese Diagnostic Criteria is a lower sensitivity (80%) and specificity (87%) than HISORt criteria (92% sensitivity and 97% specificity) (ref.[25]).

Five cardial feature of AIP are as follows:

- pancreatic histology
- serology
- imaging of pancreatic parenchyma and duct

Table 3. Comparison of type 1 and type 2 AIP.

	Type 1 AIP	Type 2 AIP
Mean Age	Sixth decade	Fourth decade
Gender	Predominantly male	Equal
Histological pattern	Lymphoplasmacytic sclerosing pancreatitis	Duct-destructive pancreatitis
Histological signs	Periductal lymphoplasmacytic infiltrates Swirling fibrosis Obliterative venulitis	Lymphoplasmacytic infiltrates Granulocyte epithelial lesions with partial/ complete duct obstruction (GEL)
IgG4 cells on immunostaining	Moderate-severe (98%)	Moderate (40%) in one study
Serum IgG4 levels	Elevated	Normal
Other organ involvement	Sclerosing sialadenitis, IgG4-associated cholangitis, retroperitoneal fibrosis, IgG4-associated tubulointerstitial nephritis, pneumonitis, prostatitis, IgG4 mastitis	Inflammatory bowel disease Primary biliary cirrhosis

Table 4. AIP with extrapancreatic lesions (n=13).

Gender	Age	Concomitant autoimmune disease
Male	36	IgG4 sclerosing cholangitis
Male	43	Sialadenitis
Male	53	Sjögren sy
Female	54	Sjögren sy, autoimmune hepatitis
Male	56	autoimmune hepatitis
Male	32	autoimmune hepatitis
Female	55	primary biliary cirrhosis
Male	51	IBD
Male	46	Xxx
Female	33	Xxx
Female	58	IgG4 positive mastitis, sialadenitis
Female	55	IgG4 sclerosing cholangitis
Male	49	IgG4 sclerosing cholangitis

Table 5. Clinical diagnostic criteria for AIP 2006.

1. Diffuse or segmental narrowing of the MPD with irregular wall and diffuse or localized enlargement of the pancreas by imaging studies, such as abdominal US, CT, and magnetic resonance.
2. High serum γ-globulin, IgG, or IgG4, or the presence of autoantibodies such as antinuclear antibodies and rheumatoid factor.
3. Marked interlobular fibrosis and prominent infiltration of lymphocytes and plasma cells in the periductal area, occasionally with lymphoid follicles in the pancreas.

Diagnosis of AIP is established when criterion 1 and criterion 2 and/or 3 are fulfilled. However, it is necessary to exclude malignant diseases.

- other organ involvement
- response to steroid therapy

Diagnostic biopsy with histological examination is usually sufficient for the diagnosis of type 1 of AIP and is a mandatory procedure in the differential diagnosis between AIP and pancreatic cancer[26-28]. Sausage-like enlargement of the gland in CT imaging and/or endosonography is present in more than 50% of patients with AIP. Dynamic CT and MRI show delayed enhancement of the swollen pancreas, in some patients forming a "capsule-like rim" surrouding the pancreas. ERCP, better than MRCP, shows diffuse narrowing of the pancreatic duct with some irregularities. Positron emission tomography /PET/ does not play any role in diagnostic work- up[25]. In the case of typical histology, serological positivity of IgG4, other organ involvement and typical imaging in CT or EUS, the diagnosis of autoimmune pancreatitis is most certain. Narrowed pancreatic duct, enlarged gland with sausage-like shape, elevation of serum IgG4 and/or compatible histology are typical for AIP type 1. Other serological markers are less specific but rheumatoid factor or high titres of ANA may also be present[11,29]. In AIP-type 2, IgG4 cells on immunostaining are usually absent and IgG4 serum level is usually normal. Histological hallmarks are lymphoplasmatic infiltration and granulocyte epithelial lesions with partial or complete duct obstruction - duct-centric destructive pancreatitis /IDCP/. The wall of the duct is usually infiltrated with neutrophils, lymphocytes and plasma cells with involvement of the duct epithelium and lumen. The ductal lesions are called GEL - granulocyte epithelial lesion[13,14].

Accurate diagnosis of the AIP-type 2 requires core biopsy of the gland. Patients with type 1 are typically males with a mean age in the sixth decade. Patients with

AIP type 2 tend to be younger with a mean age in the forth decade and with equal gender distribution[14]. From a practical point of view, the distinction between the AIP subtypes will help in clarifying the clinical features, pathogenesis and natural history of disease.

THERAPY

Most patients with AIP respond well to steroid therapy[29,30]. Corticosteroids reduce inflammation and restore both digestive enzymes and HCO3 secretion in patients with AIP by regenerating acinar cells and correcting CFTR localization in pancreatic duct cells, mislocalized to the cytoplasm of duct cells[31,32]. For the induction of remission in type 1 AIP, a dose of 30-40 mg for 2 weeks is generally recommended[11,30]. The dose of steroids is tapered by 5 mg per two weeks. The total time of therapy is usually 6-12 months. The monitoring of clinical and biochemical status is essential. Only in a few patients with obstructive jaundice, short-term biliary stent insertion is indicated[11]. The relapse of AIP can be seen in about approximately 30% of the patients with AIP. In AIP relapse (after the steroid therapy), a combination of steroids (1 mg/kg) with azathioprine (2 mg/kg) for 12 weeks is recommended[33]. A new drug, which was reported to induce remission is the CD2O antipody, ritiximab. Preliminary results with this drug are promising[34].

Reliable data on treating AIP type 2 are scarce but steroid use appears to be preferred and is effective. Whether AIP predisposes to pancreatic cancer is not known but case-report studies of pancreatic cancer complicating AIP have been published[27,28].

DISCUSION

Current research on AIP focuses on the pathogenesis of the disease. Genetic factors of AIP, humoral immunity and target antigens of cellular immunity and effector cells and the role of microbial infection (H.pylori infection and molecular mimicry) are being intensively studied[35]. Okazaki and co-workers[11] hypothesised that the pathogenesis of AIP involves a biphasic mechanism consisting of "induction" and "progression". In the early stage, the initial response to self-antigens (antilactoferrin, carbonic anhydrase II, pancreatic secretory trypsin inhibitor and alfa-fodrin) and molecular mimicry are induced by a decrease in naïve regulatory T-cells (Tregs) and T-helper (Th1) cells mediated release of proinflammatory cytokines. In the chronic stage, progression is supported by increase in memory Tregs (regulatory T cells) and Th2 immune responses. The complement system pathway may be activated by the IgG1 complex. A model published by Chari´s group from Rochester, USA is similar and considers IgG4 to be related to the differentiation phase of Treg function. During the evolution of AIP, Treg activity may be related to specific amino acid substitution of HLA class II. IgG1 immune complex may be related to IgG4-negative and granulocyte epithelial lesion (GEL)-positive AIP/idiopathic duct-centric pancreatitis IDCP. The IgG4 immune complex may correlate with IgG4-positive and GEL-negative AIP. Further research is necessary to confirm the cellular model of AIP. In 2008, Kamisawa et al.[36] proposed a new clinicopathological entity – IgG4 related sclerosing disease (IgG4–RSC) (ref.[35]). The clinical manifestation of this systemic disease is different and related to the fragmentary involvement of the pancreas, liver, bile duct, salivary gland, kidney and lung[37].Typical for this disease is abundant IgG4 positive plasma cells and T–lymphocyte organ infiltration[38,39]. Masaoki et al. extended the IgG–RSC complex into an even more extensive clinical entity – IgG4–positive multiorgan lymphoproliferative syndrome (IgG4–MOLPS). This syndrome includes inflammatory pseudotumors (liver, breast, lung, Mikulicz´s syndrome, intestinal fibrosis and autoimmune hypophysitis). Sjögren syndrom is not considered a part of IgG4-MOLPS (ref.[40]).

In 2009 experts from Europe, Japan, Korea and USA met in Honolulu to describe the entity of AIP (ref.[41]). The

Table 6. HISORt criteria of AIP.

Category	Criteria
A. Histology	1. Diagnostic (any one): a) Pancreatic histology showing periductal lymphoplasmacytic infiltrate with obliterative hlebitis (LPSP) b) Lymphoplasmacytic infiltrate with abundant (>10 cells/hpf) IgG4 positive cells in the pancreas 2. Supportive (any one) a) Lymphoplasmacytic infiltrate with abundant (>10 cells/hpf) IgG4 positive cells in involved extra-pancreatic organ b) Lymphoplasmacytic infiltrate with fibrosis in the pancreas
B. Imaging	Typical imaging features: 1. CT/MR: diffusely enlarged gland with delayed (rim) endhancement 2. ERCP: Diffusely irregular, attenuated main pancreatic duct Atypical Imaging Features: Pancreatitis, focal pancreatic mass, focal pancreatic duct stricture, pancreatic atrophy, pancreatic calcification
C. Serology	Elevated serum IgG4 level (normal 8-140 mg/dL)
D. Other Organ involvement	Hilar/intrahepatic biliary strictures, persistent distal biliary stricture, Parotid/lacrimal gland involvement, Mediastinal lymphadenopathy, Retroperitoneal fibrosis
E. Response to steroid therapy	Resolution/marked improvement of pancreatic/extrapancreatic manifestation with steroid therapy

Honolulu Consensus Document characterized AIP as a pancreatitis, which has unique histopathologic features allowing it to be distinguished from other forms of chronic pancreatitis, and with histopathological correlates of 2 distinct forms of AIP. The last international consensus - diagnostic criteria consensus, published in 2011 (ref.[42]) recognizes the spectrum of AIP as we know it today. In 2011 the criteria of the Japan Pancreas Society (HISORTs criteria) together with Korean, Asian, Italian and Mannheim criteria, led to the International Consensus Diagnostic Criteria for autoimmune pancreatitis.

The diagnostic criteria were separated into two levels. In level 1, the typical criterion is a diffuse enlargement of the pancreas with delayed enhancement. In the pancreatic duct, there is a typical sign- in more than 1/3 the length of the main pancreatic duct, there are multiple strictures without marked upstream dilatation.

Elevation of IgG4 >2x upper normal value

The diagnosis of AIP typically includes involment of other organs with histological changes-lymphoplasmatic infiltration with fibrosis and without granulocytic infiltration with storiform fibrosis, obliterative flebitis and an abundance of IgG4 positive cells-more than 10 cells / HPF. At least 3 of the pancreatic histological signs are typical for the diagnosis. An alternative to histological changes is the presence of typical radiological markers which are a segmental proximal or multiple proximal or proximal and distal bile duct stricture and retroperitoneal fibrosis.

In the histology of pancreas at least 3 of the following markers are relevant:

- periductal lymphoplasmatic infiltrate without GEL
- obliterative flebitis
- storiform fibrosis
- abundant IgG4 positive cells

The important diagnostic criterion is the response to steroid therapy, when radiologically it is possible to demonstrate the resolution or improvement in pancreatic and extrapancreatic manifestation.

For level 2 the criteria for AIP- there are no typical markers, for example no diffuse enlargement. The sign is segmental or focal enlargement of pancreatic parenchyma. Other signs are symmetrically enlarged salivary/lacrimal glands, renal involvement described in association with AIP, segmental or focal narrowing of the pancreatic duct without marked upstream dilatation (duct size <5.0 mm). There is no doubt, that autoimmune pancreatitis is still a challenge for pancreatologists, endoscopists, surgeons, histopathologists, immunologists and radiologists and it is a "hot topic" in internal medicine. Type 1 AIP is the pancreatic manifestation of the multiorgan syndrome-IgG4 related disease (called also MOLPS - MultiOrgan Lympho Proliferative Syndrome). Relapses of AIP type 1 can be prevented using immunomodulators or biological agents. Type 2 autoimmunepancreatitis is a distinct disease entity with some markers common to type 1 AIP. AIP type 2 responds promptly to steroid therapy and subsequent relapse is uncommon[43,44].

CONCLUSION

1) Autoimmune pancreatitis (AIP) is a distinct form of pancreatitis. Currently, two forms of AIP have been described - Lymphoplasmatic sclerosing pancreatitis (LPSP) and Idiopathic duct-centric pancreatitis (IDCP).

2) Clinically LPSP appears to be the pancreatic manifestation of the group of systemic diseases-IgG4 related disease. IDCP does not appear to be a systemic disease.

3) The main acute clinical symptoms are obstructive jaundice and pancreatic swelling (focal or diffuse). Typical pancreatic pain is very rare.

4) Diagnostic criteria for AIP.

- changes in pancreatic parenchyma and pancreatic duct (CT/MRI,MRCP,ERCP)
- high plasma levels of IgG, IgG4 and ANA
- histopathology of the pancreas
- steroid therapy response

5) Differential diagnosis between pancreatic tumor and AIP is essential. Endosonographically guided pancreatic biopsy is recommended.

ABBREVIATIONS

AIP, Autoimmune pancreatitis; GEL, granulocyte epithelial lesions; IDCP, Idiopathic duct-centric pancreatitis; IgG4 + MOLPS, IgG4-positive multiorgan lymphoproliferative syndrome; IgG4-RSC, IgG4 related sclerosing disease; LPSP, Lymphoplasmatic sclerosing pancreatitis.

ACKNOWLEDGEMENTS

Supported by the European Regional Development Fund - Project FNUSA-ICRC (No. CZ.1.05/1.1.00/02.0123); Grant sponsor: Ministry of Health (NT13434-4/20012).

CONFLICT OF INTEREST STATEMENT

The authors state there are no conflicts of interest regarding the publication of this article.

REFERENCES

1. Andersen BN, Pedersen NT, Scheel J, Worning H. Incidence of alcoholic chronic pancreatitis in Copenhagen. Scand J Gastroenterol 1982,17:247-52.
2. De las Heras G, Pns F. Epidemiologia y aspectos etiopatogénicos de la pancreatitis alcohólica crónica. Res Esp Enferm Dig 1993,84:253-8.
3. Lankisch PG, Assmus C, Maisonneuve P, Lowenfels AB. Epidemiology of pancreatic diseases in Luneburg Country. A study in a defined German population. Pancreatology 2002,2:469-77.
4. Dite P, Starý K, Novotný I, Precechtelová M, Dolina J, Lata J, Zboril V. Incidence of chronic pancreatitis in Czech Republic. Eur J Gastroenterol 2001,13:749-50.
5. Navarro S, Soriano A. Epidemiology of chronic pancreatitis : an infrequent disease or an infrequently diagnosed disease? In Dominguez – Munoz JE (ed.). Clinical Pancreatology for Practising Gastroenterologists and Surgeons. Blackwell, 2004,pp. 187-91.

6. Spanier BMW, Dijkgraaf MGW, Bruno MJ. Epidemiology, aetiology and outcome of acute and chronic pancreatitis. An update. Best Practice Res Clin Gastroenterol 2008,22,(1):45-53.
7. Etemad B, Whitcomb DC. Chronic pancreatitis: diagnosis, classification, and new genetic developments. Gastroenterology 2001,120:682-97.
8. Sarles H, Sarles JC, Muratore R, Guien C. Chronic anflammatory sclerosis of the pancras – an atonomous pancreatic disease? Am J Dig Dis 1961,6:688-98.
9. Yoshida K, Toki F, Takeuchi T, Watanabe S, Shiratori K, Hayashi N. Chronic pancreatitis caused by an autoimmune abnormality. Proposal of the concept of autoimmune pancreatitis. Dig Dis Sci 1995, 40:1561–68.
10. Okazaki K, Uchida K, Chiba T. Recent concept of autoimmune related pancreatitis. J Gastroenterol 2001,36:293-302.
11. Okazaki O, Uchida K, Fukui T. Recent advances in autoimmune pancreatitis: concept, diagnosis, and pathogenesis. J Gastroenterology 2008,43:409-18.
12. Nishimori I, Tamakoshi A, Otsuki M. Prevalence of autoimmune pancreatitis in Japan from a nationwide survey in 2002. J Gastroenterol 2007:42(Suppl18):6-8 .
13. Otsuki M. Autoimmune pancreatitis: a message from Japan. J Gastroenerol 2007:42(Suppl18):1-5.
14. Notohara K, Brgart LJ, Yadav D. Idiopathic chronic pancreatitis with periductal lymphoplasmacytic infiltration: clinicopathologic features of 35 cases. Am J Surg Pathol 1991,22:1119-27.
15. Zamboni G, Lüttges J, Capelli P. Histopathological features of diagnostic and clinical relevance in autoimmune pancreatitis: a study on 53 resection specimens and 9 biopsy specimens. Virchows Arch 2004,445:552-63.
16. Takeda S, Haratake J, Kasai T, Takaeda C, Takazakura E. IgG4-associated idiopathic tubulointerstitial nephritis complicating autoimmune pancreatitis. Nephrol Dial Transplant 2004,19:474-6.
17. Yamamoto M, Takahashi H, Sugai S, Imai K. Clinical and pathological characteristics of Mikulicz´s disease (IgG4-related plasmacytic exocrinopathy). Autoimmun Rev 2005,4:195-200.
18. Komatsu K, Hamano H, Ochi Y, Takayama M, Muraki T, Yoshizawa K. High prevalence of hypothyroidism in patients with autoimmune pancreatitis. Dig Dis Sci 2005,50:1052-105.
19. Taniguchi T, Ko M, Seko S, Nishida O, Inoue F, Kobayashi H. Interstitial pneumonia associated with autoimmune pancratitis. Gut 2004,53:770.
20. Ghazale A, Chari ST, Smyrk TC, Levy MJ, Topazian MD, Takahashi N. Value of serum IgG4 in the diagnosis of autoimmune pancreatitis and in distinguishing it from pancreatic cancer. Am J Gastroenterol 2007,102:1646-53.
21. Kamisawa T, Egawa N, Nakajima H, Tsuruta K, Okamoto A. Extrapancreatic lesions in autoimmune pancreatitis. J Clin Gastroenterol 2005,39:904-7.
22. Chari ST, Smyrk TC, Levy MJ, Topazian MD, Takahashi N, Zhang L. Diagnosis of autoimmune pancreatitis: the Mayo Clinic experience. Clin Gastroenterol Hepatol 2006,4:1010-6.
23. Kim MH, Lee TY. Diagnostic criteria for autoimmune pancreatitis: a proposal of revised Kim criteria. J Gastroenterol Hepatol 2007,22:A104.
24. Okazaki K, Kawa S, Kamisawa T, Naruse S, Tanaka S, Nishimori I. Clinical diagnostic criteria of autoimmune pancreatitis: revised proposal. J Gastroenterol 2006,41:626-31.
25. Naitoh I, Nakazawa T, Ohara H, Ando T, Hayashi K, Okumura F, Miyabe K, Yoshida M, Sano H, Takada H, Kanematsu T, Joh T. Comparative evaluation of the Japanese Diagnostic Criteria for autoimmune pancreatitis. Pancreas 2010,39:1173-9.
26. Chari ST, Takahahi N, Levy MJ, Smyrk TC, Clain JE, Pearson RK, Petersen BT, Topazian MA, Vege SS. A diagnostic strategy to distinguish autoimmune pancreatitis from pancreatic cancer. Clin Gastoenterol Hepatol 2009,7:1097-103.
27. Inoue H, Miyatani H, Sawada Y, Yoshida Y. A case of pancreas cancer with autoimmune pancreatitis. Pancreas 2006,33:208-9.
28. Fukuj T, Mitsuyama T, Takaoka M, Uchida K, Matsushita M, Okazaki K. Pancreatic cancer associated with autoimmune pancreatitis in remission. Intern Med 2008,47:151-5.
29. Park DJ, Kim MH, Chari ST. Recent advances in autoimmune pancreatitis. Gut 2009,58:1680-9.
30. Erkelens GW, Vleggaar FP, Lesterhuis W, van Buuren HR, van der Werf SD. Sclerosing pancreato-cholangitis responsive to steroid therapy. Lancet1999,354:43-4.
31. Tanaka S, Kobayashi T, Nakanishi K, Okubo M, Murase T, Hashimoto M. Corticosteroid-responsive diabetes mellitus associated with autoimmune pancreatitis. Lancet 2000,356:910-1.
32. Kountouras J, Zavos C, Gavalas E, Tzilves D. Challenge in the pathogenesis of autoimmune pancreatitis: potential role of Helicobacter pylori infection via molecular mimicry. Gasroenterology 2007,133:368-9.
33. Ko SBH, Mizuno N, Yatabe Y, Yoshikawa T, Ishiguro H, Yamamoto A, Azuma S, Naruse S, Yamao K, Muallem S, Goto H. Corticosteroids correct abferant CFTR localization in the duct and regenerate acinar cells in autoimmune pancreatitis. Gastroenterology 2010,138,5:1988-96.
34. Hart PA, Topazian MD, Witzig TE. Treatment of relapsing autoimmune pancreatitis with immunomodulators and rituximab: the Mayo Clinic experience. Gut Published Online First:30 Aug 2012, doi:10.1136/gutjnl-2012-302886/
35. Chari ST. Current concepts in the treatment of autoimmune pancreatitis. JOP 2007,8:1-3.
36. Kamisawa T, Okamoto A. IgG – related sclerosing disease. World J Gastroenterol 2008,14:3948-55.
37. Kamisawa T. IgG4-positive plasma cells specifically infiltrate various organs in autoimmune pancreatitis. Pancreas 2004,29:167-8.
38. Kamisawa T, Funata N, Hayashi Y, Eishi Y, Koike M, Tsuruta K. A new clinicopathological entity of IgG4 – related autoimmune disease. J Gastroenterol 2003,38:982-4.
39. Uomo G.: Autoimmune pancreatitis: An autonomous disease or a sigle entity in a complex puzzle of a multi-organ disorder? JOP (Online) 2010,5,11(2):191-2.
40. Masaki Y, Dong L, Kurose N, Kitagawa K, Morikawa Y, Yamamoto M, Takahashi H, Shinomura Y, Imai K, Saeki T, Azumi A, Nakada S, Sugiyama E, Matsui S, Origuchi T, Nishiyama S, Nishimori I, Nojima T, Yamada K, Kawano M, Zen Y, Kaneko M, Miyazaki K, Tsubota K, Eguchi K, Tomoda K, Sawaki T, Kawanami T, Tanaka M, Fukushima T, Sugai S, Umehara H. Proposal for a new clinical entity, IgG4-positive multiorgan lymphoproliferative syndrome: analysis of 64 cases of IgG4-related disorders. Ann Rheum Dis 2009;68(8):1310-5. doi: 10.1136/ard.2008.089169
41. Chari ST, Kloeppel G, Zhang L, Notohara K, Lerch MM, Shimosegawa T. Histopathologic and clinical subtypes of autoimmune pancreatitis: The Honolulu Consensus Document. Pancreatology 2010,10:664-72.
42. Shimosegawa T, Chari ST, Frulloni L, Kamisawa T, Kawa S, Mino-Kenudson M, Kim MH, Klöppel G, Lerch MM, Löhr M, Notohara K, Okazaki K, Schneider A, Zhang L. International consensus diagnostic criteria for autoimmune pancreatitis: guidelines of the International Association of Pancreatology. Pancreas 2011,40(3):352-8. doi: 10.1097/MPA.0b013e3182142fd2.
43. Kamisawa T, Chari ST, Lerch MM, Kim MH, Gress TM, Shimosegawa T. Recent advances in autoimmune pancreatitis type 1 and type 2. Gut 2013,62:1373-80. doi: 10.1136/gutjnl-2012-304224
44. Hart PA, Kamisawa T, Brugge WR, Chung JB, Culvert EL, Czako L, Frulloni L, Go WL, Gress TM, Myung-Hwan K, Kawa S, Lee KT, Lerch MM, Liao W, Lohr M, Okazaki K, Ryu JK, Schleinitz N, Shimizu K, Shimosegawa T, Soetikno R, Webster G, Yadav D, Zen Y, Chari ST. Long-term outcomes of autoimmune pacreatitis: a multicentgre, international analysis. Gut 2013;62(12):1771-6. doi: 10.1136/gutjnl-2012-303617

11

Vancomycin pharmacokinetics during high-volume continuous venovenous hemofiltration in critically ill septic patients

Petejová N, Martínek A, Zahálková J, Ďuricová J, Brozmanová H, Urbánek K, Grundmann M, Plášek J, Kacířová I

Originally published in Biomedical Papers, 2014, vol. 158, no. 1, p. 65-72

Consent to the publication of 1st April 2015

Vancomycin pharmacokinetics during high-volume continuous venovenous hemofiltration in critically ill septic patients

Nadezda Petejova[a], Arnost Martinek[a], Jana Zahalkova[b,c], Jana Duricova[d], Hana Brozmannova[d], Karel Urbanek[e], Milan Grundmann[d], Jiri Plasek[a], Ivana Kacirova[d]

Aims. To assess the influence of continuous venovenous hemofiltration (CVVH) at a filtration rate of 45 mL/kg/h on vancomycin pharmacokinetics in critically ill septic patients with acute kidney injury (AKI).
Methods. Seventeen adult septic patients with acute kidney injury treated with CVVH and vancomycin were included. All patients received first dose of 1.0 g intravenously followed by 1.0 g/12 h if not adjusted. In sixteen patients vancomycin was introduced on the day of the start of CRRT therapy. Blood samples and ultrafiltrates were obtained before and 0.5, 1, 6 and 12 h after vancomycin administration.
Results. On the first day, the median total vancomycin clearance (Cl_{tot}) was 0.89 mL/min/kg (range 0.31 - 2.16). CRRT clearance accounted for around 50-60% of the total clearance of vancomycin found in a population with normal renal function (0.97 mL/min/kg). Vancomycin serum concentrations after the first dose were below the required target of 10 mg/L as early as 6 h in 10 patients, AUC_{0-24}/MIC ≥ 400 ratio was achieved in 10 patients on the first day.
Conclusions. CVVH at a filtration rate of 45 mL/kg/h leads to high and rapid extracorporeal removal of vancomycin in critically ill patients. Due to the rapid change in patient clinical status it was impossible to predict a fixed dosage regimen. We recommend blood sampling as early as 6 h after first vancomycin dose with maintenance dose based on vancomycin serum level monitoring.

Key words: acute kidney injury, critically ill patients, renal replacement therapy, sepsis, drug monitoring, vancomycin

Received: April 16, 2012; Accepted with revision: September 18, 2012; Available online: November 6, 2012
http://dx.doi.org/10.5507/bp.2012.092

[a]Department of Internal Medicine, Faculty of Medicine, University of Ostrava and University Hospital Ostrava, Czech Republic
[b]Department of Internal Medicine III – Nephrology, Rheumatology and Endocrinology, University Hospital Olomouc and Faculty of Medicine and Dentistry, Palacky University Olomouc
[c]Stredomoravska nemocnicni, Hospital Sternberk
[d]Department of Clinical Pharmacology, Faculty of Medicine and University Hospital Ostrava
[e]Department of Clinical Pharmacology, Faculty of Medicine and Dentistry, Palacky University Olomouc and University Hospital Olomouc
Corresponding author: Nadezda Petejova, e-mail: petejova@seznam.cz

INTRODUCTION

Acute kidney injury (AKI) is a common complication of critical illness[1]. Between 45-70% of all AKI is associated with sepsis[2]. Patients with septic AKI have increased risk of death and longer hospitalization[3].

Critically ill patients in intensive care units are also at high risk of bacterial superinfection caused by nosocomial agents in particular. Both patient status and surroundings contribute to the occurrence of the infection[3].

Superinfection may be due to type of gram-positive strains of *Staphylococcus aureus* including methicillin-resistant *Staphylococcus aureus* (MRSA), and *Enterococcus*[4]. Treatment with glycopeptid antibiotic agent vancomycin is often required according to the observed sensitivity of bacterial agents[5]. Septic patients with acute kidney injury who are hemodynamically unstable and require high vasopressor support, can be treated with continuous renal replacement therapy (CRRT). Drugs with a molecular weight less than 5000 Da, low plasma protein binding, small volume of distribution, and low endogenous clearance are effectively removed by continuous venovenous hemofiltration (CVVH) (ref.[6]). Many drugs used in critically ill patients meet these criteria, complicating dosing regimens in patients receiving CVVH (ref.[7]).

The pharmacokinetics of vancomycin can be affected by the filtration dose, physical properties of elimination therapy, type of membrane and also by the properties of the antibiotic agent itself[8]. Dosing and pharmacokinetic data in patients receiving intermittent hemodialysis are not applicable to those receiving CRRT because of substantial differences in procedure, filters and timing. The clearance of vancomycin changes and can be increased using high-flux membranes[9]. An AUC/MIC ratio of ≥ 400 has been advocated as a target to achieve clinical effectiveness with vancomycin. However, trough vancomycin serum concentration C_{min} > 10 mg/L is more practical method for monitoring vancomycin effectiveness[10].

The purpose of this study was to assess the influence of CVVH at a filtration rate of 45 mL/kg/h on vancomycin pharmacokinetics in critically ill septic patients with AKI. Using pharmacokinetic modelling, we sought an optimal dosing regimen for maximising target vancomycin exposure.

PATIENTS AND METHODS

This was an open, prospective, clinical study carried out at the University hospital Ostrava, Czech Republic. The study protocol was approved by the hospital Ethics Committee. Written informed consent was obtained from patients and two unrelated physicians. Therapeutic monitoring of vancomycin levels is a standard procedure during vancomycin therapy in our hospital.

Seventeen critically ill adult patients (six women) with severe sepsis requiring CRRT in CVVH mode on vancomycin therapy were included. Acute kidney injury was classified according to the RIFLE score: eleven patients belonged to RIFLE F; six patients were in RIFLE I. They were followed up for 2 days. All received vancomycin (Edicin, Sandoz, Lek Pharmaceuticals d.d, Lek, Ljubljana, Slovenia) first dose of 1.0 g intravenously followed by 1 g/12 h if not adjusted.

In sixteen patients, vancomycin was introduced on the day of the commencement of CRRT therapy. In one patient, CRRT was initiated in the course of vancomycin treatment. Antibiotic agent was reconstituted with 0.9% Sodium Chloride 100 mL solution and administered at an infusion rate of 100 mL per hour. Blood samples and ultrafiltrates were obtained before vancomycin administration and 0.5, 1, 6 and 12 h after vancomycin administration. Blood samples were collected into 4.9 mL neutral tubes (Sarstedt-Monovette) and centrifuged. Serum and ultrafiltrate vancomycin concentrations were determined using fluorescence polarisation immunoassay method (AbboTT AxSYM™; Abbott Laboratories, Diagnostic Division, Abbott Park, IL 60064 USA). Coefficient of variation of the analysis ranged depending on the concentration from 3.36% to 6.11% with an average value of 5.04%. Vancomycin dose was adjusted according to vancomycin level simulation using a pharmacokinetic programme MWPharm, version 3.30 (MEDIWARE, Groningen, the Netherlands). A vancomycin trough concentration of 10-15 mg/L was chosen as a target concentration for vancomycin dosage adjustment. Minimal inhibitory concentration of pathogen was determined by the microdilution broth method.

The following pharmacokinetic parameters were calculated for each patient: total drug clearance (Cl_{tot}), volume of distribution (Vd), elimination half-life ($t_{1/2}$) and area under the serum concentration time curve (AUC_{0-24}). Pharmacokinetic parameters were calculated using pharmacokinetic programme KINFIT (MWPharm,

Table 1. Demografic data of the study patients.

Patient	Age (years)	Sex	Weight (kg)	RIFLE stage	SOFA	APACHE II	IL 6 (ng/L)	Diagnosis	Pathogen/ MIC
1	68	†	113	F	16	34	251	Peritonitis	*Staph.species/0.5*
2	73	¤	73	F	21	31	> 1000	MODS	*Staph. species/1.0*
3	44	†	90	F	16	31	67	Polytrauma, Sepsis	*Ent. faecium/0.5*
4	57	†	110	F	17	35	> 1000	CA - bypass,sepsis	*Staph. species/1.0*
5	71	†	90	I	21	32	> 1000	Pyartros genus l.dx	*Str. pyogenes/0.125*
6	28	†	80	F	18	26	> 1000	Infectious endocarditis	*Staph. aureus/0.5*
7	68	¤	70	F	21	31	-	Pneumonia	*Staph. species/1.0*
8	79	†	80	F	14	34	-	Infectious endocarditis	*empirically*
9	59	†	100	F	14	28	14	Pneumonia	*Staph. species/0.5*
10	45	¤	58	I	15	33	> 1000	Peritonitis	*Staph. species/-*
11	54	†	100	I	17	33	-	Sepsis	*Ent. faecalis/1.0*
12	50	†	110	I	15	33	75	Mediastinitis	*Strep. anginosus/0.25*
13	70	†	75	F	19	35	62	Wound infection	*Staph. haemolyticus/0.5*
14	51	¤	65	I	14	28	160	Spondylodiscitis	*MRSA/0.25*
15	61	†	90	F	16	34	448	Pneumonia	*MRSA/0.25*
16	61	¤	120	F	21	32	59	Mediastinitis	*Ent. faecalis/1.0*
17	34	¤	102	I	18	22	134	Sepsis	*Ent. faecalis/2.0*
Median	58		90		17	32	71		
Range	28-79		58-120		14-21	22-35	14->1000		

SOFA – sequential organ failure assessment – score, APACHE - acute physiology and chronic health evaluation - score, IL – interleukin, MIC – minimal inhibitory concentration, RIFLE – AKI classification system, F-failure, I-injury, †-men, ¤-women, MODS – multiple organ dysfunction syndrome, MRSA – methicillin resistant *Staphylococcus aureus*, CA bypass - coronary artery bypass

MEDIWARE version 3.60, Groningen, the Netherlands). The selected model was based on a one-compartment model.

CVVH was performed in all patients using a high-flux polysulphone membrane: 1.4 m^2 AV 600 (5 patients with a body weight less than 80 kg) and 1.8 m^2 AV 1000 (Fresenius Medical Care, Germany), the blood flow rate (Q_b) was 200 ml/min, ultrafiltrate flow rate (Q_f) was 45 mL/kg/h in pre-postdilution mode (50/50). This procedure was performed using a Multifiltrate machine (Fresenius Medical Care, Germany). The hemofilter was changed every 24 hours. Bicarbonate replacement fluids (Multibic K0-4) were purchased from Fresenius Medical Care, Germany. Low molecular heparin (nadroparine) was used as an anticoagulation, antiXa levels were maintained at 0.3-0.5. CVVH was performed through a double-lumen 14-F catheter inserted into the jugular or femoral vein. CRRT clearance was calculated using the following formula:

$$Cl_{CRRT} = Cl_{CRRT}(post) + Cl_{CRRT}(pre)$$

$$Cl_{CRRT}(post) = Q_f \times Sc \qquad Cl_{CRRT}(pre) = Q_f \times Sc \times CF$$

$$CF = Q_b/(Q_b+Q_{rep}) \text{ (ref.}^5\text{)}$$

where Cl_{CRRT}(post) = CRRT is the clearance from CRRT using post-filter hemodilution; Q_f is the ultrafiltration rate; Cl_{CRRT}(pre) = CRRT is the clearance from CRRT using pre-filter hemodilution; Q_b is the blood flow rate; Q_{rep} is the pre-dilution replacement rate and CF the correction factor.

Sieving coefficient was calculated following the formula $C_f/C_{pl,}$ where C_f was vancomycin concentration in ultrafiltrate fluid and C_{pl} was vancomycin serum concentration. Data are expressed as median and range. The Spearman correlation was used for correlation coefficients. A p-value of < 0.05 was considered statistically significant. GraphPad Prism for Windows version 5.0 (GraphPad Prism Software, Inc.) was used to perform the statistical analysis.

RESULTS

The clinical characteristics of the patients studied are summarized in Table 1. All patients suffered from severe sepsis and were treated with mechanical ventilation. Infections were caused by Gram-positive agents: *Staphylococcus species coagulase negat,* Methicillin-resistant *Staphylococcus aureus (MRSA), Staphylococcus haemolyticus, Streptococcus anginosus, Streptococcus pyogenes, Enterococcus faecalis* and *Enterococcus faecium.* Median Acute Physiology and Chronic Health Evaluation (APACHE II) and Sequential Organ Failure Assessment (SOFA) scores at inclusion were 32 (22-35) and 17 (14-21). Diuresis was preserved in 11 patients on the first day of the study (range 30-315 mL/h) and in 5 patients on the second study day (range 37-267 mL/h). Diuresis was supported by the diuretic agent furosemide 1.0 g/24 h (Table 2). Median estimated glomerular filtration by MDRD was 0.4 (0.1-0.6) mL/s in both study days.

Table 2. Urine output and ultrafiltration rate in study patients.

Patient	Diuresis (mL/h)		Ultrafiltration rate (mL/24 h)	
	Day 1	Day 2	Day 1	Day 2
1	160	–	3400	–
2	anuria	anuria	1700	2300
3	30	37	2800	4500
4	210	133	0	0
5	anuria	anuria	5570	6850
6	204	–	0	–
7	anuria	anuria	6000	6000
8	66	anuria	0	1700
9	36	anuria	4670	4540
10	315	–	1900	–
11	100	267	1700	2000
12	80	75	1900	5100
13	anuria	anuria	1400	2300
14	139	113	1700	4200
15	anuria	anuria	3065	4740
16	anuria	anuria	750	3250
17	81	–	800	–

Vancomycin dosage regimen and vancomycin serum concentrations during both days of the study are depicted in Tables 3 and 4. In three patients, a lower vancomycin dose of 1 g/24 h was given on the first day, due to acute surgical intervention. Vancomycin serum concentrations after the first dose were below the required target of 10 mg/L as early as 6 h in 10 patients. CRRT therapy was discontinued in 5 patients during the second day and these patients were excluded from further analysis. In the remaining 12 patients, the dose was adjusted in 8 patients. $AUC_{0\text{-}24}/MIC \geq 400$ ratio was achieved in 10 patients on the first day and in 6 patients on the second day. In 2 patients this ratio could not be determined due to unknown MIC value of pathogen (Tables 5 and 6). The pharmacokinetic parameters are summarized in Tables 5 and 6. On the first day of treatment, the total clearance of vancomycin (median 0.89 mL/min/kg, range 0.31-2.16 mL/min/kg) approached the average value of total clearance in patients without renal failure (0.97 mL/min/kg) (ref.[10]) in 7 of our patients, in 4 patients the total clearance of vancomycin was even higher. On day two the total clearance of vancomycin was equal to the average value of total clearance in only 4 patients. We found a significant correlation between the total vancomycin clearance and the dose/weight (r_s=0.8289, P=0.0009) on the second day of the treatment (Fig. 1). No significant relationship between the total clearance of vancomycin and residual renal function was found (P>0.05).

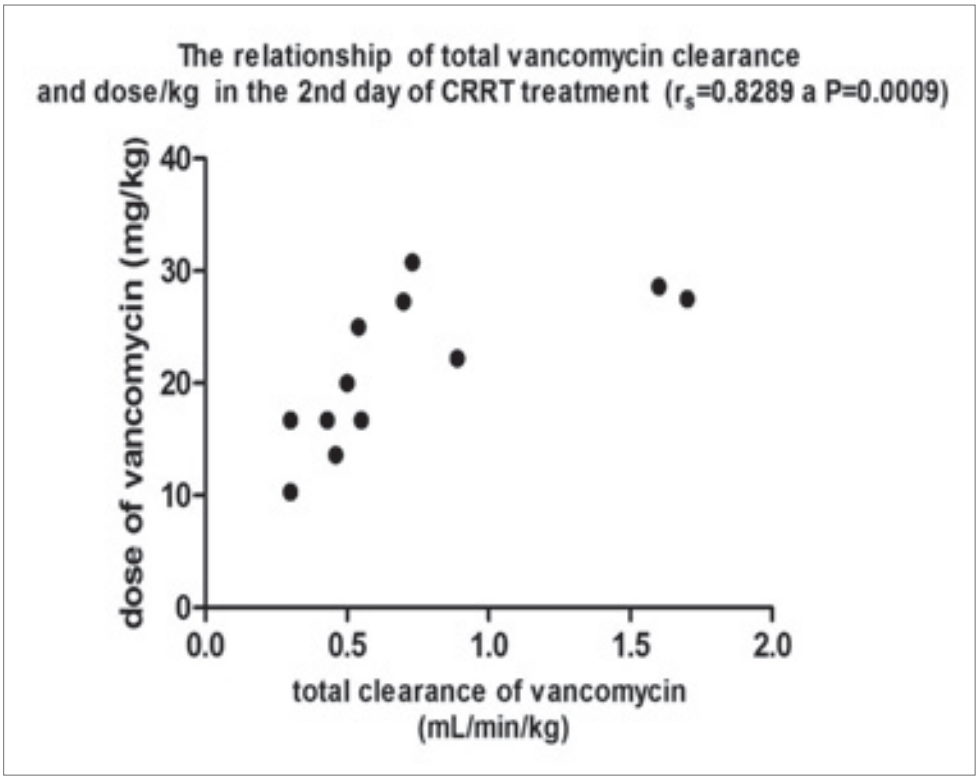

Fig. 1. The relationship between total vancomycin clearance and dose/kg on the second day of CRRT treatment (r_s=0.8289, *P*=0.0009).

Table 3. Vancomycin dose and individual serum concentrations on the first day of study.

		Day 1						
Patient	Vancomycin dose (g)	Dose/ weight (mg/kg)	1.C_{van} 1 h (mg/L)	1.C_{van} 6 h (mg/L)	1.C_{van} 12 h (mg/L)	2.C_{van} 1 h (mg/L)	2.C_{van} 6 h (mg/L)	2.C_{van} 12 h (mg/L)
1	1.0 /12 h	17.7	15.42	7.08	3.50	14.34	9.40	5.90
2	1.0 /12 h	27.4	32.50	21.10	18.38	27.28	19.49	15.66
3	1.0 /12 h	22.2	30.17	20.02	-	25.35	-	13.41
4	1.0 /12 h	18.2	16.58	5.37	4.00	13.70	6.83	-
5	1.0 /12 h	22.2	12.02	6.65	5.53	18.69	11.02	7.65
6	1-1.25-1.25	43.8	24.99	10.96	-	29.49	13.74	-
7	1.0/ 24 h	14.3	15.01	8.37	6.60	-	-	-
8	1.0 /12 h	25.0	14.63	6.53	3.53	27.20	9.81	7.00
9	1.0 /12 h	20.0	12.88	10.33	6.37	21.61	13.83	10.46
10	1.0 /12 h	34.0	22.81	4.02	3.18	20.60	8.43	5.00
11	1.0 /12 h	20.0	14.74	9.74	5.05	10.14	7.04	5.53
12	1.0 /24 h	9.1	26.55	18.10	11.25	-	-	-
13	0.75/12 h	20.0	24.18	-	12.78	19.34	-	12.22
14	1.0 /12 h	30.8	31.06	14.80	11.00	20.55	18.15	11.00
15	1.0 /12 h	22.2	10.84	7.33	5.33	16.86	11.83	9.83
16	1.0 /24 h	8.3	26.54	8.40	-	-	-	-
17	1.0 /12 h	19.6	15.21	5.42	3.19	17.37	6.39	3.99
Median		20.0	16.60	8.38	5.43	19.95	9.81	8.74
Range		8.3-43.8	10.84-32.50	4.02-21.10	3.18-18.38	10.14-29.49	6.39-19.49	3.99-15.66

1.C_{van} 1 h - vancomycin serum concentration 1 hour after 1st dose administration. 1.C_{van} 6 h –vancomycin serum concentration 6 h after 1st dose administration. 1.C_{van} 12 h - vancomycin serum concentration 12 h after 1st dose administration. 2.C_{van} 1 h - vancomycin serum concentration 1 h after 2nd dose administration. 2.C_{van} 6 h - vancomycin serum concentration 6 h after 2nd dose administration. 2.C_{van} 12 h - vancomycin serum concentration 12 h after 2nd dose administration.

Table 4. Vancomycin dose and individual serum concentrations on the second day of study.

	Day 2							
Patient	Vancomycin dose (g)	Dose/weight (mg/kg)	1.C_{van} 1 h (mg/L)	1.C_{van} 6 h (mg/L)	1.C_{van} 12 h (mg/L)	2.C_{van} 1 h (mg/L)	2.C_{van} 6 h (mg/L)	2.C_{van} 12 h (mg/L)
1	-	-	-	-	-	-	-	-
2	1.0 /24 h	10.3	25.68	18.82	16.63	-	-	-
3	1.0-0.5	16.7	21.22	22.57	15.51	18.58	18.29	12.55
4	1.0 /8 h	27.3	17.79	10.25	-	17.82	12.27	-
5	0.75/12 h	16.7	21.38	13.60	10.75	22.79	13.39	10.31
6	-	-	-	-	-	-	-	-
7	1.0/12 h	28.6	14.94	7.76	6.43	21.30	12.56	9.52
8	1.0/12 h	25.0	22.12	13.91	10.69	22.62	16.01	13.79
9	1.0/12 h	20.0	22.39	13.00	10.00	27.01	18.11	12.09
10	-	-	-	-	-	-	-	-
11	1.25-1.5	27.5	24.36	10.21	6.46	35.52	8.70	6.82
12	0.75/12 h	13.6	15.22	8.31	8.22	22.68	11.05	8.28
13	-	-	-	-	-	-	-	-
14	1.0/12 h	30.8	36.35	19.18	11.00	25.74	16.78	10.00
15	1.0/12 h	22.2	20.55	10.56	8.56	21.54	-	13.00
16	1.0/12 h	16.7	13.32	8.22	6.40	17.20	14.52	10.00
17	-	-	-	-	-	-	-	-
Median		21.1	21.30	11.78	10.00	22.62	13.96	10.16
Range		10.3-30.8	13.32-36.35	7.76-22.57	6.40-16.63	17.20-35.52	8.70-18.29	6.82-13.79

1.C_{van} 1 h - vancomycin serum concentration 1 h after 1st dose administration. 1.C_{van} 6 h - vancomycin serum concentration 6 h after 1st dose administration. 1.C_{van} 12 h - vancomycin serum concentration 12 h after 1st dose administration. 2.C_{van} 1 h - vancomycin serum concentration 1 h after 2nd dose administration. 2.C_{van} 6 h - vancomycin serum concentration 6 h after 2nd dose administration. 2.C_{van} 12 h - vancomycin serum concentration 12 h after 2nd dose administration.

DISCUSSION

We studied the pharmacokinetics of vancomycin in critically ill septic patients with acute kidney injury treated with CRRT in order to establish practical recommendations for a vancomycin dosage regimen. CVVH at a filtration rate of 45 mL/kg/h led to high and rapid extracorporeal removal of vancomycin in critically ill patients. However, due to rapid change in patient clinical status it was impossible to predict a fixed dosage regimen.

Extracorporeal elimination is clinically significant if it achieves 25-30% of total drug clearance[5]. Deldot et al. studied vancomycin clearance in 10 critically ill patients treated with continuous venovenous hemodiafiltration at a dialysis dose of 1000 mL/h and a filtration dose of 2000 mL/h. The total vancomycin clearance was 2.5±0.7 L/h and CVVHDF clearance was 76±16.5% of a total drug clearance[11]. Uchino et al. observed vancomycin clearance in 7 septic patients with multiple organ failure and AKI treated with high-volume venovenous hemofiltration at a filtration rate of 6 L/h with varying pre and postdilution flow rate[12]. They found that total vancomycin clearance increased when predilution flow rate was reduced from 4 L to 2 L in the range of 53.9 to 67.2 mL/min. Shah et al. describes a 14-year-old critically ill patient with AKI treated with CVVH at a filtration rate of 1800 mL/h, CVVH clearance was 26±0.8 mL/min[13]. In our study CRRT clearance at a filtration rate of 45 mL/kg/h accounted for approximately 50-60% of the total clearance of vancomycin found in a population with normal renal function, therefore it contributes significantly to the elimination of vancomycin in septic patients with AKI. Interestingly in three anuric patients, the total clearance of vancomycin was higher than the CRRT clearance and approached the plasma clearance of vancomycin in populations without renal impairment (0.97 mL/min/kg) (ref.[10,14,15]). In four patients, the total clearance of vancomycin was even higher than in populations without renal disease (1.24 to 2.16 mL/min/kg).

The total drug clearance is the sum of non-CRRT and CRRT clearance, which means that different factors are involved in the excretion of antibiotics. One of the important factors is residual renal function. Patients with residual diuresis may require an increased dose of vancomycin to maintain desired serum levels. In our study, however, we found no significant correlation between the total clearance of vancomycin and residual diuresis. In patients with oligoanuric AKI a substantial non-renal

Table 5. Pharmacokinetic/pharmacodynamic parameters of vancomycin during CRRT (45 mL/kg/h) treatment on the first day of study.

Day 1							
Patient	Cl_{tot} (mL/min/kg)	Vd (L/kg)	$t_{1/2}$ (h)	AUC_{0-24}	AUC_{0-24}/MIC	Cl_{CRRT} (mL/min/kg)	Sc
1	0.89	0.43	5.80	245.9	**491.8**	0.5	0.64
2	0.45	0.38	9.88	559.7	**559.7**	0.5	0.72
3	0.38	0.34	11.06	515.0	**1030.0**	0.4	0.65
4	1.24	0.46	4.32	184.8	184.8	0.5	0.68
5	0.97	0.71	8.34	233.8	**1870.1**	0.6	0.78
6	1.04	0.49	5.49	396.1	**792.2**	0.6	0.73
7	1.07	1.06	11.48	170.4	170.4	0.6	0.73
8	1.32	0.57	4.99	256.8	-	0.6	0.80
9	0.68	0.56	9.83	280.2	**560.4**	0.6	0.73
10	2.16	0.77	4.14	246.8	-	0.8	0.77
11	0.96	0.74	8.95	205.7	205.7	0.6	0.73
12	0.31	0.35	13.22	329.9	**1319.6**	0.6	0.73
13	0.49	0.51	11.68	375.0	**750.0**	0.5	0.73
14	0.73	0.55	8.88	410.9	**1640.0**	0.6	0.73
15	0.86	0.69	9.31	142.0	**568.0**	0.6	0.78
16	0.59	0.32	6.33	192.4	192.4	0.6	0.77
17	1.38	0.61	5.25	181.9	90.9	0.6	0.73
Median	0.89	0.55	8.88			0.6	0.73
Range	0.31-2.16	0.32-1.06	4.14-13.22			0.4-0.8	0.64-0.80

Cl_{tot} – total drug clearance. Vd – volume of distribution. $t_{1/2}$ – elimination half-life. Cl_{CRRT} – CRRT clearance. Sc – sieving coefficient. AUC_{0-24}/MIC – area under the serum concentration time curve 0-24 h to minimal inhibitory concentration ratio

Table 6. Pharmacokinetic/pharmacodynamic parameters of vancomycin during CRRT (45 mL/kg/h) treatment on the second day of study.

Day 2							
Patient	Cl_{tot} (mL/min/kg)	Vd (L/kg)	$t_{1/2}$ (h)	AUC_{0-24}	AUC_{0-24}/MIC	Cl_{CRRT} (mL/min/kg)	Sc
1	-	-	-	-	-	-	-
2	0.30	0.34	12.85	351.2	351.2	0.6	0.75
3	0.30	0.37	14.15	342.7	**685.4**	0.5	0.69
4	0.70	0.34	5.61	366.2	366.2	0.5	0.63
5	0.43	0.35	9.41	360.0	**2880.0**	0.6	0.74
6	-	-	-	-	-	-	-
7	1.06	0.77	8.41	278.1	278.1	0.5	0.67
8	0.54	0.53	11.77	384.5	-	0.5	0.63
9	0.50	0.38	8.67	395.1	**790.2**	0.6	0.76
10	-	-	-	-	-	-	-
11	1.07	0.43	4.71	343.6	343.6	0.5	0.68
12	0.46	0.36	9.06	287.3	**1149.2**	0.5	0.65
13	-	-	-	-	-	-	-
14	0.73	0.43	6.81	485.5	**1942.0**	0.5	0.63
15	0.89	0.78	10.85	230.3	**921.2**	0.6	0.73
16	0.55	0.54	11.66	270.5	270.5	0.5	0.63
17	-	-	-	-	-	-	-
Median	0.55	0.41	9.24			0.5	0.68
Range	0.30-1.07	0.34-0.78	4.71-14.15			0.5-0.6	0.63-0.76

Cl_{tot} – total drug clearance. Vd – volume of distribution. $t_{1/2}$ – elimination half-life. Cl_{CRRT} – CRRT clearance. Sc – sieving coefficient. AUC_{0-24}/MIC – area under the serum concentration time curve 0-24 h to minimal inhibitory concentration ratio

clearance initially has been observed[16]. The proportion of non-renal clearance can vary between 3.8 to 23.3 mL/min in patients with AKI compared with only 4-6 mL/min in patients with chronic renal failure[17]. Further vancomycin adsorption to hemofilter has also been described[18]. These factors could explain the discrepancy observed between total vancomycin clearance and CRRT clearance in our anuric patients and lack of correlation between the total clearance and diuresis. In four cases, we found paradoxically lower total clearance of vancomycin than CRRT clearance. The only explanation for this discrepancy is that these patients were disconnected from continuous elimination for several hours due to urgent intervention or due to repeated precipitation which led to the reduction in the total vancomycin clearance.

Sepsis can lead to endothelial damage with increased capillary permeability and can change the volume of distribution. Changes in the volume of distribution are important especially for hydrophilic substances. Increased volume of distribution has been observed for example in septic patients treated with aminoglycosides requiring an increase of daily dose to achieve therapeutic concentrations[19]. However, it seems that changes in fluid balance have less impact on the volume of distribution with vancomycin than with aminoglycosides. In our patients, we observed approximately the same volume of distribution as described in healthy volunteers[17]. Choi et al. describes volume of distribution of 0.55 ± 0.12 L/kg in septic patients treated with CVVH which corresponds to our findings[20]. Elimination half-life of vancomycin was longer in our patients (ranging from 4.14 h to 14.15 h) than in non-septic patients without renal impairment (approximately 4-6 h) (ref.[10,14,15]).

Trotman et al. recommends in critically ill patients an initial dose of vancomycin 15-20 mg/kg and a maintenance dose of 500 mg to 1500 mg every 24 h to 48 h in CVVHD and a dose of 1000-1500 mg every 24 h in CVVHDF to achieve trough concentration in the range of 10-15 mg/L (ref.[19]). Veltri et al. recommended an initial dose of 10-15 mg/kg parenterally followed by vancomycin concentrations monitoring in septic patients treated with CRRT in all modes[21]. The initial median daily dose of vancomycin in our group of patients was 20.0 mg/kg (8.3 to 43.8) with a loading dose of 1.0 g, maintenance dose was based on vancomycin serum concentrations. Total clearance of patients varied in a wide range and thus reflected the need for different weight-based doses of vancomycin. However, giving a standard initial dose of 1 g intravenously has lead to a drop of trough levels below 10 mg/L as early as 6 h after first drug administration in 10 of our patients. A weight-based initial vancomycin dose rather than fixed dose is proposed to rapidly achieve optimal therapeutic vancomycin concentrations. A loading dose of 25-30 mg/kg has been recommended in an effort of minimizing subtherapeutic exposures within the first 24 h (ref.[10]). However caution should be taken when applying this recommendation to the population with renal impairment. Septic patients are usually in a severe catabolic status and often need a different dose of RRT. They might often require changes in ultrafiltration flow rates leading to different elimination of antibiotics and thus making drug dosage more difficult. Boumann et al. observed a significant discrepancy between predicted and observed vancomycin removal with the need for dose adjustments and more frequent monitoring of serum levels in 45 oligoanuric patients treated with CVVH (ref.[22]). Due to rapid changes in patient clinical status and CRRT conditions, it may be therefore impossible to derive a fixed dosage regimen in critically ill septic patients and maintenance doses should be based on vancomycin concentration monitoring.

An AUC/MIC ratio ≥ 400 has been advocated as a target to achieve clinical effectiveness with vancomycin therapy[10]. However, because it can be difficult in the clinical setting to obtain multiple serum vancomycin concentrations to determine AUC and then calculate AUC/MIC, trough serum concentration monitoring, which can be used as a surrogate marker for AUC, is recommended as the most accurate and most practical method for vancomycin monitoring. Trough vancomycin serum concentrations maintained above 10 mg/L are recommended[10]. The desired $AUC_{0\text{-}24}$/MIC ≥ 400 was achieved in 67% of patients on the first day and 55% on the second day of treatment. The desired AUC/MIC ratio was achieved almost only in patients with vancomycin MIC < 1.0 mg/L. Recent study recommends a higher trough vancomycin concentration of between 15-20 mg/L especially in the treatment of complicated infections (e.g. ventilatory associated pneumonia) and for a pathogen with an MIC of 1 mg/L in order to attain target vancomycin exposure[10,23]. Higher trough vancomycin concentrations may also increase the potential for nephrotoxicity but the extent of this risk is yet to be determined. Vancomycin-induced nephrotoxicity is related to drug plasma concentrations[24]. Nephrotoxicity is a concern for those hemodialysis patients who have some residual renal function and mainly for those patients with AKI. A target AUC/MIC ≥ 400 is not achievable with conventional dosing methods if the pathogen vancomycin MIC is ≥ 2 mg/L, achievement of this ratio would lead to undesirable vancomycin toxicity. To further improve treatment options, use of predictive pharmacokinetic simulation for predicting plasma levels of vancomycin is recommended[25].

CONCLUSION

Therapeutic monitoring of vancomycin levels in critically ill septic patients treated with renal replacement therapy is a valuable tool in drug dosage adjustment. Due to the unstable patient's clinical status and possible changing conditions of RRT daily monitoring of vancomycin serum levels is necessary at least for the first days after antibiotic introduction. Achievement of adequate vancomycin concentration on the first day of treatment of septic patients is of high clinical importance. We recommend performance of blood sample as early as 6 h after first vancomycin dose in case of a need of early dose adjustment.

ACKNOWLEDGEMENTS

The authors thank all of the doctors and nurses of all the intensive care units that contributed to this study. This project was supported by grant IGA MZCR NS 103 09-3/2009.

CONFLICT OF INTEREST STATEMENT

The authors stated that there are no conflicts of interest regarding the publication of this article.

REFERENCES

1. Uchino S, Kellum JA, Bellomo R, Doig GS, Morimatsu H, Morgera S, Schetz M, Tan I, Bouman C, Macedo E, Gibney N, Tolwani A, Ronco C; Beginning and Ending Supportive Therapy for the Kidney (BEST Kidney) Investigators.Acute renal failure in critically ill patients: a multinational, multicenter study. JAMA 2005;294:813-8.
2. Bagshaw SM, Laupland KB, Doig CJ, Mortis G, Fick GH, Mucenski M, Godinez-Luna T, Svenson LW, Rosenal T.Prognosis for long-term survival and renal recovery in critically ill patients with severe acute renal failure: a population-based study. Crit Care 2005;9:R700-9.
3. Bagshaw SM, Uchino S, Bellomo R, Morimatsu H, Morgera S, Schetz M, Tan I, Bouman C, Macedo E, Gibney N, Tolwani A, Oudemans-van Straaten HM, Ronco C, Kellum JA; Beginning and Ending Supportive Therapy for the Kidney (BEST Kidney) Investigators.Septic acute kidney injury in critically ill patients: clinical characteristics and outcomes. Clin J Am Soc Nephrol 2007;2:431-9.
4. Grüneberg RN, Wilson AP.Anti-infective treatment in intensive care: the role of glycopeptides. Intensive Care Med 1994;20 Suppl 4:S17-22.
5. Choi G, Gomersall CD, Tian Q, Joynt GM, Li AM, Lipman J. Principles of antibacterial dosing in continuous renal replacement therapy. Blood Purif 2010;30:195-212.
6. Golper TA, Wedel SK, Kaplan AA, Saad AM, Donta ST, Paganini EP. Drug removal during continuous arteriovenous hemofiltration: theory and clinical observations. Int J Artif Organs 1985;8:307-12.
7. Boereboom FT, Ververs FF, Blankestijn PJ, Savelkoul TJ, van Dijk A.Vancomycin clearance during continuous venovenous haemofiltration in critically ill patients. Intensive Care Med 1999;25:1100-4.
8. Schetz M, Ferdinande P, Van den Berghe G, Verwaest C, Lauwers P. Pharmacokinetics of continuous renal replacement therapy. Intensive Care Med 1995;21:612-20.
9. Petejova N, Martinek A, Zahalkova J, Duricova J, Brozmanova H, Urbanek K, Grundmann M, Kacirova I. Vancomycin removal during low-flux and high-flux extended daily hemodialysis in critically ill septic patiens. Biomed Pap Med 2012;156:XX. DOI 10.5507/bp.2012.002, available online: January 30, 2012.
10. Rybak MJ, Lomaestro BM, Rotschafer JC, Moellering R Jr, Craig W, Billeter M, Dalovisio JR, Levine DP. Therapeutic monitoring of vancomycin in adults summary of consensus recommendations from the American Society of Health-System Pharmacists, the Infectious Diseases Society of America, and the Society of Infectious Diseases Pharmacists. Am J Health-Syst Pharm 2009;66:82-98.
11. DelDot ME, Lipman J, Tett SE.Vancomycin pharmacokinetics in critically ill patients receiving continuous venovenous haemodiafiltration. Br J Clin Pharmacol 2004;58:259-68.
12. Uchino S, Cole L, Morimatsu H, Goldsmith D, Bellomo R.Clearance of vancomycin during high-volume haemofiltration: impact of predilution. Intensive Care Med. 2002;28:1664-7.
13. Shah M, Quigley R. Rapid removal of vancomycin by continuous veno-venous hemofiltration. Pediatr Nephrol 2000;14:912-5.
14. http://www.sukl.cz/download/spc/SPC108984.doc (vancomycin product information).
15. http://www.sukl.cz/download/spc/SPC59482.doc (vancomycin product information).
16. Macias WL, Mueller BA, Scarim SK.Vancomycin pharmacokinetics in acute renal failure: preservation of nonrenal clearance.Clin Pharmacol Ther 1991;50:688-94.
17. Burton ME, Shaw LM, Scheritag JJ, Evans WE. Applied Pharmacokinetics & Pharmacodynamics Principles of Therapeutic Drug Monitoring. 4.vyd. Philadelphia PA: Lippincote Williams & Wilkins 2006:285-353.
18. Reetze-Bonorden P, Böhler J, Keller E. Drug dosage in patients during continuous renal replacement therapy. Pharmacokinetic and therapeutic considerations. Clin Pharmacokinet 1993;24:362-79.
19. Trotman RL, Williamson JC, Shoemaker DM, Salzer WL. Antibiotic dosing in critically ill adult patients receiving continuous renal replacement therapy. Clin Infect Dis 2005;41:1159-66.
20. Choi G, Gomersall ChD, Tian Q, Joynt GM, Freebairn R, Lipman J. Principles of antibacterial dosing in continuous renal replacement therapy. Critical Care Medicine 2009;7:2268-82.
21. Veltri MA, Neu AM, Fivush BA, Parekh RS, Furth SL. Drug dosing during intermittent hemodialysis and continuous renal replacement therapy: special considerations in pediatric patients. Paediatr Drugs 2004;6:45-65.
22. Bouman CS, van Kan HJ, Koopmans RP, Korevaar JC, Schultz MJ, Vroom MB. Discrepancies between observed and predicted continuous venovenous hemofiltration removal of antimicrobial agents in critically ill patients and the effects on dosing. Intensive Care Med 2006;32:2013-19.
23. Brochard L, Abroug F, Brenner M, Broccard AF, Danner RL, Ferrer M, Laghi F, Magder S, Papazian L, Pelosi P, Polderman KH; ATS/ERS/ESICM/SCCM/SRLF Ad Hoc Committee on Acute Renal Failure. An Official ATS/ERS /ESICM /SCCM /SRLF Statement: Prevention and Management of Acute Renal Failure in the ICU Patient: an international consensus conference in intensive care medicine. Am J Respir Crit Care Med 2010;181:1128-55.
24. Rybak MJ. The Pharmacokinetic and Pharmacodynamic Properties of Vancomycin. Clin Inf Dis 2006;42:S35-9.
25. Zahálková J, Strojil J, Petejová N, Urbánek K, Grundmann M, Kacířová I. Dávkování vankomycinu při kontinuální náhradě funkce ledvin. Klin Farmakol Farm 2011;25:116-21.

12

Color Doppler Ultrasound in the pre-histological determination of the biological character of major salivary gland tumors

Štrympl P, Kodaj M, Bakal T, Komínek P, Stárek I, Šišola I, Tomášková H, Matoušek P

Originally published in Biomedical Papers, 2014, vol. 158, no. 3, p. 465-469

Consent to the publication of 18th March 2015

Color Doppler Ultrasound in the pre-histological determination of the biological character of major salivary gland tumors

Pavel Strympl[a], Michal Kodaj[b], Tomas Bakaj[c], Pavel Kominek[a], Ivo Starek[c], Ivan Sisola[d], Hana Tomaskova[e], Petr Matousek[a]

Objectives. The aim of the study was to assess the use of color Doppler ultrasound in the pre-histological determination of the biological features of salivary gland tumors.
Material and Methods. Ninety-six patients with major salivary gland tumors of unknown histology were examined and operated on in our clinics. They were pre-operatively examined using ultrasound imaging with color Doppler. Peak systolic velocity (PSV) was measured and pulsatility index (PI) and resistive index (RI) were calculated on the pulsed wave traces. The Doppler flow parameters were correlated with clinical stage and tumour type (benign/carcinoma) as confirmed by final histological diagnosis. For the correlations, the tumors were categorized into 3: benign (group I), malignant stages I+II (group II), malignant stages III+IV (group III).
Results. The average PSV value was 22.15 cm/s for benign and 32.74 cm/s for all malignant tumors. The average RI value was 0.77 for benign and 0.86 for all malignant tumors. The average PI value for benign tumors was 2.85 and 3.14 for all malignant tumors. No significant differences between benign and malignant tumors in terms of SV and PI values were found. The RI values for benign tumors differed significantly from those of malignant ones (P=0.021). There were no significant differences in average PSV, PI and RI values in relation to salivary gland tumor group - I, II, III. There was no confirmation of the reported applicability of PSV and PI values in differenting benign from malignant tumors.
Conclusion. We were not able to demonstrate significant differences in Doppler flow parameters PSV and PI between benign tumors and carcinomas. Only the RI could be used to differentiate them. There were also no significant differences in PSV, PI and RI values between low (I+II) and high (III+IV) clinical tumour stage.

Key words: color Doppler ultrasound, salivary gland, tumor

Received: April 23, 2012; Accepted: July 10, 2012; Available online: September 5, 2012
http://dx.doi.org/10.5507/bp.2012.074

[a]Department of Otolaryngology, University Hospital Ostrava, Czech Republic
[b]Department of Radiology, University Hospital Ostrava
[c]Department of Otorhinolaryngology, Faculty of Medicine and Dentistry, Palacky University Olomouc
[d]Department of Radiology, Faculty of Medicine and Dentistry, Palacky University Olomouc
[e]Department of Epidemiology and Public Health, Faculty of Health Studies, University of Ostrava
Corresponding author: Pavel Strympl, e-mail: pavel.strympl@fno.cz

INTRODUCTION

Salivary gland neoplasms account for 3% of all tumors[1]. Most are benign, with the parotid being the most common site of origin. The smaller the involved salivary gland, the higher the probability of malignancy, the rate of which thus increases from 20%-25% in the parotid, through 40%-50% in the submandibular, to 50%-81% in the sublingual and minor salivary glands[2-5].

Relevant important preoperative information is the determination of their biological character. Since sole clinical investigation lacks the necessary reliability in this respect, imaging methods are being applied. Of these and due to its zero invasiveness and cost effectiveness, ultrasound is considered an essential imaging method. Its specificity can be substantially improved by the use of the color Doppler method, mapping the blood flow in tumor supplying vessels. Color Doppler criteria are used to distinguish benign from malignant tumors, particularly in terms of grade of intratumor vascularity, pattern of vascular supply, and flow parameters (Table 1) (ref.[6]). Some publications reports on the usefulness of color Doppler US in the pre-histological determination of the biological character of the tumors[3,4,6,7] while others do not[8,9].

The main aim of this study was to test the use of color Doppler US in the preoperative assessment of the biological character of salivary gland tumors which would enable us to match the extent of surgery to their real dignity.

MATERIAL AND METHODS

A total of 96 patients with parotid gland tumors were examined in this prospective study at our clinics between June 2006 and August 2011. Fifty-four women and 42 men were enrolled, average age 57.3 and 60.4 (mean 58.7) years. Sixty-six (68%) tumors were benign and 30 (32%) were malignant (Table 2). Malignant tumors were found in 17 women and 13 men. In 19 patients, the set of tested color Doppler parameters was not complete. Thus, the PSV value was measured in 95 tumors, RI in 94 tumors and PI in 74 tumors.

The color Doppler US was the basic preoperative diagnostic tool. When a deep lobe parotid tumor was suspect-

Table 1. Color Doppler ultrasound parameters in major salivary gland tumors diagnostics.

Color Doppler US parameters
Quantitative parameters
• *The number of supplying vessels*. Low-differentiated malignant tumors usually have richer vessel supply when compared with benign tumors[6,7]. We can see 3 and more tumor supplying arteries in the case of malignant tumors[2].
Qualitative parameters
• *Peak systolic velocity (PSV).* PSV in the arteries supplying benign tumors are usually lower that 25 cm/s (ref.[2]). Higher Doppler velocities can be seen in the vessels of malignant tumors. Velocity higher than 60 cm/s was found in the malignant tumor vessels. Dock et al. recommends PVS 40 cm/sec as the level for differentiation between benign and malignant tumors[3]. • *Pulsatility index (PI).* PI is the ratio between PSV and end-diastolic velocity (EDV) difference to the average velocity. The tumor with PI value 1.8 and is considered as potentially malignant[7]. • *Resistive index (RI),* so called *Pourcelot's index.* RI is the ratio between PSV and EDV (end diastolic velocity) difference to PSV. The values 0.8 and higher point to a malignant tumor[7].

ed or malignancy was confirmed on cytology, magnetic resonance imaging (MRI) or computer tomography (CT) was performed to evaluate the tumor extent and local invasion. The US examination was performed by two independent experienced radiologists. The US linear 6-9 MHz probe was used. The patients were placed in the supine position, with the neck turned to the contralateral side. The region of interest was scanned slowly with a minimal probe pressure.

Longitudinal and transverse scanning planes were used to map the color flow signals within the salivary gland parenchyma. When a tumor vessel was identified, the probe position was adapted into the optimal plane to achieve its ideal display.

The basic US parameters of the tumor (i.e. size, structure and echotexture), adjacent soft tissue invasion and the US signs of potential metastatic lymph node affection were studied. The color mapping of the tumor was then performed with the determination of the count of supplying vessels, in which three flow parameters, namely peak systolic velocity (PSV), resistive index (RI) and pulsatility index (PI) were evaluated. The PSV, RI and PI values equal to or higher than 25 cm/s, 0.8 and 1.8, were considered borderlines for malignancy in accordance with the referenced literature (Table 1) (ref.[2-4,7]).

The PSV, RI and PI values for benign tumors were compared to those of carcinomas, the differences between two groups were then evaluated with Student t–test.

Individual patients were then categorized according to the biological character and clinical stage of their tumors as follows: benign tumors (group I), malignant tumors staged I+II (group II), malignant tumors staged III+IV (group III). Sixty-six patients (68.75%) were classified as group I, 17 patients (17.71%) as group II and 13 patients (13.54%) as group III.

Table 2. Histological types of the primary epithelial salivary gland tumors in our study.

	N°	%
Benign tumors	66	68.0
pleomorphic adenoma	37	38.1
cystadenolymphoma	27	27.8
bazocellular adenoma	2	2.01
Malignant tumors	30	32.0
squamous cell carcinoma	6	6.3
adenoid cystic carcinoma	5	5.2
mucoepidermoid carcinoma	4	4.2
adenocarcinoma	4	4.2
ductal carcinoma	4	4.2
carcinoma in pleomorphic adenoma	4	4.2
small cell carcinoma	1	1.0
nondifferentiated carcinoma	1	1.0
myoepithelial carcinoma	1	1.0

Peak levels of the PSV, RI and PI in all three groups were compared, using ANOVA. All analyses were performed using the statistical software STATA version 10. Our results (PSV, PI and RI values) were compared with standard values reported in the literature. The level of significance was $P<0.05$

RESULTS

The difference in PSV, PI and RI values between benign tumors and carcinomas

The PSV values ranged from 4 to 90 cm/s (mean 25.15 cm/s) for the benign tumor group and from 4 to 68 cm/s (mean 32.74 cm/s) for carcinomas. The PI values ranged from 0.64 to 9.4 (mean 2.85) in the benign tumor group and from 0.7 to 13.0 (mean 3.14) in the carcinomas. The RI of the benign tumor group ranged from 0.41 to 1.0 (mean 0.77) and from 0.2 to 1.2 (mean 0.86) in the carcinoma group. A statistically significant difference (P=0.021) was found between the benign tumors group and the carcinomas for RI, but not PI and PSV values (Table 3).

The PSV, PI and RI values depending on clinical stage of tumor

The values of PSV 4 - 90 cm/s (mean 25.15 cm/s), RI 0.41 - 1.0 (mean 0.77) and PI 0.64 - 9.4 (mean 2.32) were found in group I. The values of PSV, RI, PI in groups II and III were 5 - 59 cm/sec (mean 24.09 cm/s), 0.2 - 0.9 (mean 0.83) PI 0.7 - 13 (mean 1.92) and 4 - 68 cm/s (mean 34.54 cm/s), 0.68 - 1.2 (mean 0.89), 1.3 - 7.68 (mean 3.21), respectively. The differences between the

Table 3. The difference of the peak systolic velocity, pulsatility index and resistive index values between benign and carcinomas (B – benign tumor, C – carcinoma, SD – standard deviation).

Index	Tumor	No	From	To	Mean	SD	*P* value
PSV	B	66	4.0	90.0	25.15	17.49	0.179
	C	29	4.0	68.0	32.74	27.50	
RI	B	66	0.41	1.0	0.77	0.16	0.021
	C	28	0.2	1.2	0.86	0.19	
PI	B	51	0.64	9.4	2.85	2.32	0.642
	C	21	0.7	13.0	3.14	2.76	

Table 4. The peak systolic velocity, pulsatility index and resistive index values depending on the clinical stage of the tumor (I, II, III – groups according to tumor clinical stage, SD – standard deviation, ANOVA – test of variance).

Index	Groups	No	Mean	SD	ANOVA *P* value
age	I	66	54.51	15.82	< 0.001
	II	17	63.47	14.48	
	III	13	72.36	11.72	
PSV	I	66	25.15	17.49	0.185
	II	17	24.09	13.45	
	III	13	34.54	21.65	
RI	I	66	0.77	0.16	0.072
	II	17	0.83	0.22	
	III	13	0.89	0.16	
PI	I	51	2.85	2.32	0.305
	II	12	1.92	1.14	
	III	10	3.21	1.88	

Table 5. Sensitivity and specificity calculation for parameter RI (B – benign tumor, C – carcinoma, T (-) – negative results, T (+) – positive results, RN – right negative result, FP – false positive result, FN – false negative result, RP – right positive result).

	B	C	Total
T (-)	36 (RN)	8 (FN)	44
T (+)	32 (FP)	20 (RP)	52
Total	68	28	96
RI: sensitivity 71.4%, specificity 52.9%.			

PSV, PI and RI values in groups I, II, III were not statistically significant (Table 4).

Using the PSV, PI, RI values reported in the literature for distinguishing benign tumors and carcinomas

Our study confirmed the use of an RI critical value of 0.8 appearing in the literature[2,3,4,7] for distinguishing benign tumors and carcinomas. Thirty-six patients had true negative results, in the group of 32 patients false positive results were described, 8 patients had false negative results and 20 patients true positive results. The sensitivity and specificity of the RI parameter in differentiating carcinomas from benign tumors were thus 71.4% and 52.9%, respectively (Table 5).

No applicability of the PSV value of 25 cm/s and PI value 1.8 for differentiation was demonstrated.

The PI parameter differentiated carcinomas from benign tumors with a sensitivity of 61.9% and a specifity of 49.1%. True negative results were obtained in 26 pa-

Table 6. Sensitivity and specificity calculation for parameter PI
(B – benign tumor, C – carcinoma, T (-) – negative results, T (+) – positive results, RN – right negative result, FP – false positive result, FN – false negative result, RP – right positive result).

	B	C	Total
T (-)	26 (RN)	8 (FN)	34
T (+)	27 (FP)	13 (RP)	40
Total	53	21	74
PI: sensitivity 61.9%, specificity 49.1%.			

Table 7. Sensitivity and specificity calculation for parameter PSV
(B – benign tumor, C – carcinoma, T (-) – negative results, T (+) – positive results, RN – right negative result, FP – false positive result, FN – false negative result, RP – right positive result).

	B	C	Total
T (-)	42 (RN)	11 (FN)	53
T (+)	25 (FP)	17 (RP)	42
Total	67	28	95
PSV: sensitivity 60.7%, specificity 62.7%.			

tients and in 27 patients false positive results. In 8 cases we found false negative results and in 13 patients true positive results. The PI value was measured in 72 tumors (Table 6).

The parameter PSV can distinguish carcinomas from benign tumors with a sensitivity of 60.7% and a specificity of 62.7%. In the case of 42 patients, true negative results were found and in 25 patients false positive results. The result from 11 patients were false negative and from another 17 true positive (Table 7).

DISCUSSION

The role of imaging methods in the evaluation of salivary gland tumors is to define their intra- vs. extraglandular position, to detect local extension, invasion and nodal metastases. All this information can be successfully obtained with US, which is a safe, inexpensive and accurate method[10], serving as a basic guide for further imaging and treatment strategy. US is also expected to provide us with information about the status of salivary gland tumors, greatly varying between, as well as within, particular histopathologic entities. However, in this aspect, the capability of standard US is rather limited.

A question which remains is whether color Doppler US could be helpful in the determination of the biological nature or even the histopathological type of salivary gland tumor.

Izzo et al.[7] followed a series of 49 patients with major salivary gland tumors who underwent color and power Doppler US examinations preoperatively. In benign tumors the peritumoral and in much lesser extent intratumoral vascularisation as measured by a color power Doppler US device with 7.5-10 MHz linear probe was modest. On the other hand, carcinomas, due to a number of arteriovenous shunts and massive neovascularization, had a non-homogenous pattern with scattered distribution of vessels.

Martinoli et al.[6] achieved similar results in their series of 62 patients with major salivary gland tumors. They described significantly more extensive blood supply in the group of malignant tumors.

Some authors found higher vascular resistance as a sign of tumor malignancy. Bradley et al.[4] examined 56 patients with major salivary gland tumors. PSV was measured and PI and RI calculations were performed and particular values were then correlated with the histolopathological diagnosis. The combination of the real time ultrasound parameters RI and PI diagnosed benign disease with a sensitivity of 89.7% and specificity of 57.1%. The positive predictive value was 93.6%. There were no significant differences in the colour Doppler appearances in terms of vessel type or intratumour distribution which could separate benign from malignant conditions. No malignant lesion showed the PI and RI lower than 1.8 and 0.8, respectively.

In a study of 49 patients with benign and 13 patients with malignant tumors Martinoli et al.[6] did not find significant differences between groups in RI values (range from 0.55 to 1.10 in benign and 0.45 to 1.10 in malignant tumors). Contrary to Martinoli, we confirmed a significant difference in RI, but not in PI values between benign and carcinomas.

PSV is another color Doppler parameter used to analyze the flows in tumor supplying vessels. In a study on 130 benign and malignant tumors (44 mammary gland, 43 liver, 43 other organs) Dock et al. detected generally increased (higher than 40 cm/s) PSV values in the latter[3]. Similar results were presented by Stárek who recommend-

ed PSV 25 cm/s as the level, critical for differentiation between benign and malignant tumors[2]. Martinoli suggested that a systolic peak flow of 60 cm/s was a threshold for differentiating benign from malignant lesions. As some of the latter were associated with lower PSV, no reliable conclusions could be drawn[6]. Bradley et al. found PSV elevation (>50 cm/s) in some carcinomas, but there was no statistical correlation with malignancy in general[4]. Schick et al. demonstrated that pulsed Doppler US distinguished benign neoplasms from malignant ones with a 72% sensitivity and 88% specificity[11]. The highest PSV observed in benign tumors was 19.9 ± 7.7 cm/s, compared with 44.4 ± 47.7 cm/s in malignant tumors. The difference between velocities of benign and malignant tumors was statistically significant[11]. The outcomes of our study are not in accord with these results.

Given different values of PSV, PI and RI considered as threshold between benign and malignant tumors[4,7,11] we, as well as Gritzmann[9], are skeptical of their practical application. This view was also shared by Bialek in her paper on US use in salivary gland diagnostics[8].

Our study, in agreement with Bialek[8] and Gritzmann[9] but in contrast to the above studies[2-4,7] failed to demonstrate the applicability of the PSV value of 25 cm/s and PI value of 1.8 as the "break points" for the tumor type. The PSV values were higher than 25 cm/s in 26 benign (27.4%) and 17 malignant tumors (17.9%) (from 95 PSV measurements in total) in our study. The PI values higher than 1.8 were demonstrated in 25 benign (34.7%) and 13 malignant tumors (18.1%) (from 72 PI measurements in total).

Our study confirmed that the parameter RI can be used for differentiating benign from malignant tumours. and confirmed an RI critical value of 0.8 for the distinguishing benign tumors from carcinomas. Doppler US parameter RI differentiates carcinomas from benign tumors with a sensitivity of 71.4% and specificity of 52.9%.

Overall, significant differences in PSV and PI between benign tumors and carcinomas were not confirmed in contrast to some published papers. Similarly, there were no significant differences in the PSV, PI and RI values for particular clinical stages of the latter.

CONCLUSION

We confirmed the usefulness of the color Doppler RI parameter in differentiating benign salivary gland tumors from malignant ones. For other parameters (PSV and PI) no significant differences between benign tumors and carcinomas were. The study failed to confirm the benefit of the color Doppler US in the differentiation between benign tumors and clinical stages of carcinomas.

ACKNOWLEDGEMENT

The authors would like to thank Ms. Vanessa DeRhen, Mr. Jiří Hynčica and Mr. Alexander Oulton for their help and corrections to get this paper in its final form.

Results described in this paper were obtained with support of Grant IGA MZ CR NT/13505.

Authorship contributions: PS: literature search; PS, PK, IS: manuscript writing; PS, IS: study design; PS, TB, MK, ISi, PM: data collection; HT, PS: data analysis and interpretation; HT: statistical analysis and figures; PS, PK, IS: final approval.

Conflict of interest statement**:** None declared.

REFERENCES

1. Lee YYP, Wong KT, King AD, Ahujab AT. Imaging of salivary gland tumours. European J Radiol 2008;66:419-36.
2. Stárek I. Choroby slinných žláz. Praha: Grada, 2000. p. 37-47.
3. Dock W, Grabenwoger F, Metz V. Tumor Vascularization: Assessment with Duplex Sonography. Radiology 1991;181:241-4.
4. Bradley M, Durham L, Lancer J. The Role of Colour Flow Doppler in the Investigation of the Salivary Gland Tumour. Clinical Radiology 2000;55:759-62.
5. Ariji Y, Kimura Y, Hayashi N. Power Doppler Sonography of Cervical Lymph Nodes in Patients with Head and Neck Cancer. Am J Neuroradiol 1998; 26:303-7.
6. Martinoli C, Delhi E, Solbiati L. Color Doppler sonography salivary glands. Amer J Roentgenol 1994;163:933-41.
7. Izzo L, Sassayanis P, Frati R. The Role of Echo Colour/Power Doppler and Magnetic Resonance in Expansive Parotid Lesions. J Exp Clin Cancer Res 2004;23:585-92.
8. Bialek EJ, Jakubowski W, Zajkowski P. Ultrasonography of salivary glands: Anatomy and Spatial Relationships, Pathologic Conditions and Pitfalls. RadioGraphics 2006; 26:745-63.
9. Gritzmann N, Rettenbacher T, Hollerweger A. Sonography of the salivary glands. Eur Radiol 2003;13:964-75.
10. Alyas F, Lewis K, Williams L, Mooby AB, Wong KT. Diseases of the submandibular gland as demonstrated using high resolution ultrasound. The British Journal of Radiology 2005;78:362-69.
11. Schick S, Steiner E, Gahleitner A. Differentiation of benign and malignant tumors of the parotid gland: value of pulsed Doppler and color Doppler sonography. Eur Radiol 1998;8:1462-7.

13

Procedure for granulocyte collection performed at the Blood Centre of the Faculty Hospital Ostrava

Čermáková Z, Blahutová Š, Papajík T, Galuszková D, Hubáček J, Sommerová M

Originally published in Biomedical Papers, 2014, vol. 158, no. 2, p. 309-312

Consent to the publication of 1st April 2015

Procedure for granulocyte collection performed at the Blood Centre of the Faculty Hospital Ostrava

Zuzana Cermakova[a,b], Sarka Blahutova[b], Tomas Papajik[c], Dana Galuszkova[d], Jaromir Hubacek[c], Martina Sommerova[b]

Background. Granulocyte apheresis is a safe and effective method for granulocyte collection. We present a five year experience (2006-2010) of the Blood Center, Faculty Hospital Ostrava, Czech Republic. Donor granulocyte transfusion is one treatment option for haemato-oncology patients with severe neutropenia complicated by bacterial/fungal infections unresponsive to standard antibiotic/antifungal treatment. In this study, we describe the experiences of the Blood Centre at the Faculty Hospital in Ostrava of granulocyte apheresis.

Methods and Results. A total of 149 granulocyte units were collected for 33 patients from the Department of Haemato-oncology, University Hospital Olomouc, over a 5-year period (2006-2010). Information on donor selection, laboratory screening, mobilization regimen and granulocyte yield was obtained and analyzed. All mandatory screening tests for infection markers, AB0 and Rh and abnormal erythrocyte antibodies were performed. The cytomegalovirus status of the donors was not investigated. Steroids were the only mobilization regimen used, and were generally well accepted. The mean granulocyte yield was 12.6×10^9/per transfusion unit (range 5.4-30.3). All granulocyte concentrates were irradiated and transfused according to AB0 Rh compatibility within 24 h after collection.

Conclusion. Based on our experience, granulocytapheresis is a safe and effective method for obtaining granulocytes but the yield can be significantly influenced by other variables. From the recipients' perspective, the use of donor granulocytes supports an effective therapeutic modality.

Key words: granulocyte apheresis, donor selection, mobilization regimen

Received: November 9, 2011; Accepted with revision: July 4, 2012; Available online: November 1, 2012
http://dx.doi.org/10.5507/bp.2012.071

[a]Department of Biomedical Sciences, Faculty of Medicine, University Ostrava, Czech Republic
[b]Blood Centre, Faculty Hospital Ostrava
[c]Department of Haemato-Oncology, University Hospital Olomouc
[d]Department of Transfusion Medicine, University Hospital Olomouc
Corresponding author: Zuzana Cermakova, e-mail: zuzana.cermakova@fno.cz

INTRODUCTION

Transfusions of allogeneic granulocytes are indicated in immunocompromised patients with severe neutropenia whose status is complicated by bacterial/fungal infection unresponsive to standard antibiotic/antifungal therapy. Other indications are primary (congenital) or secondary diseases with neutrophil dysfunction. The granulocyte product contains granulocytes suspended in plasma and is obtained by apheresis from a single donor using automated cell-separation equipment[1]. Sedimentation agents such as hydroxyethyl starch (HES) or low-molecular-weight starch (Pentastarch) are used to improve the separation of leukocytes from erythrocytes. Various mobilization regimens are used to mobilize donor granulocytes, including filgrastim (G-CSF), a combination of G-CSF and corticosteroids, and corticosteroids alone. Tests for AB0 and RhD groups, abnormal erythrocyte antibodies, human immunodeficiency virus, hepatitis C virus (HCV), HBV and syphilis are mandatory. Granulocyte concentrates must be irradiated and transfused as soon as possible after collection. In this study, we present the results of 5 year's experience of granulocyte concentrate collection.

MATERIAL AND METHODS

A total of 149 granulocyte units were prepared for 33 patients from the Department of Haemato-oncology, University Hospital Olomouc. Data were obtained for the 5-year period from 2006-2010. Each patient received a mean of 4.5 transfusion units (TU) of granulocytes for the diagnoses indicated in Table 1.

Table 1. Diagnoses of recipients of granulocyte transfusions from 2006-2010.

Diagnosis	Number of patients
Acute myeloid leukaemia	20
Chronic myeloid leukaemia	2
Myelodysplastic syndrome	2
Hodgkin's lymphoma	3
Acute lymphoblastic leukaemia	5
Aplastic anaemia	1

Granulocyte donors were obtained from a pool of healthy blood donors with previous experience of apher-

esis collection (usually recruited from plateletapheresis donors). Granulocytes were collected once every 6 months. Czech law only allows the use of G-CSF for related donors; mobilization in unrelated donors was thus achieved using corticosteroids alone,with an infusion of 40 mg methylprednisolone in 100 mL 0.9% sodium citrate 4-5 h before collection. No adverse events were reported, except for fatigue within 24 h after collection. Donors were not tested for cytomegalovirus (CMV) status because the incidence of donor CMV positivity is high (about 90%) and may change.

High-molecular-weight HES 10% (molecular weight 200.000 kDa) was used to enhance granulocyte collection. All donors underwent mandatory tests for human immunodeficiency virus, hepatitis B virus (HBV), HCV, syphilis, AB0 and Rh and abnormal erythrocyte antibodies. Red blood cell cross-matching between donor and patient was done before granulocytapheresis as granulocyte concentrates contain a significant number of red blood cells. All granulocytapheresis procedures were carried out using a Cobe Spectra separator (Caridian BCT, USA) and all granulocyte concentrates were irradiated after collection.

Blood counts were taken before and after mobilization, with a focus on donor leukocyte counts and normal blood counts. Regarding granulocytes, we focused on the haematocrit per granulocyte TU (to determine the correlation between haematocrit and yield), and yield after collection. MedCalc (MedCalc Software, Belgium) was used to analyze the correlation between haematocrit and yield.

Table 2. Patient age and number of granulocyte units transfused per patient.

	Patient age (years)	Number of granulocyte units transfused per patient
Mean	47	6
Range	22-64	1-14

RESULTS

The results are summarized in Tables 2-6 and in Fig. 1-3.

Table 3. Donor peripheral blood leukocyte and neutrophil counts before and after corticosteroid stimulation.

	Leukocytes before collection (10^9/L)	Leukocytes after collection (10^9/L)	Neutrophils before collection (%)	Neutrophils after collection (%)
Mean	6.2	7.6	54.0	88.0
Range	2.7-10.6	3.8-14.5	36.0-75.0	45.0-5.0

Table 4. Haematocrit per granulocyte unit.

Haematocrit per granulocyte unit	
Mean	0.029
Range	0.003-0.080

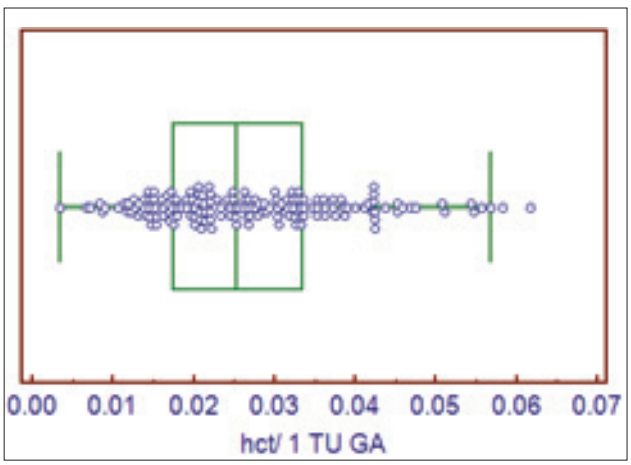

Fig. 1. Box and Whisker graph. Variable haematocrit per TU. Granulocytes were equally distributed around a theoretical midpoint. Although there were some eccentric points, these were still within the tolerance range.

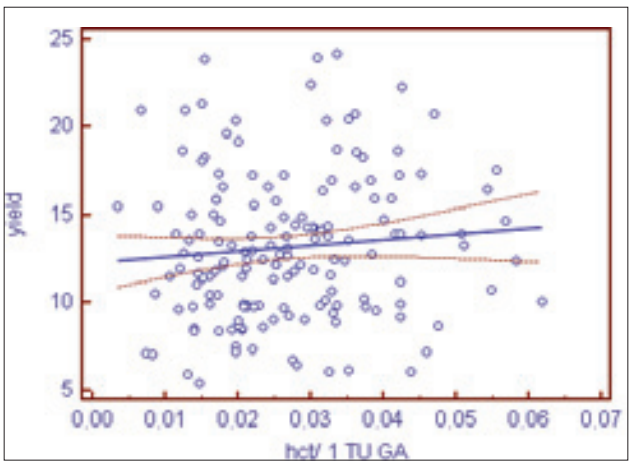

Fig. 2. Point graph of relationship between haematocrit and granulocyte yield. There was no correlation between the haematocrit per granulocyte TU and granulocyte yield.

Dependent Y	yield
Independent X	hct__1_TU_GA hct/ 1 TU GA

Sample size	158
Coefficient of determination R^2	0.009058
Residual standard deviation	4.1296

Regression Equation

$y = 12.2826 + 33.2231 x$

Parameter	Coefficient	Std. Error	95% CI	t	P
Intercept	12.2826	0.8173	10.6683 to 13.8970	15.0290	<0.0001
Slope	33.2231	27.8213	-21.7319 to 88.1780	1.1942	0.2342

Analysis of Variance

Source	DF	Sum of Squares	Mean Square
Regression	1	24.3183	24.3183
Residual	156	2660.3046	17.0532

F-ratio	1.4260
Significance level	P=0.234

Table 5. Correlation between haematocrit per TU and yield.

Table 6. Yield and volume of granulocyte apheresis, and separation time.

	Granulocyte yield (10^9/TU)	Apheresis volume (mL)	Separation time (min)
Mean	12.6	270.0	105
Range	5.4-30.3	220.0-360.0	90-120

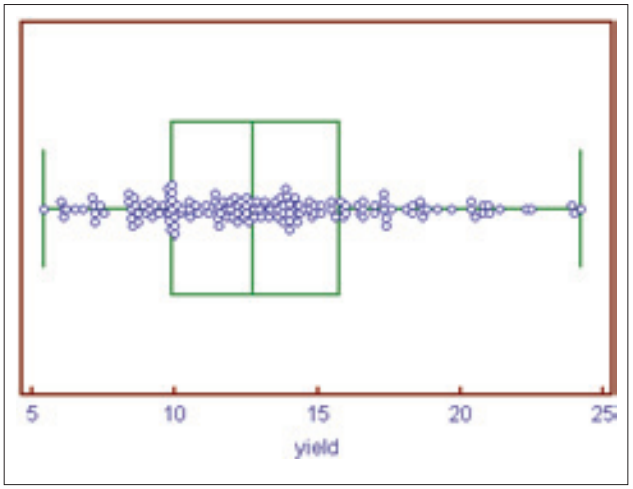

Fig. 3. Box and Whisker graph. Yield was equally distributed around a theoretical mid-point.

DISCUSSION

Granulocytapheresis donors at the Blood Centre Ostrava were healthy volunteers from a pool of apheresis donors; granulocytes were not collected from patients' relatives. The mobilization regimen thus used corticosteroids alone as national guidelines only allow the use of G-CSF mobilization in related donors. However, many European and US centres use this "off-label" administration in unrelated donors[2]. Methylprednisolone 40 mg in 0.9% sodium citrate 500 mL was well-accepted by donors, with no adverse events except for fatigue within 24 h after collection. Granulocytes were collected a maximum of twice a year. CMV status is not routinely investigated at this institution, because of its tendency to change. CMV-untested donors may be used to support CMV-negative patients if the medical benefits seem to outweigh the potential risks, in accordance with procedures at other blood centres worldwide (e.g., Department of Transfusion Medicine, Bethesda, MD, USA; University of Texas, MD Anderson Cancer Center, Houston, USA). High-molecular-weight HES was used to enhance the efficiency of granulocyte collection during the separation process in the current study. Analysis of the distribution of haematocrit per granulocyte TU showed that the collection process was stable, and the haematocrit had no effect on the granulocyte yield[3]. AB0 and Rh compatibility between donors and recipients was respected in this study. However, some blood centres do not respect AB0 Rh compatibility, though incompatible red cells are removed from the granulocyte component in these cases[4]. Granulocyte donors were not routinely screened for HLA antibodies in this study, and a different approach was used for routine HLA screening[5,6].

CONCLUSION

Granulocyte transfusions may reduce the mortality risk in patients with severe neutropenia, and thus provide valuable therapeutic support. Further randomized studies are needed to assess the global benefits of granulocyte transfusions, involving close collaboration between clinical departments and blood centres.

CONFLICT OF INTEREST STATEMENT

The authors state that there are no conflicts of interest regarding the publication of this article.

REFERENCES

1. Guide to the Preparation, Use and Quality Assurance of Blood Components. 16th Edition 2010. European Committee on Blood Transfusion
2. Leitner G, Panzer H, Reesink HW, Stiegler G, Fischer-Nielsen A, Dickmeiss E, Einsele H, Reinl P, Wiesneth M, Coluccia P, Axdorph Nygell U, Halter J, Sigle J, Gratwohl A, Buser AS, Ozturk G. Preparation of granulocyte concentrates by apheresis. Vox Sang 2010;88:567-75.
3. Bryant BJ, Yau YY, Byrne PJ, Stroncek DF, Leitman SF. Gravity sedimentation of granulocytapheresis concentrates with hydroxyethyl starch efficiently removes red blood cells and retains neutrophils. Transfusion 2010;50:1203-9.
4. Narvios AB, Reddy V, Lichtoger B. Method of removing incompatible red blood cells from granulocyte components. Transfus Apher Sci 2006;35:179-80.
5. Strauss RG, Klein HG, Price TH, Lichtiger B, Martinez F, Reesink HW, Panzer S. Preparation of granulocyte concentrates by apheresis: collection modalities in the USA. Vox Sang 2011;100:426-33.
6. Vrielink H, Koopman MMW. Preparation of granulocyte concentrates by apheresis: situation in the Netherlands. Vox Sang 2011;100:344-6.

14

Squamous cell carcinoma antigen as a marker of sinonasal inverted papilloma

Matoušek P, Zeleník K, Šafarčík K, Čábalová L, Komínek P

Originally published in European Archives of Oto-rhino-laryngology and Head & Neck, 2014, vol. 271, no. 3, p. 535-538

Consent to the publication of 19th March 2015

(licence no. 3592391004699)

Eur Arch Otorhinolaryngol (2014) 271:535–538
DOI 10.1007/s00405-013-2604-z

RHINOLOGY

Squamous cell carcinoma antigen as a marker of sinonasal inverted papilloma

Petr Matoušek · Karol Zeleník · Kristián Šafarčík · Lenka Čábalová · Pavel Komínek

Received: 12 April 2013 / Accepted: 12 June 2013 / Published online: 19 June 2013

Abstract This prospective study aimed to evaluate the usefulness of squamous cell carcinoma antigen (SCCA) as a clinical marker of sinonasal inverted papilloma (IP). The potential benefit of SCCA in the diagnosis of unilateral nasal pathology and as a marker of hidden recurrence was evaluated as well. Blood samples from patients with sinonasal IP were examined to determine serum SCCA levels before surgery, the day after surgery, and every 6 months during follow-up. Preoperative and postoperative levels of SCCA were compared. Twenty consecutive patients with histologically confirmed IP were included in the study, conducted between 2000 and 2011. The mean age of the patients was 54.2 years (range 35–72). The mean serum SCCA level before surgery was 3.885 μg/l (range 0.7–7.6). A decrease of the SCCA level to 0.885 μg/l (range 0.1–1.9) was observed on the 1 day after a radical surgical procedure. A statistically significant difference between the preoperative and postoperative levels was observed ($P < 0.001$). Elevated levels of SCCA during long-term follow-up were observed in three patients. All of them had a recurrence of IP. We conclude that the serum level of SCCA is a useful clinical marker of the presence of sinonasal IP. The level of SCC antigen was significantly lower in patients after IP was completely removed. According to our results, SCCA level also appears to be useful for long-term follow-up (hidden recurrence diagnosis).

Keywords Squamous cell carcinoma antigen · Sinonasal inverted papilloma · Clinical marker · Hidden recurrence · Surgery

P. Matoušek · K. Zeleník · L. Čábalová · P. Komínek (✉)
Department of Otorhinolaryngology, University Hospital Ostrava, 17. Listopadu Street 1790, 708 52 Ostrava-Poruba, Czech Republic
e-mail: pavel.kominek@fno.cz

P. Matoušek · K. Zeleník
Faculty of Medicine, University of Ostrava, Ostrava, Czech Republic

K. Šafarčík
Department of Nuclear Medicine, University Hospital Ostrava, Ostrava, Czech Republic

Introduction

Squamous cell carcinoma antigen (SCCA) is a protein with a strong homology to the family of protease inhibitors known as serpins. SCCAs are cytoplasmic proteins: they are found in normal squamous epithelia, and in elevated levels in the serum of patients with squamous cell carcinomas, especially in cases of uterine cervix carcinoma, lung carcinoma, and head and neck squamous cell carcinoma. SCCA is clinically useful, especially for the staging of uterine cervix carcinoma (risk of lymph node metastasis). It is also a useful marker for monitoring during follow-up and therapy, and increasing SCCA levels may predict carcinoma relapse [1]. Recent studies have shown a close relationship between SCCA and sinonasal inverted papilloma (IP) [2, 3].

IP is a relatively infrequent, benign sinonasal tumour. Careful long-term follow-up after radical surgery is necessary when treating IP, owing to its malignant potential and high recurrence rate [4, 5]. Distinguishing between inflammatory changes and recurrence of IP can sometimes be difficult. The purpose of this study was to determine the benefit of SCCA serum level evaluation in patients with IP.

Materials and methods

This prospective study was performed in accordance with the Declaration of Helsinki, the criteria of good clinical practice, and all applicable regulatory requirements. Written informed consent was obtained from all participants before the initiation of any procedure.

Patients with IP treated at the Department of Otolaryngology, Faculty of Medicine, University of Ostrava between 2000 and 2011 were included in the study. At least 3 years of follow-up after surgery was required for inclusion of a patient in the study.

Blood samples from enrolled patients were examined to determine serum SCCA levels before surgery, the day after surgery, and every 6 months during follow-up. Preoperative and postoperative SCCA levels were compared. The changes in SCCA levels during follow-up were evaluated.

Biochemical analysis

Serum SCCA levels were assayed using an immunofluorescence assay with monoclonal antibodies (B.R.A.H.M.S SCC KRYPTOR kit, Hennigsdorf, Germany). The normal serum level of SCC antigen is 0–1.5 μg/l.

Statistical analysis

Statistical analysis of the correlation between preoperative and postoperative serum SCCA levels was performed using Student's *t* test for paired data (SCCA levels before surgery and the day after surgery). Differences with $P < 0.05$ were considered statistically significant.

Results

Twenty consecutive patients with sinonasal IP treated at the Department of Otolaryngology, Faculty of Medicine, University of Ostrava between 2000 and 2011 were enrolled in the study. The mean age of patients was 54.2 years (range 35–72). Follow-up took place over 3–10 years.

The mean serum SCCA level was 3.885 μg/l (range 0.7–7.6) before surgery. A decrease in the SCCA level to 0.885 μg/l was observed after radical surgery (range 0.1–1.9). This difference was statistically significant ($P < 0.001$). Up to 18 patients out of 20 (90 %) had a normal level of SCCA after surgical treatment. Three out of 20 patients (15 %) presented with a normal level of SCCA before surgery (Table 1). The mean serum SCCA level in these three patients decreased after surgery (from 1.03 μg/l preoperatively to 0.27 μg/l postoperatively).

Table 1 Patients characteristics and squamous cell carcinoma antigen levels before and after surgery

	Number of patients	Mean	SD	Min.	Max.
Patient characteristics					
Age (years)	20	54.2	11.6	35	72
SCCA (μg/l)					
Before surgery	20	3.82	1.98	0.7	7.6
After surgery	20	0.82	0.51	0.1	1.9

SD standard deviation, *Min.* mimimum, *Max.* maximum

Elevated SCCA levels after surgery were observed in 3/20 (15 %) patients (decrease from 3.15 to 1.75) (Figs. 1, 2).

An incomplete removal (polypectomy) was performed in one case with a preoperative histopathological diagnosis of polyp. The SCCA level was high prior to surgery. After the non-radical surgery, only a slight decrease in the SCCA level was observed. After a subsequent histopathological examination indicated a diagnosis of inverted papilloma, a complete removal of IP was performed and the SCCA returned to normal levels.

We observed three cases of IP recurrence. In these cases, elevated SCCA levels were observed. In two cases, the recurrence was evident during endoscopy. In one patient with elevated SCCA levels, a computed tomography (CT) examination confirmed our suspicion of recurrence (Fig. 2).

No cases of malignant transformation were observed during the follow-up period.

Discussion

The use of tumour markers is not quite usual in otolaryngology, in comparison with other medical specialities.

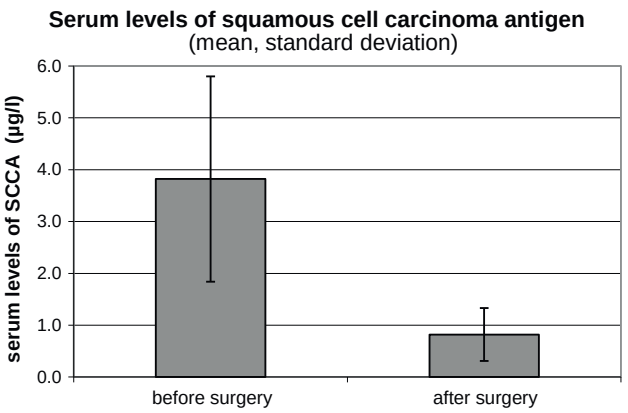

Fig. 1 Squamous cell carcinoma antigen levels before and after surgery

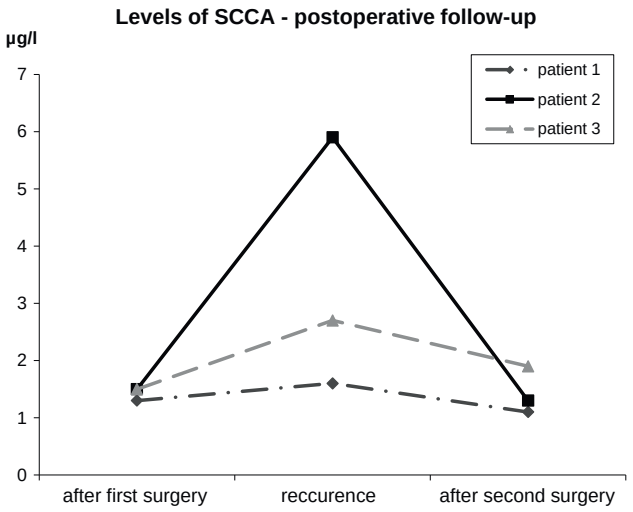

Fig. 2 Squamous cell carcinoma antigen in postoperative follow-up in patients with IP recurrence

However, recent studies have demonstrated the usefulness of SCCA in patients with carcinoma of the larynx, oesophagus, and oral cavity [1]. Most recent studies have also shown a close relationship between SCCA and sinonasal IP [2, 3].

SCCA is a tumour-associated antigen that was first isolated from squamous cell carcinoma of the uterine cervix. It is a subtraction of antigen TA 4, which was first described by Kato in 1977. Although this protein (serotonin protease inhibitor) is also expressed in normal squamous epithelium, its level is significantly elevated in cancer tissues, as well as in the serum of patients with squamous cell carcinoma. Therefore SCCA has been used as a tumour marker for squamous cell carcinoma of various organs, including the uterine cervix, skin, head and neck, oesophagus, lung, and bladder [1, 6]. Although the level of SCCA expression increases in the tissue and serum of patients with cancer, the biological function of SCCA in cancer cells remains undefined. Recent studies have indicated that SCCA may play a role as a mediator of apoptosis [6]. False positive elevations of SCCA have been observed in association with skin or saliva contamination, normal pregnancy, renal failure, and non-malignant skin diseases (e.g., eczema and pemphigus) [7].

Recent studies have revealed increased SCCA expression in cases of sinonasal IP. Yasumatsu observed that 89 % (25/28) of patients with IP had serum levels of SCCA exceeding the upper limit of normal; SCCA levels decreased in all cases after tumour removal, and he concluded that serum SCCA level is a reliable tumour marker in patients with IP [1, 3].

Sinonasal IP is a relatively uncommon benign tumour with specific behaviour: it has a high recurrence rate after surgical resection, risk of malignant transformation or possible association with malignancy, locally aggressive growth, and a tendency towards multicentricity [4, 5, 8]. Recurrent disease and metachronous carcinoma can develop several years after surgery. Because the disease can become extensive before it becomes symptomatic, careful postoperative follow-up is recommended [1, 9].

In general, complete surgical removal is recommended as a suitable treatment protocol for IP.

Tumour markers can be useful for detecting tumour development and recurrence. We focused on the clinical usefulness of SCCA and its role in sinonasal IP, mainly as a marker of hidden recurrence.

We evaluated serum SCCA levels in 20 patients with diagnosed sinonasal IP. The patients were examined before surgery, immediately after surgery, and every 6 months thereafter. A statistically significant decrease in the level of SCCA after radical surgery was observed. Moreover, an increase in SCCA levels was observed during postoperative follow-up in three patients. During the subsequent endoscopic examination, an obvious recurrence of IP was confirmed in two of these patients. In the third patient, recurrence was revealed by a CT scan. SCCA levels in these patients returned to normal after surgery.

In a separate case study, we observed only a slight decrease in SCCA levels after polypectomy (non-radical surgery). Once we performed radical surgery on this patient, the SCCA levels returned to normal. In yet another case, we suspected IP (based on endoscopy and CT), although a preoperative histological examination only revealed a polyp. A higher SCCA level was another factor that caused us to suspect the presence of IP in this patient. Our suspicions were confirmed by frozen section during surgery under general anaesthesia.

The majority of IP recurrences (approximately 90 %) occur within 5 years after surgery [10]. Thus, most surgeons follow patients during the first 5 years after surgery. The follow-up is performed by endoscopy. CT or magnetic resonance imaging (MRI) is usually performed in questionable cases.

There are two prominent issues to address with endoscopy during postoperative follow-up. The first issue is that we have limited access to the paranasal sinuses (i.e., anterior wall of maxillary sinus, floor of maxillary sinus, frontal sinus, and nasofrontal ductus). The second issue is our inability to distinguish between inflammation and IP recurrence. It is necessary to perform a CT or MRI in cases in which the primary site was in an area with limited visualisation. MRI is the most appropriate method [10].

Based on our experience, SCCA monitoring may be beneficial in distinguishing between inflammation and recurrence, as well as during the decision-making process when choosing between CT and MRI. Our findings and

findings in the relevant literature confirm the conclusion that monitoring SCCA levels in patients with IP may result in improved diagnostic procedures, treatment, and post-operative follow-up. Our study requires additional experimentation with comparison SCCA levels in IP patients with other diagnosis such as benign polyposis in chronic rhinosinusitis, squamous cell carcinoma, etc.

Conclusion

Serum SCCA level appears to be a useful clinical marker of sinonasal IP, and decreases significantly after radical surgery. Monitoring SCCA levels could be used for long-term follow-up (hidden recurrence) in patients after surgery. In addition, it can also be helpful in patients with unilateral nasal pathology; an elevated SCCA level is suspicious and may indicate a diagnosis of sinonasal IP. Our study requires additional experimentation.

Acknowledgments The authors gratefully acknowledge Hana Tomášková for performing the statistical analysis and Rob Marshall and Jiří Hynčica for their help with editing the English version of the article. This work was supported by the Institutional support of the Ministry of Health No 1 RVO-FNOs/2012.

Conflict of interest The authors declare that we have no conflict of interests.

References

1. Suminami Y, Nawata S, Kato H (1998) Biological role of SCC antigen. Tumor Biol 19:488–493
2. Yasumatsu R, Nakashima T, Kuratomi Y et al (2002) Serum squamous cell carcinoma antigen is a useful biologic marker in patients with inverted papillomas of the sinonasal tract. Cancer 1:152–158
3. Yasumatsu R, Nakashima T, Masuda M (2005) Clinical value of serum squamous cell carcinoma antigen in the management of sinonasal inverted papilloma. Head Neck 1:44–48
4. Fan GK, Imanaka M, Yang B et al (2006) Characteristic of nasal inverted papilloma and its malignant transformation: a study of cell proliferation and programmed cell death. Am J Rhinol 20: 360–363
5. Fang S, Yan JJ, Ohyama M (1998) Immunochemistry of p53 in sinonasal inverted papilloma and associated squamous cell carcinoma. Am J Rhinol 12:119–124
6. Suminami Y, Nagashima S, Vujanovic NL et al (2000) Inhibition of apoptosis in human tumour cells by tumour associated serpin. SCC antigen Br J Cancer 82:981–989
7. Kagohashi K, Hiroaki S, Kurishima K et al (2008) Squamous cell carcinoma antigen in lung cancer and nonmalignant respiratory diseases. Lung 186:323–326
8. Roh HJ, Procop GW, Batra PS et al (2004) Inflammation and the pathogenesis of inverted papilloma. Am J Rhinol 18:65–74
9. Lund V, Stammberger H, Nicolai P, Castelnuovo P et al (2010) European position paper on endoscopic management of tumours of the nose, paranasal sinuses and skull base. Rhinol Suppl 22:143
10. Petit P, Vivarrat-Perrin L, Champsaur P, Juhan V, Chagnaoud C et al (2000) Radiological follow-up of inverted papilloma. Eur Radiol 10:1184–1189

15

Lacrimal sac dacryolith (76 cases): a predictive factor for successful endonasal dacryocystorhinostomy?

Komínek P, Červenka S, Zeleník K, Pniak T, Tomášková H, Matoušek P

Originally published in European Archives of Oto-rhino-laryngology and Head & Neck, 2014, vol. 271, no. 6, p. 1595-1599

Consent to the publication of 19th March 2015

(licence no. 3592391281557)

Eur Arch Otorhinolaryngol (2014) 271:1595–1599
DOI 10.1007/s00405-013-2787-3

RHINOLOGY

Lacrimal sac dacryolith (76 cases): a predictive factor for successful endonasal dacryocystorhinostomy?

Pavel Komínek · Stanislav Červenka · Karol Zeleník · Tomáš Pniak · Hana Tomášková · Petr Matoušek

Received: 10 August 2013 / Accepted: 16 October 2013 / Published online: 26 October 2013

Abstract To evaluate whether the presence of dacryolith is a predictive factor for successful dacryocystorhinostomy. The success rate of endonasal dacryocystorhinostomy (EDCR) performed to relieve obstruction of the nasolacrimal duct was evaluated according to the presence of dacryolithiasis. The surgical results of patients with (group I) and without dacryoliths (group II) were analysed and compared 1-year post surgery. A total of 771 EDCRs performed from 1994 to 2010 were evaluated. Dacryolith was found in 76/771 procedures (9.9 %). Complete improvement was achieved significantly more frequently in group I (76/76; 100.0 %) than in group II (633/695; 91.1 %; $p < 0.001$). EDCRs were performed significantly more frequently in people aged 31–50-years, the average age of the group I was 41.1 years (range 18–72 years), of the group II 53.3 years (range 3 months–86 years; $p < 0.001$). There was no significant difference in the female-to-male ratio in the two groups. The presence of dacryoliths is a predictive factor for successful endonasal dacryocystorhinostomy.

P. Komínek (✉) · S. Červenka · K. Zeleník · T. Pniak · P. Matoušek
Department of Otorhinolaryngology, University Hospital Ostrava, Ostrava, Czech Republic
e-mail: pavel.kominek@fno.cz

S. Červenka
Department of Ophthalmology, Otrokovice, Czech Republic

K. Zeleník · P. Matoušek
Department of Surgical Studies, Faculty of Medicine, University of Ostrava, Ostrava, Czech Republic

H. Tomášková
Department of Epidemiology and Public Health, Faculty of Medicine, University of Ostrava, Ostrava, Czech Republic

Keywords Dacryolithiasis · Endonasal · Dacryocystorhinostomy · Predictive factor · Surgical results

Introduction

Finding a dacryolith is a relatively common "surprise" during dacryocystorhinostomy (DCR). While the incidence of dacryoliths in patients with DCR ranges from 6.0 to 16.0 %, the incidence of dacryoliths has not been evaluated in the general population [1–4]. Although the presence of a dacryolith may sometimes be expected due to patient symptoms or examination results, it is underdiagnosed and can only be confirmed surgically [2, 3, 5, 6]. The success rate in primary DCR is 70–99 % (7–12). Unfortunately, most studies of DCR and dacryoliths are small, and the role of dacryoliths in DCR outcome is not clear. In this study, we evaluated whether finding a dacryolith during endonasal dacryocystorhinostomy (EDCR) was a predictive factor for surgical outcome.

Materials and methods

Study design

A total of 908 primary EDCR procedures were performed at the Department of Otorhinolaryngology of the University Hospital Ostrava between 1995 and 2011. Patients with presaccal obstruction and with incomplete follow-up were excluded from the study. The study cohort thus included 771 patients with EDCRs performed for postsaccal stenosis/obstruction. The following data were obtained from patient records: age, gender, involved side, duration of epiphora,

etiology of the nasolacrimal duct (NLD) obstruction, and history of prior episodes of acute dacryocystitis. The surgical results were analysed statistically according to the presence of dacryolith, with patients categorized as group I patients (with dacryolith) or as group II patients (without dacryolith). Group I included 76 cases with dacryolith, and group II included 695 patients without dacryolith.

The goal of the papers was not to perform chemical and morphological analysis of dacryoliths.

EDCR procedure

EDCR was performed under general inhalation anaesthesia using a rigid fiberoptic endoscope. Our standard EDCR procedure was described in detail previously [8].

Follow-up clinical examination

Lacrimal system drainage was assessed 1-year after surgery using the fluorescein dye disappearance test (FDT), medical history, clinical examination (tear retention and conjunctival sac evaluation, medial canthus observation, and/or palpation), and endoscopic examination of the nasal cavity (Table 1). Syringing of the system was also performed in some cases, but the medical history and the FDT results were considered to be the major endpoints.

Complete therapeutic success was defined as FDT grade 0–1 plus complete resolution of previous symptoms. Partial success was defined as FDT 0–1 plus substantial improvement and some residual symptoms. Failure was defined as the absence of improvement or worsening of symptoms.

Statistical analysis

For statistical analysis, the binomial confidence intervals (CI) for the success rates were calculated as the 95 % CI.

Table 1 Fluorescein dye disappearance test (design)

Design
One drop of fluorescein is instilled into the lower fornix of each conjunctival sac. The infant must be watchful sitting on a parent's knee or being held on arms. After 5 min the thickness of the fluorescence of the tear meniscus is measured with the help of cobalt blue filter
Evaluation
0, no fluorescence in the conjunctival sac
1, thin fluorescing marginal tear strip persists
2, more fluorescein persist
3, wide, brighly fluorescing tear strip
FDT 0 and 1 are considered to be normal, i.e., drainage function is good
FDT 2 and 3 are considered to be abnormal, lacrimal drainage system is obstructed

The two-sample t test and χ^2 test were used to analyse differences in age, sex, and surgical success between groups I and II, with $p < 0.05$ considered statistically significant.

Results

The success rate for all EDCRs was 709/771 (92.0 %) 1-year after the surgery. The success rate was 76/76 (100.0 %) in group I patients and 633/695 (91.1 %) in group II patients (95 % CI 89–93.2 %). The distributions of the primary EDCR success rates in the groups were statistically significant $p < 0.001$.

The most common cause of NLD obstructions was primary acquired nasolacrimal duct obstruction (PANDO), and congenital nasolacrimal duct obstruction (CNLDO) (Table 2). In group I patients (with dacryoliths), PANDO was the cause of obstruction in 75/76 (98.7 %) cases and CNLDO was the cause in 1/76 (1.3 %).

In the group that included all EDCRs ($n = 771$), the average patient age was 52.1 years, ranging from 3 months to 86 years. The average age of the female patients was significantly different than that of the male patients, mean age 53.5 ± 18.8 versus 48.6 ± 22.0 years, respectively ($p = 0.0019$). In terms of gender distribution, there were significantly more women than men in the group that included all EDCRs: 547/771 (71 %; 95 % IC 67.6–74.1 %). The gender distribution was very similar in group I, in which 55/76 (72.4 %) patients were women, and in group II, in which 492/695 (70.8 %) of the patients were women. Thus, the female-to-male ratio was not significantly different in group I (2.6:1) versus group II (2.4:1) ($p = 0.774$).

The average age of group I patients (with dacryolith) was 41.1 years (range, 18–72 years) and that of group II patients (without dacryolith) was 53.3 years (range, 3 months–86 years). The difference in the average age in the two groups was statistically significant ($p < 0.001$). Most EDCRs were performed in patients aged 31–50 years in group I, whereas in group II, most EDCRs were performed in patients aged 51–70 years ($p < 0.001$) (Figs. 1, 2). If we compared groups under 50 years, the success rate in the group I (aged up to 50 years) was 62/62 (100 %) and in the group II (aged up to 50 years) was 228/247 (92.7 %, 95 %CI 89.4–96.0 %). If we compared both groups over 50 years, in the group I the success rate was 14/14 (100 %) and in the group II 404/448 (90.2 %, 95 % CI 87.4–92.9 %). In the group I the success rate was 100 % in the both age groups. In the group II the difference between the age groups (under 50 years and over 50 years) was not statistically significant ($p = 0.262$).

Of the preoperative symptoms and clinical findings, epiphora was the most common and was reported by all patients (100.0 %). Symptom duration ranged between

Table 2 Etiology of the nasolacrimal duct obstruction in the different groups

	PANDO	CNLDO	Trauma	Iatrogenic (sinonasal surgery)	Other
All EDCR (771)	670/771 (86.9 %)	49/771 (6.4 %)	21/771 (2.7 %)	20/771 (2.6 %)	11/771 (1.4 %)
Group I (76)	75/76 (98.7 %)	1/76 (1.3 %)	0/76	0/76	0/76
Group II (695)	595/695 (85.6 %)	48/695 (6.9 %)	21/695 (3.0 %)	20/695 (2.9 %)	11/695 (1.6 %)

PANDO primary acquired nasolacrimal duct obstruction, *CNLDO* congenital nasolacrimal duct obstruction, *EDCR* endonasal dacryocystorhinostomy

1 month and 20 years (mean 3.1 years) in group I and between 10 days and 62 years (mean 4.5 years) in group II. Acute dacryocystitis was observed in 30/76 cases (39.5 %) in group I and in 56/695 (8.1 %) in group II. Symptom duration and the presence of acute dacryocystitis were significantly different between the two groups ($p = 0.0142$ and $p < 0.001$, respectively).

In the group that included all EDCRs ($n = 771$), EDCR was performed only on the right side in 231 patients, only on the left side in 238 patients, and on both sides in 151 patients. Dacryolith 76/771 (9.9 %) EDCRs were observed unilaterally in 66 patients and bilaterally in five patients. In these 5 patients, dacryoliths were observed on both sides during EDCRs that were performed bilaterally in the same session in three patients, while in two patients the dacryoliths were found during EDCRs that were performed separately (i.e., in two sessions). The dacryoliths copied usually the shape of the lumen of the lacrimal sac, the size of the dacryoliths was mostly 5–8 mm, ranging from 4 to 14 mm (Fig. 3).

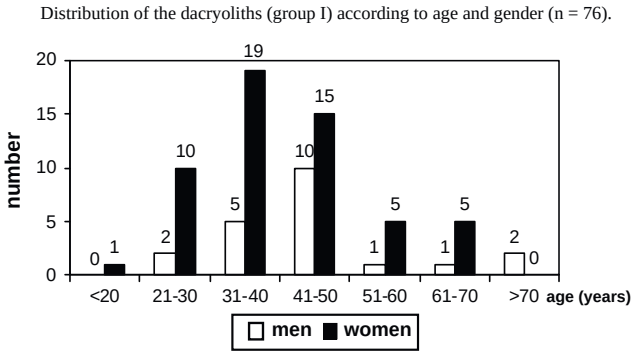

Fig. 1 Distribution of the dacryoliths (group I) according to age and gender ($n = 76$)

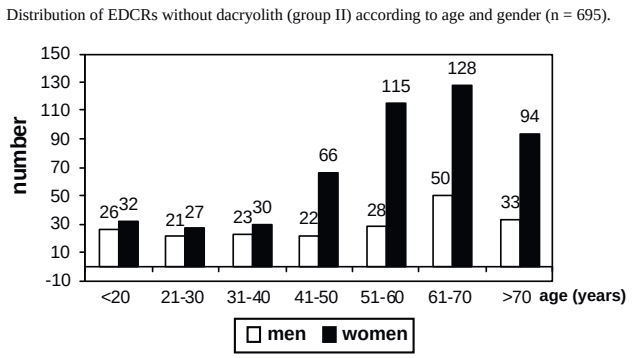

Fig. 2 Distribution of EDCRs without dacryolith (group II) according to age and gender ($n = 695$)

Discussion

The most common causes of DCR failure are obstructions at rhinostomy and canaliculi [1–3, 12, 13]. To improve the surgical success rate, silicone tubing is used to intubate the lacrimal system, mitomycin C is applied to the intranasal ostium, and septoplasty and partial middle concha resection are performed [8]. Although the success rate of primary DCR is 70–99 %, it is desirable to be able to predict the EDCR outcome as accurately as possible [7–12]. The question of whether the presence of dacryolith in the lacrimal sac during surgery is a predictive factor for successful EDCR has not been addressed by previous studies [5, 11]. Unfortunately, most of the published studies on DCR and dacryoliths are mainly small, with the largest studies including slightly over a hundred procedures at most. In these studies, the incidence of dacryolithiasis ranges between 6.0 and 16.0 % [1–4, 13, 14]. In our study of 771 EDCRs performed for postsaccal obstruction, which is the largest study to date, dacryolith was observed in 76 procedures (9.9 %). The exact frequency of dacryoliths in the general population would be difficult to evaluate [1].

The pathophysiology of dacryoliths remains unclear [1, 2, 6], although it seems that they are one of the causes of PANDO [2]. The present study confirmed earlier results and PANDO was found as a cause of dacryoliths in 75/76 (98.7 %), and only one patient with dacryolith had a history of CNLDO. Several predisposing factors in dacryoliths have been suggested, such as increased incidence in females, patient age less than 50 years, and increased frequency subsequent to previous occurrence of dacryocystitis [1, 2, 15]. Unfortunately, the results have not been consistent or clear and have sometimes even been contradictory, probably due to the lack of cases/small series.

Between 68 and 95 % of patients with dacryolithiasis are reported to be female [4, 14, 16, 17]. On the other hand, Yazici et al. [1] found male gender more likely to be

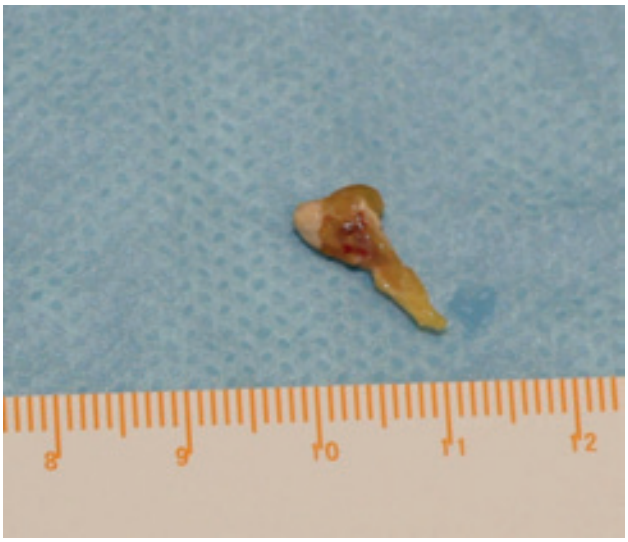

Fig. 3 The large dacryolith follows the shape of the lacrimal sac and duct

associated with dacryoliths. In their study of 163 DCRs, they found dacryolith in 12 patients and the female/male ratio was 1:2 [1]. In our study of 76 cases with dacryolith, we confirmed that there was a higher dacryolith frequency in women, with a female-to-male ratio of 3.6:1.

We also confirmed that dacryoliths are observed much more frequently in people under 50 years old. Moreover, patients with dacryolith were significantly younger than patients without dacryolith. There were only 14 patients with dacryolith who were over 50 years old in our study, and the procedure was performed most frequently on patients between 31 and 50 years old. Thus, the ratio of patients under 50 year old to patients over 50 years old was approximately 5–6:1 in group I.

The frequency of partial NLD obstruction with dacryoliths has been reported as high as 65–70 % [3, 4, 16]. In the Yazici et al. [1] study, the partial obstruction was noted in 6/12 (50 %) of the patient with dacryoliths compared with 23 % in patients without dacryoliths. With respect to preoperative symptoms and findings, we observed partial obstruction (stenosis) of the NLD in approximately 30–40 % of patients with dacryolithiasis. Nevertheless, we were not able to analyse this symptom statistically due to the lack of information in many patient's medical records. We confirmed a greater frequency of acute dacryocystitis with dacryoliths, as reported in earlier studies [1, 2, 18].

Dacryolithiasis has been noted as a contraindication to EDCR in some, but not all, studies [9, 12, 20]. According to the often-cited study by Mannor and Millman, the lacrimal sac size, as evaluated using dacryocystography, is an important factor for predicting the success of EDCR, and patients with large lacrimal sacs are recommended to undergo EDCR [19]. In the present study, dacryoliths were found only in large sacs; however, we use dacryocystography only very rarely before EDCR for cases that are not clear or that appear complicated. Neither CT nor MRI scans were performed before surgery in our study. Those examinations are performed only rarely in some patients after the facial trauma with lacrimal pathways obstruction at our clinic.

The main outcome of our study was that the surgical success rate in the group with dacryoliths (group I) was 100 % (76/76). This success rate was significantly higher than the success rate in the group without dacryoliths (group II), which has important clinical implications. We conclude that if dacryolith is found during EDCR, the surgeon can be very optimistic in terms of expecting a successful result. That is, finding a dacryolith is a predictive factor for successful EDCR, and a nearly 100 % succes rate can be expected for such EDCRs. The predictive risk factors for development of dacryoliths are age 30–50 years and female gender.

Conclusion

Dacryolithiasis was observed in nearly 10 % of the EDCRs that were performed to treat postsaccal obstruction. Dacryoliths were most often observed in patients aged 31–50 years, and the female-to-male ratio of patients with dacryoliths was 2.6:1 in the study presented here. Thus, age and gender were found to be predictive risk factors for the development of dacryoliths. EDCRs were successful 100 % of the time for patients with dacryolith in the lacrimal sac. Thus, failure of the surgeries can be considered exceptionally rare and a dacryolith finding is a very good predictive factor for successful EDCR.

Acknowledgments This work was supported by the Institutional support of the Ministry of Health No 2 RVO-FNOs/2013.

Conflict of interest The authors declare that we have no conflict of interests.

References

1. Yazici B, Hammad AM, Meyer DR (2001) Lacrimal sac dacryoliths predictive factors and clinical characteristics. Ophthalmology 108:1308–1312
2. Paulsen F (2007) Pathophysiological aspects of PANDO, dacryolithiasis, dry eye, and punctum plugs. In: Weber RK, Keerl R, Schaefer SD, Della Rocca RC (eds) Atlas of lacrimal surgery, Springer, Berlin pp 15–27
3. Rosen WJ, Rose GE (2000) Intranasal passage of dacryoliths. Br J Ophthalmol 84:799–804
4. Berlin AJ, Rath R, Rich L (1980) Lacrimal system dacryoliths. Ophthalmic Surg 11:435–436

5. Wilkins RB, Pressly JP (1980) Diagnosis and incidence of lacrimal calculi. Opthalmic Surg 11:787–789
6. Repp DJ, Burkat CN, Lucarelli MJ (2009) Lacrimal excretory system concretions: canalicular and lacrimal sac. Ophthalmology 116:2230–2235
7. Hammoudi DS, Tucker NA (2011) Factors associated with outcome of endonasal dacryocystorhinostomy. Ophthal Plast Reconstr Sug. 27:266–269
8. Komínek P, Červenka S, Pniak T, Zeleník K, Tomášková H, Matoušek P (2011) Revision endonasal dacryocystorhinostomies: analysis of 44 procedures. Rhinology 49:375–380
9. Sprekelsen MB, Barberán MT (1996) Endoscopic dacryocystorhinostomy: surgical technique and results. Laryngoscope 106(2):187–189
10. Choi JC, Moon YE, Kim MS, Oh JK, Kim HA, Choi MY, Shim WS (2009) The surgical outcome of endoscopic dacryocystorhinostomy according to the obstruction levels of lacrimal drainage system. Clin Exp Otorinolarnygol 2:141–144
11. Stupp T, Spaniol K, Prokosch V, Thanos S, Pavlidis M (2010) Einflussfaktoren auf den langfristigen erfolg von tränenwegoperationen und der prognostische wert der dakryozystografie. Klin Monbl Augenheilkd 227:43–46
12. Zenk J, Karathanis AD, Psychogios G, Franzke K, Koch M, Hornung J, Velegrakis GA, Iro H (2009) Long-term results of endonasal dacryocystorhinostomy. Eur Arch Otorhinolaryngol 266:1733–1738
13. Özer Ö, Eskiizmir G, Ünlü H, Isisag A, Aslan A (2011) Chronic inflammation: a poor prognostic factor for endosopic dacryocystorhinostomy. Eur Arch Otorhinolaryngol 269:839–845
14. Hawes MJ (1988) The dacryolithiasis syndrome. Ophthal Plast Reconstr Surg 1988(4):87–90
15. Herzig S, Hurwitz JJ (1979) Lacrimal sac calculi. Can J Opthatomol 14:17–20
16. Jones LT (1965) Tear-sac foreign bodies. Am J Ophthalmol 60:111–113
17. Berlin AJ, Rath R, Rich L (1980) Lacrimal system dacryoliths. Ophthalmic Surg 11:435–436
18. Baratz KH, Bartley GB, Campbell RJ, Garrity JA (1991) An eyelash nidus for dacryoliths of the lacrimal excretory and secretory systems. Am J Ophthalmol 111:624–627
19. Andreou P, Rose GR (2002) Clinical presentation of patients with dacryolithiasis. Ophthalmology 109:1573–1574
20. Mannor GE, Millman AL (1992) The prognostic value of preoperative dacryocystography in endoscopic intranasal dacryocystorhinostomy. Am J Ophthalmol 113:134–137

16

Inter-rater reliability of carotid atherosclerotic plaque quantification by 3-dimensional sonography

Bar M, Roubec M, Farana R, Ličev L, Tomášková H, Školoudík D

Originally published in Journal of Ultrasound in Medicine, 2014, vol. 33, no. 7, p. 1273-1278

Consent to the publication of July 2015

Inter-Rater Reliability of Carotid Atherosclerotic Plaque Quantification by 3-Dimensional Sonography

Michal Bar, MD, PhD, FESO, Martin Roubec, MD, PhD, Radim Farana, PhD, Lacezar Ličev, PhD, Hana Tomášková, MSc, PhD, David Školoudík, MD, PhD, FESO

Objectives—Embolization from atherosclerotic carotid plaques is the most common cause of ischemic stroke; therefore, identification of high-risk plaques by sonography is important. The aim of this study was to investigate the agreement between 2 investigators in the evaluation of sonographic parameters relating to plaque stability.

Methods—The following plaque parameters were assessed: echogenicity, homogeneity, surface, maximum content, and total volume. Serial 2-dimensional (2D) image sequences were obtained. Linear motion of the probe was automatically synchronized with the electrocardiogram. The edges of the plaque in each image were manually identified by the investigators. The total plaque volume was calculated after computer transformation of 2D images into a 3-dimensinoal (3D) format. Inter-rater reliability for echogenicity, homogeneity, and the surface was assessed by the weighted κ coefficient. Parametric values were tested by a paired *t* test.

Results—We enrolled 30 patients (22 male; mean age ± SD, 72 ± 13 years) in the study and evaluated 28 atherosclerotic plaques. Inter-rater agreement values were as follows: homogeneity, 96% ($\kappa = 0.84$; $P < .001$); surface, 90% ($\kappa = 0.77$; $P < .001$); and echogenicity, 86% ($\kappa = 0.60$; $P < .001$). The significance values for plaque content and volume measurement agreement were $P = .311$ and .312, respectively, and the correlation coefficient was 0.808.

Conclusions—In our study, the agreement between 2 examiners in the evaluation of 2D and 3D sonographic parameters related to plaque stability was good to excellent. The sonographic measurement of plaque volume growth was the most accurate parameter; therefore, 3D sonography may be used for risk assessment of plaques in the future.

Key Words—atherosclerotic plaque; inter-rater reliability; 3-dimensional sonography; vascular ultrasound; volume

Received September 6, 2013, from the Department of Neurology and Faculty of Medicine, Faculty Hospital of Ostrava, Ostrava University, Ostrava, Czech Republic (M.B., M.R., D.Š.); Faculty of Mechanical Engineering (R.F.) and Electrical Engineering and Computer Science (L.L.), Vysoká Škola Báňská–Technical University of Ostrava, Ostrava, Czech Republic; and Department of Epidemiology and Public Health, Faculty of Medicine, Ostrava University, Ostrava, Czech Republic (H.T.). Revision requested September 23, 2013. Revised manuscript accepted for publication November 4, 2013.

This work was presented in part at the European Stroke Conference; May 28–30, 2013; London, England; and was supported by the Grant Agency of Czech Republic (grant 101/06/0491).

Address correspondence to Michal Bar, MD, PhD, FESO, Department of Neurology, Faculty Hospital of Ostrava, 17 Listopadu 1790, 70852 Ostrava, Czech Republic.

E mail: michal.bar@fno.cz

Abbreviations

ECG, electrocardiogram; 3D, 3-dimensional; 2D, 2-dimensional

doi:10.7863/ultra.33.7.1273

Stroke is one of the leading causes of death and disability.[1] Thirty percent to 50% of stroke survivors do not regain functional independence, and 15% to 30% of all stroke survivors are permanently disabled. Twenty percent of patients require 3 months of poststroke institutional care.[2]

Embolization from atherosclerotic carotid plaques is the most common cause of ischemic stroke.[3] Several recent studies have also suggested that measurement of carotid plaques is also an important predictor of cardiac risk.[4,5] Measuring plaques improves therapy in cardiovascular prevention clinics.[6] Therefore, identification of high-risk plaques by sonography is important.

There are several ways of classifying the risk of carotid plaques using sonography. Conventional 2-dimensional (2D) sonography is an adequate and cost-effective method for evaluation of the composition (echogenicity and homogeneity) and surface features of plaques.[7–10] Three-dimensional (3D) sonography is used for total plaque volume measurement.[11] It has the potential to allow quantification of plaque volume changes, which can provide important information on a plaque's response to therapy.[12,13] The aim of this study was to investigate the agreement between 2 examiners in the evaluation of sonographic parameters relating to plaque stability.

Materials and Methods

Patients

We conducted a single-center prospective study with a predefined protocol. Thirty consecutive patients who had ischemic atherothrombotic strokes and who were examined in the Ultrasound Laboratory at the Faculty Hospital of Ostrava were enrolled in the study. The study was conducted in accordance with the Declaration of Helsinki of 1975 (as revised in 1983) and was approved by the local Ethics Committee of the Faculty Hospital of Ostrava. Informed consent was obtained from each patient. The following demographic and clinical data were evaluated and recorded: age, sex, and medical history, including diabetes mellitus, arterial hypertension, hyperlipidemia, and lipid-lowering drugs.

Image Acquisition

Serial 2D image sequences of the carotid bifurcation and proximal carotid internal artery were obtained with a Vivid 7 Pro ultrasound device (GE Vingmed Ultrasound AS, Horten, Norway) equipped with a linear 5–10-MHz probe. A plaque was defined as local intima thickening greater than 1.5 mm in thickness. The beginning and end of each plaque was identified by the investigators.

The probe was fixed on a linear motion system (Figure 1). The motion was automatically synchronized with the patient's electrocardiogram (ECG). Each image was obtained during heart diastole only. The positioning device was composed of components made by Haberkorn Ulmer (Opava, Czech Republic). The base was fixed to the patient's bed. The base could be moved manually with a longitudinal mechanism, which allowed the physician to set the position of the ultrasound probe according to the patient's position. The position of the probe relative to the patient's neck could be adjusted with a mechanism that moved the probe in the transverse direction. The ultrasound sensor was located on a shift platform, which was implemented by a Microcon (Prague, Czech Republic) stepper engine. The range of the probe movement was 2 to 3 cm. We used an SM2321-1400 motor as the stepper motor (static torque of 1.5 N-m, 200 steps per revolution) and a threaded rod with a 5-mm rise for a thread. These parameters showed that a shift of 0.025 mm was achieved during a single step of the stepper engine. In terms of positioning accuracy of the ultrasound probe, we achieved accuracy of 0.5 mm. The ECG signal was used for synchronization of the probe movement control. Figure 2 shows the ECG waveform with a gap in the middle. The space between the heartbeats was used for image capture. The experiments were performed on a multipurpose portable patient monitor (S5 compact anesthesia monitor; Datex-Ohmeda, Inc, Madison, WI), which was used to monitor the ECG, heart rate, temperature, and other parameters. The amplified output of the ECG signal (1 V/1 mV) was used to synchronize the movement of the ultrasound probe.[14]

Figure 1. Automatic linear positioning device with ECG synchronization of probe motion.

Figure 2. Electrocardiographic and sonographic synchronization.

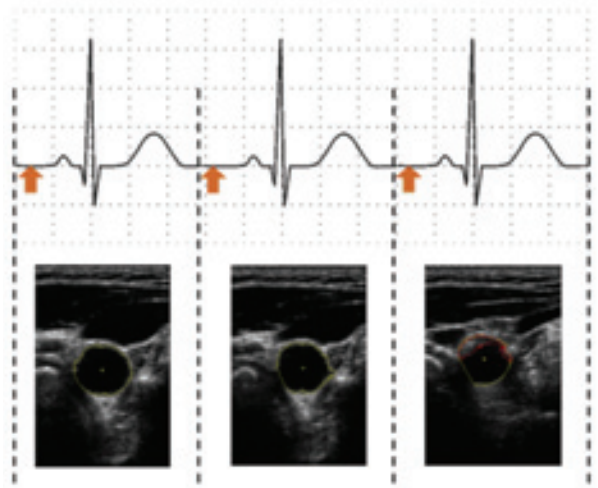

Three-Dimensional Reconstruction and Display

The 2D images were obtained with the Vivid 7 Pro ultrasound device. The borders of the plaque on each image slice were manually identified by the investigators (Figure 3). Plaque volume measurements were performed with the 3D quantification software FOTOM PC, which was developed by the Faculty of Electrical Engineering and Computer Science at the Technical University of Ostrava (Figure 4).[14]

Plaque Evaluation

The following plaque parameters were assessed: echogenicity, homogeneity, surface, maximum content, and total volume. We used a plaque definition according to the Mannheim carotid-intima thickness and plaque consensus.[15] The scale for echogenicity was as follows: (1) anechoic, (2) echogenic, and (3) hyperechoic; the scale for homogeneity was as follows: (1) heterogeneous and (2) homogeneous; and the scale for surface was as follows: (1) smooth, (2) irregular (defect <2 mm), and (3) ulcerated (defect >2 mm).[7,15,16] Individual sonograms of carotid plaques in patients after ischemic stroke were evaluated independently by 2 experienced examiners.

Figure 3. Outline of a plaque boundary.

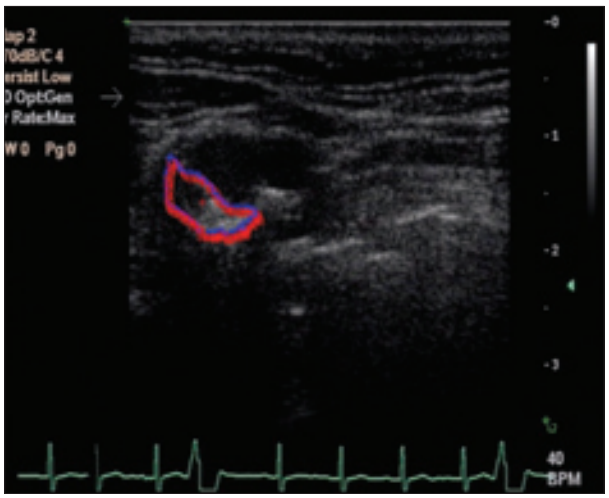

Figure 4. Three-dimensional model of a plaque (FOTOM PC).[11]

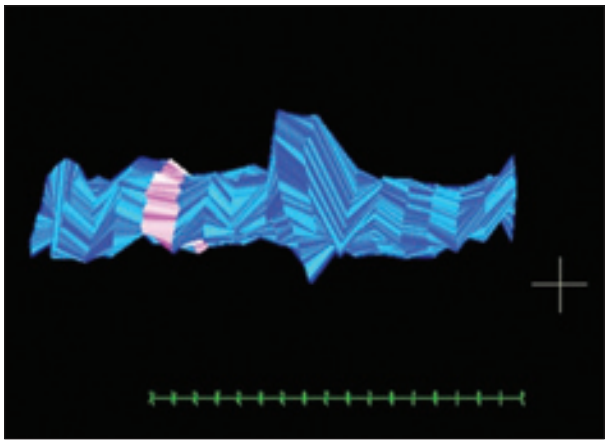

Data and Statistical Analyses

Inter-rater reliability for categorical variables (echogenicity, homogeneity, and surface) was assessed by the weighted κ coefficient. The agreement was considered poor when the κ was less than 0.4, good when the κ was 0.41 to 0.75, and excellent when the κ was greater than 0.75. Parametric values (content and volume) were tested by a paired *t* test. The strength and direction of the linear relationship between 2 parametric variables (content and volume) were measured by the Pearson correlation coefficient (0 means no correlation; 1 means absolute agreement). Statistical tests were evaluated at the significance level of $P < .05$. Data analysis was performed with Stata version 10 statistical software (StataCorp, College Station, TX).

Results

Thirty consecutive patients who had ischemic strokes were enrolled in the study (22 male; mean age ± SD, 72 ± 13 years). Demographic data are shown in Table 1. Four patients were excluded from the measurements due to poor image quality. In 2 cases, 2 different plaques were measured; thus, 28 plaques were evaluated overall.

Inter-rater agreement values for composition features were as follows: homogeneity, 96% ($\kappa = 0.84$; $P < .001$); surface, 90% ($\kappa = 0.77$; $P < .001$); and echogenicity, 86% ($\kappa = 0.60$; $P < .001$; Tables 2–4). The significance values for plaque content and volume measurement agreement were $P = .311$ and .312, respectively, and the correlation coefficient was 0.808 (Figure 5 and Tables 5 and 6).

Table 1. Patient Characteristics

Characteristic	Value
Patients enrolled, n	30
Mean age ± SD, y	72 ± 13
Male, n (%)	22 (73)
Hypertension, %	61
Hyperlipidemia, %	38
Diabetes mellitus, %	24
Lipid-lowering drugs, %	42

Discussion

Because of their superficial location, the extracranial carotid arteries are ideal for color and duplex Doppler sonography.[16] The features of at-risk carotid plaques have been evaluated in previous studies.[16–19]

Traditional 2D sonography is an adequate and cost-effective method for screening patients with carotid atherosclerosis. Two-dimensional imaging can also be used for evaluation of carotid plaque morphologic characteristics or composition; however, the clinical importance of this evaluation remains uncertain.[7,20] Intima-media thickness is associated with risk factors for stroke, whereas plaques are more directly associated with prevalent ischemic heart disease.[5,21]

Hartmann et al[22] reported low inter-rater agreement regarding visual assessment of static B-mode images in assessing plaque composition. Nevertheless, 2D imaging has one crucial disadvantage: once the 2D slices have been captured, images of other planes can no longer be extracted.[23] This step may affect the accuracy of plaque characterization because the information is only sampled from one section of the plaque. Three-dimensional sonography also allows assessment of the carotid bulb in all planes, whereas 2D imaging allows assessment of only one section, and sometimes we can miss the plaque.[4]

In the first phase of our study, we developed a unique device used to move the probe, which was synchronized with the heart. Using this device, we avoided emergent motion artifacts due to carotid pulsation. In the second phase of our study, we tested inter-rater reliability of plaque characteristics. Strong correlations were observed for each parameter.

In addition to the 2D examination, we also measured total plaque volume using 3D sonography. Images were obtained by the examiner by slicing the plaque, moving from one edge to the other and outlining the boundary of each slice by using a mouse cursor. The images were then reconstructed with the FOTOM PC program.[14] We consider plaque volume measurement to be the best method and most accurate for plaque progression (regression) evaluation. Total plaque volume measurement also requires a small number of patients to prove progression of the plaque; therefore, it is also an appropriate method for testing the efficacy of drugs.[13]

Total plaque volume measurement is also superior to intima-media thickness for assessing new antiatherosclerotic therapies. Studies based on intima-media thickness require hundreds of patients per group, and the patients have to

Table 2. Inter-Rater Reliability for Plaque Homogeneity

	Measurement A		
Measurement B	Homogeneous	Heterogeneous	Total, n (%)
Homogeneous	3	1	4 (14)
Heterogeneous	0	24	24 (86)
Total, n (%)	3 (11)	25 (89)	28 (100)

Agreement: 96% ($\kappa = 0.837$; $P < .001$).

Table 3. Inter-Rater Reliability for Plaque Surface

	Measurement A			
Measurement B	Smooth	Irregular (Defect <2 mm)	Ulcerated (Defect >3 mm)	Total, n (%)
Smooth	3	0	0	3 (11)
Irregular (defect <2 mm)	3	18	0	21 (75)
Ulcerated (defect >3 mm)	0	0	4	4 (14)
Total, n (%)	6 (21)	18 (64)	4 (14)	28 (100)

Agreement: 90% ($\kappa = 0.774$; $P < .001$).

Table 4. Inter-Rater Reliability for Plaque Echogenicity

	Measurement A			
Measurement B	Anechoic	Echogenic	Hyperechoic	Total, n (%)
Anechoic	3	1	0	4 (14)
Echogenic	1	20	1	22 (79)
Hyperechoic	0	1	1	2 (7)
Total, n (%)	4 (14)	22 (79)	2 (7)	28 (100)

Agreement: 86% ($\kappa = 0.600$; $P < .001$).

be followed for 2 years. The 3D plaque volume method allows measurement of substantial regression in 3 months with 20 patients per study.[24]

The 3D variability of total plaque volume was tested in 11 previous studies. In these studies, the sample volumes ranged from 10 to 105 carotid plaques. All studies confirmed good inter-rater variability and reproducibility of 3D sonography in carotid plaque volume measurement.[11,25] However, ECG synchronization with a probe motion system was only used in 1 of these studies.[11] The superiority of 3D evaluation of plaque morphologic characteristic over 2D sonography has not yet been demonstrated.[26]

This study had some limitations. The 3D sonograms were acquired with a mechanical scanning system developed in our laboratory. This step eliminated examiner variability in individual positioning of the transducer; however, the examination was strictly linked to our laboratory only.

Figure 5. Correlation and linear regression for plaque volume.

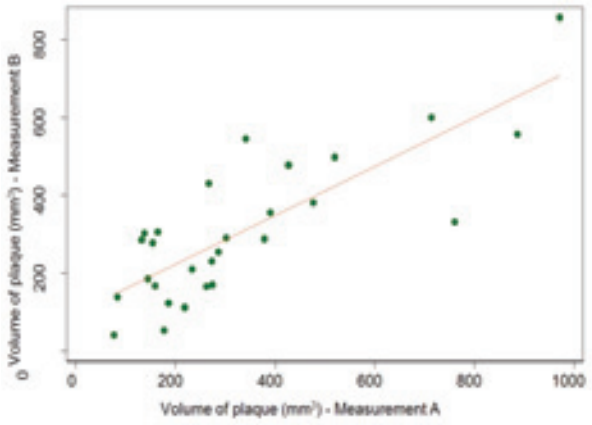

Table 5. Maximum Plaque Content

Maximum Plaque Content, mm	Measurement (n = 28)		Difference
	A	B	
Mean	30.52	28.05	2.4
SD	16.70	12.99	2.3

Paired *t* test ($t = 1.031$; $P = .311$).

Table 6. Plaque Volume

Plaque Volume, mm^3	Measurement (n = 28)		Difference
	A	B	
Mean	333.5	308.1	27.4
SD	238.3	185.2	140.5

Paired *t* test ($t = 1.036$; $P = .312$).

The number of evaluated plaques was relatively small, but it was sufficient for statistical analysis. Fixation of the probe on the linear motion system and manual outlining of multiple slices were time-consuming and took approximately 30 minutes longer per measurement than conventional 2D sonography.

In conclusion, embolization from atherosclerotic carotid plaques is the most common cause of ischemic stroke; therefore, identification of high-risk plaques by sonography is important because it can then lead to targeted aggressive medical or invasive treatment in patients at increased risk. We have demonstrated a 3D technique that allows evaluation and quantification of carotid plaque volume. In our study, the inter-rater reliability of 2D and 3D sonographic evaluations of atherosclerotic plaque parameters was good to excellent. Two-dimensional sonography is a simple, quick, and cost-effective screening method, and 3D measurement of total plaque volume is an accurate method; therefore, 3D sonography may be used for risk assessment of plaques in the future.

References

1. Kochanek KD, Xu JQ, Murphy SL, Miniño AM, Kung HC. Deaths: final data for 2009. *Natl Vital Stat Rep* 2011; 60:1–117.
2. Novakovic R, Toth G, Purdy PD. Review of current and emerging therapies in acute ischemic stroke. *J Neurointerv Surg* 2009; 1:13–26.
3. Barnett HJ, Gunton RW, Eliasziw M, et al. Severity of ischemic stroke in patients with internal carotid artery stenosis. *JAMA* 2000; 283:1429–1436.
4. Johri AM, Chitty DW, Matangi M, et al. Can carotid bulb plaque assessment rule out significant coronary artery disease? A comparison of plaque quantification by two- and three-dimensional ultrasound. *J Am Soc Echocardiogr* 2013; 26:86–95.
5. Nambi V, Chambless L, Folsom AR, et al. Carotid intima-media thickness and presence or absence of plaque improves prediction of coronary heart disease risk: the ARIC (Atherosclerosis Risk in Communities) study. *J Am Coll Cardiol* 2010; 55:1600–1607.
6. Spence JD, Hackam DG. Treating arteries instead of risk factors: a paradigm change in management of atherosclerosis. *Stroke* 2010; 41:1193–1199.
7. Devuyst G, Piechowski-Jóźwiak B, Bogousslavsky J. Arterial wall imaging. *Front Neurol Neurosci* 2006; 21:19–26.
8. Školoudík D, Bar M, Vaclavík D, et al. Risk of vascular events during treatment with fluvastatin and fenofibrate E. *Cesk Slov Neurol N* 2007; 70/103:163–167.
9. Widder B, Paulat K, Hackspacher J, et al. Morphological characterization of carotid artery stenoses by ultrasound duplex scanning. *Ultrasound Med Biol*. 1990; 16:349–354.
10. Hennerici MG. The unstable plaque. *Cerebrovasc Dis* 2004; 17(suppl 3):17–22.

11. Makris GC, Lavida A, Griffin M, Geroulakos G, Nicolaides AN. Three-dimensional ultrasound imaging for the evaluation of carotid atherosclerosis. *Atherosclerosis* 2011; 219:377–383.
12. Landry A, Spence JD, Fenster A. Measurement of carotid plaque volume by 3-dimensional ultrasound. *Stroke* 2004; 35:864–869.
13. Ainsworth CD, Blake CC, Tamayo A, Beletsky V, Fenster A, Spence JD. 3D ultrasound measurement of change in carotid plaque volume: a tool for rapid evaluation of new therapies. *Stroke* 2005; 36:1904–1909.
14. Farana R, Ličev L, Bar M, et al. Equipment for 3-D picturing and measurement of atherosclerotic plaque. *Acta Mech Slov* 2010; 14:88–93.
15. Touboul PJ, Hennerici MG, Meairs S, et al. Mannheim carotid intima-media thickness and plaque consensus (2004-2006-2011): an update on behalf of the advisory board of the 3rd, 4th and 5th watching the risk symposia, at the 13th, 15th and 20th European Stroke Conferences, Mannheim, Germany, 2004, Brussels, Belgium, 2006, and Hamburg, Germany, 2011. *Cerebrovasc Dis* 2012; 34:290–296.
16. European Carotid Plaque Study Group. Carotid artery plaque composition: relationship to clinical presentation and ultrasound B-mode imaging. *Eur J Vasc Endovasc Surg* 2011; 42(suppl 1):S32–S38.
17. Grønholdt ML, Nordestgaard BG, Wiebe BM, Wilhjelm JE, Sillesen H. Echo-lucency of computerized ultrasound images of carotid atherosclerotic plaques are associated with increased levels of triglyceride-rich lipoproteins as well as increased plaque lipid content. *Circulation* 1998; 97:34–40.
18. Gaitini D, Soudack M. Diagnosing carotid stenosis by Doppler sonography: state of the art. *J Ultrasound Med* 2005; 24:1127–1136.
19. Tegos TJ, Kalomiris KJ, Sabetai MM, Kalodiki E, Nicolaides AN. Significance of sonographic tissue and surface characteristics of carotid plaques. *AJNR Am J Neuroradiol* 2001; 22:1605–1612.
20. Joakimsen O, Bønaa KH, Stensland-Bugge E. Reproducibility of ultrasound assessment of carotid plaque occurrence, thickness, and morphology: the Tromsø Study. *Stroke* 1997; 28:2201–2207.
21. Ebrahim S, Papacosta O, Whincup P, et al. Carotid plaque, intima media thickness, cardiovascular risk factors, and prevalent cardiovascular disease in men and women: the British Regional Heart Study. *Stroke* 1999; 30:841–850.
22. Hartmann A, Mohr JP, Thompson JL, Ramos O, Mast H. Interrater reliability of plaque morphology classification in patients with severe carotid artery stenosis. *Acta Neurol Scand* 1999; 99:61–64.
23. Ainsworth CD, Spence JD, Landry AM, et al. 3-D ultrasound carotid plaque volume: a tool for quickly measuring effects of treatment on atherosclerosis. *Stroke* 2005; 36:1904–1909.
24. Spence JD. Carotid plaque measurement is superior to IMT. Invited editorial comment on: carotid plaque, compared with carotid intima-media thickness, more accurately predicts coronary artery disease events: a meta-analysis—Yoichi Inaba, MD, Jennifer A. Chen MD, Steven R. Bergmann MD, PhD. *Atherosclerosis* 2012; 220:34–35.
25. Fenster A, Blake C, Gyacskov I, Landry A, Spence JD. 3D ultrasound analysis of carotid plaque volume and surface morphology. *Ultrasonics* 2006; 44(suppl 1):e153–e157.
26. Denzel C, Balzer K, Merhof D, Lang W. 3D cross sectional view to investigate the morphology of internal carotid artery plaques: is 3D ultrasound superior to 2D ultrasound? *Ultraschall Med* 2009; 30:291–296.

J Ultrasound Med 2014; 33:1273–1278

17

Tissue ischemia microdialysis assessments following severe traumatic haemorrhagic shock: lactate/pyruvate ratio as a new resuscitation end point?

Burša F, Pleva L, Máca J, Sklienka P, Ševčík P

Originally published in BMC Anesthesiology, 2014, vol. 14, no. Article ID 118, p. 1-8

Consent to the publication of 24th March 2015

Burša et al. BMC Anesthesiology 2014, 14:118
http://www.biomedcentral.com/1471-2253/14/118

BMC Anesthesiology

RESEARCH ARTICLE Open Access

Tissue ischemia microdialysis assessments following severe traumatic haemorrhagic shock: lactate/pyruvate ratio as a new resuscitation end point?

Filip Burša[1*], Leopold Pleva[2], Jan Máca[1], Peter Sklienka[1] and Pavel Ševčík[1]

Abstract

Background: Intensive care of severe trauma patients focuses on the treatment of haemorrhagic shock. Tissues should be perfused sufficiently with blood and with sufficient oxygen content to ensure adequate tissue oxygen delivery. Tissue metabolism can be monitored by microdialysis, and the lactate/pyruvate ratio (LPR) may be used as a tissue ischemia marker. The aim of this study was to determine the adequate cardiac output and haemoglobin levels that avoid tissue ischemia.

Methods: Adult patients with serious traumatic haemorrhagic shock were enrolled in this prospective observational study. The primary observed parameters included haemoglobin, cardiac output, central venous saturation, arterial lactate and the tissue lactate/pyruvate ratio.

Results: Forty-eight patients were analysed. The average age of the patients was 39.8 ± 16.7, and the average ISS was 43.4 ± 12.2. Hb < 70 g/l was associated with pathologic arterial lactate, $ScvO_2$ and LPR. Tissue ischemia (i.e., LPR over 25) developed when CI ≤ 3.2 l/min/m^2 and Hb between 70 and 90 g/l were observed. Severe tissue ischemia events were recorded when the Hb dropped below 70 g/l and CI was 3.2-4.8 l/min/m^2. CI ≥ 4.8 l/min/m^2 was not found to be connected with tissue ischemia, even when Hb ≤ 70 g/l.

Conclusion: LPR could be a useful marker to manage traumatic haemorrhagic shock therapies. In initial traumatic haemorrhagic shock treatments, it may be better to maintain CI ≥ 3.2 l/min/m^2 and Hb ≥ 70 g/l to avoid tissue ischemia. LPR could also be a useful transfusion trigger when it may demonstrate ischemia onset due to low local DO_2 and early reveal low/no tissue perfusion.

Keywords: Microdialysis, Shock, Lactate, Pyruvate, Haemoglobin, Cardiac output, Transfusion, Trauma

Background

Trauma is a serious cause of morbidity and mortality. In adults up to 40 years of age, polytrauma is the most frequent cause of death [1]. The overall mortality rate in severely injured patients is approximately 30% [1], and following haemorrhagic shock, a loss of more than 40% intravascular volume can result in irreversible shock and death if it is not treated effectively [2].

Intensive care focuses on haemorrhagic shock and trauma-induced coagulopathy treatments during initial care. Shock is primarily a microcirculatory disorder, in which the oxygen supplied to tissues does not meet their metabolic demand, causing tissue ischemia. Manifest and occult shock is the result of decreased oxygen delivery due to low cardiac output and/or low oxygen content to tissues. Tissue ischemia may then develop, potentially causing multi-organ failure [3]. The physiological response to traumatic distress is intended to ensure oxygen delivery to vital organs, such as the brain and heart, by the centralisation of circulation and hyperdynamic circulation (i.e., high cardiac output). Distressed tissues with inadequate

* Correspondence: bursaf@seznam.cz
[1]Department of anesthesiology and intensive care medicine, University Hospital Ostrava, Faculty of Medicine Universitas Ostrava, 17. listopadu 1790, Ostrava-Poruba, Czech Republic
Full list of author information is available at the end of the article

oxygen and substrate delivery react by switching their metabolism to the anaerobic pathway; lactate production in tissue is also proportional to the amount of energy produced [4,5]. To avoid tissue ischemia and microcirculatory dysfunction, shock treatments must be effective, quick and as aggressive as possible to provide sufficient oxygen to distressed tissues. The global oxygen delivery (DO_2) is determined by the haemoglobin concentration (Hb) and its saturation (SaO_2), the amount of dissolved oxygen in the plasma and the cardiac output (CO); this can be defined by $DO_2 = COx(HbxSaO_2x1.34 + PaO_2x0.003)$. Tissues should be perfused with sufficient blood and oxygen content to ensure adequate tissue oxygen delivery; however, tissue requirements could differ from the global DO_2 value. Monitoring tissue conditions could provide information about shock resolutions more quickly and precisely than global parameters, which include arterial lactate, $ScvO_2$, Hb and CO levels. Tissue ischemia is poorly assessed by commonly used perfusion markers, and more detailed monitoring could be beneficial.

Haemostatic resuscitation, which is the primary treatment for haemorrhagic shock, attempts to restore and sustain tissue perfusion using an appropriate amount of fluid, transfusion and vasopressor administration; it also emphasises effective clotting and not impairing bleeding by increasing inadequate arterial pressure [6,7]. Resuscitation guidelines have been developing particularly in the field of transfusions and fluids. Metabolic monitoring could be beneficial for the evaluation of resuscitation efficiency. New markers of ischemia could also help in decision-making processes.

Tissue ischemia is one of the primary causes of multiorgan dysfunction due to shock, which increases mortality [3]. Tissue conditions are not usually observed by traditional monitoring techniques, which typically only observe global parameters. Monitoring of tissue metabolisms could provide more precise assessments for shock management. Tissue metabolisms could be monitored by microdialysis. The lactate/pyruvate ratio (LPR) is a tissue ischemia marker [8], and LPR ≥ 25 indicates the onset of anaerobic metabolism [9]. The observed population consisted of severe blunt trauma patients, between 18 and 60 years of age with ISS > 25 and a blood loss estimated over 1 litre, who were admitted to the Emergency Department (ED). Measured parameters were of LPR, haemoglobin, cardiac output, arterial lactate and $ScvO_2$. The aims of this study were to determine the adequate cardiac output and amount of haemoglobin required to prevent tissue ischemia; the study aims to define the association between the lactate/pyruvate ratio (LPR) on the haemoglobin (Hb) and the cardiac output (CO) or cardiac index (CI). The authors also compare LPR with arterial lactate and $ScvO_2$. Adequate Hb and CI levels to avoid tissue ischemia were determined as outcomes.

Methods

Severe blunt trauma patients with ISS > 25 between 18 and 60 years of age were enrolled in this prospective observational study between 2010 and 2013. Minimum required amount of 40 patients were enrolled due to preliminary power analysis. All participants presented with serious traumatic haemorrhagic shock with an estimated blood loss exceeding 1 l and hypotension (MAP ≤ 60 mm Hg). They were admitted to the Ostrava University Hospital Level 1 Trauma Centre Emergency Department as an inclusion criterion. Exclusion criteria included paediatric patients, penetrating trauma, non-serious haemorrhagia (blood loss up to 1 litre), ISS ≤ 25, no hypotension (MAP > 60 mm Hg), different ICU (non study) admission, dead in ED and dead within 6 hours from admission to ED; undergoing surgery was not an exclusion criterion. Monitoring was initiated as soon as possible and no later than 6 hours from admission. Study patients underwent prehospital care, ensuring treatment and transport. Diagnostic and therapeutic interventions were followed at the trauma centre according to the best clinical practises.

The observed parameters included haemoglobin concentration (Hb, haemoglobin g/l), central venous saturation ($ScvO_2$, %), arterial lactate (L, mmol/l), cardiac output as cardiac index (CI, cardiac index, l/min/m^2), and tissue lactate and pyruvate levels, which are displayed as the lactate/pyruvate ratio (LPR). The authors also recorded age, ISS, gender, weight, height, pre-hospital care time, and care time in the ED, theatre (if surgery was performed), and ICU. Haemoglobin, central venous saturation and arterial lactate were measured immediately after ED admission using a biochemical analyser (Roche Cobas b221 OMNI S) at 8-hour intervals but also at least three times for two hours following the administration of blood products. Cardiac output (CO) analysis was performed with a haemodynamic monitor (LiDCO Rapid), which analysed pulse characteristics in the arteria radialis beat-to-beat. Hourly CO averages were also recorded. Tissue monitoring was performed by extracellular fluid collected by a microdialysis probe inserted into certain tissues. Extracellular fluid samples were analysed in a biochemical bedside analyser. Tissue monitoring was performed using a CMA 60 microdialysis probe (CMA Microdialysis AB, Stockholm, Sweden), which was placed into each patient's deltoid muscle. The authors used CMA Perfusion Fluid T1 dialysis solution (i.e., a lactate-free Ringer solution), and perfusion was accomplished with a CMA 106 pump at a constant flow of 0.3 μL/min. Subsequent analyses were performed with a CMA Iscus Flex analyser (CMA Microdialysis AB) using a set of reagents for the analysis of the lactate, pyruvate, glycerol and glucose levels (CMA Reagent Set A). These tissue values were analysed at 1-hour intervals. The data analysed included only those from the first 24 hours after trauma because shock is always eliminated after this

period. All Hb, CI, $ScvO_2$ and L levels were assigned to the corresponding LPR for the same moment in time for all patients. Then, data from all patients were divided into groups, which were created according to Hb and CI values: Hb ≤ 70 g/l; Hb 70-90 g/l; Hb ≥ 90 g/l and CI ≤ 3.2 l/min/m^2 (i.e., "low"); CI 3.2-4.8 l/min/m^2 (i.e., "normal"); and CI ≥ 4.8 l/min/m^2 (i.e., "supranormal"). The measured variables (i.e., LPR, $ScvO_2$ and arterial lactate) were also assigned to the created groups.

The study was performed in a single centre at the University Hospital in Ostrava. The Ethics Committee of the University Hospital Ostrava in the Czech Republic approved the study, which conformed to the tenets of the Declaration of Helsinki. Each of the awake and conscious study subjects signed the Informed Consent Form approved by the Ethics Committee of the University Hospital Ostrava. The Ethics committee waived the need to sign the Informed Consent in unconscious study subjects, who were unable to sign it.

The authors used R software (version 2.15.2) to perform the statistical analyses in this study. Missing values were extrapolated using a linear approximation with respect to measurement's date and time. The resulting p-values were adjusted for multiple comparisons using the Kruskall-Wallis test. Figure 1.

Results

The authors observed an association between LPR on haemoglobin, cardiac output, $ScvO_2$ and arterial lactate levels in the 48 patients. The authors analysed 967 records of LPR and the appropriate markers. The median time of pre-hospital care was 58 minutes; in the ED, patients spent 90 minutes, and the median time in theatre was 140 minutes. The average and median ages were 39.8 ± 16.7 and 36 years, respectively; the average and median ISS were 43.4 ± 12.2 and 43; and the average Hb was 97.70 ± 18.67 g/l Tables 1, 2 and Figure 2.

Monitored values during the first 24 hours after trauma are displayed in Table 2 and Figure 2. The median L, $ScvO_2$ and LPR values and their association with Hb groups are also shown. Hb < 70 g/l was associated with pathologic arterial lactate, $ScvO_2$ and LPR values. Pathologic arterial lactate in all Hb groups in the first 24 hours after trauma was observed, but higher Hb was associated with lower L. When Hb 70-90 g/l and Hb ≥ 90 g/l, $ScvO_2$ and LPR was found to be normal Table 3 and Figure 3.

According to the concurrent values of Hb and CI, values of LPR are shown in Table 3 and Figure 3. Tissue ischemia developed when a low CI and haemoglobin between 70 and 90 g/l were observed. Severe tissue ischemia was registered when haemoglobin levels dropped below 70 g/l with a normal CI; CI above 4.8 l/min/m^2 was not associated with tissue ischemia, even at haemoglobin values below 70 g/l. Note that CI below 3.2 l/min/m^2 with concomitant haemoglobin values below 70 g/l were observed only in a few measurements; the statistical significance of LPR in these cases could thus not be determined. Another view of the data is shown in Figure 4, which displays

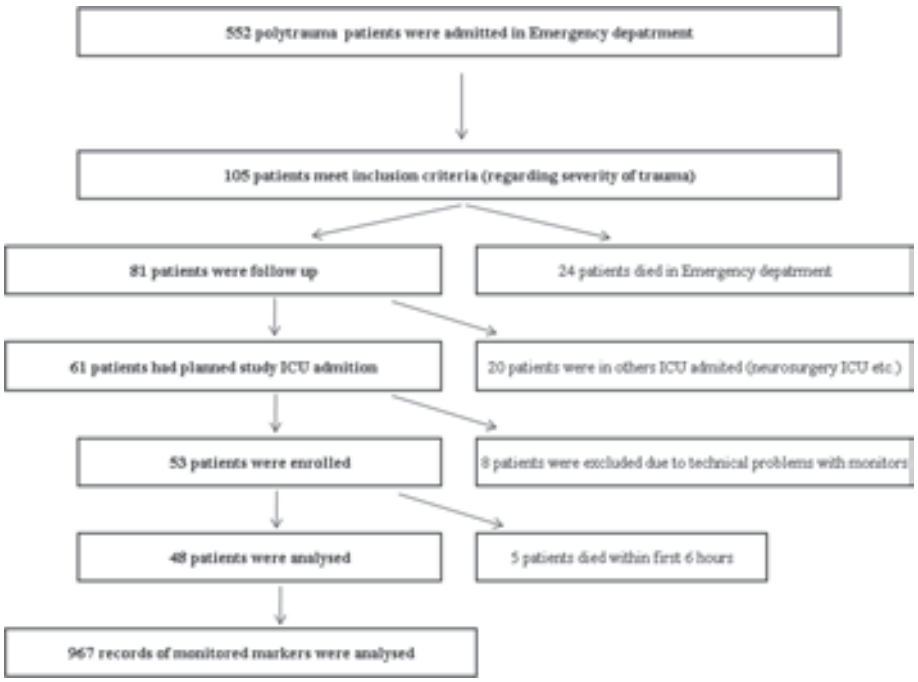

Figure 1 Flow diagram of the study.

Table 1 Demographics description of study population

	Median	Percent
Age (years)	36	
ISS	43	
Male gender		83
Weight (kg)	82	
Height (cm)	178	
Pre-hospital care (minute)	58	
ED care (minute)	90	
Theatretime (minute)	140	
ICU stay (days)	10.5	

cardiac output, haemoglobin and $ScvO_2$ in association to LPR category (i.e., non-ischemic, border and severe ischemic LPRs). All results were statistically significant ($p < 0.05$) Figure 4.

Discussion

Severe trauma patient transfusion management is challenging; the identification of both occult and inadequately resuscitated shock is a major clinical problem with traditional markers. Additionally, occult shock can present with normal global haemodynamics [10]. Severe polytrauma patient triage is crucial for good decision making regarding massive transfusion protocol (MTP) activation, which improves trauma haemorrhage outcomes [11]. Transfusion recommendations in trauma management attempt to maintain haemoglobin levels at 70-90 g/l [7]. Transfusions can be life saving but may also cause serious complications (i.e., TRALI, DIC, etc.) [12,13]; inadequate transfusion and over-transfusion (Hb ≥ 110 g/l) are also harmful [14]. Fewer transfusions can lead to low DO_2 with global or local (i.e., different local DO_2 in tissues and organs according to local perfusion) ischemia development with regard to oxygen consumption. Many articles have discussed the benefits of the restriction transfusion strategy compared with liberal transfusions [14]. Haemoglobin could not be evaluated separately in traumatic haemorrhagic shock treatments; however, other markers may account for patient comorbidities (i.e., coronary disease), age and clinical status. Hb targets could differ according to the treatment period; Hb values of approximately 70 g/l could be low during initial treatments, particularly with a low CI or with severe comorbidities. This value could be sufficient in the next period of critical care, which starts after the initial shock and bleeding are resolved. Higher haemoglobin levels in the initial treatment period could reduce haemodilutions and decrease any potential ischemia if re-bleeding occurs; thus, mortality could be reduced [15]. Additional transfusion benefits could include restored blood viscosity and enhanced rheological properties of the blood. Transfusion of PRBC, which are the most frequent transfusion media, compared to fresh blood transfusions, may not provide immediate increase of oxygen delivery to tissues primarily due to transfusion storage length. A decrease in LPR could delay an increase in haemoglobin levels for 7-10 hours, and tissue ischemia could be eliminated over long time intervals [16]. Similarly, this phenomenon could be observed with LPR and $ScvO_2$ trends, whereby a decrease in LPR could delay an increase in $ScvO_2$ for 10 hours [16]. The average observed haemoglobin in the first 24 hours of this study, which included the suspected haemoconcentration period, were 97.70 ± 18.67 g/l; therefore, it could be speculated that if this value was approximately 70 g/l, then tissue ischemia could be eliminated at a much later period, and organ dysfunction could be worsened.

Table 2 Association of L, $ScvO_2$ and LPR to Hb groups

Hb groups	L		$ScvO_2$		LPR	
g/l	mmol/l		Percent		Dimensionless	
	median	IQR	median	IQR	median	IQR
<70	5.538	5.036	65.00	16.47	28.66	26.08
70 - 90	3.105	4.095	73.7	17.72	16.02	7.68
>90	2.3	3.072	77.7	11.52	17.16	9.83

Hb, hemoglobin (g/l); L, arterial lactate (mmol/l); $ScvO_2$, central venous oxygen saturation(%); LPR, lactate/pyruvate ratio. Values are median ± interquartile range (IQR) ($p < 0.05$).

Additionally, fluid administration, which is a core treatment for shock and hypovolemia for preserving effective haemodynamic functions and tissue perfusion, has limits and adverse effects. Excessive fluid amounts lead to diluted coagulation factors, hypothermia [17] and endothelial glycocalyx damage [18]. Hypervolemia and fluid overload also lead to interstitium expansion. These influence the transcapillary gas and substrate exchange and decrease oxygen transport to tissues [19]. Hypovolemia leads to vasoconstriction and microvasculatory blood flow restriction, which cause ischemia due to low oxygen and substrate delivery [19]. Tissue perfusion could be altered with the administration of vasoactive agents, and knowledge of metabolic tissue conditions (i.e., LPR) during haemostatic resuscitation could help guide treatment.

Lactataemia evaluation in shock is typically difficult in practice; elevated arterial lactate levels are associated with increased mortality and morbidity [7], and lactate normalisation is one of most frequent resuscitation targets. Arterial lactate could be elevated without clinical signs of shock but could also be an indication of on-going ischemia [20]. In contrast, during a shock state, lactate could accumulate in low or non-perfused tissues, and serum levels could be falsely determined to be low. After tissue perfusion is restored, lactate levels increase as a sign of reperfusion, and high lactate levels could be connected with normal aerobic metabolism. The normalisation of

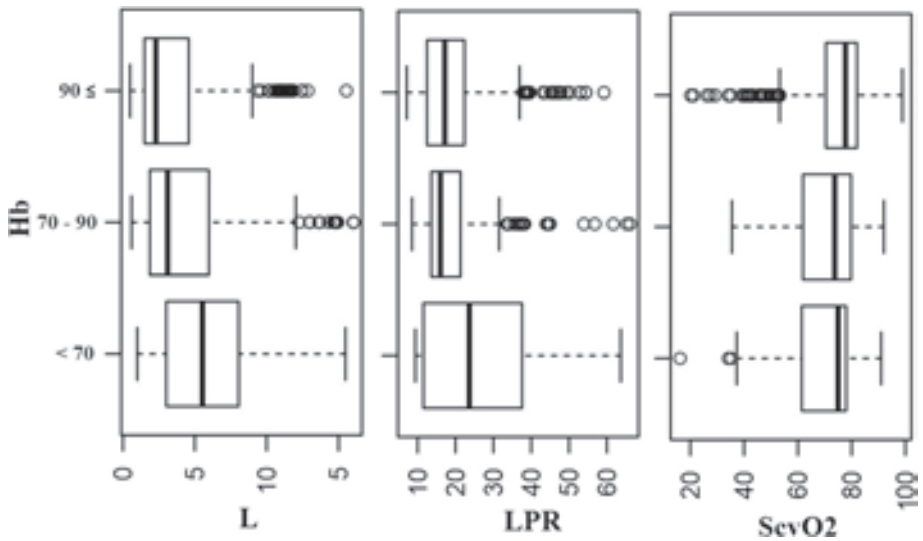

Figure 2 Association of L, LPR and $ScvO_2$ to Hb groups. Hb, hemoglobin (g/l); L, arterial lactate (mmol/l); $ScvO_2$, central venous oxygen saturation(%); LPR, lactate/pyruvate ratio.

lactate values depends on the hepatic clearance of lactate or its consumption in tissues, which could also decrease during shock. It is expected that lactate levels will follow the oxygen debt, but in some clinical conditions, lactate levels may normalise without the resolution of tissue oxygen debt [21]. There are also a number of non-ischemic factors that elevate lactate levels (e.g., stress and catecholamines) [22]. Arterial lactate levels should, therefore, be critically evaluated because assessment of the lactate levels alone fails to discriminate between ischemia and aerobiosis [23].

The measurement of LPR could be more useful than that of arterial lactate levels alone when discriminating between occult shock with ischemic tissue conditions and aerobic metabolism. LPR may be used as an early indicator of emerging ischemia during shock [24,25] and could also help to discriminate between elevated ischemic or non-ischemic lactate levels and to distinguish between the anaerobic aspects of hyperlactataemia [26].

Table 3 Association of lactate/pyruvate ratio (LPR) on hemoglobin (Hb) and cardiac index (CI) groups simultaneously

CI groups	Hb groups g/l					
l/min/m^2	<70		70 - 90		>90	
	Median	IQR	Median	IQR	Median	IQR
<3.2			29.13	22.05	17.88	12.28
3.2-4.8	50.04	1.02	15.81	7.18	16.19	9.03
>4.8	10.54	3.29	14.76	4.24	15.67	7.27

CI, cardiac index (l/min/m^2); Hb, hemoglobin (g/l); LPR, lactate/pyruvate ratio. Values are median ± interquartile range (IQR) ($p < 0.05$).

Hyperlactataemia with elevated LPR levels is associated with higher mortality than hyperlactataemia with normal LPR levels [26]. LPR levels over 25 indicate anaerobic metabolism onset [9] and are a more precise marker of ischemia than lactate levels alone [27].

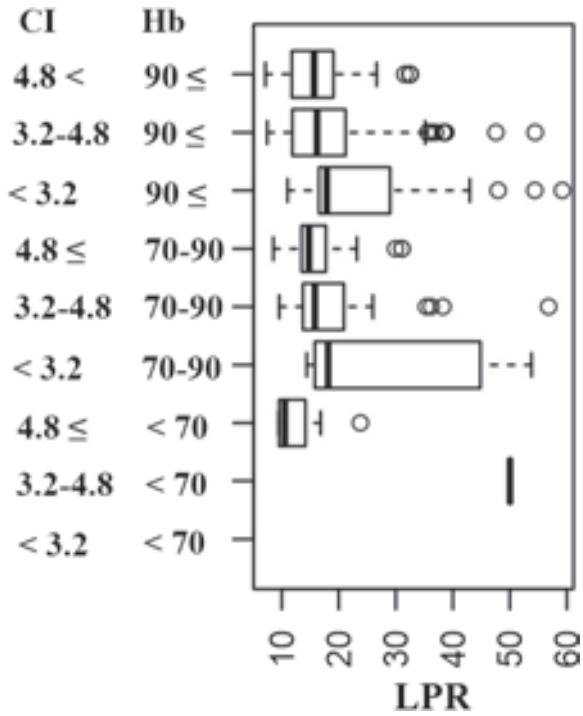

Figure 3 Association of LPR (axis X) on Hb and CI groups simultaneously (axis Y). CI, cardiac index (l/min/m^2); Hb, hemoglobin (g/l); LPR, lactate/pyruvate ratio.

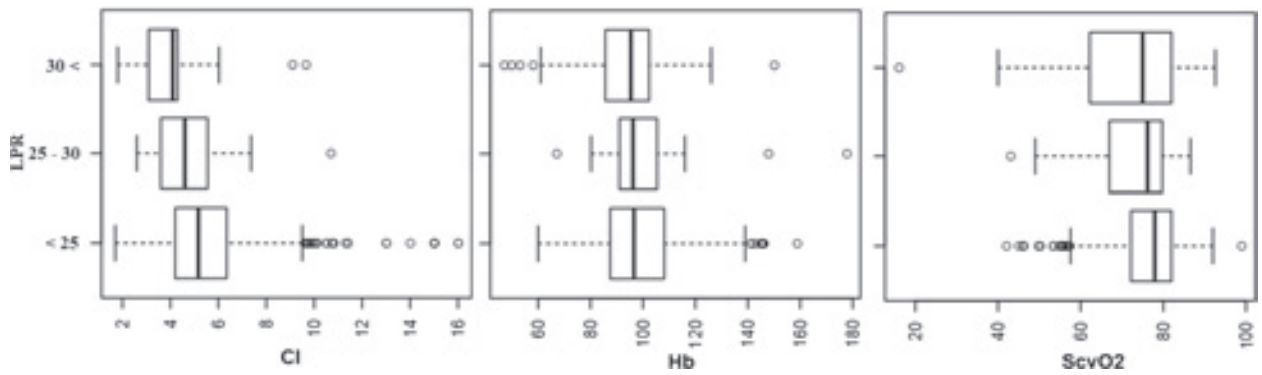

Figure 4 Association of CI, Hb and $ScvO_2$ on LPR devided to non-ischemic (<25), border ischemic (25-30) and severe ischemic (30<). CI, cardiac index (l/min/m^2); Hb, hemoglobin (g/l);); $ScvO_2$, central venous oxygen saturation(%); LPR, lactate/pyruvate ratio.

$ScvO_2$ is a frequently used marker that is useful in guiding fluid, catecholamine and transfusion therapy [28]. It is a global parameter of the oxygen extraction sum from the blood, and therefore, normal values do not exclude severe local tissue damage or regional tissue ischemia. It is expected that low $ScvO_2$ could reflect low DO_2. The most respected target value for shock resuscitation is an $ScvO_2$ value above 70% [29]; however, emerging ischemia originates at the cellular level, and changes in the LPR value could precede that in the $ScvO_2$ value by 10 or 11 hours [16]. A low $ScvO_2$ could lead to DO_2 manipulation, but a normal or high $ScvO_2$ could lead to false satisfaction due to treatment, allowing background cell dysfunction to occur.

Haemodynamic monitoring of CO is typically the next most frequent measurement in the evaluation of traumatic haemorrhagic shock. Trauma patients may have a low CI in the first hours after trauma (i.e., the ebb phase of shock). Tachycardia could then occur to preserve CI during hypovolemia, and later, CI rises to supranormal values to act as a physiologic reserve marker and as a compensatory reaction to overcoming distress (i.e., the flow phase of shock). In contrast, a normal CI value may not ensure adequate tissue perfusion [10]. Many authors have examined the evaluation of the VO_2/DO_2 relationship. A normalised VO_2 seems to be essential for organism recovery, and oxygen supply independency is a key strategy for haemodynamic optimisation [30]. Increasing DO_2 to supranormal values, however, was found to be beneficial in some studies [31], but not in others [32]. Additionally, excessive oxygen supply may be deleterious due to ineffective metabolic costs; however, it may be reasonable to increase the DO_2 to 20% above the critical DO_2 value (i.e., the limit of DO_2/VO_2 dependency) [30]. Velmahos GC demonstrated that patients who achieved supranormal haemodynamic parameters (i.e., CI > 4.5 l/min/m^2, DO_2I > 600 ml/min/m^2 and VO_2I > 170 ml/min/m^2) after severe trauma had better outcomes than patients who did not achieve those limits [31]. A spontaneously high DO_2 could be used as a simple physiologic reserve marker and a predictor of outcomes. An excessive artificial increase in DO_2 without a functional organism reserve could be detrimental [31]. Resuscitation efforts should be limited to what is only necessary with respect to human variability [33].

In this study, Hb < 70 g/l (i.e., without a CI distinction, whereby different CI are included) was associated with pathologic lactate, $ScvO_2$ and LPR values; therefore, treatment interventions or more intensive monitoring were inevitable (Table 2.). Pathologic blood lactate levels in all Hb intervals were also observed and certainly influenced the reduced lactate clearance during the first 24 hours after trauma.

To eliminate tissue ischemia (i.e., normalise LPR), it is rational to increase the DO_2, but only in patients with Hb values of 70-90 g/l and a low CI; with a normal CI and Hb < 70 g/l; or, most likely, with a low CI and Hb < 70 g/l (Table 3.). An artificial CI increase to supranormal values could be beneficial, but only if it is accomplished when Hb < 70 g/l to avoid an ischemic LPR; however, potential adverse vasoactive medication effects may occur. It may be beneficial to transfuse to Hb 70-90 g/l and a normal CI, which will also lead to a normal LPR. An ischemic LPR with supranormal CI values was not observed, supporting the benefits of the physiologic reaction to trauma discussed above. Increasing a low CI to normal is rational in patients with Hb levels at 70-90 g/l and most likely <70 g/l. In cases where Hb > 90 g/l, the increase of a low CI to normal levels leads to a decrease in LPR; however, the LPR in both of these situations is under the ischemic threshold. A low CI should be avoided.

To avoid tissue ischemia, transfusions are applicable in patients with Hb < 70 g/l and a normal CI and most likely in low CI cases as well. An Hb increase to over 90 g/l could only be warranted when patients have a low CI; however, it is preferable to increase a low CI. With regard to LPR, it was shown that supranormal CI levels

could be used to treat tissue ischemia, but the artificial elevation of CI could be dangerous [31]. Another requirement is to adequately correct the blood oxygen content using not only Hb but also SaO_2 and PaO_2.

Limitations

This study has several limitations. Tissue monitoring in the early phase of management of severe trauma patients is typically difficult. In this timeframe, physicians employ several necessary interventions, including diagnostic and therapeutic methods. The observations of this study were performed in addition to and did not influence the standard care of the examined critically ill patients; tissue monitoring was begun within 6 hours after admission. The study was performed in full working Trauma centre. The authors enrolled only 48 patients, and each patient was enrolled by a physician associated with this study. The authors also had limited human and economic resources. The study was financial supported partially by a grant, and certain technical problems with encountered with equipment during testing.

Conclusion

LPR is shown to be a useful marker to manage traumatic haemorrhagic shock therapies. LPR is the result of cell metabolic functions and thus reflects the sum of all interventions. LPR target therapies could be better than traditional management, which use other global markers that only assume good tissue conditions; tissue conditions could be directly monitored by the proposed method. In initial traumatic haemorrhagic shock treatments, it may be better to maintain CI ≥ 3.2 l/min/m^2 and Hb ≥ 70 g/l. Additionally, LPR may be very important and useful as a transfusion trigger in normal or low CI situations with decreased haemoglobin; it could be used to predict the onset of ischemia due to low local DO_2 levels and effectively reveal low tissue perfusion.

Abbreviations

CO: Cardiac output; PaO_2: Partial pressure of oxygen in arterial blood; Hb: Haemoglobin; LPR: Lactate/pyruvate ratio; CI: Cardiac index; SaO_2: Arterial saturation of oxygen; PRBC: Packed red blood cells; MTP: Massive transfusion protocol; TRALI: Transfusion-related acute lung injury; $ScvO_2$: Central venous oxygen saturation; VO_2: Oxygen consumption; DO_2: Oxygen delivery; VO_{2i}: Oxygen consumption index; DO_{2i}: Oxygen delivery index; L: Arterial lactate; ISS: Injury severity score; ED: Emergency department; DIC: Disseminated intravascular coagulation.

Competing interests

First two authors are funded by the Internal Grant Agency of the Ministry of Health of the Czech Republic. The authors declare no other competing interests.

Authors' contributions

FB - conception and design, data collection and analysis, manuscript writing and final approval of the manuscript. LP - conception and design, financial support, final approval of manuscript. JM - data analysis, critical revision and final approval of the manuscript. PS - data analysis, critical revision and final approval of the manuscript. PŠ - critical revision and final approval of the manuscript. All authors have substatially contributed to the conception and design of the study, read and then approved the final manuscript.

Acknowledgments

The authors with to thank Michal Burda from IT4Innovations Division, University of Ostrava, Institute for Research and Applications of Fuzzy Modelling, Department of Biostatistics, Czech Republic for statistical processing. The authors would also like to express their gratitude to the staff of the intensive care unit at KARIM, University Hospital Ostrava, Czech Republic, for their help collecting and analyzing the data.

Source of funding

Project is partially funded by the Resort Programme of Science and Development - MZ III for the period of 2010-2015, from the Internal Grant Agency of the Ministry of Health of the Czech Republic: NT11371-5/2010 "Metabolic Response of the Organism in Polytraumas", principle investigator Leopold Pleva, MD, CSc.; co-investigators Filip Burša, MD; Tomáš Olos, MD; Jan Jahoda, MD; Roman Kula, MD CSc.; Vaclav Prochazka, MD, PhD; and Ivo Kopáček, MD.

Author details

[1]Department of anesthesiology and intensive care medicine, University Hospital Ostrava, Faculty of Medicine Universitas Ostrava, 17. listopadu 1790, Ostrava-Poruba, Czech Republic. [2]Traumatology Centre, University Hospital Ostrava, Faculty of Medicine Universitas Ostrava, 17. listopadu 1790, Ostrava-Poruba, Czech Republic.

Received: 1 September 2014 Accepted: 10 December 2014
Published: 15 December 2014

References

1. Schoeneberg C, Schilling M, Keitel J, Kauther MD, Burggraf M, Hussmann B, Lendemans S: **TraumaNetwork, Trauma Registry of the DGU®, Whitebook, S3 Guideline on Treatment of Polytrauma/Severe Injuries: An Approach for Validation by a Retrospective Analysis of 2304 Patients (2002-2011) of a Level 1 Trauma Centre.** *Zentralbl Chir* 2014, doi:10.1055/s-0033-1360225.
2. Rush BF: **Irreversibility in post-transfusion phase of hemorrhagic shock.** *Adv Exp Med Bio* 1971, **23:**215–221.
3. Shoemaker WC, Appel PL, Kram HB: **Tissue oxygen debt as a determinant of lethal and nonlethal postoperative organ failure.** *Crit Care Med* 1988, **16**(11):1117–1120.
4. Barbee RW, Reynolds PS, Ward KR: **Assessing shock resuscitation strategies by oxygen debt repayment.** *Shock* 2010, **33**(2):113–122.
5. Bonanno FG: **Physiopathology of shock.** *J Emerg Trauma Shock* 2011, **4**(2):222–232.
6. Dutton RP: **Hemostaticresuscitation.** *British J Anesthesia* 2012, **109**(S1):i39–i46.
7. Spahn DR, Bouillon B, Cerny V, Coats TJ, Duranteau J, Fernández-Mondéjar E, Filipescu D, Hunt BJ, Komadina R, Nardi G, Neugebauer E, Ozier Y, Riddez L, Schultz A, Vincent JL, Rossaint R: **Management of bleeding and coagulopathy following major trauma: an updated European guideline.** *Crit Care* 2013, **17**(2):R76.
8. Bursa F, Olos T, Pleva L, Kula R, Jahoda J, Procházka V, Kopácek I: **Metabolism monitoring with microdialysis in the intensive care.** *Cas Lek Cesk* 2011, **150**(11):605–609.
9. Waelgaard L, Dahl BM, Kvarstein G, Tønnessen TI: **Tissue gas tension and tissue metabolites for detection of organ hypoperfusion and ischemia.** *Acta Anaesthesiol Scand* 2012, **56**(2):200–209.
10. Suistomaa M, Uusaro A, Parviainen I, Ruokonen E: **Resolution and outcome of acute circulatory failure does not correlate with hemodynamics.** *Critical Care* 2003, **7:**R52–R58.
11. Khan S, Allard S, Weaver A, Barber C, Davenport R, Brohi K: **A major haemorrhage protocol improves the delivery of blood component therapy and reduces waste in trauma massive transfusion.** *Injury* 2013, **44**(5):587–592.
12. Hsu JM, Hitos K, Fletcher JP: **Identifying the bleeding trauma patient: predictive factors for massive transfusion in an Australasian trauma population.** *J Trauma Acute Care Surg* 2013, **75**(3):359–364.
13. Elmer J, Wilcox SR, Raja AS: **Massive transfusion in traumatic shock.** *J Emerg Med* 2013, **44**(4):829–838.
14. Tien H, Nascimento B Jr, Callum J, Rizoli S: **An approach to transfusion and hemorrhage in trauma: current perspectives on restrictive transfusion strategies.** *Can J Surg* 2007, **50**(3):202–209.

15. Morel N, Delaunay F, Dubuisson V: **Management of bleeding following major trauma: is a targethaemoglobin of 7 to 9 g/dl high enough?** *Critical Care* 2013, **17:**442.
16. Burša F, Pleva L: **Anaerobic metabolism associated with traumatic hemorrhagic shock monitored by microdialysis of muscle tissue is dependent on the levels of hemoglobin and central venous oxygen saturation: a prospective, observational study.** *Scand J Trauma Resusc Emerg Med* 2014, **22**(1):11.
17. Chappell D, Jacob M, Hofmann-Kiefer K, Conzen P, Rehm M: **A rational approach to perioperative fluid management.** *Anesthesiology* 2008, **109:**723–740.
18. Rhee P, Wang D, Ruff P, Austin B, DeBraux S, Wolcott K, Burris D, Ling G, Sun L: **Human neutrophil activation and increased adhesion by various resuscitation fluids.** *Crit Care Med* 2000, **28:**74–78.
19. Nohé B, Ploppa A, Schmidt V, Unertl K: **Volume replacement in intensive care medicine.** *Anaesthesist* 2011, **60**(5):457–464. 466-473.
20. Meregalli A, Oliveira RP, Friedman G: **Occulthypoperfusion is associated with increased mortality in hemodynamically stable, high-risk, surgical patients.** *Critical Care* 2004, **8:**R60–R65.
21. Sakr Y, Dubois MJ, De Backer D, Creteur J, Vincent JL: **Persistent microcirculatory alterations are associated with organ failure and death in patients with septic shock.** *Crit Care Med* 2004, **32**(9):1825–1831.
22. Brucculeri S, Urso C, Caimi G: **The role of lactate besides the lactic acidosis.** *ClinTer* 2013, **164**(3):e223–e238.
23. De Backer D: **Lactic acidosis.** *Intensive Care Med* 2003, **29:**699–702.
24. Ohashi H, Kawasaki N, Fujitani S: **Utility of microdialysis to detect the lactate/pyruvate ratio in subcutaneous tissue for the reliable monitoring of haemorrhagic shock.** *J Smooth Muscle Res* 2009, **45**(6):269–278.
25. Larentzakis A, Toutouzas KG, Papalois A, Lapidakis G, Doulgerakis S, Doulami G, Drimousis P, Theodorou D, Katsaragakis S: **Porcine model of haemorrhagic shock with microdialysis monitoring.** *J Surg Res* 2013, **179**(1):e177–e182.
26. Dimopoulou I, Nikitas N, Orfanos SE, Theodorakopoulou M, Vassiliadi D, Ilias I, Ikonomidis I, Boutati E, Maratou E, Tsangaris I, Karkouli G, Tsafou E, Diamantakis A, Kopterides P, Maniatis N, Kotanidou A, Armaganidis A, Ungerstedt U: **Kinetics of adipose tissue microdialysis-derived metabolites in critically ill septic patients:associations with sepsis severity and clinical outcome.** *Shock* 2011, **35**(4):342–348.
27. Suistomaa M, Ruokonen E, Kari A, Takala J: **Time-pattern of lactate and lactate to pyruvate ratio in the first 24 hours of intensive care emergency admissions.** *Shock* 2000, **14**(1):8–12.
28. Tánczos K, Molnár Z: **The oxygen supply–demand balance: a monitoring challenge.** *Best Pract Res Clin Anaesthesiol* 2013, **27**(2):201–207.
29. Della Rocca G, Pompei L: **Goal-directed therapy in anesthesia: any clinical impact or just a fashion?** *Minerva Anestesiol* 2011, **77**(5):545–553.
30. Caille V, Squara P: **Oxygen uptake-to-delivery relationship: a way to assess adequate flow.** *Crit Care* 2006, **10**(3):S4.
31. Velmahos GC, Demetriades D, Shoemaker WC, Chan LS, Tatevossian R, Wo CC, Vassiliu P, Cornwell EE 3rd, Murray JA, Roth B, Belzberg H, Asensio JA, Berne TV: **Endpoints of resuscitation of critically injured patients: normal or supranormal? A prospective randomized trial.** *Ann Surg* 2000, **232**(3):409–418.
32. Hayes MA, Timmings AC, Yau EH, Palazzo M, Hinds CJ, Watson D: **Elevation of systemic oxygen delivery in the treatment of critically ill patients.** *N Engl J Med* 1994, **330:**1717–1722.
33. Sisak K, Manolis M, Hardy BM, Enninghorst N, Bendinelli C, Balogh ZJ: **Acute transfusion practice during trauma resuscitation: who, when, where and why?** *Injury* 2013, **44**(5):581–586.

doi:10.1186/1471-2253-14-118
Cite this article as: Burša *et al.*: Tissue ischemia microdialysis assessments following severe traumatic haemorrhagic shock: lactate/pyruvate ratio as a new resuscitation end point? *BMC Anesthesiology* 2014 **14**:118.

18 Radiofrequency energy in surgery: state of the art

Ihnát P, Ihnát Rudinská L, Zonča P

Originally published in Surgery Today, 2014, vol. 44, no. 6, p. 985-991

Consent to the publication of 19th March 2015

(licence no. 3592400026817)

Surg Today (2014) 44:985–991
DOI 10.1007/s00595-013-0630-5

REVIEW ARTICLE

Radiofrequency energy in surgery: state of the art

Peter Ihnát · Lucia Ihnát Rudinská · Pavel Zonča

Received: 21 March 2013 / Accepted: 30 April 2013 / Published online: 1 June 2013

Abstract Over a period of more than 100 years, radiofrequency energy has been introduced in many fields and applications in medicine. At present, radiofrequency constitutes the basis of numerous medical devices employed in almost all medical specialties. It is particularly applicable and valuable in various minimally invasive procedures for its locally focused effects. Radiofrequency energy is a technical term established to describe high-frequency alternating electrical currents (with a frequency ranging from 300 kHz to 3 MHz) and their impact on biological tissue. The application of RF energy causes controlled tissue heating with consequent cell protein denaturation and desiccation, which leads to cell death and tissue destruction. The primary principle of radiofrequency is that the generated heat can be used to cut, coagulate or induce metabolic processes in the target tissue. The authors of this paper offer a comprehensive and compact review of the definition, history, physics, biological principles and applications of radiofrequency energy in current surgery.

Keywords Radiofrequency · History · Definition · Biological effects · Applications

P. Ihnát · P. Zonča
Department of Surgical Studies, Faculty of Medicine, University of Ostrava, Syllabova 19, 703 00 Ostrava, Czech Republic

P. Ihnát (✉) · P. Zonča
Department of Surgery, University Hospital Ostrava, 17. listopadu 1790, 708 52 Ostrava, Czech Republic
e-mail: peterihnat@yahoo.com

L. Ihnát Rudinská
Department of Forensic Medicine, University Hospital Ostrava, Ostrava, Czech Republic

Introduction

Radiofrequency energy presently forms the basis of numerous medical device systems used in the treatment of various medical disorders. The characteristics, methods of application and design of medical devices using radiofrequency (RF) energy are highly varied; however, the fundamental effects of energy on biological tissue are the same. The application of RF energy generates heat, which can be used to cut, coagulate or induce metabolic processes in the target tissue [1–3].

The basic characteristics of RF energy determine its application primarily in minimally invasive procedures and make it likely the most extended minimally invasive method in medicine at present. Many of today's surgical procedures and techniques owe their existence and success to radiofrequency [1, 4, 5].

Very limited information regarding the fundamentals of radiofrequency energy is currently available to practicing specialists in standard textbooks. A search of the current scientific literature found no available complex or compact reviews evaluating the use of radiofrequency energy in surgery.

Methods

A comprehensive literature search was performed to identify studies regarding the application of radiofrequency energy in surgery. The search combined the following terms: radiofrequency, electrosurgery, radiofrequency ablation and radiofrequency resection. The sources were MEDLINE, PubMed and the Google Scholar database.

In this paper, we review the history of radiofrequency energy in medicine and the definition, physics, biological

principles and applications of radiofrequency energy in surgery. The primary outcome of this paper is to offer a complete, well-structured and up-to-date review of the current status of the use of radiofrequency in surgery.

Results

History of radiofrequency energy in medicine

Radiofrequency technology has been deployed in medicine for over 100 years. The first experiments to apply radiofrequency energy in humans were conducted at the end of the 19th century. In 1881, Morton found that an oscillating current with a 100-KHz frequency can pass through the human body without inducing pain, spasms or burns [6].

In 1893, Arsene D'Arsonval published similar findings with the current frequency lowered to 10 kHz. He reported that a current passing through the tissue leads to the elevation of tissue temperature and increased oxygen absorption and carbon dioxide elimination [6, 7].

In 1900, the Parisian physician, Joseph Rivere, used a high-frequency alternating current to treat a carcinomatous ulcer on the hand of a patient, which is noted to be the first use of radiofrequency electricity in surgery. Consequently, he continued to apply electricity in the treatment of hemorrhoids and various superficial lesions of the skin, oral cavity and bladder [8].

In 1911, William Clark altered an electrosurgical device (amperage increased, voltage decreased) to produce deeper penetration of heat into tissue and used this device to remove malignant lesions of the skin, breast and cervix. He described the term *desiccation* as the destruction of tissue via dehydration without carbonization [6, 9].

The first attempts to utilize radiofrequency currents in the operating theater are found at the beginning of the 20th century. In 1926, Wiliam Bowie (a physicist from Harvard) constructed an operating room electrosurgical device that offered both coagulating and cutting currents. The device was first used by Harvey Cushing (a neurosurgeon at Peter Bent Brigham Hospital) to stop bleeding and cut through tissue [10]. Since that time, a worldwide revolutionary spread of this technology occurred, and radiofrequency electrosurgery quickly became accepted by the scientific community. This led to the evolution of various and numerous types of electrosurgical instruments for cutting and achieving coagulation in the operating theater.

In the 1970s, several experiments studying the effects of radiofrequency and microwave currents on animals (pigs, rats and Rhesus monkeys) were conducted. Unaffected internal homeostasis was observed, and the pattern of tissue heating was studied (both on the surface of and deep within the body) [2, 5].

The utilization of RF energy to induce focal thermal tissue destruction deep within the human body (without its opening) was first described in the field of cardiology in the 1980s. In 1989, Langberg reported successful catheter ablation of the atrioventricular junction using RF energy. The safety of the procedure led to the widespread adoption of catheter ablation as a therapeutic modality in cardiology for the treatment of supraventricular and ventricular dysrhythmias caused by stable arrhythmic foci [11, 12].

The idea to apply RF energy to solid tumors to cause tissue destruction via focal thermal injury came in the early 1990s. Investigators modified RF equipment to induce focal thermal injuries deep within the liver parenchyma. Histopathologic examinations of the ablated livers showed well-defined concentric regions of coagulative necrosis around the active electrode tips [13, 14].

Rossi and colleagues became leaders in the field of percutaneous imaging-guided tumor ablation. In 1990, they reported the findings of experiments in guinea pig and pig livers using 480-KHz localized RF currents and determined the size and shape of achievable areas of ablation in the liver. Subsequently, they published the preliminary and final results of the use of RF ablation in the treatment of inoperable liver tumors. In particular, their study published in 1996 constituted a milestone with respect to percutaneous RF ablation of liver tumors, proving the effectiveness and safety of this new method [13, 15].

In 2002, Habib and colleagues developed the innovative method of radiofrequency-assisted liver resection. This new technique employs the heat produced by an RF needle electrode to coagulate liver tissue before cutting it, thus permitting the surgeon to perform liver resection with minimal blood loss [16]. The technique can be used in both open and minimally invasive surgery.

Definition and physical principles of radiofrequency energy

Radiofrequency energy is the biophysical conception established to describe high-frequency alternating electrical currents (with a frequency ranging from 300 kHz to 3 MHz) and their impact on biological tissue [17].

Radiofrequency alternating current is a technical term in biophysics created by the fusion of the names of two different physical quantities: electromagnetic radio broadcast waves and high-frequency alternating electrical currents. Intermediate frequencies of electromagnetic waves (300 kHz–3 MHz) are used to modify the amplitude (AM) of a radio broadcast. For this reason, alternating electrical currents with high frequencies in the range of 300 kHz–3 MHz are referred to as radiofrequency alternating currents [1, 5, 17].

Radiofrequency currents create the desired clinical effect by passing through tissue. In the course of current RF

application, electromagnetic energy is first converted in cells to kinetic energy then to thermal energy. Thermal energy production causes tissue heating around the active electrodes [1, 17].

The resulting effects of an RF current in the tissue are determined according to a number of factors: the electrical properties of the current (the frequency, amperage, voltage, power and waveform of the output), exposure time, properties of the tissue (impedance, water content) and size and shape of the surface of the electrode [3, 18].

The electrical energy is transformed into heat in accordance with Joules Law and can be expressed using the following formula:

$$\text{Energy} = (\text{current}/\text{cross} - \text{sectional area})^2 \times \text{time} \times \text{resistance}.$$

The heat generated in the tissue around the active electrode is a function of the current density (the current per cross-sectional area), time and resistance. The larger the current and voltage, the more heat is produced in the tissue. The RF current spreads around the electrode in a relatively uniform manner and creates a spherical zone of thermal tissue destruction. The RF power density decreases in proportion to the square of the distance from the electrode, which leads to a rapid decrease in temperature in association with an increase in the distance from the electrode [1, 5, 17, 19, 20].

The application of RF energy requires the formation of a closed-loop electrical circuit consisting of a radiofrequency generator, the patient and wires and electrodes. The RF generator takes an alternating electrical current from a socket (with a frequency of 50 or 60 Hz) and converts it into an alternating current with a frequency in the range of 300–700 kHz. Generators can be used to produce a number of different waveforms (low-voltage continuous mode, interrupted high-voltage mode and various blended modes) that allow the surgeon to change the impact of the RF energy on the tissue [3, 18].

The electrical circuit must be complete. For this reason, there are always two electrodes in direct contact with the patient. Monopolar devices include one dispersive electrode with a large surface and one active electrode with a small surface. A significant discrepancy between the surfaces of the active and passive electrodes results in the concentration of heat production in the tissue surrounding the active electrode. When bipolar devices are used, both electrodes are located within the surgical instrument, with the electrical current passing and concentrating between the electrodes.

The primary principle of bipolar devices is that only the tissue interposed between the two electrodes is part of the electrical circuit. This allows for more accurate measurement of the tissue temperature and impedance and decreases the number of possible complications caused by current diversion [1, 18, 21].

Biological effects of radiofrequency energy

Alternating electrical currents with a low frequency have the ability to depolarize muscle and neural cells. Depolarization is caused by opening voltage-gated sodium and calcium ion channels localized within neural and muscular cell membranes. Depolarization of heart muscle cells can lead to cardiac rhythm disorders, and depolarization of muscles and nerves is associated with muscle fasciculation and pain [1, 17]. If the current frequency is increased in excess of 100,000 Hz, sodium and calcium ion channels do not open, and cellular membrane depolarization does not occur. In addition, the functions of muscle and neural cells are not altered. For these reasons, RF currents can be used in medicine without causing undesired clinical effects on cardiac, muscular or neural cells [22, 23].

The application of RF energy causes controlled tissue heating with consequent cell protein denaturation and desiccation, which leads to cell death and tissue destruction. The primary use of generating heat via the application of RF energy is to cut, coagulate or induce metabolic processes in the target tissue. Radiofrequency currents do not affect cellular macromolecules and are, therefore, neither carcinogenic nor teratogenic [22–24].

The elevation of cellular and tissue temperature is the principal property of RF currents used to achieve the desired clinical effects. There are three basic mechanisms through which RF currents increase tissue temperature. The most important is the conversion of electromagnetic energy to mechanical energy. High-frequency alternating currents cause rapid oscillation of electrically charged particles (ions) within the cellular cytoplasm. Rapid ion movement leads to frictional forces that induce thermal energy production and elevation of intracellular and tissue temperature. The second mechanism of RF-induced increased tissue temperature is the so-called resistive heating, which is based on the physical concept of an increased temperature in a resistor due to the flow of current. The third mechanism is indirect: conductive heat transfer. The increase in tissue temperature leads to the conduction of thermal energy to the adjacent tissue with elevation of the tissue temperature [1, 17, 22, 23].

Two crucial factors determine the biological effects of RF energy on tissue: the amount of thermal energy delivered to the tissue and the speed of tissue heating. RF-induced thermal damage to tissue is reversible when the achieved cellular temperature is below 45 °C. When the tissue temperature reaches 50 °C, cell death occurs within

approximately 6 min. A local temperature of 60 °C or higher results in immediate cell death [19, 25, 26].

Tissue temperatures between 60 °C and 95 °C lead to cellular death via two simultaneous biological processes: protein denaturation and the loss of cellular water (desiccation). Protein denaturation is caused by the temperature-induced breaking of the hydrothermal bonds that exist between protein molecules and consequent reforming of broken bonds as the local temperature cools, which leads to a loss of structural protein integrity. The loss of cellular water occurs through the thermally damaged cellular wall. Tissue temperatures above 95 °C result in a process of vaporization: intracellular water turns to steam leading to massive expansion of the intracellular volume and cell explosion. When the tissue temperature reaches 200 °C or higher, a process of carbonization takes place in which organic tissue molecules are reduced to carbon [1, 17, 25, 27].

Applications of radiofrequency energy in surgery

Over a period of more than 100 years, radiofrequency energy has been introduced in many fields and applications in medicine. The currently accepted medical applications of RF energy are shown in Table 1. At present, RF energy is widely used in operating rooms in the vast majority of surgical procedures. Several types of RF-based systems are used in surgery: monopolar and bipolar electrosurgical units, endovenous RF ablation of varicose veins, RF ablation of tumors and RF-assisted resection of parenchymal organs.

Monopolar and bipolar electrosurgical units

Electrosurgical units based on the use of RF energy are widely applied in operating rooms to assist in surgical procedures by providing methods of cutting and achieving hemostasis. These devices are also called diathermy or electrocautery apparatuses.

Electrosurgical units utilize the effects of RF energy to cut or achieve coagulation and/or fulguration. Cutting (tissue incision) is performed using the RF-induced biological process of cellular vaporization. Hemostasis is achieved by two simultaneous processes: desiccation and protein denaturation. Fulguration is a process of rapid superficial coagulation caused by the biological processes of desiccation, denaturation and carbonization [1, 3, 17].

The output from the electrosurgical unit (RF generator) can be modulated to produce different waveforms for a particular mode of action. As the waveforms change, so too do the corresponding tissue effects. The RF oscillator provides the basic high-frequency signal, which is amplified and modulated to produce cutting, coagulation and blended waveforms. The RF power output is turned on and

Table 1 Applications of radiofrequency energy in medicine

Medical field	Type of procedure	Indications
Cardiology	RF catheter ablation	Cardiac arrhythmias
Coloproctology	Secca procedure	Fecal incontinence
Cosmetic surgery	Skin rejuvenation and tightening RF systems	Skin wrinkles
		Cellulitis
ENT (otolaryngology)	RF palatoplasty	Obstructive sleep apnoea syndrome
		Habitual snoring
Gastroenterology	Stretta procedure	Gastroesophageal reflux syndrome
Neurosurgery	Percutaneous RF neurotomy	Chronic back pain from facet or sacroiliac joints
Ophthalmology	Conductive Keratoplasty	Vision correction of hyperopia and presbyopia
Surgery	Monopolar and bipolar electrosurgical units	Cutting and haemostasis in the operating rooms
	Endovenous radiofrequency ablation	Saphenous vein reflux
	RF ablation	RFA of solid tumours of liver, kidney, lung, adrenal gland, bone
	RF-assisted resection	Resection of tumours of liver, kidney, spleen, pancreas
Urology	Transurethral resection of the prostate (TURP)	Benign prostatic hyperplasia
	Transurethral RF needle ablation of the prostate (TUNA)	Benign prostatic hyperplasia
	Renessa procedure	Stress urinary incontinence

off by means of a control circuit connected to either a hand switch on the active electrode or a foot switch that can be operated by the surgeon. In cutting mode, the generator delivers constant, continuous, sinusoidal waveforms of alternating current. A generator working in coagulation mode delivers interrupted (the current is relative to the continuous cutting mode only approximately 6 % of the time) high-voltage current. Blended modes include various modifications of the duty cycle to achieve varying mixtures of cutting and coagulation [1, 3, 5, 18].

Electrosurgical units can apply RF energy in either a monopolar or bipolar fashion. Both methods of RF energy delivery are applicable via various instruments designed for use in open or laparoscopic surgery.

Monopolar systems are the most commonly used electrosurgical modalities at present. The active electrode is designed to focus the current (and its tissue effects) on the surgical target. The current then passes through the patient and completes the circuit through the dispersive, large-surface electrode positioned on the patient at a location distant from the surgical site.

Bipolar systems are designed to have both electrodes positioned on the same surgical instrument at the site of surgery. The only part of the patient involved in the electrical circuit is the tissue between the two electrodes. For this reason, bipolar systems are safer, provide more accurate measurements of local tissue parameters (temperature, impedance) and prevent complications related to unintended dispersal of the electrical current [18, 21].

Progressive evolution of bipolar electrosurgical instruments has led to the creation of vessel sealing technology. This technology is designed to reliably seal vascular structures up to 7 mm in diameter via the complete fusion of the vascular intimal layers. Vessel sealing systems are equipped with sophisticated closed-loop feedback control algorithms and combine RF energy and high pressure to achieve fusion of the vessel walls, thus creating a permanent seal with minimal thermal spread.

Seal strengths have been proven to be significantly stronger than other energy-based techniques, such as standard bipolar systems or ultrasonic coagulation. Electrosurgically sealed vessels are comparable to mechanical ligation tools, such as sutures and clips. Several studies have demonstrated low complication rates and low amounts of operative blood loss associated with the use of vessel sealing technology in laparoscopic and open surgery [1, 17, 18].

Endovenous RF ablation of varicose veins

Reflux of the great saphenous vein is the most common cause of chronic venous insufficiency (CVI), whose symptoms include varicose veins, leg swelling, skin discoloration and ulceration, and is usually associated with substantial effects on the patient's quality of life. Surgery (high saphenofemoral ligation, stripping of the saphenous vein and varicose vein removal) is the traditional modality for treating CVI. In recent years, minimally invasive endovenous treatments (endovenous laser therapy, radiofrequency ablation and endovenous foam sclerotherapy) have gained popularity and become widely used in the treatment of saphenous vein reflux [28, 29].

Endovenous radiofrequency ablation (RFA) involves the delivery of RF energy to induce thermal injury and seal the saphenous vein. This procedure is usually performed under ultrasound guidance to confirm and map all areas of reflux and monitor the course of the procedure. The majority of RFA treatments are currently performed in the office setting. A catheter is passed through a small incision near the knee into the sheath and advanced to the desired location. RF energy is then applied and delivered directly to the vein walls without coagulating blood. Heat delivered to the vessel wall causes the vein to shrink and seal off. The catheter tip is then slowly withdrawn along the course of the vein at a rate of approximately 1 cm per minute.

This procedure is typically used to treat truncal varicose veins (the great saphenous vein and small saphenous vein) because RFA catheters cannot easily be passed through tortuous veins or vessels with many turns and bends. Published studies have demonstrated endovenous RFA to be a minimally invasive technique that is safe, well-tolerated by patients and able to achieve good cosmetic results. In comparison with standard surgery, endovenous RFA offers comparable efficacy with lower morbidity and a faster recovery. The primary advantages of RFA are reduced periprocedural pain, a high vein occlusion rate and an early return to normal activities [28–31].

Solid tumor ablation

Primary and secondary liver tumors present a challenging problem in clinical oncology due to very high morbidity and mortality worldwide. Surgical resection is undoubtedly the "gold standard" for patients with liver metastases or primary liver tumors. Unfortunately, resection of hepatic malignancies is possible in only 10–25 % of patients at the time of initial detection as a result of tumor extent and localization, an inadequate hepatic reserve and/or significant comorbidities. Patients with unresectable disease may be candidates for local ablative techniques, chemoembolization and/or systemic or local chemotherapy [4, 20, 25, 26].

Several local ablative techniques for performing chemical or thermal tumor ablation have been developed in the past two decades. Radiofrequency ablation (RFA) has become the ablative modality of choice on the grounds of

multiple randomized controlled trials of patients with unresectable liver tumors [4, 26, 32].

RFA is based on the application of RF energy to the tumor, thereby causing thermal destruction, i.e., ablation. The most common method of performing RFA is the percutaneous approach under ultrasonography or CT guidance. RFA can also be performed in the operating theater during open surgery or laparoscopy. During the course of the RFA procedure, an active electrode is placed on the tumor, and RF energy is delivered. The entire targeted volume must be subjected to cytotoxic temperatures in order to be destroyed. The initial major limitation of RFA was the small volume of lesions created by ablation. Early RF electrodes were monopolar, able to create 1.5–2 cm cylindrical zones of ablated tissue; therefore, only tumors less than 2 cm in diameter could be ablated [19, 20, 25].

The continuous development of RF technology allowed surgeons to achieve larger volumes of tissue ablation. There are several different strategies for increasing the field of ablation using RFA. The most successful involve bipolar electrodes, internal electrode cooling via circulating fluid, the use of pulsed RF ablation and multi-applicator systems. Multi-applicator systems are composed of several straight, parallel electrodes (cluster) or curved, radially arranged electrodes (expandable electrodes). Due to technical improvements in RF technology, it is currently possible to effectively ablate lesions with a diameter of 5–7 cm under optimal conditions [25, 26, 32].

According to many studies published in the last two decades, RFA can be used to treat primary and secondary liver tumors, with a success rate of 90 %. It is a safe technique with a low rate of complications, offering benefits for life expectancy in patients with locally advanced disease [4, 20, 25, 26, 32]. The spectrum of clinical applications of RFA has been widened from unresectable liver tumors to unresectable tumors of the kidneys, adrenal glands, bones, lungs and breast [4].

Radiofrequency-assisted resection of parenchymal organs

Liver resection is the accepted treatment of choice for patients with primary or secondary liver tumors. Intraoperative blood loss and the subsequent need for blood transfusions remain significant risk factors for postoperative morbidity and mortality associated with hepatic resection. Over the years, different techniques have been developed to allow for safer liver resection with minimal blood loss. One of the techniques offering "bloodless" liver resection is radiofrequency-assisted liver resection, which was introduced by Habib's team in 2002 and is, therefore, also called Habib's resection. It is a simple method in which the principle of radiofrequency-induced coagulative necrosis is used to achieve hemostasis and biliostasis [16, 33, 34].

RF energy induced by an RF generator is repeatedly applied through a special RF needle (Habib^{TM} 4X) along the intended resection line. This leads to the creation of an approximately 2-cm wide zone of coagulative necrosis in the liver parenchyma. The created zone represents an avascular resection plane, along which the liver parenchyma can be divided using a scalpel with minimal blood loss. In this manner, hemostasis is obtained using RF energy only; no additional devices (e.g., stitches, knots, clips or glue) are needed [16].

Radiofrequency-assisted liver resection can be performed in both open and minimally invasive surgery. The Habib^{TM} 4X is a handheld instrument designed for use in liver resection during open surgery. It is a bipolar device that releases RF energy between two pairs of active electrodes spaced at the corners of a rectangle. The laparoscopic Habib^{TM} 4X is a similar device (bipolar with four electrodes) designed for use in minimally invasive surgery [16, 33, 35].

This technique can be used in all types of liver resection, from small wedge resection to hemihepatectomy. It allows the surgeon to perform minor hepatic resection at the expense of major hepatectomy, thereby saving the patient's normal hepatic parenchyma for future resection.

Published studies indicate that Habib's resection is associated with minimal blood loss, a reduced need for perioperative blood transfusions and low morbidity and mortality. The use of the radiofrequency-assisted technique in parenchymal resection has expanded from liver resection to resection of the kidneys, spleen and pancreas [16, 33–36].

Conclusion

Radiofrequency energy has been used in medicine for more than 100 years. The spectrum of RF energy application has been expanded in the last decades from tissue coagulation and cutting in operating room electrosurgical units to the development of a high number of diverse devices used in almost every medical specialty.

Currently accepted medical applications of radiofrequency energy include: monopolar and bipolar electrosurgical units for tissue coagulation and cutting; vessel sealing systems; conductive keratoplasty in vision correction; RF ablation of the soft palate and tongue in the treatment of obstructive sleep apnea and snoring; RF catheter ablation in the treatment of cardiac arrhythmias; RF skin rejuvenation and tightening technology in cosmetic surgery; endovenous RF ablation of varicose veins; RF neurotomy in the treatment of chronic back pain; transurethral resection and transurethral needle ablation of benign prostatic

hyperplasia; the Stretta procedure in the treatment of gastroesophageal reflux disease; the Renessa procedure in the treatment of stress urinary incontinence; the Secca procedure in the treatment of fecal incontinence; RF ablation of unresectable solid tumors; and RF-assisted resection of the parenchymal organs (liver, kidneys, spleen, pancreas).

Radiofrequency energy is a principal component of numerous medical devices and, thus, functions as an extremely valuable tool in the hands of practicing clinicians. It is, therefore, absolutely necessary for all health care professionals to understand the fundamental physical principles and biological effects of radiofrequency energy on the human body. Such awareness would give rise to the proper use of RF energy and increase the safety of procedures.

Conflict of interest Peter Ihnat and the other coauthors have no conflicts of interest to declare.

References

1. Massarweh NN, Cosgriff N, Douglas PS. Electrosurgery: history, principles, and current and future uses. J Am Coll Surg. 2006;202(3):520–30.
2. Schwaitzberg SD. Evolutions and revolutions in surgical energy. In: Feldman LS, Fuchshuber P, Jones DB, editors. The fundamental use of surgical energy (FUSE) manual. New York: Springer; 2012. p. 3–13.
3. Pearce JA. Electrosurgery. New York: John Wiley; 1986.
4. Friedman M, Mikityansky I, Kam A, Libutti SK, Walther MM, Neeman Z, et al. Radiofrequency ablation of cancer. Cardiovasc Interv Radiol. 2004;27:427–34.
5. Filingeri V, Gravante G, Cassisa D. Physics of radiofrequency in proctology. Eur Rev Med Pharmacol Sci. 2005;9:349–54.
6. Kelly HA, Ward GE. Electrosurgery. Philadelphia: WB Saunders; 1932. p. 1–9.
7. D'Arsonval A. Action physiologique des courants alternatis a grande frequency. Arch Physiol Porm Pathol. 1893;25:401.
8. Glover JL, Bendick PJ, Link WJ. The use of thermal knives in surgery: electrosurgery, lasers, plasma scalpel. Curr Probl Surg. 1978;15:1.
9. Clark WL. Oscillatory dessication in the treatment of accessible malignant growths and minor surgical conditions. J Adv Ther. 1911;29:169–83.
10. Cushing H, Bovie W. Electrosurgery as an aid to the removal of intracranial tumors. Surg Gynecol Obstet. 1928;47:751–84.
11. Langberg JJ, Chin MC, Rosenqvist M, Cockrell J, Dullet N, Van Hara G, et al. Catheter ablation of the atrioventricular junction with radiofrequency energy. Circulation. 1989;80(6):1527–35.
12. Morady F. Radio-frequency ablation as treatment for cardiac arrhythmias. N Engl J Med. 1999;340:534–44.
13. Rossi S, Fornari F, Pathies C, Buscarini L. Thermal lesions induced by 480KHz localized current field in guinea pig and pig liver. Tumori. 1990;76:54–7.
14. McGahan JP, Browning PD, Brock JM, Tesluk H. Hepatic ablation using radiofrequency electrocautery. Invest Radiol. 1990;25:267–70.
15. Rossi S, Di Stasi M, Buscarini E, Quaretti P, Garbabnati F, Squassante L, et al. Percutaneous RF interstitial thermal ablation in the treatment of hepatic cancer. AJR Am J Roentgenol. 1996;167:759–68.
16. Weber JC, Navarra G, Jiao LR, Nicholls JP, Jensen SL, Habib NA. New technique for liver resection using heat coagulative necrosis. Ann Surg. 2002;236:560–3.
17. Munro MG. Fundamentals of electrosurgery Part I: Principles of radiofrequency energy for surgery. In: Feldman LS, Fuchshuber P, Jones DB, editors. The fundamental use of surgical energy (FUSE) manual. New York: Springer; 2012. p. 15–60.
18. Pearce JA. Electrosurgical unit. In: Webster JG, editor. Encyclopedia of medical devices and instrumentation. New York: Wiley; 2006. p. 156–77.
19. Goldberg SN, Gazelle GS, Halpern EF, Rittman WJ, Mueller PR, Rosenthal DI. Radiofrequency tissue ablation: importance of local temperature along the electrode tip exposure in determining lesion shape and size. Acad Radiol. 1996;3:212–8.
20. Strasberg SM, Linehan D. Radiofrequency ablation of liver tumors. Curr Probl Surg. 2003;40:451–98.
21. Nduka CC, Super PA, Monson JR, Darzi AW. Cause and prevention of electrosurgical injuries in laparoscopy. J Am Coll Surg. 1994;179:161–70.
22. Lacourse JR, Miller WT, Vogt M, Selikowitz SM. Effect of high-frequency current on nerve and muscle tissue. IEEE Trans Biomed Eng. 1985;32:82–6.
23. Repacholi MH. Low-level exposure to radiofrequency electromagnetic fields: health effects and research needs. Bioelectromagnetics. 1998;19:1–19.
24. Schwan HP. Biological effects of non-ionizing radiations: cellular properties and interactions. Ann Biomed Eng. 1988;16:245–63.
25. Periera PL. Actual role of radiofrequency ablation of liver metastases. Eur Radiol. 2007;17:2062–70.
26. Lencioni R, Cioni D. Percutaneous methods for ablation of hepatic neoplasms. In: Blumgart LH, editor. Blumgart's surgery of the liver, biliary tract, and pancreas. Philadelphia: Elsevier; 2007. p. 1269–77.
27. Nikfarjam M, Muralidharan V, Christophi C. Mechanisms of focal heat destruction of liver tumors. J Surg Res. 2004;127:208–23.
28. Dietzek AM. Endovenous radiofrequency ablation for the treatment of varicose veins. Vascular. 2007;15(5):255–61.
29. Murad MH, Coto-Yglesias F, Zumaeta-Garcia M, Elamin MB, Duggirala MK, Erwin PJ, et al. A systematic review and meta-analysis of the treatments of varicose veins. J Vasc Surg. 2011;53(Suppl 5):49S–65S.
30. Gohel MS, Davies AH. Radiofrequency ablation for uncomplicated varicose veins. Phlebology. 2009;24(Suppl 1):42–9.
31. Van den Bos R, Arends L, Kockaert M, Neumann M, Nijsten T. Endovenous therapies of lower extremity varicosities: a meta-analysis. J Vasc Surg. 2009;49(1):230–9.
32. Zogakis TG, Bilchik J. Radiofrequency thermal ablation of liver tumors. In: Blumgart LH, editor. Blumgart's surgery of the liver, biliary tract, and pancreas. Philadelphia: Elsevier; 2007. p. 1288–97.
33. Ayav BP, Habib NA, Pellicci R, Tierris J, Milicevic M, Jiao LR. Impact of radiofrequency assisted hepatectomy for reduction of transfusion requirements. AM J Surg. 2007;193:143–8.
34. Milicević M, Bulajić P, Zuvela M, Dervenis C, Basarić D, Galun D. A radiofrequency-assisted minimal blood loss liver parenchyma dissection technique. Dig Surg. 2007;24:306–13.
35. Hompes D, Aerts F, Penninck F, Topal B. Laparoscopic liver resection using radiofrequency coagulation. Surg Endosc. 2007;21:175–80.
36. Pai M, Jiao LR, Khorsandi S, Canelo R, Spalding DR, Habib NA. Liver resection with bipolar radiofrequency device: Habib^{TM} 4x. HPB. 2008;10:256–60.

Poznámky / Notes:

www.fno.cz

ISBN 978-80-905684-9-5 (print)
ISBN 978-80-906002-0-1 (on-line)

ISSN 2336-4041 (Print)
ISSN 2336-405X (On-line)